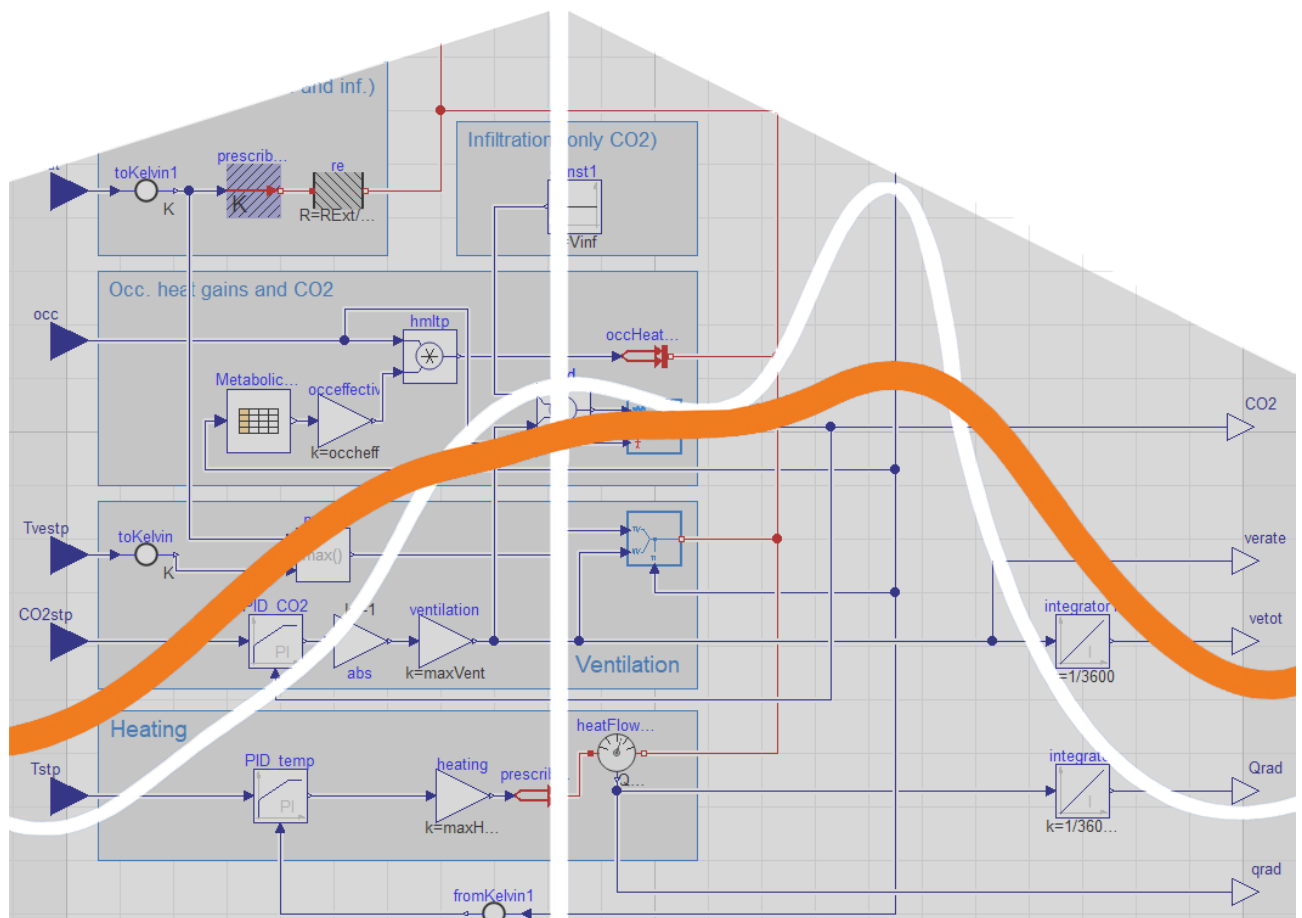


International Energy Agency

# Control strategies and algorithms for obtaining Energy Flexibility in buildings

Energy in Buildings and Communities Programme  
 Annex 67 Energy Flexible Buildings

November 2019





International Energy Agency

# Control strategies and algorithms for obtaining Energy Flexibility in buildings

---

**Energy in Buildings and Communities Programme**  
**Annex 67 Energy Flexible Buildings**

July 2019

## **Editors**

University of Southern Denmark, Denmark

Athila Quaresma Santos, [ags@mmmi.sdu.dk](mailto:ags@mmmi.sdu.dk)

Bo Nørregaard Jørgensen, [bnj@mmmi.sdu.dk](mailto:bnj@mmmi.sdu.dk)

## **Authors**

University of Southern Denmark, Denmark

Athila Quaresma Santos, [ags@mmmi.sdu.dk](mailto:ags@mmmi.sdu.dk)

Bo Nørregaard Jørgensen, [bnj@mmmi.sdu.dk](mailto:bnj@mmmi.sdu.dk)

Enervalis, Houthalen-Helchteren, Belgium

Hussain Kazmi, [hussain.kazmi@enervalis.com](mailto:hussain.kazmi@enervalis.com)

VTT Technical Research Centre of Finland Ltd.

Reino Ruusu, [reino.ruusu@semantum.fi](mailto:reino.ruusu@semantum.fi)

Ala Hasan, [ala.hasan@vtt.fi](mailto:ala.hasan@vtt.fi)

IREC Catalonia Institute for Energy Research

Thibault Péan, [tpean@irec.cat](mailto:tpean@irec.cat)

The Hong Kong Polytechnic University, Hong Kong SAR, China

Yuekuan Zhou, [yuekuan.zhou@connect.polyu.hk](mailto:yuekuan.zhou@connect.polyu.hk)

Sunliang Cao, [sunliang.cao@polyu.edu.hk](mailto:sunliang.cao@polyu.edu.hk)

Young Jae Yu, [young.jae.yu@iee.fraunhofer.de](mailto:young.jae.yu@iee.fraunhofer.de)

Norwegian University of Science and Technology (NTNU), Norway

John Clauß, [john.clauss@ntnu.no](mailto:john.clauss@ntnu.no)

Technical University of Denmark, Denmark

Rune Grønberg Junker, [rung@dtu.dk](mailto:rung@dtu.dk)

Eindhoven University of Technology, Netherlands

Christian Finck, [c.j.finck@tue.nl](mailto:c.j.finck@tue.nl)

University College Dublin (UCD)

Despoina Christantoni, [despoina.christantoni@ucdconnect.ie](mailto:despoina.christantoni@ucdconnect.ie)

Donal P. Finn, [donal.finn@ucd.ie](mailto:donal.finn@ucd.ie)

Concordia University, Montreal, Canada

Ali Saberi Derakhtenjani, [ali.saberi.mech@gmail.com](mailto:ali.saberi.mech@gmail.com)

Jose Agustin Candanedo, [jose.candanedoibarra@canada.ca](mailto:jose.candanedoibarra@canada.ca)

Andreas Athienitis, [aathieni@encs.concordia.ca](mailto:aathieni@encs.concordia.ca)

University College Dublin (UCD)

Anjukan Kathirgamanathan, [anjukan.kathirgamanathan@ucdconnect.ie](mailto:anjukan.kathirgamanathan@ucdconnect.ie)

Donal P. Finn, [donal.finn@ucd.ie](mailto:donal.finn@ucd.ie)



© Copyright Danish Technological Institute 2019

All property rights, including copyright, are vested in Danish Technical Institute, Operating Agent for EBC Annex 67, on behalf of the Contracting Parties of the International Energy Agency Technology Collaboration Programme of Research and Development on Energy in Buildings and Communities. In particular, no part of this publication may be reproduced, stored in a retrieval system or transmitted in any form or by any means, electronic, mechanical, photocopying, recording or otherwise, without the prior written permission of Danish Technological Institute.

Published by Danish Technological Institute, Denmark

Disclaimer Notice: This publication has been compiled with reasonable skill and care. However, neither Danish Technological Institute nor the EBC Contracting Parties (of the International Energy Agency Technology Collaboration Programme of Research and Development on Energy in Buildings and Communities) make any representation as to the adequacy or accuracy of the information contained herein, or as to its suitability for any particular application, and accept no responsibility or liability arising out of the use of this publication. The information contained herein does not supersede the requirements given in any national codes, regulations or standards, and should not be regarded as a substitute for the need to obtain specific professional advice for any particular application.

ISBN: ISBN: 978-87-93250-11-6

ISSN: 1600-3780

Participating countries in EBC:

Australia, Austria, Belgium, Canada, P.R. China, Czech Republic, Denmark, Finland, France, Germany, Greece, Ireland, Italy, Japan, Republic of Korea, the Netherlands, New Zealand, Norway, Poland, Portugal, Singapore, Spain, Sweden, Switzerland, Turkey, United Kingdom and the United States of America.

Additional copies of this report may be obtained from:

[www.iea-ebc.org](http://www.iea-ebc.org)

[essu@iea-ebc.org](mailto:essu@iea-ebc.org)

Special thanks to the internal Annex 67 reviewers:

Achim Geissler, University of Applied Sciences Northwestern Switzerland,

Søren Østergaard Jensen, Danish Technological Institute, Denmark.

# Preface

## The International Energy Agency

The International Energy Agency (IEA) was established in 1974 within the framework of the Organisation for Economic Co-operation and Development (OECD) to implement an international energy programme. A basic aim of the IEA is to foster international co-operation among the 28 IEA participating countries and to increase energy security through energy research, development and demonstration in the fields of technologies for energy efficiency and renewable energy sources.

## The IEA Energy in Buildings and Communities Programme

The IEA co-ordinates research and development in a number of areas related to energy. The mission of the Energy in Buildings and Communities (EBC) Programme is to develop and facilitate the integration of technologies and processes for energy efficiency and conservation into healthy, low emission, and sustainable buildings and communities, through innovation and research. (Until March 2013, the IEA-EBC Programme was known as the Energy in Buildings and Community Systems Programme, ECBCS.)

The research and development strategies of the IEA-EBC Programme are derived from research drivers, national programmes within IEA countries, and the IEA Future Buildings Forum Think Tank Workshops. The research and development (R&D) strategies of IEA-EBC aim to exploit technological opportunities to save energy in the buildings sector, and to remove technical obstacles to market penetration of new energy efficient technologies. The R&D strategies apply to residential, commercial, office buildings and community systems, and will impact the building industry in five focus areas for R&D activities:

- Integrated planning and building design
- Building energy systems
- Building envelope
- Community scale methods
- Real building energy use

## The Executive Committee

Overall control of the IEA-EBC Programme is maintained by an Executive Committee, which not only monitors existing projects, but also identifies new strategic areas in which collaborative efforts may be beneficial. As the Programme is based on a contract with the IEA, the projects are legally established as Annexes to the IEA-EBC Implementing Agreement. At the present time, the following projects have been initiated by the IEA-EBC Executive Committee, with completed projects identified by (\*) and joint projects with the IEA Solar Heating and Cooling Technology Collaboration Programme by (☼):

- Annex 1: Load Energy Determination of Buildings (\*)
- Annex 2: Ekistics and Advanced Community Energy Systems (\*)
- Annex 3: Energy Conservation in Residential Buildings (\*)
- Annex 4: Glasgow Commercial Building Monitoring (\*)
- Annex 5: Air Infiltration and Ventilation Centre
- Annex 6: Energy Systems and Design of Communities (\*)
- Annex 7: Local Government Energy Planning (\*)
- Annex 8: Inhabitants Behaviour with Regard to Ventilation (\*)
- Annex 9: Minimum Ventilation Rates (\*)
- Annex 10: Building HVAC System Simulation (\*)
- Annex 11: Energy Auditing (\*)
- Annex 12: Windows and Fenestration (\*)
- Annex 13: Energy Management in Hospitals (\*)
- Annex 14: Condensation and Energy (\*)

- Annex 15: Energy Efficiency in Schools (\*)
- Annex 16: BEMS 1- User Interfaces and System Integration (\*)
- Annex 17: BEMS 2- Evaluation and Emulation Techniques (\*)
- Annex 18: Demand Controlled Ventilation Systems (\*)
- Annex 19: Low Slope Roof Systems (\*)
- Annex 20: Air Flow Patterns within Buildings (\*)
- Annex 21: Thermal Modelling (\*)
- Annex 22: Energy Efficient Communities (\*)
- Annex 23: Multi Zone Air Flow Modelling (COMIS) (\*)
- Annex 24: Heat, Air and Moisture Transfer in Envelopes (\*)
- Annex 25: Real time HVAC Simulation (\*)
- Annex 26: Energy Efficient Ventilation of Large Enclosures (\*)
- Annex 27: Evaluation and Demonstration of Domestic Ventilation Systems (\*)
- Annex 28: Low Energy Cooling Systems (\*)
- Annex 29: Daylight in Buildings (\*)
- Annex 30: Bringing Simulation to Application (\*)
- Annex 31: Energy-Related Environmental Impact of Buildings (\*)
- Annex 32: Integral Building Envelope Performance Assessment (\*)
- Annex 33: Advanced Local Energy Planning (\*)
- Annex 34: Computer-Aided Evaluation of HVAC System Performance (\*)
- Annex 35: Design of Energy Efficient Hybrid Ventilation (HYBVENT) (\*)
- Annex 36: Retrofitting of Educational Buildings (\*)
- Annex 37: Low Exergy Systems for Heating and Cooling of Buildings (LowEx) (\*)
- Annex 38: ☀ Solar Sustainable Housing (\*)
- Annex 39: High Performance Insulation Systems (\*)
- Annex 40: Building Commissioning to Improve Energy Performance (\*)
- Annex 41: Whole Building Heat, Air and Moisture Response (MOIST-ENG) (\*)
- Annex 42: The Simulation of Building-Integrated Fuel Cell and Other Cogeneration Systems (FC+COGEN-SIM) (\*)
- Annex 43: ☀ Testing and Validation of Building Energy Simulation Tools (\*)
- Annex 44: Integrating Environmentally Responsive Elements in Buildings (\*)
- Annex 45: Energy Efficient Electric Lighting for Buildings (\*)
- Annex 46: Holistic Assessment Tool-kit on Energy Efficient Retrofit Measures for Government Buildings (EnERGo) (\*)
- Annex 47: Cost-Effective Commissioning for Existing and Low Energy Buildings (\*)
- Annex 48: Heat Pumping and Reversible Air Conditioning (\*)
- Annex 49: Low Exergy Systems for High Performance Buildings and Communities (\*)
- Annex 50: Prefabricated Systems for Low Energy Renovation of Residential Buildings (\*)
- Annex 51: Energy Efficient Communities (\*)
- Annex 52: ☀ Towards Net Zero Energy Solar Buildings
- Annex 53: Total Energy Use in Buildings: Analysis & Evaluation Methods (\*)
- Annex 54: Integration of Micro-Generation & Related Energy Technologies in Buildings
- Annex 55: Reliability of Energy Efficient Building Retrofitting - Probability Assessment of Performance & Cost (RAP-RETRO) (\*)
- Annex 56: Cost Effective Energy & CO<sub>2</sub> Emissions Optimization in Building Renovation (\*)
- Annex 57: Evaluation of Embodied Energy & CO<sub>2</sub> Emissions for Building Construction (\*)
- Annex 58: Reliable Building Energy Performance Characterisation Based on Full Scale Dynamic Measurements (\*)
- Annex 59: High Temperature Cooling & Low Temperature Heating in Buildings (\*)
- Annex 60: New Generation Computational Tools for Building & Community Energy Systems (\*)
- Annex 61: Business and Technical Concepts for Deep Energy Retrofit of Public Buildings (\*)
- Annex 62: Ventilative Cooling (\*)
- Annex 63: Implementation of Energy Strategies in Communities (\*)
- Annex 64: LowEx Communities - Optimised Performance of Energy Supply Systems with Energy Principles (\*)
- Annex 65: Long-Term Performance of Super-Insulation in Building Components and Systems (\*)
- Annex 66: Definition and Simulation of Occupant Behaviour in Buildings

- Annex 67: Energy Flexible Buildings
- Annex 68: Indoor Air Quality Design and Control in Low Energy Residential Buildings
- Annex 69: Strategy and Practice of Adaptive Thermal Comfort in Low Energy Buildings
- Annex 70: Building Energy Epidemiology: Analysis of Real Building Energy Use at Scale
- Annex 71: Building Energy Performance Assessment Based on In-situ Measurements
- Annex 72: Assessing Life Cycle Related Environmental Impacts Caused by Buildings
- Annex 73: Towards Net Zero Energy Public Communities
- Annex 74: Energy Endeavour
- Annex 75: Cost-effective Strategies to Combine Energy Efficiency Measures and Renewable Energy Use in Building Renovation at District Level
- Annex 76: ☀ Deep Renovation of Historic Buildings towards Lowest Possible Energy Demand and CO<sub>2</sub> Emissions
- Annex 77: ☀ Integrated Solutions for Daylight and Electric Lighting
- Annex 78: Supplementing Ventilation with Gas-phase Air Cleaning, Implementation and Energy Implications
- Annex 79: Occupant-Centric Building Design and Operation
- Annex 80: Resilient Cooling
- Annex 81: Data-Driven Smart Buildings

- Working Group - Energy Efficiency in Educational Buildings (\*)
- Working Group - Indicators of Energy Efficiency in Cold Climate Buildings (\*)
- Working Group - Annex 36 Extension: The Energy Concept Adviser (\*)
- Working Group - HVAC Energy Calculation Methodologies for Non-residential Buildings
- Working Group - Cities and Communities
- Working Group - Building Energy Codes
- Working Group - International Building Materials Database

# Management summary

This report constitutes one of the contributions of the IEA EBC Annex 67 which aims to increase the knowledge, identify critical aspects and possible solutions concerning the energy flexibility that buildings can provide. Control strategies and algorithms were developed and together with components and systems these were evaluated in controlled environments. Example cases were selected and documented under realistic energy prices, weather conditions, user behavior and load profiles.

This deliverable contains fifteen chapters with twelve cases (shown in Table 2). The Introduction summarizes the investigation of the Energy Flexibility potential in different buildings and contexts. Following a literature review of applied and tested control is presented that show potential for providing demand side flexibility in residential or commercial buildings. The further chapters presents each a case study that discuss their methodology to achieve Energy Flexibility and the obtained results. Chapters 4-15 with case studies are structured to include an introduction, control scope, methodology, implementation, results and a conclusion. In total, twelve authors have contributed to different parts of the report (shown in Table 2).

## Reading guide

This section provides a guide to find useful information regarding the case studies presented in the next sections. The features are grouped in five areas: Building typology, Energy system, Source of flexibility, Control system and what Results based on. These five areas are further subdivided in to different technologies which are briefly explained in Table 1. Table 2 helps the reader in finding the examples/features of most interest.

The case studies describe results from investigations applying different boundary conditions (weather, energy prices, etc.) and constrains (use of buildings, comfort range, etc.) so the results may differ between the examples or even contradict in some cases.

Table 1 The features of the different case studies of Tables 2.

	Icon	Technology	Explanation
<b>Building typology</b>		Single-family house	Only one single house or a flat is considered
		Multi-family house	The considered building is a multi-family building with a number of flats
		Non-residential building	These buildings are in this report offices or multi-use e.g. university buildings
		Cluster of buildings	The flexibility of several buildings are considered at an aggregated level. The buildings can either be located physically next to each other or not be physically connected but have the same aggregator controlling their energy flexibility – e.g. buildings with the same

	Icon	Technology	Explanation
			type of heating system e.g. a heat pump, and are controlled as a group
Energy system		Heat pump	The utilized heat pumps are located in the buildings and may both be ground source or air source heat pumps
		District heating	Is considered in the sense, that the building(s) heat demand is covered by district heating via typically a heat exchanger in the building
		Other HVAC system	This includes any other ventilation and/or cooling systems
		PV	PV systems located at the building make the building a prosumer, which may put extra stress on the grid when they export electricity to the grid
Source of flexibility		Constructions	The thermal mass of the building (walls, floors, ceilings but also furniture) are utilised for storage of heat
		Thermal storage	Thermal storage are here both DHW tanks, buffer tanks in space heating and cooling systems but also swimming pools or PCM storage
		Battery	Batteries may both be a stationary battery in the building (e.g. in connection with a PV system) or the battery of an electrical vehicle owned by the user of the building
		Fuel switch	Energy flexibility obtained in a building, which has two or more energy systems covering the same demand – e.g. a gas boiler and a heat pump
Control system		Rule based	Traditional control where the energy service systems are controlled by a set of predefined rules. A traditional PI thermostat is a simple rule based controller
		Model based	The controller is based on a model of the energy demand of the building in the form of a white box model (e.g. TRNSYS), a grey box model (typically a low order RC (resistance-capacitance) model) or a black box model (where the model is generated from measurements and the parameters of the model give no direct physical meaning). Model based controllers give the possibility of applying forecasts and can thereby make them more efficient but also more complex
Results based on		Simulations	The results of the example/teaser are based on simulations using typically white box modelling but can also be based on grey and black box models
		Measurements	The obtained results are from measurements on real building or from test facilities utilizing hardware-in-the loop where parts of the test are real physical components while the building and weather are simulated

Twelve case studies (listed in Table 2) around the world (Denmark , Belgium, Finland, Spain, China, Germany, Norway, Netherlands, Ireland and Canada) were developed in order to demonstrate control strategies and algorithms implementation that can provide Energy Flexibility in buildings.

Table 2 Case studies.

Case study	Name	Managed by	Location
1	Multi-objective genetic algorithm for model predictive control in buildings	University of Southern Denmark	Denmark
2	Deep reinforcement learning for optimal control of space heating	Enervalis and KU Leuven	Belgium
3	A Model Predictive Controller for Multiple-Source Energy Flexibility in Buildings	Technical Research Centre of Finland Ltd	Finland
4	Model predictive control for carbon emissions reduction in residential cooling loads	Catalonia Institute for Energy Research	Spain
5	Investigation of the Energy Flexibility of a residential net-zero energy building involved with the dynamic operations of hybrid energy storages and various energy conversion strategies	The Hong Kong Polytechnic University	China
6	Rule-based load shifting with heat pumps for single family houses	Fraunhofer IEE	Germany
7	Predictive rule-based control to perform heating demand response in Norwegian residential buildings	Norwegian University of Science and Technology	Norway
8	CO <sub>2</sub> -aware heating of indoor swimming	Technical University of Denmark	Denmark
9	Economic model predictive control for demand flexibility of a residential building	Eindhoven University of Technology	Netherlands
10	Implementation of demand response strategies in a multi-purpose commercial building	University College Dublin	Ireland
11	Experimental assessment of Energy Flexibility potential of a zone with radiant floor heating system	Concordia University	Canada
12	Aggregation of Energy Flexibility of commercial buildings	University College Dublin	Ireland

Table 3 Examples of how to obtain Energy Flexibility from buildings.

Chapter	Building typology				Energy system				Source of flexibility				Control system		Results based on	
																
	Single-family house	Multi-family house	Non-residential building	Cluster of buildings	Heat pump	District heating	Other HVAC systems	PV	Constructions	Thermal storage	Batteries	Fuel switch	Rule based	Model based	Simulation	Measurements
4			X			X	X		X				X	X	X	X
5	X				X				X					X	X	
6	X				X	X	X	X		X	X		X	X	X	
7	X	X			X				X	X				X	X	
8	X				X			X			X		X		X	
9	X				X				X	X			X		X	
10	X						X		X	X			X		X	
11	X			X	X					X				X		X
12	X				X		X	X	X					X		X
13			X				X		X				X		X	
14	X						X		X				X			X
15			X				X	X	X		X		X		X	

# Table of content

Reading guide	5
Abbreviations	7
1 Introduction to Annex 67	11
1.1 IEA EBC Annex 67	13
1.1.1 Terminology for and characterization of Energy Flexibility in buildings	13
1.1.2 Determination of the available Energy Flexibility of devices, buildings and clusters of buildings	13
1.1.3 Demonstration of and stakeholders perspective on Energy Flexible Buildings	14
1.1.4 Deliverables from IEA EBC Annex 67	14
2 Introduction to the report	16
3 Review of applied and tested control possibilities for energy flexibility in buildings	18
3.1 Terminology of control methods	18
3.2 Strengths and weaknesses of different control methods	19
3.3 Control strategies for heating and cooling using MPC	21
3.4 Control objectives, inputs, disturbances, constraints, and signals	22
3.4.1 Control objectives	22
3.4.2 Control constraints	25
3.4.3 Control inputs	27
3.4.4 Control disturbances	27
3.4.5 Control signals	27
3.5 Models supporting model-based control	28
3.5.1 Modelling of buildings	28
3.5.2 Modelling of TES systems	31
3.5.3 Advanced mathematical techniques for flexibility control	32
4 Multi-objective genetic algorithm for model predictive control in buildings	33
4.1 Building and system description	33
4.2 Control scope	33

4.2.1	Ventilation	34
4.2.2	Heating	35
4.2.3	Lights	35
4.2.4	Blinds	36
4.2.5	Energy flexibility mechanism	36
4.3	Methodology: control strategies	36
4.4	Implementation: genetic algorithm	39
4.4.1	Negotiation	42
4.5	Results and conclusions	43
5	Deep reinforcement learning for optimal control of space heating	48
5.1	Building and system description	48
5.1.1	Influencing variables	49
5.2	Methodology	49
5.2.1	Background	49
5.2.2	Context	50
5.2.3	Formulation	51
5.3	Implementation	52
5.3.1	Control objectives	52
5.3.2	Rule based control	53
5.3.3	Model predictive control	53
5.3.4	Model-based reinforcement learning	53
5.3.5	Model-free reinforcement learning (D-DNFQI)	54
5.4	Results	55
5.4.1	Quality of model learnt in model-based learning	55
5.4.2	Flat price signal	56
5.4.3	Dual price signal	57
5.4.4	Robustness to changing constraints	58
5.4.5	Robustness to incorrect model	59
5.5	Conclusion	59
6	A Model Predictive Controller for Multiple-Source Energy Flexibility in Buildings	61

6.1	Building and system description	61
6.2	Methodology: control strategies	63
6.3	Results and conclusion	63
7	Model predictive control for carbon emissions reduction in residential cooling loads	69
7.1	Building and system description	69
7.2	Methodology: control strategies	70
7.3	Implementation: control algorithms	72
7.4	Results and conclusion	73
8	Investigation of the energy flexibility of a residential net-zero energy building involved with the dynamic operations of hybrid energy storages and various energy conversion strategies	76
8.1	Building and system description	76
8.1.1	Parameters for the building facade, the infiltration and internal gains	77
8.1.2	Building services system	78
8.1.3	The renewable system, the battery and the electric vehicle	79
8.2	Methodology: control strategies	80
8.2.1	Demand responsive energy control strategy	81
8.2.2	Structural thermal mass storage	81
8.3	Implementation: control algorithms	82
8.4	Results and conclusion	82
8.4.1	Excess renewable-recharging strategy for hybrid thermal storages	87
8.4.2	The structural thermal mass storage	89
8.4.3	Conclusions	90
9	Rule-based load shifting with heat pumps for single family houses	92
9.1	Building and system description	92
9.2	Methodology: control strategies	96
9.3	Implementation: control algorithms	97
9.4	Results and conclusion	99
10	Predictive rule-based control to perform heating demand response in Norwegian residential buildings	104

10.1 Building and system description	104
10.2 Methodology: control strategies	106
10.3 Implementation: control algorithms	107
10.4 Results and conclusion	108
11 CO <sub>2</sub> -aware heating of indoor swimming	110
11.1 Building and system description	110
11.2 Methodology: control strategies	110
11.3 Implementation: control algorithms	111
11.4 Results and conclusion	112
12 Economic model predictive control for demand flexibility of a residential building	117
12.1 Building and system description	117
12.2 Methodology: control strategy	117
12.3 Implementation: control algorithm	118
12.4 Results and conclusion	119
13 Implementation of demand response strategies in a multi-purpose commercial building	123
13.1 Building and system description	123
13.2 Methodology: control strategies	127
13.3 Implementation: control algorithms	128
13.4 Results	129
13.5 Conclusions	135
14 Experimental assessment of energy flexibility potential of a zone with radiant floor heating system	136
14.1 Building and system description	136
14.2 Methodology: control strategies and implementation	138
14.3 Control algorithms	138
14.4 Results and conclusion	139
15 Aggregation of energy flexibility of commercial buildings	144
15.1 Building and system description	144
15.2 Research aim	145
15.3 Methodology	146

15.3.1	Demand response strategies	146
15.3.2	Flexibility indicators	147
15.4	Implementation: control algorithms	147
15.5	Results and conclusion	148
16	Conclusion	152
	References	153



# Abbreviations

Abbreviations	Meaning
ACH	Air changes per hour
ADR	Active Demand Response
AEEF	Available Electrical Energy Flexibility
AHU	Air handling unit
ANN	Artificial neural network
APX	Amsterdam Power Exchange
BAU	Business-as-usual
BCVTB	Building Controls Virtual Test Bed
BIM	Building information modelling
BMS	Building Management System
BOS	Building Operation System
BZ	Bidding zone
CA	Concern Agents
CAV	Constant Air Volume
CEM	Cross entropy method
CHP	Co-generation of Heat and Power
CI	Carbon intensity
CIBSE	Chartered Institute of Building Service Engineers
COP	Coefficient Of Performance
CS	Control strategy
CSC	Control strategy carbon
CSP	Control strategy price
CWT	Chilled Water Temperature
D-DNFQI	Double deep neural fitted Q iteration

Abbreviations	Meaning
DHW	Domestic Hot Water
DP	Dynamic Programming
DR	Demand Response
DSO	Distribution System Operator
EH	Electric Heating
EMPC	Economic Model Predictive Control
EMS	Energy Management System
ER	Electric radiator
ERL	EnergyPlus Runtime Language
ETP	Equivalent thermal parameter (model)
EW	External wall
FCU	Fan Coil Unit
FF	Flexibility Factor
FMI	Functional Mock-Up Interface
G	Goodness Of Fit
GA	Genetic algorithm
GHG	Greenhouse Gas
GSA	Global Setpoint Adjustment
GSHP	Ground-Source Heat Pump
GTH	Green Tech House
HCT	High Carbon threshold
HDS	Heat distribution system
HP	Heat Pump
HVAC	Heating, Ventilation and Air Conditioning
HWST	Hot-Water Storage Tank
IAQ	Indoor Air Quality

Abbreviations	Meaning
ICT	Information and Communications Technology
IW	Internal wall
LCT	Low carbon threshold
MA	Manager Agent
MAE	Mean Absolute Error
MAPE	Mean Absolute Percentage Error
MBRL	Model-based reinforcement learning
MDP	Markov Decision Process
MEF	Marginal Emissions Factor
MFRL	Model-free reinforcement learning
MOGA	Multi-Objective Genetic Algorithm
MPC	Model Predictive Control
PER	Primary energy ratio
PH	Passive house
PI	Proportional Integral
PIR	Passive InfraRed
PMV	Predicted Mean Vote
PPD	Predicted Percentage of Dissatisfied
PRBC	Predictive rule-based control
PV	Photovoltaics
PZTC	Perimeter Zone Test Cell
RE	Renewable Energy
RBC	Rule-Based Control
RC	Resistance-Capacitance
RL	Reinforcement learning
RLS	Recursive Least Squares

Abbreviations	Meaning
RMSE	Root Mean Square Error
S	Safety factor
SC	Space Cooling
SLLS	Student Learning Leisure and Sports Facility
SLP	Successive Linear Programming
SH	Space Heating
SPF	Seasonal performance factor
SSEC	Solar Simulator Environmental Chamber
TES	Thermal Energy Storage
TEK10	Norwegian building standard
TM	Temperature measurement
TOU	Time Of Use
TRNSYS	Transient System Simulation Tool
TSE	Thermal Energy Storage
TSP	Temperature SetPoint
VAV	Variable Air Volume
VSHP	Variable Speed Heat Pump
ZEB	Zero emission building

# 1 Introduction to Annex 67

Substantial and unprecedented reductions in carbon emissions are required if the worst effects of climate change are to be avoided. A major paradigmatic shift is, therefore, needed in the way heat and electricity are generated and consumed in general, and in the case of buildings and communities in particular. The reduction in carbon emissions can be achieved by firstly: reducing the energy demand as a result of energy efficiency improvements and secondly: covering the remaining energy demand by renewable energy sources. Applying flexibility to the energy consumption is just as important as energy efficiency improvements. Energy flexibility is necessary due to the large-scale integration of central as well as decentralized energy conversion systems based on renewable primary energy resources, which is a key component of the national and international roadmaps to a transition towards sustainable energy systems where the reduction of fuel poverty and CO<sub>2</sub>-equivalent emissions are top priorities.

In many countries, the share of renewable energy sources (RES) is increasing parallel with an extensive electrification of demands, where the replacement of traditional cars with electrical vehicles or the displacement of fossil fuel heating systems, such as gas or oil boilers, with energy efficient heat pumps, are common examples. These changes, on both the demand and supply sides, impose new challenges to the management of energy systems, such as the variability and limited control of energy supply from renewables or the increasing load variations over the day. The electrification of the energy systems also threatens to exceed already strained limits in peak demand.

A paradigm shift is, thus, required away from existing systems, where energy supply always follows demand, to a system where the demand side considers available supply. Taking this into consideration, flexible energy systems should play an important part in the holistic solution. Flexible energy systems overcome the traditional centralized production, transport and distribution-oriented approach, by integrating decentralized storage and demand response into the energy market. In this context, strategies to ensure the security and reliability of energy supply involve simultaneous coordination of distributed energy resources (DERs), energy storage and flexible schedulable loads connected to smart distribution networks (electrical as well as thermal grids).

Looking further into the future, the ambition towards net zero energy buildings (NZEB) imposes new challenges as buildings not only consume, but also generate heat and power locally. Such buildings are commonly called prosumers, which are able to share excess power and heat with other consumers in the nearby energy networks. Consequently, the energy networks must consider the demand of both heat and electricity as well as the local energy generation. If not, it may result in limitations of the amount of exported energy for building owners to avoid power quality problems; for example, Germany has already enforced restrictions on private PV generation exported to the grid. Furthermore, today the distribution grid is often sized based on buildings that are heated by sources other than electricity. However, the transition to a renewable energy system will, in many areas, lead to an increase in electrical heating, by heat pumps for example, which will lead to an increase in the electricity demand even if the foreseen reduction in the space heating demand via energy renovation is realized. The expected penetration of electrical vehicles will increase the loads in the distribution grids, but they may also be used for load shifting by using their batteries; they could in effect become mobile storage systems. All these factors will, in most distribution grids, call for major reinforcement of the existing grids or for a more intelligent way of consuming electricity in order to avoid congestion problems. The latter approach is holistically referred to as a 'Smart Grid' (or as a Smart Energy Network, when energy carriers other than electricity are considered as well) where both demand and

local production are controlled to stabilize the energy networks and thereby lead to a better exploitation of the available renewable energy sources towards a decarbonisation of the building stock. Buildings are, therefore, expected to have a pivotal role in the development of future Smart Grids/Energy networks, by providing Energy Flexibility services.

As buildings account for approximately 40 % of the annual energy use worldwide, they will need to play a significant role in providing a safe and efficient operation of the future energy system. They have the potential to offer significant flexibility services to the energy systems by intelligent control of their thermal and electric energy loads. More specifically, a large part of the buildings' energy demand may be shifted in time and may thus significantly contribute to increasing flexibility of the demand in the energy system. In particular, the thermal part of the energy demand, e.g. space heating/cooling, ventilation, domestic hot water, but also hot water for washing machines, dishwashers and heat to tumble dryers, can be shifted. Additionally, the demand from other devices like electrical vehicles or pool pumps, can also be controlled to provide Energy Flexibility.

All buildings have thermal mass embedded in their construction elements, which makes it possible to store a certain amount of heat and thereby postpone heating or cooling from periods with low RES in the networks to periods with excess RES in the networks without jeopardizing the thermal comfort. The amount of thermal storage available and how quickly it can be charged and discharged affect how this thermal storage can be used to offer flexibility. Additionally, many buildings may also contain different kinds of discrete storage (e.g. water tanks and storage heaters) that can potentially contribute to the Energy Flexibility of the buildings. A simple example of a discrete storage system is the domestic hot water tank, which can be pre-heated before a fall in available power. From these examples, it is evident that the type and amount of flexibility that can be offered will vary among buildings. A key challenge is, therefore, to establish a uniform framework that describes how flexibility can be offered in terms of quantity and quality.

Storage (thermal or electrical) is often necessary in order to obtain energy flexibility. However, storage has "roundtrip" energy conversion losses, which may lead to a decrease in the energy efficiency in the single building. But as energy flexibility ensures a higher utilization of the installed RES, the efficiency of the overall energy system will increase. A decrease in efficiency will mainly be seen in well-controlled buildings, however, most buildings are not well-controlled. In the latter case, the introduction of energy flexibility may typically lead to a more optimal control of the buildings and in this way simultaneously increase the energy efficiency of the buildings.

Various investigations of buildings in the Smart Grid context have been carried out to date. However, research on how Energy Flexibility in buildings can actively participate the future energy system and local energy communities, and thereby facilitate large penetration of renewable energy sources and the increasing electrification of demand, is still in its early stages. The investigations have either focused on how to control a single component - often simple on/off controlled - or have focused on simulations for defining indicators for Energy Flexibility, rather than on how to optimize the Energy Flexibility of the buildings themselves.

The concept of flexible loads, demand side management and peak shaving is of course not new, as demand response already in the 1970s was utilized in some power grids. Although the concept is not new, before now there was no overview or insight into how much Energy Flexibility different types of building and their usage may be able to offer to the future energy systems. This was the main, although not sole, reason why IEA EBC Annex 67 Energy Flexible Buildings was initiated.

## **1.1 IEA EBC Annex 67**

The aim of IEA EBC Annex 67 was to increase the knowledge, identify critical aspects and possible solutions concerning the Energy Flexibility that buildings can provide, plus the means to exploit and control this flexibility. In addition to these technical aims, Annex 67 also sought to understand all stakeholder perspectives - from users to utilities - on Energy Flexibility, as these are a potential barrier to success. This knowledge is crucial for ensuring that the Energy Flexibility of buildings is incorporated into future Smart Energy systems, and thereby facilitating the transition towards a fossil free energy system. The obtained knowledge is also important when developing business cases that will utilize building Energy Flexibility in future energy systems – considering that utilization of Energy Flexibility in buildings may reduce costly upgrades of distribution grids.

The work of IEA EBC Annex 67 was divided into three main areas:

- terminology and characterization of Energy Flexibility in buildings
- determination of the available Energy Flexibility of devices, buildings and clusters of buildings
- demonstration of and stakeholder's perspective on Energy Flexible buildings

### ***1.1.1 Terminology for and characterization of Energy Flexibility in buildings***

A common terminology is important in order to communicate a building's or a cluster of buildings' ability to provide Energy Flexible services to the grid. The available Energy Flexibility is often defined by a set of generally static Key Performance Indicators. However, the useful Energy Flexibility will be influenced by internal factors such as the form or function of a building, and external factors, such as local climatic conditions and the composition and capacity of the local energy grids. There is, therefore, a need for a dynamic approach in order to understand the services a building can provide to a specific energy grid. A methodology for such a dynamic approach has been developed during the course of IEA EBC Annex 67.

The findings in the area of terminology and characterization of Energy Flexibility in buildings are reported in the deliverable "Characterization of Energy Flexibility in Buildings" mentioned below.

### ***1.1.2 Determination of the available Energy Flexibility of devices, buildings and clusters of buildings***

Simulation is a powerful tool when investigating the possible Energy Flexibility in buildings. In IEA EBC Annex 67, different simulation tools have been applied on different building types and Common Exercises have been carried out on well-defined case studies. This approach increased the common understanding of Energy Flexibility in buildings and was useful for the development of a common terminology.

Simulations are very effective to quickly test different control strategies, among which some may be more realistic than others. Control strategies and the combination of components were, therefore, also tested in test facilities under controllable, yet realistic, conditions. Hardware-in-the-loop concepts were utilized at several test facilities, where, for example, a heat pump and other components were tested combined with the energy demand of virtual buildings and exposed to virtual weather and grid conditions.

The results of the investigations are described in several of the below mentioned publications by IEA EBC Annex 67.

### ***1.1.3 Demonstration of and stakeholders perspective on Energy Flexible Buildings***

In order to be able to convince policy makers, energy utilities and grid operators, aggregators, the building industry and consumers about the benefits of buildings offering Energy Flexibility to the future energy systems, proof of concept based on demonstrations in real buildings is crucial. Example cases of obtaining Energy Flexibility in real buildings have, therefore, been investigated and reported in reports, articles and papers and as examples in the deliverables of IEA EBC Annex 67.

When utilizing the Energy Flexibility in buildings, the comfort, economy and normal operations of the buildings can be influenced. If the owner, facility manager and/or users of a building are not interested in exploiting Energy Flexibility to increase building smartness, it does not matter how energy flexible the building is, as the building will not be an asset for the local energy infrastructure. However, the involvement of utilities, regulators and other stakeholders, for example, building automation providers, can provide incentives and increase awareness of and thereby participation in providing Energy Flexibility. It is, therefore, very important to understand which barriers exist for the stakeholders involved in the Energy Flexible buildings and how they may be motivated to contribute with Energy Flexibility in buildings to stabilize the future energy grids. Investigating the barriers and benefits for stakeholders is, therefore, of paramount importance and work was completed in IEA EBC Annex 67 to understand these in more detail. Findings from this work are described in the report “Stakeholder perspectives on Energy Flexible Buildings” mentioned below.

### ***1.1.4 Deliverables from IEA EBC Annex 67***

Many reports, articles and conference papers have been published by IEA EBC Annex 67 participants. These can be found on [annex67.org/Publications](http://annex67.org/Publications).

The main publications by IEA EBC Annex 67 are, however, the following reports, which all may be found on [annex67.org/Publications/Deliverables](http://annex67.org/Publications/Deliverables).

**Principles of Energy Flexible Buildings** summarizes the main findings of Annex 67 and targets all interested in what Energy Flexibility in buildings is, how it can be controlled, and which services it may provide.

**Characterization of Energy Flexibility in Buildings** presents the terminology around Energy Flexibility, the indicators used to evaluate the flexibility potential and how to characterize and label Energy Flexibility.

**Stakeholder perspectives on Energy Flexible buildings** displays the view point of different types of stakeholders towards Energy Flexible Buildings.

**Control strategies and algorithms for obtaining Energy Flexibility in buildings** reviews and gives examples on control strategies for Energy Flexibility in buildings.

**Experimental facilities and methods for assessing Energy Flexibility in buildings** describes several test facilities including experiments related to Energy Flexibility and draws recommendations for future testing activities.

**Examples of Energy Flexibility in buildings** summarizes different examples on how to obtain Energy Flexible Buildings.

**Project Summary Report** brief summary of the outcome of Annex 67.

## 2 Introduction to the report

The development needs by new socio-economic requirements have led to a substantial increase in the energy consumption and the environmental concerns in recent years. Buildings are one of the fastest growing energy consumers, responsible for approximately 50 % of the greenhouse gas (GHG) emissions (European Environment Agency (EEA), 2004). On the other hand, the energy production sector is struggling to meet the required demand. In this context, efforts are being directed on the flexibility of energy demand for efficient buildings, by assuring the operational needs with the minimum possible energy cost and environmental protection (Doukas, et al., 2007).

One of the greatest difficulties of energy efficient buildings is to combine the reduction in power consumption with the costumers' comfort. Although buildings account for approximately 40 % of the global energy consumption (World Business Council for Sustainable Development, 2008), this number can increase significantly in order to address indoor environment comfort demands, for example for heating, cooling, lighting, ventilation, and office equipment (Wang, et al., 2012).

In order to reduce GHG emissions in the energy sector, sustainable and renewable sources are being proposed because of their social and environmental benefits, such as the reduction of air pollutants and declining energy costs. As a result, challenges such as high intermittence of generation and storage capacities have to be addressed. The built-in Energy Flexibility in buildings may be utilized for stabilizing the energy grid.

As a natural consequence, buildings are gradually moving towards modernizations that increase their performance. Automation of new and existing processes using state-of-the-art technologies in remote sensing operations, communication, control and information technology is essential. The purpose is to align automation and optimization to the actions of all elements of a building in order to provide a sustainable, economic and secure energy supply.

Energy flexibility of buildings is a focus area in many countries directives because society is facing an urgent need to find new innovative methodologies and tools to guarantee the required demand for the future energy consumers. The ability to manage the demand and generation according to local climate conditions, user needs and grid requirements allows demand side management, load control and thereby demand response based on the requirements of the surrounding grids.

In this way, the search for attractive solutions grows in order to control building operations due to their inherent flexibility, considering relevant factors such as occupant behavior patterns, weather conditions, thermal properties and their complex interactions, without compromising the occupants' comfort (Maasoumy, et al., 2014). In order to use the potential of both commercial and residential buildings as providers of flexibility to the smart grid, it is fundamental to redesign the way a building and its HVAC system is controlled.

Since buildings are unpredictable consumers of electrical energy (Zavala, 2013), optimization-based control is a key technology in next-generation energy-efficient building systems. Traditional control strategies are still being used even with the development of better alternatives presented over the past years. In addition, more focus needs to be done on building-wide optimization, exploiting the entire system in order to achieve significant energy savings (Zavala, et al., 2010).

Furthermore, the building-wide optimization is a non-linear and multivariate problem having no guarantee of a unique solution where competitive objectives arise in practice, involving interdependent issues distributed among multiple building climate zones. In this way, the coordinated

operation of interconnected subsystems performing autonomous control is essential to achieve the overall system goals.

In this context, where the control process of buildings should be optimized, there is a need to seek new methods and technologies that provide fast and optimized management and control. Appropriate methods must be efficient and robust, performing inter-context considerations among each building zone micro-climate and ensuring reliability and security in several operating conditions of the system (Zavala, et al., 2010). Other approaches are described in literature and it are the focus of the Annex 67 technical report (Finck, et al., 2018), which lists different control possibilities. A summary of (Finck et al, 2018) is given in the next chapter.

In order to achieve an emerging overall optimization of the building energy performance, control architectures must be developed, enabling the estimation of weather, occupancy behavior trends and energy consumption within each building zone. More importantly, control methods are multi-variable systems that can exploit the interactions between states to optimize performance, making buildings more adaptive to system variations and reducing the energy and environment cost. In addition, the sensor information helps to better understand the building performance and the provided services, like air-conditioning, lighting and heating systems and their equivalent parameters, as well as its indoor environmental quality and comfort level in a real-time format.

In order to model/simulate the Energy Flexibility in buildings it is necessary to define control strategies. Different studies described in this report investigate algorithms for efficient implementation of strategies for realizing the Energy Flexibility in buildings, including strategies for storage capacities (thermal and electrical) and local renewables sources, like PV panels. Different control algorithms and strategies are introduced, ranging from simple low-level control of single devices over complex control of several devices to decision making based on different types of forecast (weather, prices, occupancy).

Currently, there is no overview or insight into the types and usages of control strategies on future energy systems. The aim of this report is thus to increase knowledge on and demonstrate which flexibility services buildings can provide for the energy grids, and to identify critical aspects and possible solutions to manage Energy Flexibility.

# 3 Review of applied and tested control possibilities for Energy Flexibility in buildings

Christian Finck, Eindhoven University of Technology, The Netherlands,  
Paul Beagon, School of Mech. and Materials Eng., UCD, Dublin, Ireland  
John Clauß, Norwegian University of Science and Technology, Norway  
Thibault Péan, Catalonia Institute for Energy Research, Barcelona, Spain  
Pierre J.C. Vogler-Finck, Neogrid Technologies ApS / Aalborg University, Denmark  
Kun Zhang, Polytechnique Montreal, Canada

The here presented literature research aims to present control strategies that show potential for providing demand side flexibility in residential or commercial buildings. The control techniques and strategies discussed here focus on heating and cooling systems including heat pumps and thermal energy storage.

## 3.1 Terminology of control methods

There are two main types of control: (1) control of a single component, also known as local control, and (2) control of a whole energy system, also known as supervisory control. The local controller makes sure that the process is stable and a proper setpoint is kept at all times, whereas the supervisory controller coordinates all the local controllers in a way that the overall operation of the energy system works smoothly (Naidu & Rieger 2011a).

Control methods can be divided into hard control, soft control and hybrid control. Naidu et al. (Naidu & Rieger 2011a) include classical controls in hard controls, whereas Afram et al. (Afram & Janabi-Sharifi 2014) see classical controls as a distinct group of HVAC control methods. Dounis et al. (Dounis & Caraiscos 2009) on the other hand only distinguish between classical controllers and optimal, predictive and adaptive controllers. An overview of different HVAC control methods is given in Figure 3.1.

Classical control refers to the most commonly used control techniques, such as on/off control, P, PI or PID control. An on/off controller regulates a process within a predefined lower and upper threshold so that the process stays within these boundaries. P, PI and PID controllers modulate a controlled variable by using error dynamics, so that accurate control is achieved. Research related to PID controllers focuses on auto-tuning or optimal tuning methods of these controllers (Afram & Janabi-Sharifi 2014).

Hard controllers follow the theory of control systems based on nonlinear control, robust control, optimal control, adaptive control and Model Predictive Control (MPC) (Naidu & Rieger 2011a), (Afram & Janabi-Sharifi 2014). Hard controllers are usually rather straightforward to analyze. They have a predictable overall behavior and stability and usually a low to moderate computational burden of practical algorithms (Ovaska et al. 2002).

Soft control systems are based on fuzzy logic, neural networks or genetic algorithms.

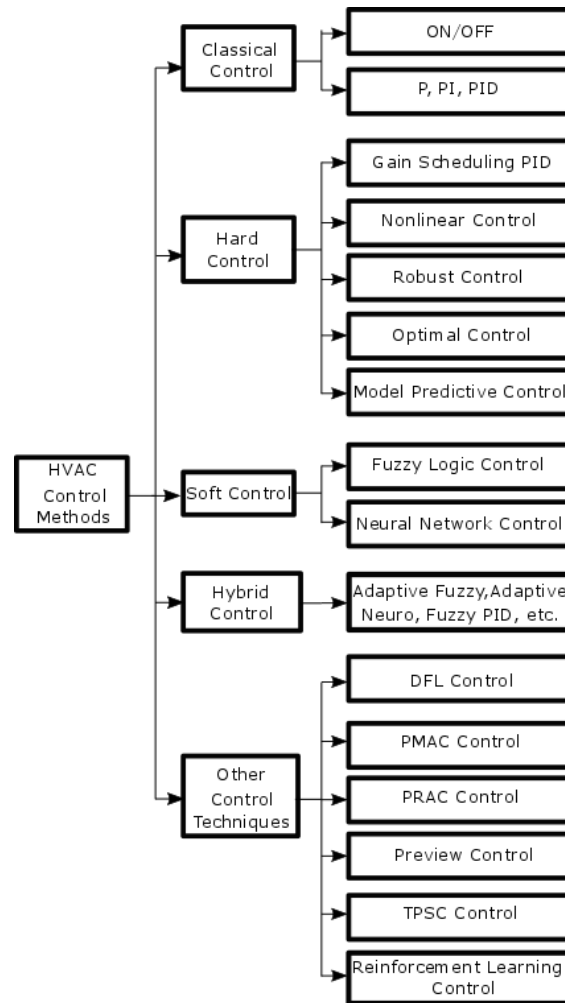


Figure 3.1 Overview of control methods for HVAC systems (Afram & Janabi-Sharifi 2014).

Hybrid controls are a combination of hard and soft control techniques and benefit from the advantages of each of them. The soft control is usually applied for supervisory control, whereas the hard controller is used for local control (Afram & Janabi-Sharifi 2014) even though MPC can be used for supervisory control.

### 3.2 Strengths and weaknesses of different control methods

On/off controllers are not able to control dynamic processes with time delays well. A good performance of PID controllers is ensured only if the operating conditions do not vary from the tuning conditions (Afram & Janabi-Sharifi 2014). Gain-Scheduling PID show improved stability compared to “normal” PID controllers (Leith & Leithead 2000), but it is necessary to spot the linear regions and to develop a logic for switching the regions. Manual tuning of the PID controller is required and can be laborious.

Table 3.1 Summary of the most common control methods.

Type of controller	Working principle	Implementation maturity	References
<b>Thermostatic on/off control</b>	Regulates a process within a predefined lower and upper threshold so that the process stays within these boundaries	State-of-the-art in buildings	(Afram & Janabi-Sharifi 2014), (Yu et al. 2015), (Dounis & Caraiscos 2009), (Naidu & Rieger 2011a)
<b>P, PI, PID control</b>	Modulates a controlled variable by taking into account error dynamics	State-of-the-art in buildings	(Afram & Janabi-Sharifi 2014), (Yu et al. 2015), (Dounis & Caraiscos 2009), (Naidu & Rieger 2011a)
<b>Gain Scheduling PID</b>	Controls non-linear systems by a family of linear controls which are used to control different operating points of the non-linear system	State-of-the-art for hydronic-radiator-based HVAC systems	(Afram & Janabi-Sharifi 2014), (Afram & Janabi-Sharifi 2014), (Leith & Leithead 2000)
<b>Non-linear</b>	A control law (derived from Lyapunov's stability theory, feedback linearization and adaptive control techniques) for reaching a stable state of the non-linear system while keeping the control objectives	State-of-the-art for AHUs and cross-flow water to air heat exchanger	(Afram & Janabi-Sharifi 2014)
<b>Robust</b>	Controller works well for changing parameters as well as time-varying disturbances / Considers model uncertainty and non-linearities of the system	State-of-the-art for supply air temperature, supply airflow rate and zone temperature control	(Afram & Janabi-Sharifi 2014), (Naidu & Rieger 2011a)
<b>Optimal</b>	Solves an optimization problem (optimizing a cost function) → minimization of energy consumption and control effort, maximizing thermal comfort	State-of-the-art for active TES, energy optimization for HVAC systems, VAV system control, building heating and cooling control	(Afram & Janabi-Sharifi 2014), (Naidu & Rieger 2011a)
<b>Adaptive</b>	Controller learns to adapt to changes and learns from the characteristics of a building or/and environment by self-regulation	Used for single cases, but not widespread Used for AHUs with VAV	(Dounis & Caraiscos 2009), (Naidu & Rieger 2011a), (Yu et al. 2015)
<b>MPC</b>	Applies a system model for predicting future system states and optimizes a cost function over a sliding planning horizon / takes disturbances and constraints into account	Applied at building design stage, but not yet widespread for practical operation	(Afram & Janabi-Sharifi 2014), (Naidu & Rieger 2011a)
<b>Neural Network</b>	A mathematical representation of neurons relating inputs and outputs as a huge network / Black-box modelling technique / A controller which is tuned/trained on the performance data of a system / Fits a non-linear mathematical model to the historical data	For fan control of an air-cooled chiller and for AC setback time based on the outdoor temperature	(Afram & Janabi-Sharifi 2014), (Naidu & Rieger 2011b)
<b>Fuzzy Logic</b>	Control actions as if-then-else statement / Methodology to represent human knowledge and reasoning by remembering rules and functions / Can be applied as supervisory control in combination with a local PID controller	Used in AHUs	(Afram & Janabi-Sharifi 2014), (Naidu & Rieger 2011b)

Hard controllers are a common technique in control system design. Nonlinear control is effective but requires a rather complex mathematical analysis when designing the controller as well as an identification of stable states. Optimal and robust control can handle time-varying parameters and disturbances, but robustness is difficult to obtain because of varying conditions for HVAC systems in buildings. According to (Afram & Janabi-Sharifi 2014) specification of additional parameters is required for hard controllers and thus an integration in HVAC systems may be difficult or impractical.

Soft controllers are not very common in real building applications. Neural-networks-based control systems need an extensive amount of historical data for training purposes, in order to cover a wide range of operating conditions. Similarly, fuzzy logic controllers require an extensive knowledge of the building operation under different conditions.

Hybrid controllers inherit the benefits and weaknesses of both hard control and soft control systems.

### **3.3 Control strategies for heating and cooling using MPC**

Some of the main challenges facing a HVAC system are non-linear dynamics, time-varying dynamics, time-varying disturbances and supervisory control. MPC is a control method that overcomes these problems.

(Afram & Janabi-Sharifi 2014) summarize the main features of MPC:

- MPC is not a corrective control, but anticipates future system evolution
- An integrated disturbance model can handle disturbances in an explicit manner
- It has the ability to explicitly handle uncertainties and constraints
- It is capable of dealing with processes with time delays
- Energy saving strategies can be integrated in the controller formulation
- Multiple objectives can be achieved by using adequate formulations of the cost function
- MPC can be used for supervisory as well as local control
- Explicitly includes the prediction of occupant behavior, equipment use and weather conditions

The reviews of (Afram & Janabi-Sharifi 2014), (Dounis & Caraiscos 2009), and (Naidu & Rieger 2011a), (Naidu & Rieger 2011b) include several metrics for comparing the performances of different controllers. However, they do not consider the potential for flexibility deployment in detail.

The research on MPC has intensified during the last decade. It is well understood and proven that this control method can achieve energy savings while maintaining or even improving thermal comfort in buildings. Researchers show different approaches for applying MPC for controlling HVAC systems in buildings in combination with thermal energy storages in order to deploy the demand side flexibility that a building may offer.

(Huang 2011) shows that the control signal for zone temperature regulation is much smoother when using a MPC compared to a PI controller. Zone temperature regulation has also been investigated by (Moroşan et al. 2010) who simulated the performance of a PI controller and a distributed MPC. The MPC achieved 13 % energy savings and a 37 % improvement of the thermal comfort. More studies are presented in (Afram & Janabi-Sharifi 2014).

The zone temperature is also the typical control variable in experiments. (Hong LüLei JiaShulan KongZhaosheng Zhang 2007) implemented a MPC into a HVAC system and showed an improved robustness as well as greater tracking performance of the MPC compared to a PID controller.

(Aswani et al. 2012) implemented a learning-based MPC into a heat pump test facility at a university and showed that the energy consumption can be reduced by 30 to 70 % compared to on/off control.

Economic MPCs (Halvgaard et al. 2012) include electricity prices from the day-ahead market into the cost function and suggest an optimized schedule for electricity consumption over the planning horizon based on these prices. Energy consumption is shifted to periods with low electricity prices. For instance, the controller of a heat pump can compute an optimized schedule for the compressor based on dynamic electricity prices as well as weather conditions (outdoor temperature and solar radiation).

### **3.4 Control objectives, inputs, disturbances, constraints, and signals**

The aim of the applied control strategies presented in this report is to improve the Energy Flexibility, or implement demand-side management (DSM). However, this objective remains general, and DSM can take several forms, such as load-shifting, peak shaving etc. For this reason, this section intends to identify more precisely objectives that have been addressed by different control strategies, as well as other parameters taken into account (disturbances, constraints, control inputs and signals) in their design.

This identification process is not always straightforward. In MPC and optimal control, the objective function is explicit: its expression represents the quantity that the control should optimize, for instance, the energy cost. This function can also contain multiple terms that represent multiple objectives, which are balanced with appropriate weights. In rule-based controls (RBC), the final objective is more difficult to identify, and is not always explicitly mentioned in the reviewed papers. A certain method is often analysed under different angles (impact on the energy use, comfort, flexibility...), without a clear statement of the goals to achieve. There can also be a short-term goal (e.g. shifting loads to a certain time of the day), and a more general goal on the long-term (e.g. enabling the integration of more RES in the grid).

Due to the conceptual difference, the two types of control (RBC and MPC) have been separated when analysing their respective objectives. The constraints, control inputs, disturbances and signals present similarities and therefore have been reviewed jointly. It should be noted too that there is not always a consensus on the boundaries between these different elements, as different studies would address these with different approaches. For instance, comfort can be considered as an objective (minimize discomfort) or as a constraint (with boundaries for the indoor temperature for example).

#### **3.4.1 Control objectives**

##### ***In rule-based controls***

The simplest flexibility objective consists in load shifting according to a predefined fixed schedule. Regular daily peak periods can usually be identified in a national energy grid. The controller can therefore try to avoid or force the operation of the systems during fixed hours. For instance, (Lee et al. 2015) use set-point modulation to reduce the energy use during the grid peak hours (14:00 to 17:00 in summer and 17:00 to 20:00 in winter). (Carvalho et al. 2015) completely shut down the heat pump during peak hours (9:00 to 10:30 and 18:00 to 20:30). Fixed scheduling can also be used to force the charging of a Thermal Energy Storage (TES) tank, like presented by (De Coninck et al. 2010). In another study, (De Coninck et al. 2014) used clock control, raising the DHW heating set-point from 12:00 to 16:00 in order to reduce PV curtailing losses at that time because a heat pump

can be run to charge the DHW storage. Overall, fixed scheduling strategies are simple and easy to implement, and they can already achieve a substantial performance. However, the fixed schedule cannot adapt to changing conditions in the daily profile of the grid.

Another objective targeted by RBC strategies is peak shaving, i.e. the reduction of the demand peak, in order to support the grid operation. In these cases, the power exchange of the building with the grid is monitored, and thresholds can be defined both for the import and export (when a production unit is present, i.e. when the customer is a prosumer<sup>1</sup>) of power. When the thresholds are passed, an action is taken by the controller to stop or force the operation of certain elements, such as mechanical systems, batteries, etc., and thus limit the peak to the predefined threshold. For instance, (Dar et al. 2014) set an import limit of 2500 W and an export limit of 5000 W in a nZEB equipped with a PV system, while (De Coninck et al. 2010) present a similar “grid-load strategy”, with both import and export thresholds set at 3500 W.

Certain control strategies aim at reducing the energy costs for the end-users. In general, these approaches rely on time-varying energy prices, and the controller aims at operating the energy-using systems during low-price periods, or at avoiding their operation during high-price periods. Identifying the thresholds for low and high-price periods therefore becomes the key elements of these RBC strategies. (Schibuola et al. 2015) propose two different approaches in this regard: the first one analyzes the price data of two entire years (2012 and 2013), and fixes thresholds based on this distribution. The second approach compares the current electricity price with the forecasted price over the next 12 hours, hence relying on prediction data rather than on past data. (Le Dréau & Heiselberg 2016) also based their approach on recorded past data: their thresholds were calculated using the first and the third quartiles from the price distribution of the two weeks prior to the current moment.

Finally, other rule-based controls aim at improving the use of energy from renewable energy sources (RES). This can be done at the scale of the building with a local generation unit (in the case of a prosumer), where the objective consists in increasing self-consumption. It can also be done at the scale of the overall power grid, which means the control relies on the analysis of the residual load calculated at a national level. The methods employed can then take different forms. The heating systems can be switched on simply when the local PV are generating electricity (Schibuola et al. 2015), or when this production exceeds the non-heating loads (Dar et al. 2014). Thus, a thermal storage is charged to temperatures which are higher than the usual set point. This leads to a better coincidence between production and demand. (De Coninck et al. 2014) use a different trigger for the activation of DSM: voltage measurement. Their study works on the assumption that an excess PV production induces an increase of voltage of the distribution feeder. The voltage is therefore monitored, and when it surpasses a defined value (around 250 V), the setpoint for the DHW tank is raised in order to utilize more electricity and avoid the curtailment of PV production due to inverter shutdown. (Miara et al. 2014) use the residual load profile at the national level to design their own Time Of Use (TOU) signal and thus use energy at times of low residual load.

### ***In optimized control and MPC***

As recalled in the introduction of this section, the objective is easier to identify for MPC configurations, since it is explicitly formulated in the cost function which the controller optimizes. In the reviewed papers, one sort of MPC clearly stands out: Economic MPC (EMPC), where the objective is to reduce monetary costs. This method utilizes the variation of energy prices in time to

---

<sup>1</sup> A prosumer is a customer who is both a consumer and a producer of electricity. A prosumer thus sometimes retrieves electricity from the grid, and sometimes feeds it into the grid.

perform a cost optimization. The objective function  $J_e$  can for example take the following form, taken from (Masy et al. 2015):

$$J_e = \sum_i p_{el}(i) W_{el}(i)$$

Where  $W_{el}$  is the manipulated variable (the heat pump power in this case),  $p_{el}$  is the electricity price (varying in time according to different tariffs). The optimization process then minimizes this cost function over the receding horizon, logically leading to monetary savings.

Even though the formal objective is to reduce the costs, this method will implicitly result in load shifting towards periods of lower energy prices. Depending on how the price profile is constructed, this load shifting can constitute a valuable form of Energy Flexibility. A similar cost function is used in (De Coninck & Helsen 2016) (considering also a term for the cost of natural gas), (Halvgaard et al. 2012), (Ma et al. 2014), (Mendoza-Serrano & Chmielewski 2014), (Zong et al. 2012), (Santos et al. 2016), (Bianchini et al. 2016), (Sichilalu & Xia 2015) (including the monetary benefits of selling PV electricity) and (Oldewurtel et al. 2013). As it appeared from the survey, EMPC seems to be a dominant form of MPC in studies of Energy Flexibility in buildings.

Comfort can also constitute an objective of MPC, or more precisely the minimization of thermal discomfort. The objective function can for instance take the following form, taken from (De Coninck & Helsen 2016):

$$J_d = \sum_i \theta_{occ}(i) (T_{zon}(i) - T_{set}(i))^2$$

Where  $\theta_{occ}$  is an occupancy factor (0 or 1),  $T_{zon}$  is the actual zone temperature, and  $T_{set}$  is the tracked set-point temperature. By minimizing this term, the optimization problem will reduce the difference between the actual and the desired temperature (setpoint), hence improving the comfort conditions. (Masy et al. 2015) use the same principle but with a slightly different formulation. (Váña et al. 2014) introduce two different comfort ranges in their objective function:

$$J_d = \sum_k (|Q(y_k - z_k)|_2^2 + |Q^c(y_k - z_k^c)|_2^2)$$

Where  $y_k$  represent the zone temperatures from system states  $k$ ,  $z_k$  represent soft comfort constraints (comfort range 1) that can be violated from time to time, while  $z_k^c$  represent soft comfort constraints (comfort range 2) that should not be violated at almost any cost. The hierarchy between comfort ranges 1 and 2 is realized through the weight matrices  $Q$  and  $Q^c$ . It should be noted that comfort is often also implemented in the form of constraints (see following paragraph).

In some cases, the objective function includes a term for the reduction of the energy use. For instance, (Sturzenegger et al. 2013) present an MPC which aims at minimising the non-renewable primary energy use. The formulation is the following:

$$J_{pe} = \sum_k c_k^T u_k$$

Where  $c_k$  is the cost vector element (depending on the systems efficiency) and  $u_k$  the manipulated variables (or control inputs).  $c_k$  put different weights on the energy consumption depending on the operating conditions, which leaves room for a minimisation of non-renewable primary energy.

Few articles use a term for peak shaving within their objective function. Notably (Ma et al. 2014) present the following formulation:

$$J_p = \sum_k D_c(k) \max\{P(k)\}$$

Where  $D_c$  represents the peak demand cost, and  $P$  is the average power consumption during the time interval  $k$ . In this way, the peak power is penalized in the objective function, therefore the MPC will try to reduce it, leading to peak shaving.

Reducing the CO<sub>2</sub> intensity is another objective that may be implemented in MPC. (Dahl Knudsen & Petersen 2016) notably introduce the following term:

$$J_c = \sum_k e_k u_k$$

Where  $e_k$  is a vector representing the prediction of the CO<sub>2</sub> intensity associated with the electricity production (i.e. the amount of CO<sub>2</sub> equivalent emissions per unit of energy, expressed in g CO<sub>2</sub>eq /kWh). The MPC optimization will therefore intend to minimise the total CO<sub>2</sub> emissions incurred by the energy used for operation of the building.

Finally, other terms can be introduced in the objective function to increase the robustness of the control. They do not represent a flexibility objective on their own, but enable a smoother operation of the systems. For example, (Váňa et al. 2014) introduce the following term:

$$J_r = \sum_k \delta |u_k - u_{k-1} - p_k|_2^2$$

Where  $\delta$  is a penalty factor and  $p_k$  a slack variable. Introducing such terms in the objective function enables to avoid too drastic changes in the control inputs, and decreases the sensitivity to model mismatch and imperfect disturbance predictions. (Santos et al. 2016) and (Halvgaard et al. 2012) also introduce slack variables in order to soften the constraints imposed on the output, and thus enable the optimization to always find a solution outside the strict range, although at the cost of a certain penalty.

Finally, it is important to mention that these different objectives can be combined in a single objective function. Most papers use linear combinations of the different terms, setting different weights to put more emphasis on certain aspects of the optimization. For instance, (Masy et al. 2015) and (De Coninck & Helsen 2016) present a global objective function of the form  $J = J_e + \alpha J_d$ , which is an EMPC but also taking into account discomfort term  $J_d$  with weight  $\alpha$ .

### 3.4.2 Control constraints

As recalled by (Camacho & Bordons 2007), in practice all processes are subject to constraints: a heating system cannot provide more heat than its maximum thermal capacity, or a ventilation system cannot provide more air than the capacity of its fans. Limits can also be set for safety or constructive reasons. The control algorithm needs to know these boundaries in order to yield physically meaningful solutions to the numerical optimisation problem in the case of MPC (e.g. exclude negative flow rates).

A distinction can be made between the constraints implemented on the control inputs and the control outputs (or system states). The first type can always be respected, since the controller decides the control inputs, therefore it can choose them within the defined boundaries. In the case of MPC, the constraints on control outputs and states must be anticipated beforehand, since these variables depend on the behavior and inertia of the modelled plant, as well as disturbances. Therefore, imposing hard constraints on these outputs and states may lead to infeasibility of the receding horizon optimisation (Löfberg 2012), which is why these constraints are usually softened in practise.

It should be kept in mind that adding constraints to a MPC problem, even though it is probably necessary in the kind of applications reviewed in this report, makes it impossible to find an explicit solution of the optimization problem; a numerical method must be used.

The constraints on the control inputs mostly represent the physical limitations of the devices in use. For instance, (Dahl Knudsen & Petersen 2016) bound the power of the heating system to 0–0.5 kW, and (Masy et al. 2015) to 0–3 kW, which corresponds to the devices used in their respective studies. The MPC controller can then pick a thermal power within this interval at every time step. In (Oldewurtel et al. 2013) and (Sturzenegger et al. 2013), the MPC also controls blinds or ventilation, therefore constraints are also imposed on these systems (e.g. minimum and maximum air supply temperature, non-closed position for the blinds during occupancy hours to guarantee some daylighting). A minimum air ventilation flow rate is also implemented as a constraint for health reasons, to guarantee air renewal indoors.

Time constraints can also be applied to the inputs of the control strategies. In (Le Dréau & Heiselberg 2016), the DSM activation can only last for a predefined amount of hours. In (Carvalho et al. 2015), the systems can operate only between a start hour and a stop hour which are fixed beforehand. In (Dar et al. 2014), a minimum cycle length is imposed to the heat pump, and in (Santos et al. 2016) and (Halvgaard et al. 2012) the successive changes in the control inputs are penalized. These methods enable to avoid frequent cycling that may reduce the lifetime of the equipment.

As for the constraints on control outputs, they include almost in every case reviewed a temperature comfort range (as defined in the standards EN 15251 (CEN 2007) or ASHRAE 55 (ASHRAE 2013) for instance). This range can apply to indoor operative temperature: for example, 22-25 °C in winter and 22-27 °C in summer mentioned by (Sturzenegger et al. 2013), 21-24 °C in (Ma et al. 2014), 20-22 °C in (Masy et al. 2015). The constraints can be relaxed during non-occupancy periods: in (Hong et al. 2012) and (Masy et al. 2015), the problem is unconstrained when the building is not occupied. (Halvgaard et al. 2012) changes the constraints at night, with a minimum output temperature of 18 °C, while this lower bound is set to 21 °C during daytime. The temperature constraint can also be formulated as a setpoint around which a dead-band is applied. For instance in (Schibuola et al. 2015), an additional check is performed and actions are taken if the temperature deviates by more than 5 K from the setpoint. When a storage tank is used, a temperature range can also be applied to it, for instance when using DHW water storage that needs to be kept above 55 °C to avoid Legionnaire's disease (Lee et al. 2015). In (Dar et al. 2014), the temperature constraint is transformed into a state of charge parameter to be kept in the buffer storage tank.

It should be noted that in MPC, the temperature constraints can be formulated as hard constraints (with fixed boundaries), or as soft constraints, integrating slack variables in the objective function, and penalizing the violation of these constraints with a high cost (see also section on the control objectives). Another remark raised by (Ma et al. 2014) concerns the use of unconstrained temperature ranges in real building applications: it might cause problems because the actuators (room thermostats) might have a specific acceptable range of temperature setpoints.

### 3.4.3 Control inputs

The control strategies act upon certain parameters, which are called control inputs (or manipulated variables). No major difference was found for the control inputs between RBC and optimized control. In the reviewed papers, the following control inputs have been identified:

- **Temperature set-points:** several control strategies modulate the temperature setpoints, whether in the room thermostats, the supply of the systems, or in a water storage tank.
- **On/Off control:** other control strategies directly force the systems to switch on or off, depending on the control algorithm decisions. The manipulated variable is therefore binary.
- **Thermal power:** when the power of the mechanical systems can be modulated (electric heating, inverter-controlled heat pump...), the controller can decide to adjust it in time. This control input is mostly used in simulations, in practice the modulation of the thermal power can also be obtained through changes in the setpoints.

### 3.4.4 Control disturbances

Unknown disturbances always affect the behaviour of a controlled system. In general, RBC strategies take into account very few of them. On the other hand, MPC strategies need to forecast some of them, in order to predict the future response of the model to these disturbances, and not only to the control inputs.

The most common disturbance taken into account by MPC is the outside weather conditions, since they will affect the heating or cooling needs of the building the most. The external temperature is considered in the model in almost all of the reviewed papers. A notable exception is the paper of (Ma et al. 2014), where the authors found out that the outside temperature did not have as much influence on the output as the setpoints or the heating power, and therefore neglected it. (Sturzenegger et al. 2013), (Oldewurtel et al. 2013), (Sichilalu & Xia 2015) and (De Coninck & Helsen 2016) only consider the external temperature when accounting for weather conditions. Several papers additionally consider the solar irradiation: (Bianchini et al. 2016), (Halvgaard et al. 2012), (Váña et al. 2014), and (Dahl Knudsen & Petersen 2016). Besides the external temperature and the solar irradiation, (Santos et al. 2016) and (Masy et al. 2015) also take into account the effects of wind speed. In many cases, it is assumed that the forecast of these disturbances is perfect. When the MPC is implemented in a real building, weather forecast is retrieved from external services or derived from a local measurement.

Another major source of disturbance are the internal gains. They group the heat gains from occupants, appliances and equipment. Most commonly, a deterministic approach is applied, with a fixed schedule for these internal gains ((Váña et al. 2014), (Bianchini et al. 2016), (Masy et al. 2015)). When a MPC is implemented in real buildings, other methods can be employed: an occupancy sensor like in (Sichilalu & Xia 2015), or deriving the internal gains from measurements of the plugs and lighting electricity circuits (De Coninck & Helsen 2016).

### 3.4.5 Control signals

Several external parameters can be monitored to support the decisions made by the controller. For simplification, it can be considered that each RBC only monitors one specific control signal, and

reacts upon it. Usually, a threshold is pre-set on this parameter, and when the threshold is passed, an action is triggered on the system. MPC strategies can monitor several signals and penalize excursions from a given reference profile.

For instance, the strategies aiming at peak shaving monitor the net power exchange between the building and the grid, and take actions when this exchange reaches too high values ((Dar et al. 2014), (De Coninck et al. 2010), (De Coninck et al. 2014)).

The strategies that aim at reducing the energy cost (notably EMPC) monitor the electricity price, and decide to use energy or not based on how expensive the current price is considered, always taking into account the thermal comfort requirements ((Schibuola et al. 2015); (Le Dréau & Heiselberg 2016)). Time-of-use electricity tariffs are applied most often, with different values for peak periods and off-peak periods, and sometimes with an additional medium price in-between. In other papers, hourly tariffs are applied, reflecting day-ahead prices on the spot market.

The strategies which tend to increase the consumption of renewables can use different parameters in this objective. A measurement of the electricity production of a local generation unit can be used, be it a PV system like in (Dar et al. 2014) and (Schibuola et al. 2015) or a wind turbine like in (Hong et al. 2012). In (De Coninck et al. 2014), a voltage measurement is used, because it is assumed that a sub- or overproduction of electricity in the grid will result in voltage fluctuations at the feeder level. Finally, the residual load at local or national level can be monitored like in (Miara et al. 2014) and (Reynders et al. 2013).

At the level of the local controller, weather compensation is often implemented, through the use of heating curves. They consist in adapting the supply temperature of the heating/cooling systems, according to the ambient temperature, in order to save energy. They rely therefore on an outside temperature sensor.

### **3.5 Models supporting model-based control**

Modelling and simulation allow engineers to investigate and analyze physical systems so that design flaws or failures can be avoided before being deployed in practice. In the domain of building engineering, models are created for different reasons. Here, the discussion is focused on models for control purposes.

Modelling of building systems can be generally divided into two parts: modelling of the building itself and modelling of mechanical and thermal systems supplying service to buildings, such as HVAC, domestic hot water system, solar thermal collectors, PVs etc. Here, mainly modelling approaches for buildings and thermal energy storage (TES) systems are discussed, given that these two components contribute directly to the Energy Flexibility of buildings.

#### **3.5.1 Modelling of buildings**

From the degree how detailed a model represents a building, a building model in the literature can be roughly categorized into three groups: white-box, grey-box and black-box models.

### White-box models

The white-box model, often referred to as a physical model, describes a building in details based on first principles of building physics. Building performance simulation (BPS) programs commonly used by building modellers all adopt this approach, for instance, EnergyPlus, TRNSYS, ESP-r etc. Based on physical parameters and thermodynamic laws familiar to building engineers, the white-box model is a very intuitive representation of a building, for example, information about geometry and materials of building constructions are required for this type of model. Thus, it allows building engineers to easily use, understand, analyze or even re-develop these parameters. However, because of the large amount of information input, it suffers from the complexity of model construction. (Pr??vara et al. 2013) advocated that modelling was the most expensive part of the predictive control. In addition, it causes difficulty in real-time control application due to its high computation power demand.

Several studies however explored the “offline” control application based on the white-box model. (Coffey et al. 2010) proposed a model predictive control strategy using a detailed TRNSYS building model in the controller for the purpose of peak shaving. A software framework was outlined where the optimization work was done externally by GenOpt with a genetic algorithm. The optimal decision was handled yet in another organization layer with outputs to the building energy management system. (Zhang et al. 2014) took a similar approach with a TRNSYS building model coupled with GenOpt optimisation. The TRNSYS building model acted as the “real house”, as well as the model in the controller, which facilitated the study without concerning model mismatch, an issue commonly existing in model-based control studies. (May-Ostendorp et al. 2012) developed a model of a small office building in EnergyPlus, which was used for the extraction of supervisory building control rules.

Besides offline control application, the white-box model is more often used to generate a synthetic database which is further utilized for system identification and validation of simplified models. Several of its typical applications will be covered in the section below after introduction of the grey-box and black-box models.

### Grey-box models

The grey-box model uses simplified physical representations, for instance, using a network of resistors and capacitors based on the electric analogy of building Resistance and Capacitance (RC) to describe a building. In the RC network model, a node of the network represents a space or a layer of a wall/floor with a homogenous temperature; the thermal mass of the space or construction is represented by a capacitor. Figure 3.2 shows examples of RC network representations of a wall (left), a house with radiators (middle) and with a floor heating system (right).

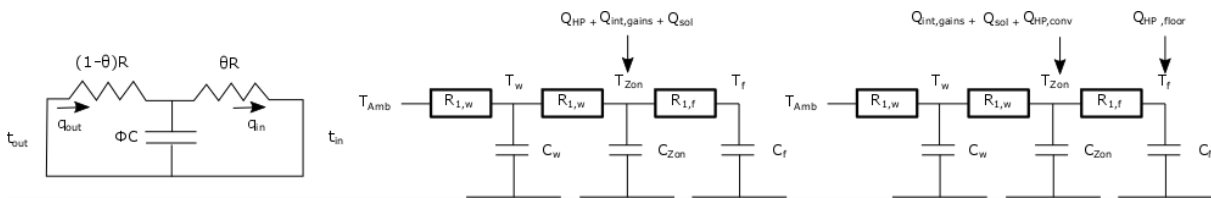


Figure 3.2 RC network representations of a building wall as 2R-1C (left), a house with radiators only (middle) and with a floor heating system additionally (right) (Masy et al. 2015).

As in the electric RC network, the number of capacitors decides the order of the dynamic system; and similarly, the research findings of RC networks as well as linear systems can therefore be transplanted to the building system for analysis and controller design. This type of model appears to be the most widely applied in the literature.

The RC network model is included in the category of the grey-box model because the system parameters can be physically interpreted, for instance, time constant, resistance and capacitance of the system may be analyzed and paralleled in the building system. Therefore, observations and findings can still be physically sought. (Candanedo et al. 2013) analyzed the capacitance ratio of the central zone and perimeter zone of an office after identifying these parameters. They claimed that the bigger capacitance of the central zone showed a slower change than the perimeter zone. According to (Madsen & Holst 1995), a RC model may or may not describe the long-term dynamics of a building, depending on the number of time-constants of the corresponding RC network. They suggested using at least two time-constants for a single-story building. This recommendation is not difficult to understand since the physical building system is nonlinear, while the RC network approximates it using a linear system. To what extent a RC network represents a building system well enough was further investigated by (Bacher & Madsen 2011). Different scenarios of envelope, heater and sensor combinations were examined and discussed. A non-RC network based grey-box model is also possible, such as the one proposed by (Aswani et al. 2012) .

Compared to the white-box model, the grey-box model is much simpler. It requires much less computational power and can be easily implemented in real-time control applications. However, some researchers are concerned about the accuracy of grey-box models and propose some in-between models. In the study of (Wang & Xu 2006), a model was created by combining functions based on thermodynamic laws with grey-box models. Then parameter identification technique was applied with operation data to obtain the model. Besides the dynamics of different thermal zones, the model also took into account the dynamics of internal mass and multilayer external walls and roof.

### ***Black-box models***

Unlike grey-box models, black-box models cannot necessarily be understood from a physical point of view. They are often purely mathematical models, derived from data based on different machine learning algorithms, such as polynomial models (e.g. autoregressive moving average (ARMA) models), artificial neural networks (ANN) and so on.

(Jiménez et al. 2008) presented a detailed guidance on how to identify an ARMA with exogenous terms (ARMAX) model for a building using the Matlab system identification toolbox IDENT. The relationship between the RC network and the polynomial models (or parametric models) were also explored. (Huang et al. 2014) developed an ANN model based on the model structure of nonlinear autoregressive with exogenous terms (ARX). A three-layer Multilayer Perceptions (MLP) was chosen and the Levenberg-Marquardt algorithm was used as the training algorithm to minimize the mean square errors between the predicted and measured data. In this study, a RC-network model was also created and results showed that the ANN model gave slightly better predictions than the ARX model. Research from (Ruano et al. 2006) showed that the ANN model could perform even better than the white-box model. However, choosing the correct order number for the ANN model is challenging and its model structure is complicated, which could result in a non-convex optimization problem that is difficult to solve. (Dong & Lam 2014) examined the feasibility and applicability of the support vector machine (SVM) algorithm in building load forecasting. In this case, coefficients of variance and the percentage errors of all prediction results were within 5 %.

### ***Comparison of model types***

The advantage of black-box models is their flexibility of model structure, compared to grey-box models. (Jiménez et al. 2008) have shown that the RC network model is just one special type of the polynomial models. However, since the polynomial model is more flexible in its parameters and structure, the original physical meaning of the RC network model cannot be retained in the expansion

of parameters and structure. As to other machine learning algorithms, the choices can be abundant, but each has its own limitations, too.

Nonetheless, the black-box and grey-box models have lower complexity than the white-box one, so they are more widely applied in real-time control practice. However, the former two types rely heavily on measurement data, which can remain an obstacle in reality. In the literature, one common approach is using the white-box model built in BPS programs to generate a synthetic database, as mentioned previously, for system or parameter identification for the simplified models. This approach diminishes the potential problems existing in system identification using real measurements, such as sampling rates selection, satisfaction of excitation conditions and data duration requirements etc. Moreover, the simplified models can also be validated with the white-box model ((Masy et al. 2015), (Ma et al. 2012), (Ma et al. 2014)).

In a study from (Ma et al. 2012), the Building Control Virtual Test Bed (BCVTB) environment was utilized to integrate EnergyPlus and Matlab. The input-output information of the EnergyPlus model was used to identify the ARX model in Matlab. This simplified model was used in the MPC to provide optimal cooling setpoints for a five-zone building (see Figure 3.3).

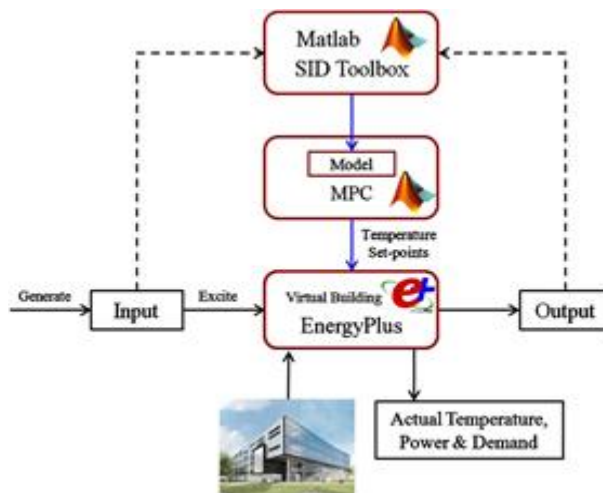


Figure 3.3 A system framework in BCVTB (Ma et al. 2012).

The study from (Garnier et al. 2015) describes the creation of a complex building model in EnergyPlus, and an ANN model was then identified based on the input-output data generated by the EnergyPlus model. The optimal network topology was identified with 18-24 hidden neurons using a dataset of two months.

Although different types of models exist, each of them has its own advantages and disadvantages, as well as its application field as discussed above. Selecting the most appropriate model and tool to solve a problem is a critical step for reasonable building simulation. Most models are highly dependent on the specific case.

### 3.5.2 Modelling of TES systems

Like the building thermal mass within the building itself, controlling the charging and discharging of a TES system can contribute to the Energy Flexibility of buildings, such as reducing peak power demands.

Common TES systems found in buildings are hot water tanks for service water and ice storage tanks for cooling, often installed in commercial buildings. Currently, only simplified TES models and low-order RC-networks have been applied for model-based control. (Salpakari & Lund 2016) integrate a one-node model for a water tank into an MPC. (Berkenkamp & Gwerder 2014) developed a linearized model of a stratified water tank for an optimal control problem. Figure 3.4 shows the different layers or nodes of the tank model.

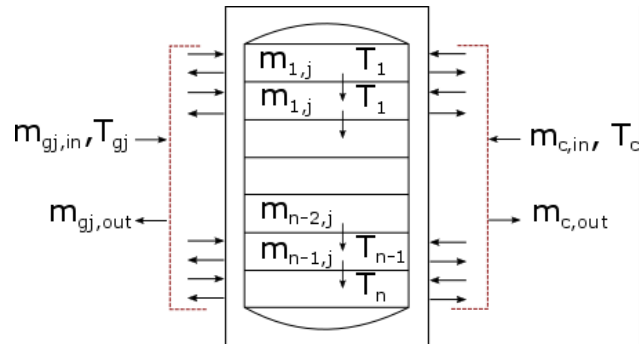


Figure 3.4 Stratified hot water tank (Berkenkamp & Gwerder 2014).

(Beghi et al. 2014) assumed a lumped-capacitance model for ice storage that considered both sensible and latent heat transfer. The model regarded the average temperature of water/ice (storage medium), heat exchange efficiency and heat loss as the function of insulation (self-discharge).

Such simplified TES models integrated into MPC and optimal control are sometimes not capable of capturing the dynamics in the complex process of heat and mass transfer. For this reason, researchers have introduced model-free reinforcement learning and model-based solutions, such as ANN models (Rosiek & Batlles 2011). The reinforcement learning and ANN models can solve nonlinear problems with fast computation. However, the computation time extends substantially as the number of states increases in the optimization and state-space model.

### 3.5.3 Advanced mathematical techniques for flexibility control

As discussed earlier, most business cases for energy flexible buildings depend on time varying energy pricing. Predictable time of use pricing alters tariffs at known times of the day, while a dynamic market offers real-time pricing. Real-time electricity pricing that reflects intermittent renewables is analysed as a stochastic process (Kitapbayev et al. 2015).

Mathematical finance techniques take stochastic input data to quantify the flexibility of a possible investment; in this case a district energy system. One technique, “real options”, assists business decision making. Applied to a district energy system equipped with CHP, the high-level control decision is to operate or idle the local CHP plant in favour of dynamically priced utility energy.

(Kitapbayev et al. 2015) find that the real options technique surpasses discounted cash flow analysis of investments, by modelling uncertainty and operational flexibility. In summary, they prove by simulation that “short-term flexibility can change the long-term business case”. Research of large energy systems with flexible operation and pricing will drive advanced mathematical modelling and simulation.

# 4 Multi-objective genetic algorithm for model predictive control in buildings

Athila Santos and Krzysztof Arendt, Center for Energy Informatics, University of Southern Denmark

## 4.1 Building and system description

OU44 is a teaching/office building of 9,600 m<sup>2</sup> spread over three floors and a basement constructed at the campus of the University of Southern Denmark – see Figure 4.1. The building is designed as a benchmark pilot project for energy efficiency and automated performance testing. It has been operational since 2015 and built according to the Danish Building Code BR2015 with a \$18,5 million budget. The energy consumption of the building also complies with the BR2020 requirements due to the high performance quality and commissioning process. The building is connected to the campus' local electricity and district heating grids.

In Denmark, a building may be classified as class 2015 when the total demand for energy supply (kWh/m<sup>2</sup> heated floor area per year) for heating, <sup>TM</sup>ventilation, cooling and domestic hot water, as well as lighting (except for dwellings) may be no more than  $41 + 1000/A$  (kWh/m<sup>2</sup>/year), where A is the total heated floor area (PAROC, 2017). The introduction of an energy factor of 0.8 for district heating for class 2015 and of 0.6 for class 2020 reflects the fact that district heating is generally more energy-efficient to produce than other types of heating. The requirements for airtightness in low energy buildings have also been tightened. Denmark is so far the only country in Europe to have a definition of a “nearly zero” building (ECOFYS, 2013). The purpose of OU44 was to establish a living lab for improving the energy efficiency of public buildings based on Information and Communications Technology (ICT) solutions that also account for the behavior of occupants.

This building is under normal use by its occupants and has room for approximately 1200 students. The OU44 building is equipped with a Building Management System (BMS) controlling multiple building-related sensors, such as temperature, CO<sub>2</sub>, humidity, window and door sensors, as actuators in systems like Heating, Ventilation and Air Conditioning (HVAC), lighting and power outlets. Although it is an advanced system in terms of the current engineering standards, it is still based on a set of expert rules with little or no overall optimization coordination from the global point of view. Figure 4.2 shows an example of how the different sensors and actuators are organized in different control zones. The BMS system is organized based on room levels and the logic nodes are distributed on Schneider Electric Automation Servers.

## 4.2 Control scope

The current BMS does not introduce any flexibility. The aim is to boost the performance and the flexibility of the BMS system with a multi-objective model predictive control.

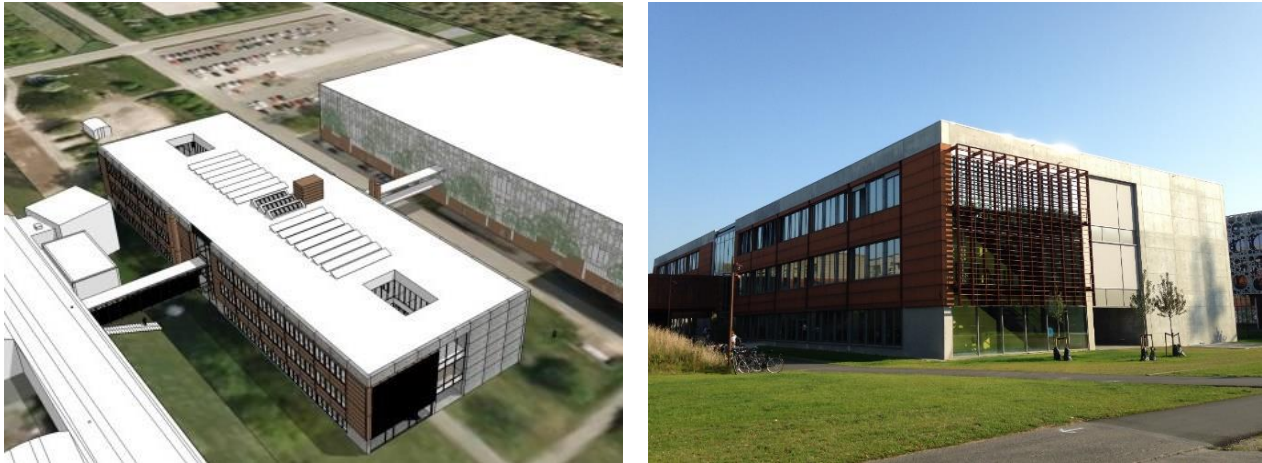


Figure 4.1 The OU44 Site.

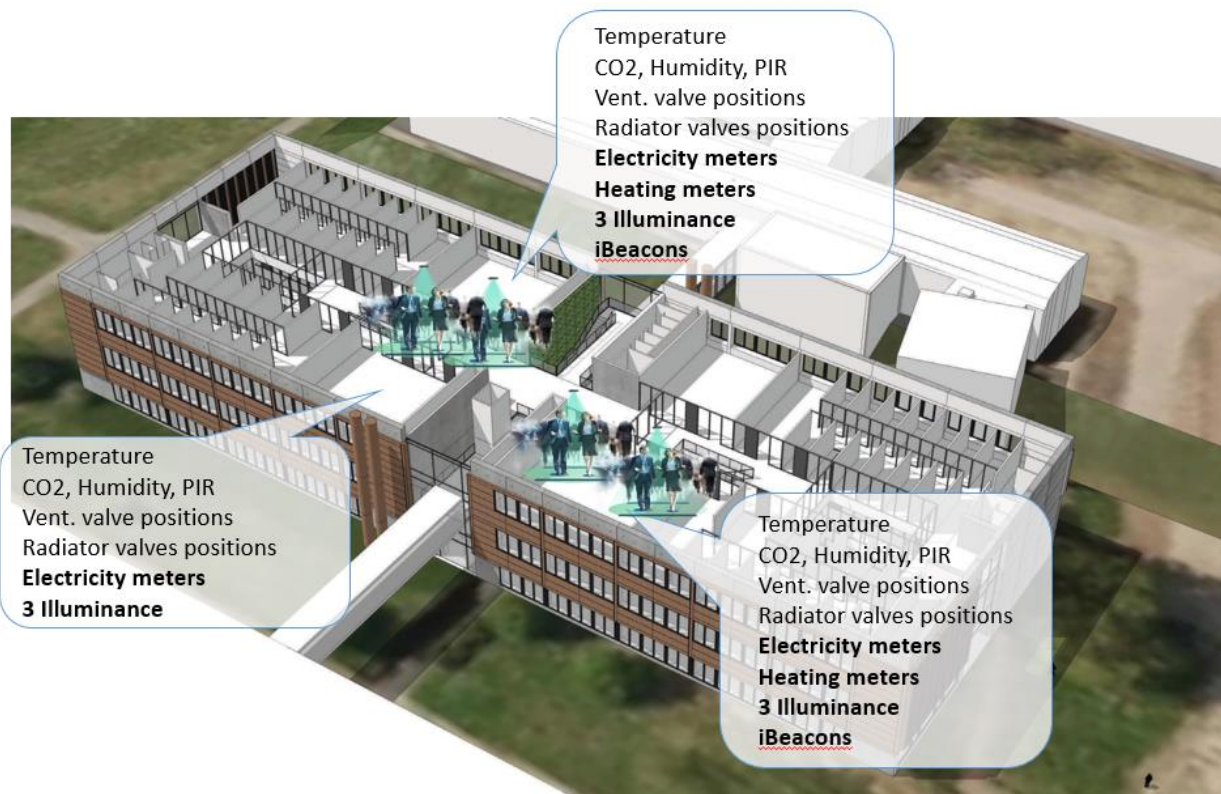


Figure 4.2 Example of sensors in OU44.

### 4.2.1 Ventilation

The ventilation is organized in 4 different modules, each with a rotary heat exchanger for heat recovery from the exhaust to the fresh supply air. The flow rates are controlled based on the indoor CO<sub>2</sub> concentration, room booking and Passive InfraRed (PIR) sensor measurements and heating capacity from district heating. In each zone, the damper opening is controlled based on prescribed CO<sub>2</sub> thresholds: 600 ppm/45 %, 750 ppm/70 %, 900 ppm/100 %. Additionally, rooms are pre-

ventilated before the booked meetings. The pre-ventilation starts 30 minutes before the planned meeting. The amount of the fresh air supply during the pre-ventilation is, however, not specified in the documentation. During the meetings a minimum ventilation rate can be specified, but this option is currently disabled and only CO<sub>2</sub>-based ventilation is in use.

Ventilation is used also for cooling. If the air temperature exceeds the setpoint by more than 2 °C (adjustable), the airflow gradually increases. The airflow vs. temperature increase is, however, also not specified in the documentation. Figure 4.3 shows the fresh air intakes (Bygningsstyrelsen, 2016).



Figure 4.3 Air intake chimneys for ventilation systems (construction phase).

#### **4.2.2 Heating**

The heating system is based on district heating to maintain the setpoint temperatures using radiators and the ventilation systems. Different setpoints are used for day and nighttime. The room temperatures can be adjusted by the users within a narrow range ( $\pm 1.5$  °C).

#### **4.2.3 Lights**

The lights can be turned on and off by the users, but the dimming is controlled by the BMS to maintain a 200 lux setpoint in each controlled zone. When there is no activity in the room, the lights turn off after 30 minutes.

#### 4.2.4 Blinds

The blinds are roman blinds and are controlled on a per room basis based on the outdoor illuminance. If the illuminance exceeds a prescribed threshold (20000 lux on the South façade and 25000 lux on the East facade), the blinds move down. There is a built-in 15-minute delay between up/down movements to avoid too frequent movements on cloudy days. The blind control can be overridden by the room users.

#### 4.2.5 Energy flexibility mechanism

The system was designed to take advantage of building dynamics (passive heating/cooling), which may result in temporary lower occupant comfort. The system was, however, constrained to not allow the thermal comfort to be outside the PMV range -1.0, ..., +1.0. Table 4.1 describes the Energy Flexibility mechanisms and how they are implemented in the system.

Table 4.1 Energy flexibility mechanism.

Type	Description
Load Shifting	<ul style="list-style-type: none"> <li>- Pre-ventilation or postponed ventilation</li> <li>- Pre-heating and utilization of thermal mass</li> </ul>
Valley filling	<ul style="list-style-type: none"> <li>- Nighttime free cooling (using ventilation) during summer</li> </ul>
Target	<ul style="list-style-type: none"> <li>- Decreased ventilation rate in low occupancy periods</li> <li>- Passive heating (absorption of solar heat gains into thermal mass for later use)</li> <li>- Light dimming</li> </ul>

### 4.3 Methodology: control strategies

The control strategy is implemented as a direct control of the ventilation dampers, radiator valves, setpoints for the air pressure in the ventilation duct system, ventilation air temperature (heating only), and light systems. The control is based on a multi-objective model predictive control of the heating and ventilation systems and blinds. The system objectives are to maximize indoor thermal comfort, minimize energy consumption and minimize energy costs. In addition, the system can react to the Demand Response (DR) events by temporarily sacrificing other objectives. The system utilizes simulation models to predict the indoor environment conditions and energy consumption based on the weather and occupancy forecasts. These predictions can be used to minimize the negative effect of DR events, because the system will be able to optimize the overall strategy to the DR event. The exemplary strategies the system can apply are related to the building dynamics, e.g. pre-heating, pre-cooling, pre-ventilating. Table 4.2 describes the algorithm implementation for each control strategy.

Table 4.2 Algorithm implementation of the control strategy.

Algorithm	Description
Genetic Algorithm	Used to estimate building specific steady state parameters of all zones and to optimize overall control strategy
Unscented Kalman Filter	Used to estimate specific transient parameters of the model (e.g. occupancy in rooms without cameras)
Probabilistic Classification	Used to predict indoor occupancy based on 3D camera data or the UKF estimates

The optimization framework consists of the following parts (Figure 4.4):

- Multi-Objective Genetic Algorithm (MOGA) (Sørensen & Jørgensen, 2017),
- Simplified gray-box models calibrated using ModestPy – Functional Mock-up Unit parameter estimation toolbox (Arendt, et al., 2018),
- Archiver with the sMAP interface (Dawson-Haggerty, 2013).

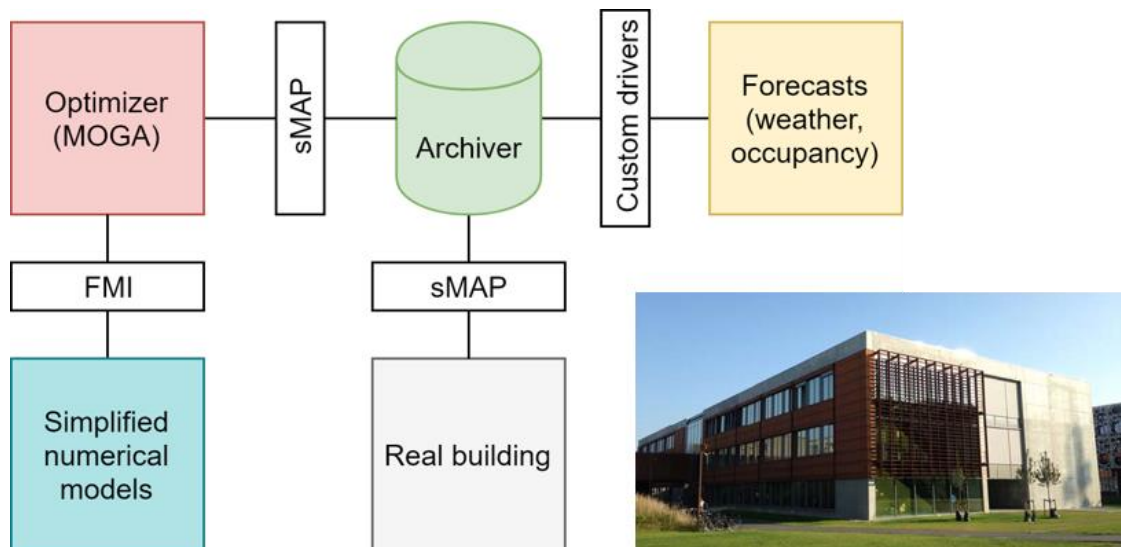


Figure 4.4 Optimization framework based on the MOGA.

Due to the use of Functional Mock-Up Interface (FMI) (Blochwitz & Otter M., 2016) and sMAP interfaces, the framework is model and system-independent. E.g. the same interface can be used to communicate with a virtual building (simulator) as with the actual building (real application).

The optimizer is based on the MOGA (Sørensen & Jørgensen, 2017) that constructs a Pareto frontier with respect to the considered objectives. Each individual in the population represents a specific control policy, e.g. specific heating and ventilation profiles, that is tested in a simulation. The Pareto frontier (Branke, et al., 2008) construction is iterative and based on the genetic algorithm operations: selection, crossover, and mutation. Whenever a new individual with a better fitness with respect to at least one of the objectives appears in the evolution, it joins the Pareto frontier. When one of the stopping criteria is met, the evolution stops and the algorithm proceeds to the second phase in

which the final policy is selected. There are two stopping criteria in use: (1) no improvement in the Pareto frontier for a defined number of generations, (2) maximum computational time reached.

The policy selection in the second phase is conducted recursively. In each step  $i$  the subset of individuals optimal with respect to the priority level  $L_i$  (Figure 4.5) is selected. Each priority level can contain either one or more objectives. In the case there are two or more objectives at the same level, the objectives are normalized in order to identify the optimal population subset. However, no normalization is required for priority levels with a single objective. Finally, after traversing through all the levels, one or more equally optimal policies are left, out of which one is selected randomly.

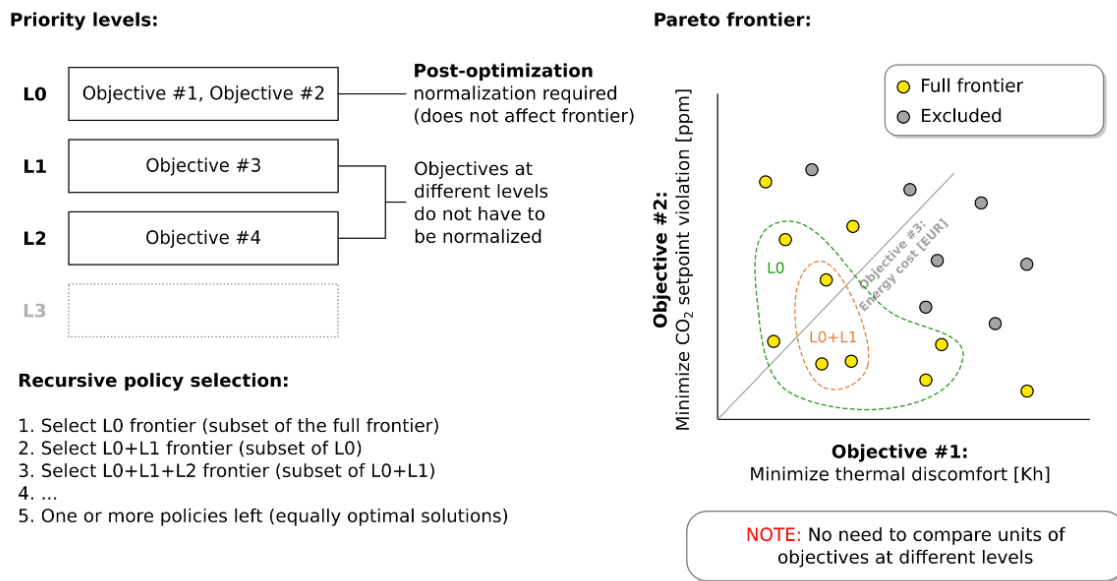


Figure 4.5 Pareto frontier in the multi-objective genetic algorithm optimization

Due to the FMI-compatibility and the use of MOGA the framework is essentially model independent. The models can be implemented in any FMI-compliant tool, and they can be non-linear, non-differentiable or even non-continuous. In addition, since the optimization is not based on a cost function, adding new objectives is straightforward. The objectives do not have to be normalized with respect to one another. Therefore, the framework is potentially more flexible than MPC systems based on collocation or shooting methods. Such features might especially be relevant for building systems, which are often non-linear (e.g. HVAC) and non-continuous (e.g. on/off controllers). On the other hand, MOGA is expected to be more computationally demanding than gradient-based methods.

MOGA uses 7 gray-box zone models to simulate the effects of control policies on the thermal zones in the analyzed building. The zone models are based on the RC thermal network, and each zone model has the same structure (Figure 4.6), but different parameters. The models are implemented in Modelica (Mattsson and Elmqvist, 1997). The zone model parameters were estimated by minimizing the error in indoor temperature and  $\text{CO}_2$  compared to the EnergyPlus outputs using the ModestPy toolbox (Arendt et al. 2018).

The performance of the framework is compared with the rule-based control (RBC) in a one-month long simulation, based on the climate data for January from Typical Meteorological Year for Copenhagen. It is assumed that the framework has control over the room temperature setpoints (each room can have a different setpoint) and has access to room occupancy schedules. In the real

applications the occupancy schedules would be replaced with occupancy predictions. The influence of the quality of the occupancy predictions on the performance of the framework is not considered in this study. Two MOGA-based scenarios are considered:

1. CTRL-EE – optimization of temperature setpoints to minimize energy consumption and maintain indoor thermal comfort,
2. CTRL-DK1 – optimization of temperature setpoints to minimize energy price (based on the Nord Pool market data) and maintain indoor thermal comfort. Electric heating is assumed in this case.

In both scenarios the maintenance of indoor thermal comfort has the highest priority. In the RBC strategy the temperature setpoints are scheduled to 20 °C during weekdays between 5:00-16:00, and 15 °C otherwise. The RBC strategy is implemented directly in EnergyPlus.

The occupancy schedules for the seven zones were generated based on the reference schedule for office buildings available in OpenStudio, with additional time/value offsets, so that there are no two same schedules in the building.

#### **4.4 Implementation: genetic algorithm**

The system is a Multi-Objective Genetic Algorithms (MOGA) framework and it is built as a component-based system from software components intended to be units of independent production, acquisition and deployment (Sørensen & Jørgensen, 2017). It is divided into four types of components: Objectives, Core, Data and Services components, see Figure 4.7. Each component encompasses an individual unit of software functionality and it is implemented as loosely coupled plug-in components.

An objective component provides one or more objective functions. Each objective function can be formulated either as a minimization cost function or as a constraint. The objective function evaluates the set of solutions proposed by the MOGA component during the optimization process. A solution can have multiple different types of domain specific decision variables; e.g., temperature, CO<sub>2</sub> or light-plane. The result of an optimization is a population of non-dominated Pareto optimal solutions (Kalyanmoy & Dhish, 2005). Objective functions implement the Objective interface and represent minimization cost functions. The decision variables are provided by implementing a specific Variable interface from the Variable platform. The variables can be of different types and can be customized for the domain specific problems. This is important as some domain problems are difficult to encode into a generic data types, e.g., a binary string. Dynamic Links are used to connect decision variables and objectives of unrelated types and promote extensibility and late configuration of the problem context (Jensen & Jørgensen, 2010) (Jensen & Jørgensen, 2011). Furthermore, the open/closed principle is supported, as the problem context is open to extension but closed to modification. This principle is important when the problem context can change dynamically over time.

Figure 4.8 shows the pseudocode for the default evolutionary algorithm implementation used by the core of the MOGA (Ghoreishi, et al., 2015). The algorithm is separated into the following phases: Initialization, Ranking, Mutation, Crossover and Termination. The MOEA function has three arguments: 1) the extensible problem object, 2) a time-stamp time for when the algorithm is executed, and 3) the population oldPop from previous executions. For each optimization, the variables attached to the problem object are updated using the Decouplink CONTEXT function, see Line 2-3. Line 5 checks if the previous population oldPop is empty. The population oldPop is empty

the first time the algorithm is executed. If the population `oldPop` exists from previous executions, it is copied into the new non-dominated population `pop` (Line 7). The time-stamp time is used for optimization problems that use the start time of the optimization to initialize the population. A domain specific initialization operator `INIT` is implemented for each type of decision variable (Line 11). The function `ADDNONDOMSOLUTION` ranks all solutions in the population `pop` according to the Pareto dominance relation and is called during initialization and after crossover and mutation.

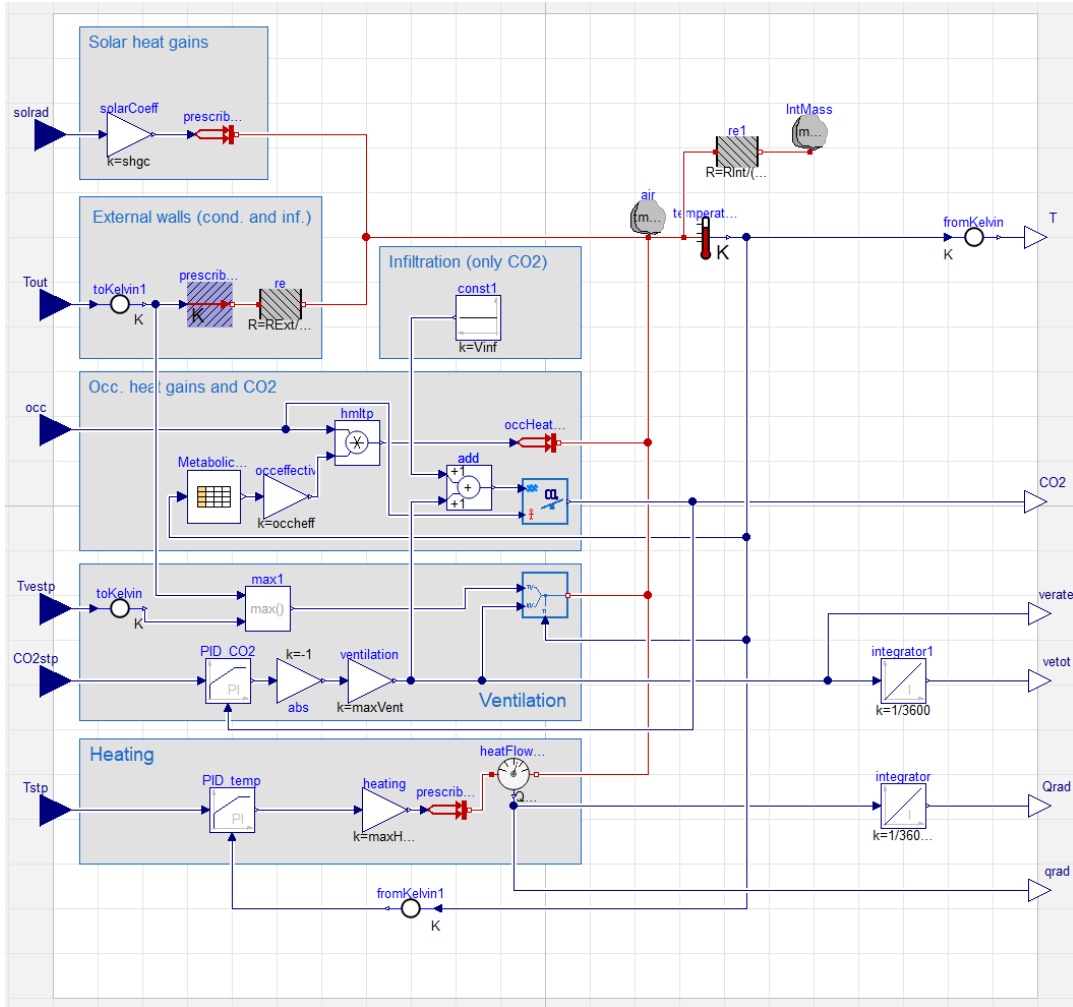


Figure 4.6 Gray-box model of a zone based on a R2C2 thermal network implemented in Dymola/Modelica.

For each generation, solutions are selected a number of times for mutation or crossover based on the added selection strategy implementation. The default implementation of the `SELECT` function selects a pseudorandom solution from the population. Finally, a priority-based post selector function is applied to select one solution out of the resulting Pareto optimal set. The values of the objectives with same priority level are summarized and then the population is sorted in lexical order based on the priority levels. The most important priority level is sorted first and the top solution of the sorted population is then selected as the best solution.

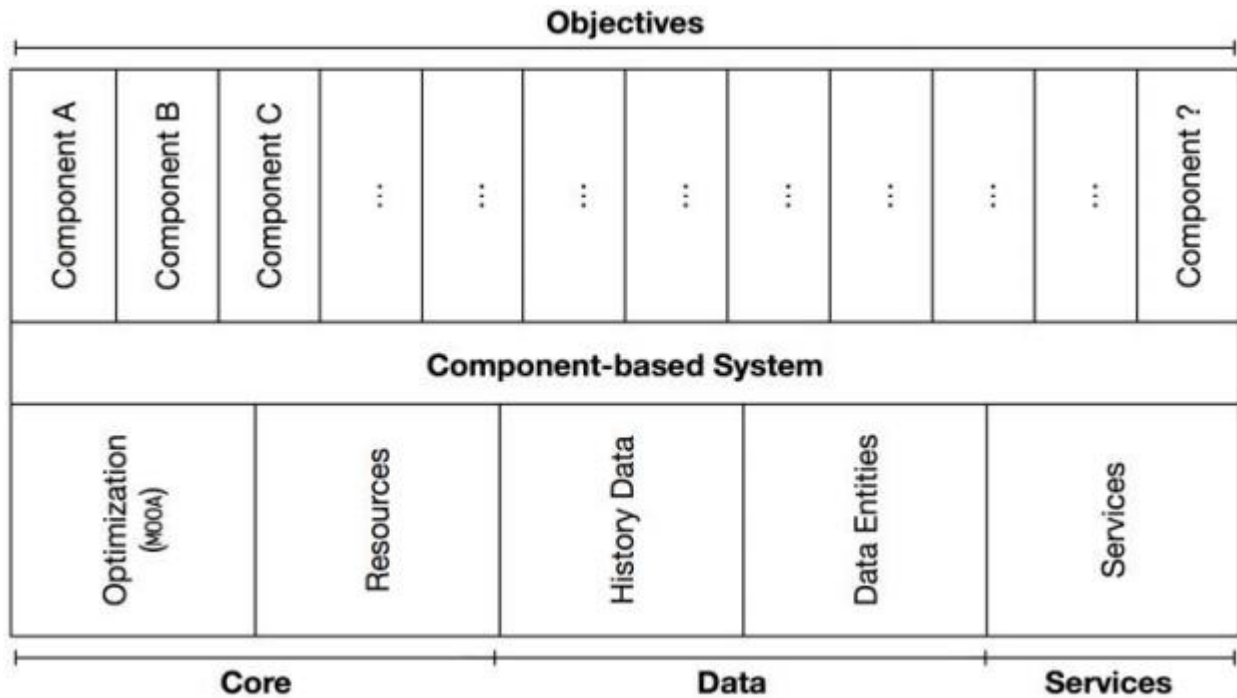


Figure 4.7 Component-based view of the MOGA framework.

```

1 MOGA(problem, time, oldPop)
2 for each variable  $\in$  AllVariables(Context(problem)) do
3   | Update(variable)
4 end
5 if oldPop.isNotEmpty then
6   for each oldSolution  $\in$  oldPop do
7     | AddNonDomSolution(Copy(problem, time, oldSolution))
8   end
9 end
10 for  $i \leftarrow 0$  to PopSize do
11   | AddNonDomSolution(Init(problem, time))
12 end
13 while not Termination() do
14   for  $i \leftarrow 0$  to  $i \leq$  PopSize do
15     if RandomDouble()  $j$  MutationRate then
16       | child = SolutionMutation(Select(pop))
17     else
18       | child = SolutionCrossover(Select(pop), Select(pop))
19     end
20     AddNonDomSolution(child)
21   end
22 end

```

Figure 4.8 MOGA algorithm.

### 4.4.1 Negotiation

Negotiation is a process in which disputing agents decide how to divide the gains from cooperation between themselves (Fatima & Kattan, 2011), (Kattan, et al., 2013). Each agent negotiates a set of resources on the basis of maximizing or minimizing a utility fitness function. When negotiation involves a set of multiple resources it is denominated "multi-issue negotiation".

This framework is applicable to a broad range of application domains, offering multi-objective and conflicting-goals solution search in the decision-making process. Decision problems are formulated using the following abstractions (Clausen, et al., 2014):

- **Issue:** A variable describing a social construct or physical phenomenon whose value must be decided by the framework. The type and range of this value are domain specific.
- **Information:** User inputs from sensors and other systems.
- **Concern Agents:** A set of independent agents that implement domain requirements. Each agent attempts to influence the values assigned to its concerned issues. For this, a fitness function is modeled.
- **Contract:** A set of values for each defined issue. A contract becomes satisfying if it is added to a Pareto-front of contracts either by replacing an existing satisfying solution (i.e., its values improve fitness for one or more agents without deteriorating other fitness values) or by extending the Pareto-front (i.e., no existing satisfying contracts is able to replace the proposed contract and vice-versa).

The negotiation context consists of several Concern Agents (CA), which negotiate over a set of issues, and a Manager Agent (MA), responsible for managing the negotiation process and finding an optimal contract. A contract is defined as a set of determined issues, that satisfies the goals of the CA.

Figure 4.9 shows the negotiation process where the MA generates a population of random contracts which will be submitted to each CA for evaluation. The evaluation assigns a cost value to each contract in the population, representing the degree to which the proposed contract adheres to the goal of the CA. In order to select the best contracts to optimize the overall system performance, the Pareto criteria is applied over the contract set to elect the best candidates. A new set of contracts is generated at each iteration based on the previous one.

Each building zone represents a negotiation context where interdependent issues are distributed across multiple coupled control domains. The framework is responsible for the negotiation of an optimal solution to the issue allocation problem among the self-interested CA.

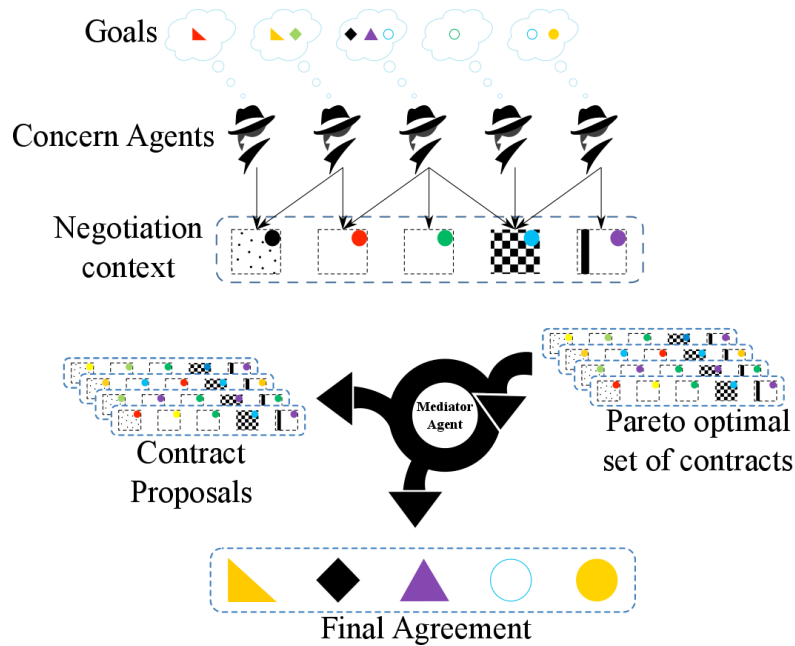


Figure 4.9 Multi-objective Multi-issue Negotiation.

## 4.5 Results and conclusions

In the initial tests on a virtual building (simulator) the framework was able to save around 24-25 % of the heating energy as compared to a rule-based control (RBC) (Table 4.3). Along the energy savings, the framework increased the indoor thermal comfort by reducing the number of occupied hours during which the indoor temperature was below the defined comfort level.

Table 4.3 Total heating energy consumption per scenario.

Scenario	Total heating energy [kWh]	Relative [% of RBC]
RBC	5368.66	100.0
MOGA-EE	4050.43	75.4
MOGA-DK1	4091.90	76.2

Based on the indoor temperature profiles (Figures 4.10 and 4.11) it can be concluded that most of the energy savings were due to the demand driven heating, as opposed to the fixed schedule-based behavior in the case of RBC. The indoor temperature profiles in the RBC were repetitive and, in many periods, not reflecting the actual occupancy, e.g. see large deviations between RBC and MOGA results on January 4, zones 2-7 in Figure 4.10. In addition to the demand-driven behavior, in most cases MOGA was able to preheat the zones before the actual occupancy occurred, with some exceptions when it did not start the preheating early enough, e.g. on January 4, zone 4 in Figure 4.10. The similar monthly profiles of indoor temperature in MOGA-EE and MOGA-DK1 (Figure 4.11) suggest that the highest priority objective, i.e. the thermal comfort maintenance, dominated the solution.

The framework reduced the discomfort (measured in Kh) by around 70% (Figure 4.12). The discomfort metric used in the study was calculated as the product of the temperature difference

between the setpoint of 20°C and the actual temperature and the time in which the difference was observed. Only occupancy periods and only the negative temperature differences were taken into account, i.e. when the indoor temperature was lower than 20°C. E.g. 1 Kh means that the temperature was below the setpoint by 1 degree during 1 h of occupancy. The obtained discomfort metrics were 287.85, 42.18, 41.58 for RBC, MOGA-EE, MOGA-DK1, respectively. The result depends on the chosen reference RBC schedules, however the discomfort in RBC could only be decreased at the cost of increased energy consumption.

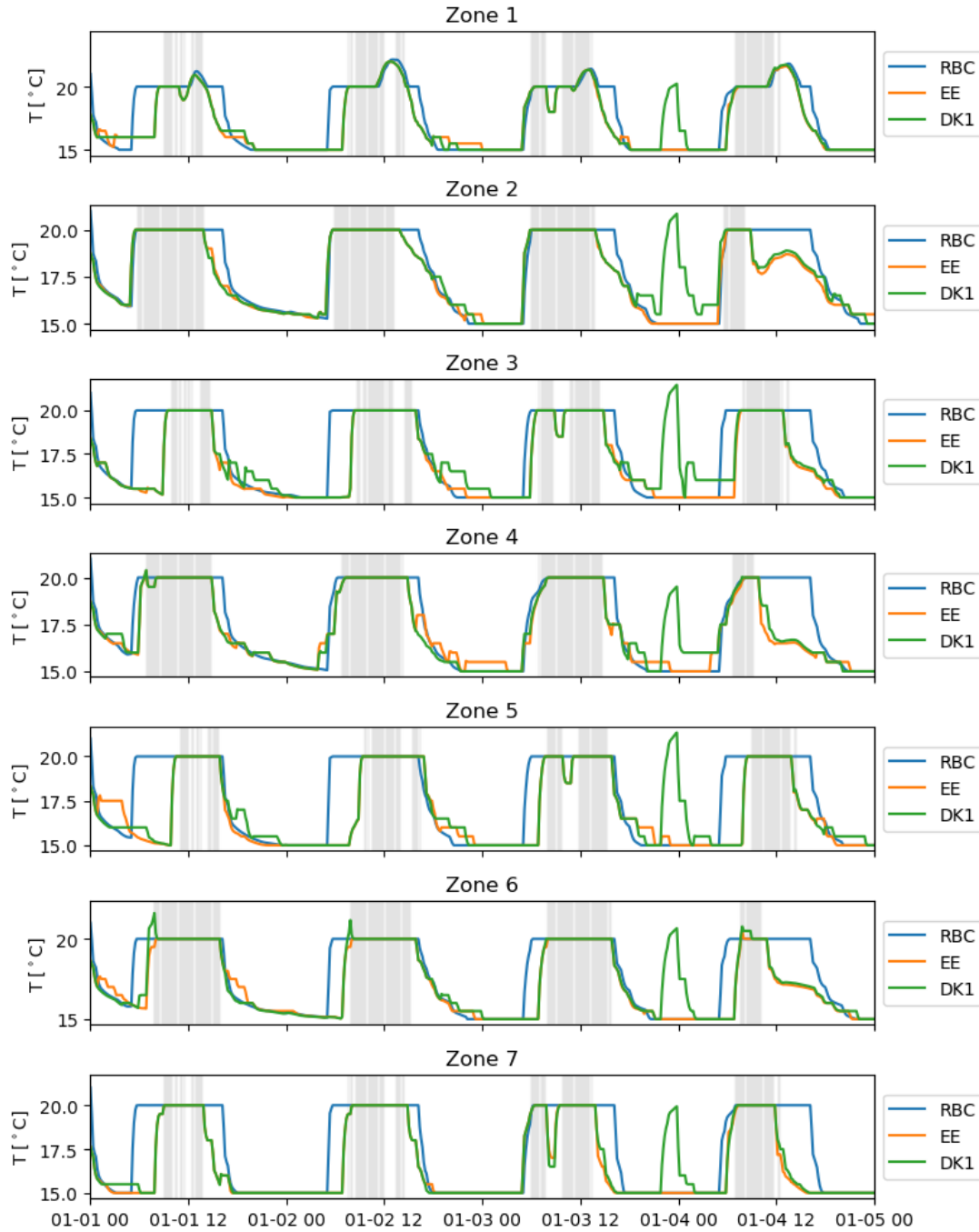


Figure 4.10 MOGA-optimized indoor temperature vs. RBC indoor temperature in three selected rooms of the virtual building (areas shaded in gray mark occupancy periods).

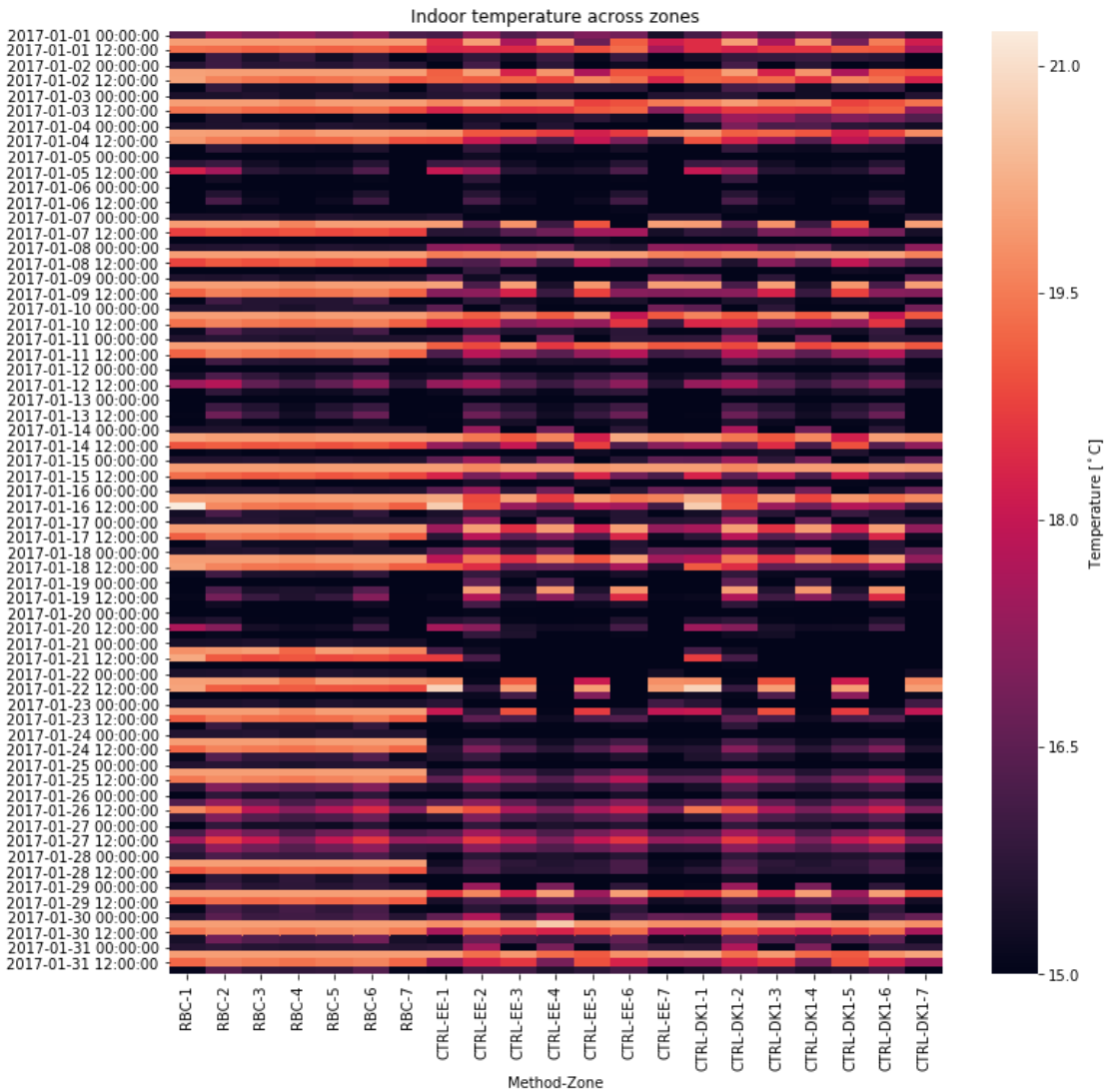


Figure 4.11 One-month indoor temperature profiles for the three considered scenarios (RBC, MOGA-EE, MOGA-DK1). Each column represents a single zone (profile name - zone number).

We believe that the slightly lower discomfort in MOGA-DK1 as compared to MOGA-EE is likely due to the stochastic nature of the optimization algorithm. Since the framework had access to 100% accurate occupancy “predictions”, it could theoretically minimize the discomfort to 0 Kh. The fact that the discomfort metric was non-zero indicate that either the solution was still suboptimal, e.g. due to the maximum CPU time reached. The suboptimality of the solution is at least partially true as can be seen in the case of zone 5, MOGA-EE, January 3 in Figure 4.10, where the indoor temperature setpoint at night is slightly above actually needed. The influence of the objectives hierarchy and optimization settings should be investigated further in the future.

The indoor heating profiles and the energy price during a subperiod of the analyzed month can be compared in Figure 4.13. As in the case of temperature, MOGA-EE and MOGA-DK1 followed a similar trend with one major exception on January 4 when the electric energy price was negative for a short period of time. The controller in MOGA-DK1 decided to consume as much energy as possible in that time, meaning that the second priority objective came into play. However, for most of the time

the price signal had no influence on the solution. Possibly higher price variations or different objective hierarchy would be needed to effectively optimize for the total energy cost in a real application.

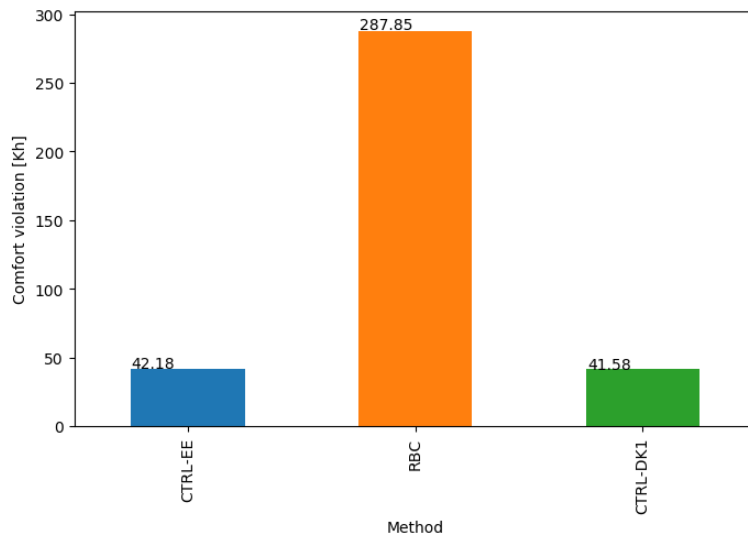


Figure 4.12 Indoor comfort violations for the three considered scenarios

Contrary to expectations, the MOGA-DK1 yielded slightly higher energy cost than MOGA-EE. However, as argued before, this is likely due to the stochastic nature of the optimization algorithm and the dominant role of the highest priority objective of the thermal comfort maintenance.

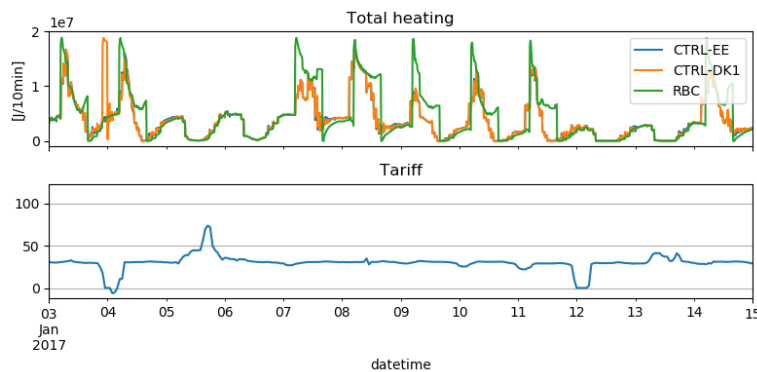


Figure 4.13 Total heating profiles for the three scenarios (top) vs. energy price (bottom).

The presented results were computed using code that was only partially parallelized, e.g. Pareto frontier detection was performed on multiple cores. However, the main bottleneck with respect to the CPU time was the simulation of the gray-box zone models, which was performed on a single core. Due to the nature of MOGA, the zone model simulations need to be repeated thousands of times. In this setup a maximum allowed optimization time per each 7h optimization horizon was five minutes. After each optimization, a one-minute time slot was used to synchronize the measurements and control strategy between MOGA and the virtual building. The optimization was repeated every 1h of the virtual building's time. In total, around 3 days of real time were needed to perform a one-month emulation of the virtual building with the MOGA framework (for one scenario). Although the computational requirements of the framework are considerable, they are feasible for implementation in real buildings. However, implementation in large buildings (with hundreds of zones) may require

parallelization of the zone model simulations. In general, more investigations regarding the scalability of the framework are required.

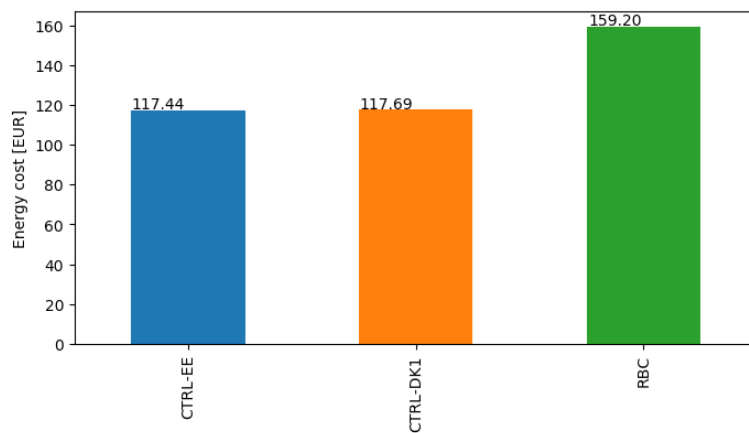


Figure 4.14 Total energy cost per scenario

Summarily, the MOGA framework reduced the energy consumption by around 25% (compared to RBC), however most of the saving were due to the demand-driven heating and not due to the utilization of the building dynamics. This may be due to either a low thermal inertia of the studied building or due to the deficiency of the dynamic optimization method. The relatively small difference in the results between the case based on the energy efficiency objective and the case based on the energy cost minimization objective shows that dynamic energy pricing might not be a sufficient incentive for increasing Energy Flexibility in the analyzed building.

# 5 Deep reinforcement learning for optimal control of space heating

Hussain Kazmi, Enervalis and KU Leuven, Belgium

Classical methods to control heating systems often suffer from suboptimal performance, caused by an inability to adapt to dynamic conditions and unrealistic assumptions often based on early-planning stage building models. This case study explores the use of a novel deep reinforcement learning algorithm which can control space heating in buildings in a computationally efficient manner, and benchmarks it against other known techniques. The proposed algorithm outperforms rule-based control by between 5-10 % in a simulation environment for a number of price signals. We conclude that, while not optimal, the proposed algorithm offers additional practical advantages such as faster computation times and increased robustness to non-stationarities in building dynamics against other well-established methods which are also discussed in this section.

## 5.1 Building and system description

This study uses the building simulator described in (Ruelens, 2016) to test and benchmark the learning characteristics and abilities of the proposed Reinforced Learning (RL) algorithm. The simulator, implemented in Python, is an Equivalent Thermal Parameter model (ETP), which simulates the heating and cooling of a building interior as a function of a limited number of lumped parameters, such as outdoor temperature and characteristics of the heating equipment. It is a deterministic second order model, which takes into account the heat being stored in the building envelope and causes it to cool down in a delayed manner in case of an outdoor temperature drop, or in the absence of introduced thermal energy. The simulation is modelled according to the typical thermal response of highly efficient buildings in Belgium and The Netherlands, and treats the entire building as a single thermal zone. The building is considered to be equipped with a modulating air-source heat pump for space heating; a depiction of the control environment is shown in Figure 5.1.

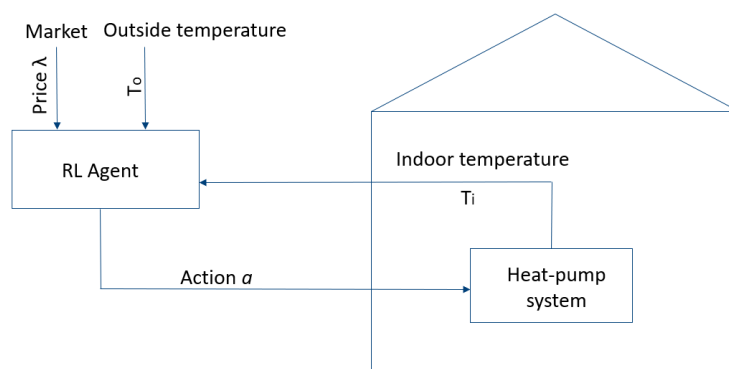


Figure 5.1 Heat pump thermostat control environment (Ruelens, 2016).

### 5.1.1 Influencing variables

In the following, all the variables influencing the system dynamics as defined by the simulator are listed:

1. Ambient air temperature  $T_a^t$  is an exogenous variable and reflects the environmental disturbance in this scenario. It can't be influenced by the RL agent. For this research, five months of ambient temperature data was used and is visualized in Figure 5.2.
2. Building envelope temperature  $T_{mass}^t$  is a measure of the energy embodied by the building at time instant  $t$ , and is not directly observable.
3. Indoor air temperature  $T_i^t$  which is a function of the following:

$$T_i^t = f(T_a^{t-1}, T_{mass}^{t-1}, T_i^{t-1}, a^{t-1}) \quad (1)$$

4. The indoor temperature is measured and can be influenced by the control action chosen by the reinforcement agent,  $a^{t-1}$ .
5. Control action  $a^t$  reflects the input power of the heat pump that it injects into the zone at time  $t$ , which is a continuous value between 0 and  $P_{max}$  [Watt].
6. Energy consumption  $c^t$  follows directly from the control action,  $c^t = f(a^{t-1})[kWh]$ .

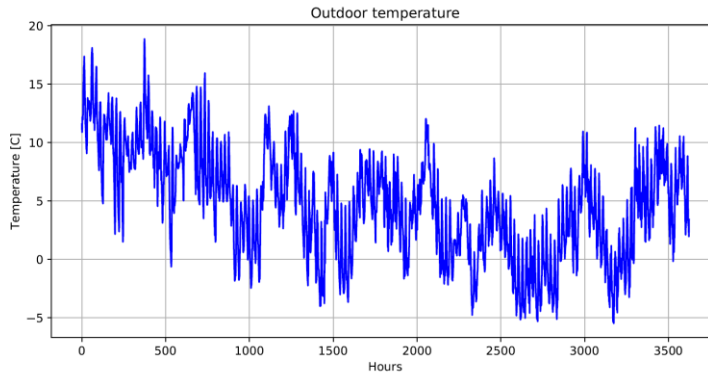


Figure 5.2 Ambient temperature variation over 5 winter months in 2016 – 2017 (observation data from Soesterberg, The Netherlands).

## 5.2 Methodology

### 5.2.1 Background

It is possible to reduce energy consumption for space conditioning by leveraging the flexibility inherent in buildings. This can be done by automatic control of the heating equipment (for instance, by modulating the power or varying the thermostat setpoints) while respecting occupant defined comfort bounds (Gill, 2014). To improve energy efficiency, these automatic controllers have to go

beyond classical rule-based control (RBC) formulations, which are usually implemented as naive hysteresis loops (i.e. reheat the building every time a temperature threshold is met).

Model Predictive Control (MPC) offers an obvious improvement over RBC in the quality of control by bringing anticipative prowess to the control procedure (Afram, 2014). The building is reheated in this case while optimizing towards a secondary objective such as reducing costs. The primary objective is naturally to preserve occupant comfort. MPC, while outperforming RBC, introduces complexity to the system and assumes the existence of a model explaining the dynamics of the system. This model is often based on building physics models and has to be constructed offline – an assumption that is usually not valid for residential buildings as creating a detailed and accurate model would be too costly in practice. Furthermore, building information models (BIM) and energy models, even when they are available, can have significant discrepancies between theoretical and practical performance (Majcen, 2015). Data-driven control can alleviate some of these limitations of requiring an accurate model (Kazmi, 2016); however, the computational expense and data requirements to continuously learn and plan can be significant.

In recent years, reinforcement learning (RL) has emerged as a viable alternative to MPC in many domains. The allure of RL lies in its ability to approach (or exceed) the level of optimal control offered by model predictive controllers while learning directly from sensor data, i.e. not requiring the presence of a model beforehand. A number of reinforcement learning algorithms have been proposed in literature, which can be broadly classified as model-based and model-free RL algorithms (Sutton, 2017) (Kazmi, 2017).

### **5.2.2 Context**

While both model-based and model-free RL algorithms are data driven and have their advantages and disadvantages, the focus here is on developing a model-free controller because of the computational advantages this class of algorithms offers. This model-free controller can then be compared with an ideal MPC (which has access to the true system dynamics model) and a data driven model-based controller to determine its efficacy.

Some studies proposing reinforcement learning strategies for different aspects of building control have recently appeared (Barrett, 2015), (Wei, 2017), (Ali, 2017) (Kazmi, 2018), however, there has been no thorough comparative study on the pros and cons of different reinforcement based controllers. Knowing how these algorithms stack up against each other and known model-based controllers is vital for practitioners to determine which one is best suited to solve practical problems. This example is intended to quantify the performance of the state of the art of RL algorithms for optimal control of buildings towards better energy or cost efficiency by leveraging the Energy Flexibility afforded by its thermal inertia. In doing so, it also aims to provide future directions for research in data driven building control and help researchers apply and report their findings in more standardized settings.

A note on terminology is necessary here. While the distinction between MPC and model-free RL is obvious (one makes use of a model while the other doesn't), the difference between model-based RL and data-driven MPC is harder to define. There are two dimensions to this. The first is exploration and the second is policy-side learning (Sutton, 2017) (Finck, et al., 2018). Actively exploring the state space of the system under consideration with the primary purpose of improving the learnt dynamics model is usually exclusively an RL construct. As such, it is seldom seen in data-driven MPC implementations. While exploration might sometimes lead to degraded performance momentarily, it improves performance over the long run by improving the model quality. Likewise, while both data-

driven MPC and model-based RL algorithms improve their representation of the system dynamics through observation data, model-based RL algorithms can go an extra step and learn the optimal policy as a corollary to this learning. This is evidenced in the popular family of Dyna algorithms (Sutton, 2017) and can help improve the quality and speed of control. Data-driven MPC usually does not include any policy-side learning, thereby solving an optimization problem at every time step (including for states it has already visited and optimized for before).

### 5.2.3 Formulation

The focus of this study is to develop reinforcement learning based controllers and benchmark them against classical controllers on their ability to leverage building Energy Flexibility. The reinforcement learning problem can be formulated as a Markov Decision Process (MDP):  $\{s, a, T, R\}$  (Sutton, 2017) where each individual element is defined as follows:

State space: continuous, where  $s^t \in S$  is the state at time t, consisting of n previous indoor temperatures including the current one, and the current ambient temperature. This variable is the state estimate and is meant to approximate the true state of the building which cannot be observed directly:

$$s^t: (T_i^t, T_i^{t-1}, T_i^{t-2}, \dots, T_i^{t-n}, T_a^t) \quad (2)$$

The action space: discretized between 0 and  $P_{max}$ , where  $a^t \in A$ , and is the energy injected by the heat pump into the thermal zone; in this case,  $P_{max}$  is 2000 W. Thus the action taken by the controller (also referred to as the control agent or simply agent) at any given time can be one of the following:

$$a^t \in [0, 400, 800, 1200, 1600, 2000][W]$$

There is no cooling functionality implemented so the agent takes no control action if the temperature exceeds the maximum allowable temperature.

The transition function,  $T^t(s^t, a^t, s^{t+1})$  represents the system dynamics and is learnt from observation data

Reward function  $R^{t+1}(s^t, a^t, s^{t+1})$  represents the reward system that the agent has to maximize over time. The rewards are shaped so that higher priority is given to occupant comfort compared to energy or cost reduction. The negative signs reflect that this is a negative reward stream (or penalty). This reward stream is then split into these two components where the reward (or penalty) accrued because of energy consumption is given by:

$$R_{cons}^{t+1} = -c^t \lambda^t \quad (3)$$

Which depends on the price of energy consumption  $c$  and the energy consumption  $\lambda$  at time t itself. The reward function for loss of occupant comfort, on the other hand, is defined as:

$$R_{userComfortLoss}^{t+1} = \begin{cases} -3 \cdot 1.3^{T_i^t - T_{max}}, & \text{if } T_i^t > T_{max} \\ -4 \cdot 1.35^{T_{min} - T_i^t}, & \text{if } T_{min} > T_i^t \\ 0, & \text{otherwise} \end{cases} \quad (4)$$

Where  $T_{max}$  and  $T_{min}$  are the maximum and minimum comfortable indoor air temperatures of the thermal zone. Figure 5.3 shows the reward function. The numerical values given for the reward function for loss of occupant comfort were derived empirically. However, a sensitivity analysis showed that the RL agent is capable of learning even if these rewards varied substantially. The

slightly asymmetric loss function derives from a review of literature on thermal user comfort (De Dear, 2002), (ASHRAE, 2010). An additional reason for the asymmetry in the loss function derives from the fact that in this particular control problem the reinforcement learner can only control the heating of the building (i.e. there is no air conditioning for cooling). Since the building is assumed to be in a North-Western European climate, the loss of comfort in lower temperatures is much more relevant.

Based on ASHRAE studies, the optimal indoor temperature is 21 °C with a band of 2 °C which results in 90 % occupant acceptability. Of course, the comfort range is extremely subjective and depends on individual preferences, something which takes into account by making the reward system parametrized over the choice of minimum and maximum acceptable temperatures. The RL agent is supposed to work for a range of user comfort valuations as long as it is prioritized over energy consumption. The total reward at any given time instant is then a simple summation of these two reward streams.

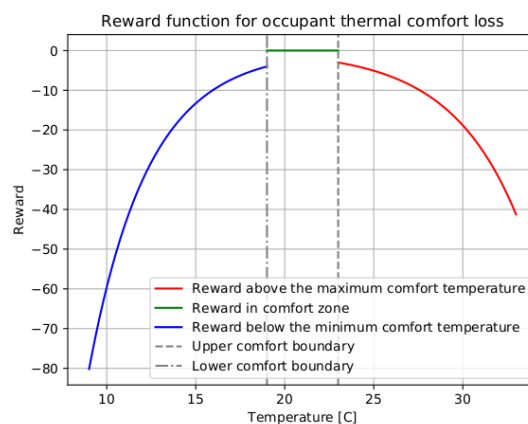


Figure 5.3 Reward function for occupant comfort loss.

The time horizon for optimization is considered to be 24 hours; the time step used by the emulator is one hour, which is also the resolution at which the control agent issues new commands.

## 5.3 Implementation

### 5.3.1 Control objectives

The reinforcement learning agent is expected to balance two reward streams. The first derives from respecting occupant comfort bounds while the second is to consume as little energy or money as possible while still meeting the first objective. The reinforcement agent has no prior information about the building dynamics at the beginning of control.

### 5.3.2 Rule based control

As mentioned earlier, the baseline controller implemented in many buildings today is rule based. This provides the lower bound of the performance and serves as the benchmark on which the proposed algorithms have to improve upon. This control takes the following form:

$$a_t = \begin{cases} P_{max} & \text{if } T_i^t < T_{min} - \Delta T \\ 0 & \text{otherwise} \end{cases} \quad (5)$$

Which implies that the heat pump starts consuming full power as soon as the temperature falls below the minimum threshold limit of the occupant comfort by a predefined hysteresis band.

### 5.3.3 Model predictive control

A model predictive controller is implemented which assumes full knowledge of system dynamics. This provides an upper bound for the performance when compared with rule based control and the research question is how close a reinforcement learning based agent can approximate this solution.

### 5.3.4 Model-based reinforcement learning

The final benchmark, the proposed model-free controller is compared against, is a model-based reinforcement learning agent (which can also be considered to be a data-driven MPC). Here, the RL agent needs to learn the transition function to represent the system dynamics from observed data. This is achieved using a neural network. This neural network takes as input the feature vector defined in Eq. 2, and produces a scalar continuous valued output reflecting the indoor temperature at the next time step. It is possible to build future trajectories of arbitrary length by repeating this process multiple times. The model-based agent interleaves learning and planning to identify the action vector, which would maximize long-term reward. Multiple options were explored for the planning step. These include a cross entropy method (CEM) based planner (De Boer, 2005) and a genetic algorithm (GA) based planner (Fortin, 2012).. Finally, the agent uses an  $\epsilon$ -greedy algorithm to take exploratory steps to improve its learnt dynamics model. Here  $\epsilon$  is given by a harmonic sequence, which decays over time with  $1/d^x$ . The details of the implemented algorithm are summarized in the following pseudocode Algorithm 1.

---

**Algorithm 1** Model-based RL control with  $\epsilon$ -greedy exploration

---

- 1: Initialize sample memory  $\mathcal{D}$  with capacity  $N$ , exploration rate  $\epsilon$ , transition ANN model  $\hat{T}_r$ .
- 2: **while** end of simulation **do**
- 3:     Initialize state  $s$
- 4:     For next horizon  $h$  obtain policy  $\pi_h$  by *planning* using transition model  $\hat{T}_r$ .
- 5:     **for** k number of steps **do**
- 6:         With probability  $\epsilon$  select random action  $a$ ,
- 7:         otherwise select  $a$  from  $\pi_h$
- 8:         Execute  $a$ , observe  $r, s'$ , construct sample  $S \leftarrow \langle s, a, s', r \rangle$
- 9:         Store  $S$  in  $\mathcal{D}$
- 10:     **end for**
- 11:     With a daily frequency, improve transition ANN model  $\hat{T}_r$  on samples from  $\mathcal{D}$  and update  $\epsilon$
- 12: **end while**

---

Figure 5.4 Pseudocode for model-based RL control.

The hyper-parameters of the neural network are chosen by grid search based on known design practices followed by tuning to obtain the best performance (Bengio, 2010).

### 5.3.1 Model-free reinforcement learning (D-DNFQI)

For the model-free algorithm, a variant of fitted Q iteration (Bengio, 2010) is used. This algorithm makes use of deep neural networks to approximate the optimal Q values for planning control actions:

$$Q(s, a, w) \approx Q^*(s, a) = Q^\pi(s, a) \quad (6)$$

The Q value is the goodness of a state-action pair, and identifies the value of different actions, given a state  $s$ . Here  $w$  reflects the weight parametrizations of the neural network. The objective of this neural network is to minimize the mean squared error (MSE) with respect to the observed target value. Because of known issues with model-free learning such as convergence problems and instability in learning, target Q networks and prioritized experience replay are implemented in the algorithm (Volodymyr, 2013), (T. Schaul, 2015).. Finally, to tackle the upward bias problem of Q estimations, Double Q learning is also implemented (V. Mnih, 2015). The final algorithm takes on the form of a double deep neural fitted Q iteration (D-DNFQI) with experience replay and  $\epsilon$ -greedy exploration.

As before, the hyper-parameters of the neural network are optimized using search and existing guidelines. The structure of the output neural network is different than in the model-based RL case however. The Q-network directly outputs a 6 dimensional vector which reflects the ‘goodness’ of all possible control actions given an input state-action pair. The model-free algorithm is summarized in the following pseudocode Algorithm 2.

---

**Algorithm 2**  $\epsilon$ -greedy Double Deep Neural Fitted Q Iteration (D-DNFQI)

---

- 1: Initialize experience replay memory  $\mathcal{D}$  with capacity  $N$ , exploration rate  $\epsilon$ , network  $Q$ , target network  $Q^-$ ,
- 2: **while** end of simulation **do**
- 3:     **while** end of horizon  $h$  **do**
- 4:         Initialize state  $s$
- 5:         With probability  $\epsilon$  select random action  $a$ ,
- 6:         otherwise  $a \leftarrow \arg \max_a Q(s, a; w)$
- 7:         Execute  $a$ , observe  $r, s'$ , construct sample  $S \leftarrow \langle s, a, s', r \rangle$
- 8:         **if**  $s'$  is not terminal state **then**
- 9:             Obtain target:  $Tg(S) \leftarrow r + \gamma Q^-(s', \arg \max_{a'} Q(s', a'; w^-); w^-)$      ▷
- 10:         Double Q learning update rule
- 11:         **else**
- 12:             Obtain target:  $Tg(S) \leftarrow r$
- 13:         **end if**
- 14:         Calculate  $priority_S$  from  $Tg(S)$  and  $Q(s, a; w)$
- 15:         Store  $S$  in  $\mathcal{D}$  with  $priority_S$
- 16:     **end while**
- 17:      $mini\text{-}batch \leftarrow \mathcal{D}$
- 18:     Train  $Q$  network on  $mini\text{-}batch$
- 19:     Update  $w^-$  of  $Q^-$  with  $\tau$  and  $w$
- 20:     Update each  $priority_S$  in  $mini\text{-}batch$  using updated  $Q$  and  $Q^-$
- 21:      $\mathcal{D} \leftarrow$  updated  $mini\text{-}batch$
- 22: **end while**

---

Figure 5.5 Pseudocode for model-free RL control (D-DNFQI).

## 5.4 Results

In this section, the proposed algorithm (D-DNFQI) is compared with more well-known controllers to establish its efficacy. For each test, the heating system is left uncontrolled with no input for 24 hours. After this initial period, the RL algorithms were given control whereupon learning started from scratch. In the following, the performance of the proposed RL agent is considered according to these pricing signals:

The case of flat electricity pricing, which translates to a purely energy efficiency metric.

The case of a dual pricing scheme, with fixed high prices during the day and fixed low prices during the night. This reflects the reality for many residential connections in countries with smart meters; the prices used were consumer tariffs from Belgium.

The case of real time pricing, where prices vary hourly on a daily basis. However, such pricing is usually valid only for aggregations of houses and not individual households, so it is not discussed further.

Additionally, boundary cases of interest are also considered after this discussion to evaluate the performance of different controllers on tasks where a classic model predictive controller would not be applicable. These include robustness to an incorrect model, and to changing environmental conditions and constraints.

### 5.4.1 Quality of model learnt in model-based learning

For model-based RL, the quality of the learnt model is of paramount importance. Since the building is simulated in this example, the model predictions can be directly compared against actual ‘measurements’ for a large number of possible inputs. To visualize the evolution of this model’s performance over time, several snapshots were taken from the model at monotonically increasing times, i.e. as the neural network gathered more data. Figure 5.6 shows that both the mean error and the variance around this error (obtained on an unseen test dataset) decays rapidly over time. The neural network exhibits acceptable performance after only a week’s worth of experiences and after about 20 days the model has already learnt system dynamics almost perfectly.

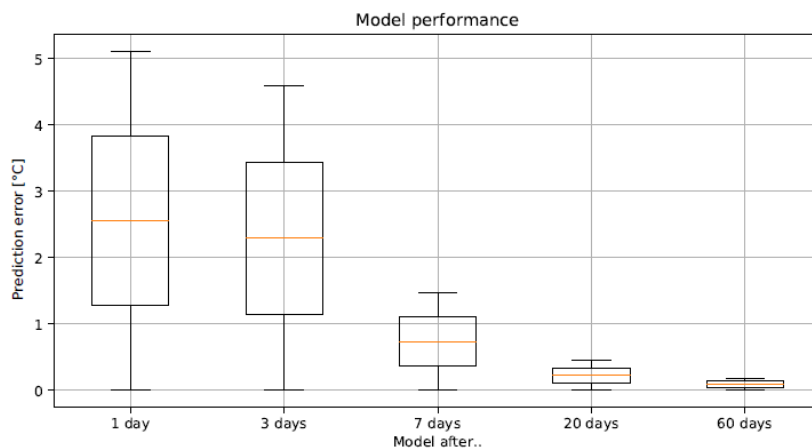


Figure 5.6 Model performance over time given as the difference between predicted and measured temperature [°C]

### 5.4.2 Flat price signal

As discussed earlier, the results obtained have to be evaluated along two dimensions of interest: the impact on occupant comfort and the consequent energy or cost reductions.

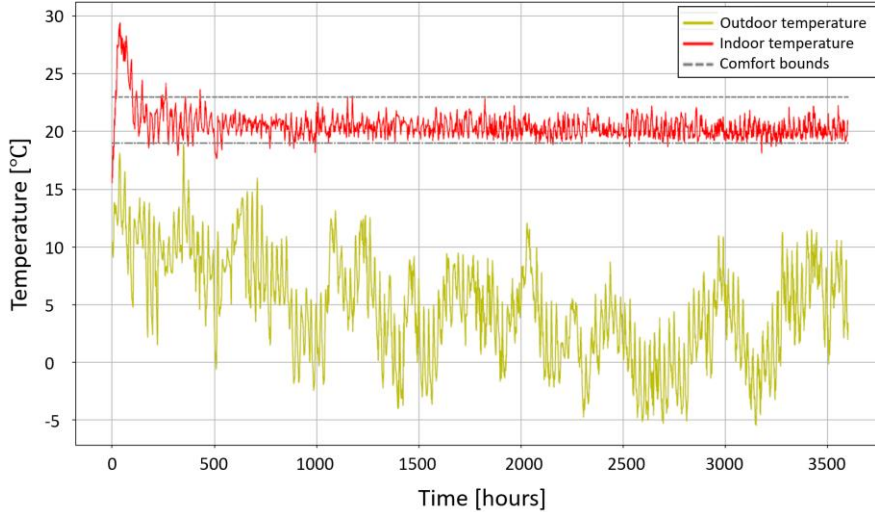


Figure 5.7 Model-free RL performance in time, where the red and yellow plots show the indoor and ambient temperature respectively; acceptable band ranges from 19 - 23 °C.

Figure 5.7 presents the indoor and outdoor temperature evolution for the period under consideration with the proposed model-free controller. It is obvious that the model-free controller exhibits a high peak indoor temperature during the exploration phase but then settles inside the comfort bounds quickly.

One difference between the model-free and the model-based controller is that the model-free controller tried to keep the indoor temperature as close to the lower comfort bound as possible, resulting in the heat pump providing some power (i.e. greater than zero) to the building almost continuously. This is visualized in Figure 5.8 where it can be seen that the heat pump is in the OFF state much less frequently for the model-free controller when compared with its model-based counterpart. While this increased the cost somewhat, it had the useful side benefit of reducing the peak power demand for heating, which can be beneficial for the overall grid (assuming a number of similar heat pumps operating in a neighborhood).

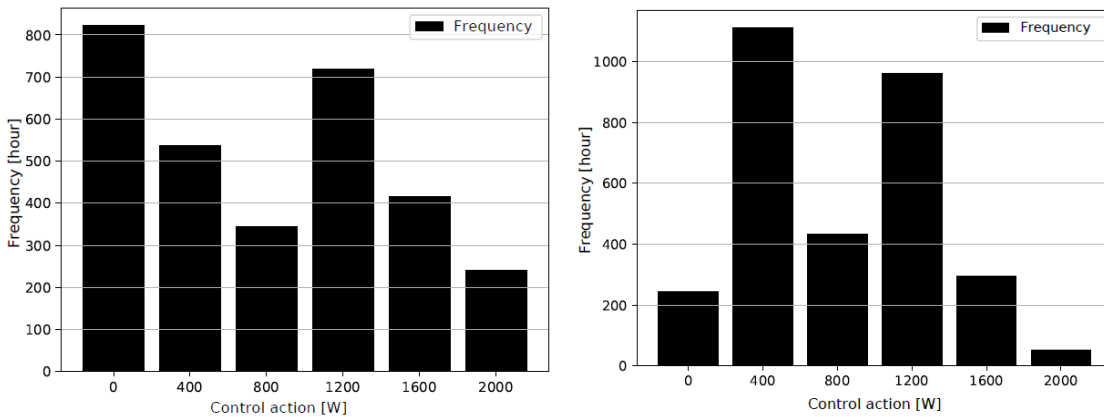


Figure 5.8 The frequency of chosen control action by the RL agent for (left) Model-based; (right) Model-free.

In addition to the very different control commands sent by the reinforcement agent, it is also instructive to compare the two controllers with the lower and upper performance bounds obtained by rule based and ideal model predictive controllers respectively. It is obvious from Table 5.1 that the model-free controller outperforms the rule-based controller in terms of cost reduction. At the same time, it is also evident that the model-free controller underperforms both the theoretical upper bound (achieved by MPC with perfect knowledge of the system model) and the performance obtained by model-based RL. The loss of occupant comfort, as calculated by the thermal comfort reward function shown in Fig. 5.3, arose mostly during the initial training period where exploratory steps caused wild fluctuations of the indoor temperature. These results are summarized in Table 5.1.

Table 5.1 Experimental results for a flat price profile.

Algorithm	Demand change (%)	Cost change (%)	Loss of comfort
Rule based	0	0	0
Perfect MPC	-8.8	-8.8	0
Model-based RL	-7.2	-7.2	0.5
Model-free RL	-6.4	-6.4	5.23

### 5.4.3 Dual price signal

The learning problem becomes more challenging when switching from flat to dual tariffs. However, similar behaviour was observed (Figure 5.9). The model-free controller, as before, cycles between the ON states for the heat pump much more when compared to the model-based one leading to a substantial reduction in peak power consumption both during high and low-price periods. On the other hand, the model-based controller has learnt that keeping the heat pump OFF during the high price signal is a desirable behaviour. The profiles on the histogram of the model-based controller make much more intuitive sense than the one for model-free control as the fraction of ON actions during low prices far outnumbers the fraction of ON actions for high price signal. However, as before the actions chosen by the model-free controller have a beneficial effect on the local low-voltage grid. This is not reflected in the costs shown in Table 5.2 however, which shows that, as before, while the model-free controller improves vastly on the rule-based controller; it is still not as efficient as the model-based controllers.

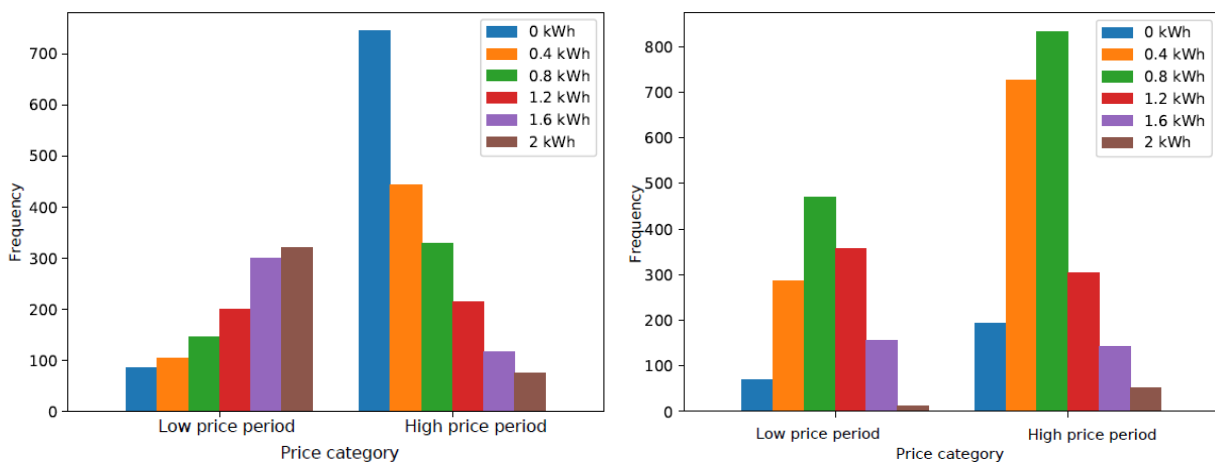


Figure 5.9 The frequency of chosen control action by the RL agent for (left) Model-based; (right) Model-free.

It is also interesting to note how demand varies as a function of the profile in time. This is visualized in Figure 5.10 where it is obvious that when the price is low, the heat pump is turned on more frequently. The two controllers have learnt strikingly different behaviours however. The model-based controller turns on the heat pump at (close to) full power as soon as the price shifts to low but seldom otherwise unless occupant comfort is at risk of being violated. The model-free controller offers a much smoother response however with the majority of operations being in the mid-power regime regardless of the price point. There is a subtle shift however, with higher power control actions (1200 W) prioritized when the price signal is low as compared to when it is high. The summarizing rewards as well as the cost and energy reductions can be seen in Table 5.2.

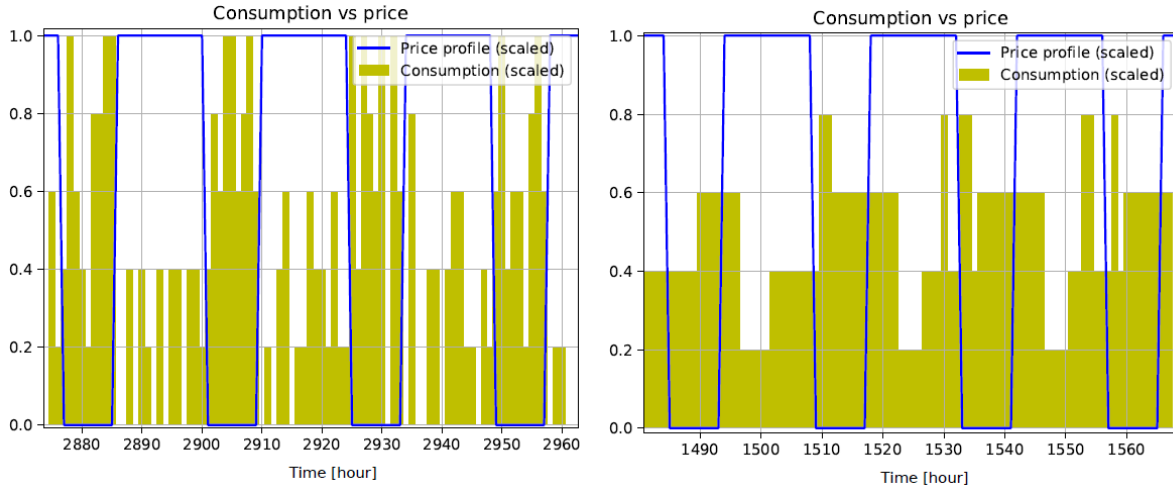


Figure 5.10 Temporal behaviour of the RL agent with dual pricing for (left) Model-based; (right) Model-free.

Table 5.2 Simulation results obtained for a dual price profile.

Algorithm	Demand change (%)	Cost change (%)	Loss of comfort
Rule based	0	0	0
Perfect MPC	-5.0	-10.7	0
Model-based RL	-4.9	-10.6	3.2
Model-free RL	-7.7	-8.0	8.0

#### 5.4.4 Robustness to changing constraints

In real world settings, occupants can interact with the thermal system of the building to adjust the indoor climate according to their needs by altering the temperature setpoint. So far, this setpoint has been considered static. When occupants change this setpoint, the reinforcement learning agent has to adapt the policy it is following to make sure that it continues to perform in a desired manner. Figure 5.11 illustrates the case for a temperature setpoint that is first raised and then lowered before being set back to the original value. It is evident that model-based learning, where planning is decoupled from learning, quickly adapts to the new situation. Model-free learning however performs poorly because existing state-action pairs do not correspond to the updated Q-values anymore. By the time it has begun to learn the new representation, the constraints have changed again. This reflects an aspect of control where model-based learning is better suited than model-free control. However,

given sufficient training data, the model-free controller is also theoretically capable of learning optimal policies in this shifting-constraints regime.

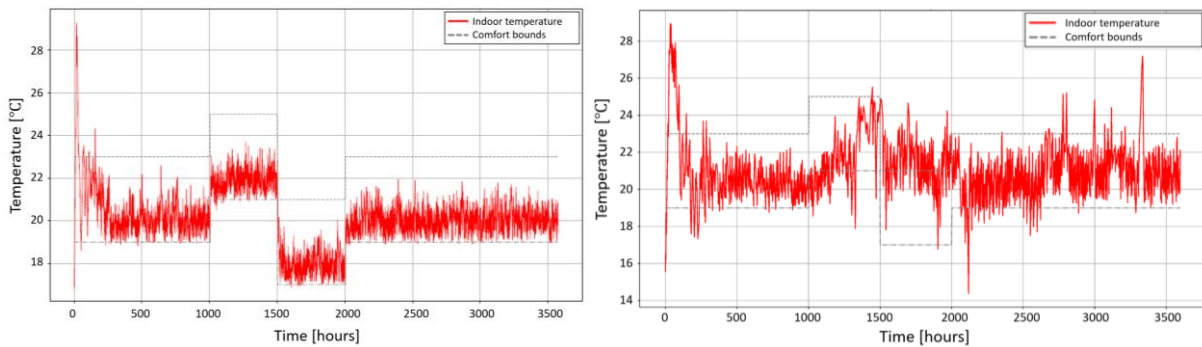


Figure 5.11 Effect of temporally changing constraints for (left) Model-based; (right) Model-free RL.

### 5.4.5 Robustness to incorrect model

In the previous section, it was highlighted how the presence of a model helps the model-based controller to adapt quickly to dynamic conditions. This can, under some circumstances, also be a weakness. More specifically, problems can occur if the model learnt by the agent is incorrect or (as is more often the case) something changes in the environment.

To demonstrate this change in the simulation environment, the backup-controller of the heat pump has been turned on. This is a simple rule-based controller acting as a filter where control actions are overridden if the indoor temperature goes out of the comfort range, turning the heat pump on or off accordingly.  $T_i$  is always kept around the desired limits, but the behaviour of the underlying filter also needs to be learned for simulating transitions. Results are shown in Figure 5.12 for the model-based and model-free controllers. For the model-based agent, close to the comfort boundaries where actions are often overridden, the model fails to predict correctly and the search for optimal policy goes on a wrong trajectory. Since the model is never learned well during the simulation period, wrong commands are issued continuously, and the temperature is regulated entirely by the safety controller, resulting in continued comfort violations as the room temperature often is below the lower comfort level. As opposed to the model-based controller, the model-free RL is less sensitive to changes of the environment dynamics. As seen in Figure 5.12 (right), the controller had no problem in learning a good policy and successfully steering the temperature within an acceptable temperature region.

## 5.5 Conclusion

This chapter has considered applying different types of controllers to a building model simulation with the objective of improving its operation. These operational improvements are made possible by the inherent Energy Flexibility in the building's thermal mass which allows the controller to shift the heating demand forward or backwards in time. Results vary with the choice of the price signal; however, the overall trends remain quite stable: costs can be reduced substantially with reinforcement learning strategies. These findings are summarized in Table 5.3.

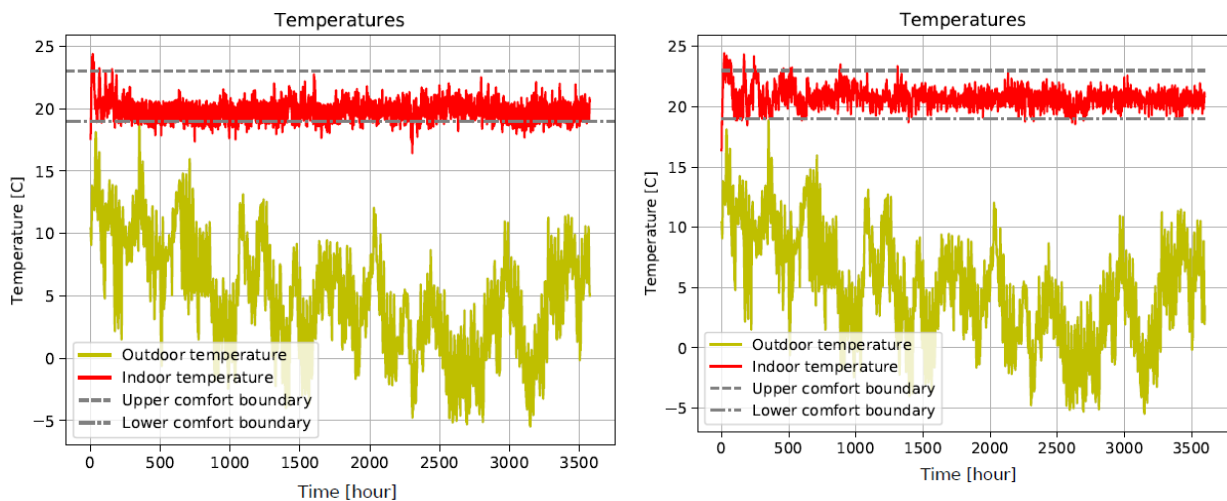


Figure 5.12 Behaviour of the RL agent when the environment has changed for (left) model-based; (right) model-free

Table 5.3 Comparison of key indicators of model-based and model-free RL.

Indicator	Model-based	Model-free
Data efficiency	Low	High
Consumption reduction	4.5-7%	5 -6%
Cost reduction	7-18%	5.5-10%
Exploration cost	Low	High
Comfort loss	Low	High
Computational expense	High	Low

By shifting the demand from times when prices are high to times when prices are low means that the building under consideration can be used as energy storage. The exact extent of this usage and its implications on using building thermal mass for providing services to the electric or thermal grid is an area for future consideration.

While model-free controllers generally under-perform their model-based counterparts, computational complexity is one avenue that might cause model-free algorithms to become more attractive for control in the future. This is especially true in distributed settings where computational budgets are relatively constrained. For instance, for real time planning, control actions have to be generated in limited time horizons which might limit the applicability of model-based algorithms.

# 6 A Model Predictive Controller for Multiple-Source Energy Flexibility in Buildings

Reino Ruusu and Ala Hasan, Technical Research Centre of Finland Ltd., VTT

In this chapter, the development and implementation of a new energy management system (EMS) used for the optimal interaction of a building with the energy networks is presented. The aim of the EMS operation is to reduce the energy cost for electricity and heating of a residential building that has multiple options for flexibility in its energy conversion and storage systems.

The flexibility sources include use of energy storage (electricity in a battery and heat in a hot-water storage tank), operation of a Ground-Source Heat Pump (GSHP), electric heating element and best management of the renewable electricity and heat generated by onsite PV panels, wind turbine and solar-thermal collectors, as well as import and export to the electricity grid and the district heating network.

The EMS is a nonlinear optimization-based model predictive controller (MPC) utilizing successive linear programming (SLP), which makes continuous approximations of the discrete control variables. The EMS is implemented in a 0.1 h time-step in a simulation environment in Matlab and deals with demand and generation data coming from TRNSYS.

The implemented method is shown to be fast, have a low computational complexity and to be accurate compared with a high computational demanding exhaustive search method like Mixed-Integer Linear programming MILP.

Results of the building's energy performance simulation for a whole year indicate reduced energy cost and increased average Coefficient Of Performance (COP) of the heating system. A Rule based control (RBC) showed that energy matching of onsite-generated heat and electricity with the demand is a good rule when the energy export price is lower than the import price. Compared with the RBC, the MPC shows better performance depending on the quality of the forecasted data. The EMS is also suitable for online real-life control of building's energy system operation.

## 6.1 Building and system description

The EMS is used here in a simulation study for the performance of a 150 m<sup>2</sup> single-family house located in Helsinki Finland that has different sources of onsite renewable energy harvesting and storage. The building's energy system is shown in Figure 6.1. It is composed of:

- PV panels 30.27 m<sup>2</sup>
- Small-scale wind turbine (4 kW)
- Solar-thermal collectors SolT (8.6 m<sup>2</sup>)
- Ground source heat pump GSHP (heat output/COP: 4.5 kW/3) at operating temperatures of 60/0 °C.
- Two compartments stratified hot water storage tank (HWST) (0.5 m<sup>3</sup>)
- Electric heating element (EH) at the top of the tank (6 kW, efficiency 0.95)

- Electric battery (12 kWh effective capacity)
- Connections to the electrical and thermal networks

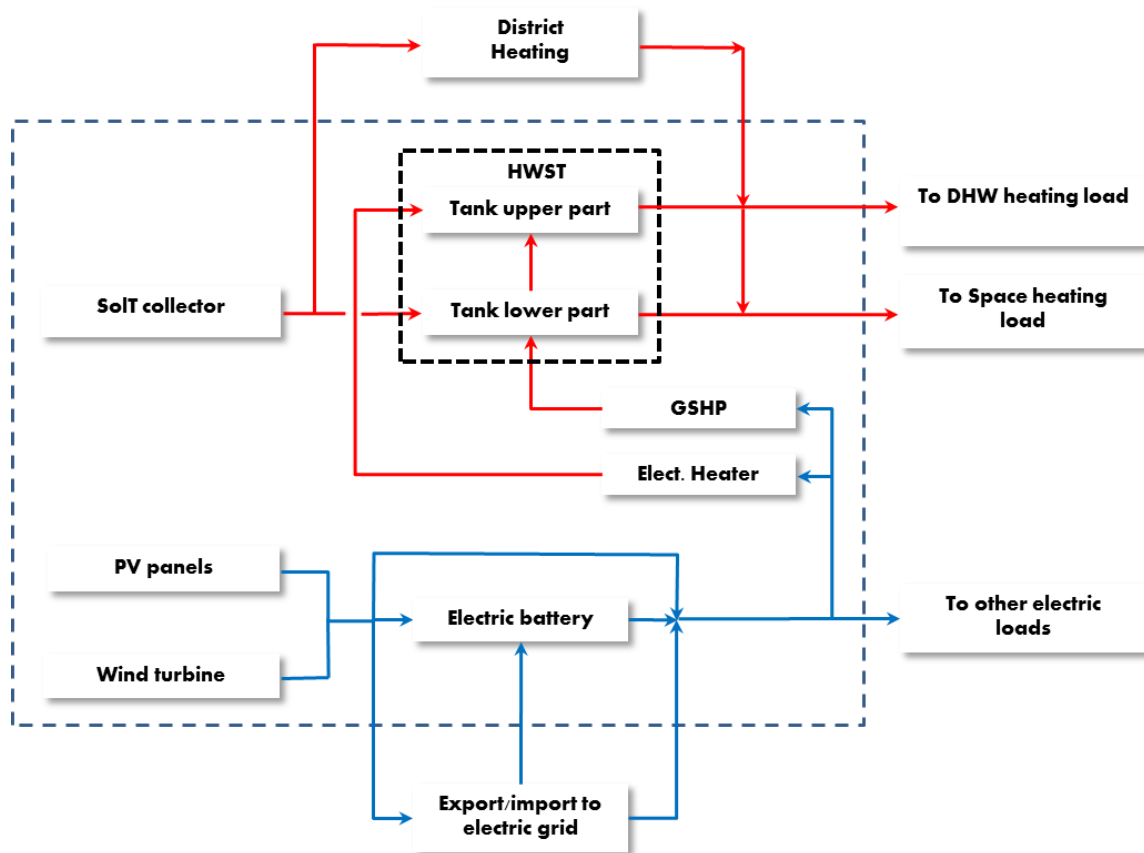


Figure 6.1 Components of the house energy system.

The house space heating system is a low temperature (40 °C supply/30 °C return) hydronic radiator heating. One important detail in the operation of the energy system is the configuration of the different heat flows inside the HWST and its connections (Figure 6.2). Water is circulated for space heating (SpH) from the tank at a minimum temperature of 40 °C. The GSHP supplies heat to the tank at a maximum temperature of 60 °C. The electric heating element (EH) is located in the upper part to keep a minimum temperature of 60 °C for the domestic-hot water (DHW) but can increase the temperature to a maximum of 90 °C when feasible.

The connection of the DHW two heat exchangers in series (for pre-heating in the lower part and after heated by the electric heating element in the upper part – see Figure 6.2) is one main source of non-linearity in this system. Heat can also be taken from a low-temperature district heating network for both space heating and DHW. Heat produced by the solar-thermal collector can be exported to an assumed low temperature return line of the district heating network, which is done by the brine flowing back from the HWST to the collector when the tank average temperature is higher than 68 °C

The EMS aims at covering the building's heat and electricity demands by optimal use of the GSHP, EH and the energy stored in the battery and HWST taking into consideration the next 24 hours forecast of onsite renewable energy harvest and the demand of the building and energy price using 0.1 h time-steps.

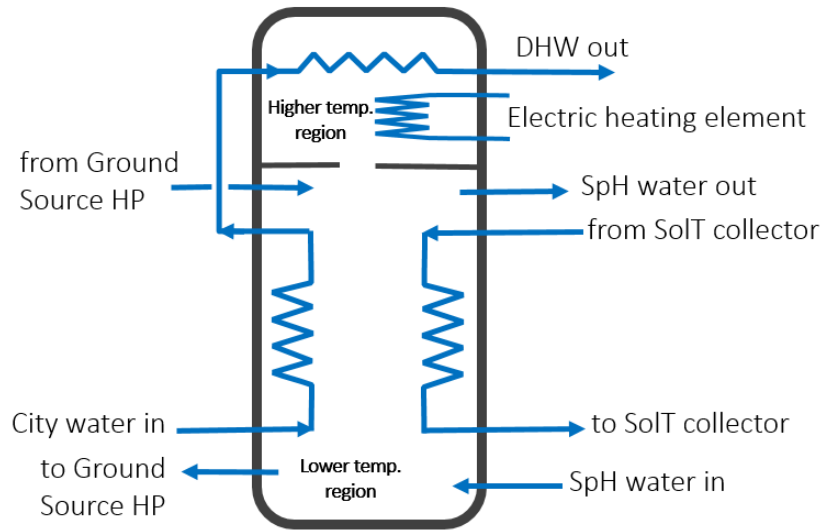


Figure 6.2 Piping and connections of the hot-water storage tank (HWST).

## 6.2 Methodology: control strategies

The objective is to develop a method to minimize energy cost using optimization methods, which should be computationally fast enough to perform full year simulations in a maximum of few days. This is important in both the simulation environment and the real-time operation. The proposed method allows performing whole-year simulations for a non-linear system of non-trivial complexity using 0.1 h and even shorter time-steps. The performance of the MPC during a whole calendar year can be evaluated in only a few days using a detailed simulation model of the energy system (Ruusu et al., 2019).

## 6.3 Results and conclusion

Samples of results of the performance of the EMS for the direct flexibility quantification are demonstrated in this section. Figures 6.3, 6.4 and 6.5 present the case when the exported energy price from the building to the grids is lower than the import price. These three figures show the simulation results for one day in April, which is extracted from the full year simulation performance demonstrating a sample of the results for ease of the analysis. The indicated numbers on the x-axis are the simulation time-steps, each of 0.1 h. The contents of these figures show, from top to bottom, decides to charge electricity to the battery, after that it supercharges the hot-water tank to a higher temperature by using the electric heating element before exporting any left energy to the grids.

The behaviour of the RBC according to the above-mentioned logic can be seen in the simulation results of the day under consideration in Figure 6.3. The increased generated electricity goes to the battery, where the battery state of charge starts to increase at around time-step 70 (7 am) until it is full at around time-step 100 (10 am). After that, the electric heating element is used extensively until it reaches its full power of 6 kW, which brings the top of the HWST to the highest temperature of 90 °C. After having the battery filled and the water tank at the highest temperature, the system starts to export electricity to the grid (bottom graph). The solar-thermal collector heat can be exported to the

district heating network when the temperature of the bottom of the HWST is higher than 68 °C, which was only possible for some instants when the tank was at its highest temperature.

The model predictive controller behaviour is presented in Figures 6.4 and 6.5 with two forecast assumptions: perfect forecast and past 24 hours forecast. Perfect forecast (Figure 6.4) refers to using the exact data of demand and generation for the next 24 hours in the optimization allowing to explore the maximum utilization of the flexibility potential of the energy system. On the other hand, Figure 6.5 shows the model predictive controller behaviour using past 24 hours data that assumes repetition of demand and generation copied from the past 24 hours.

In Figure 6.4, the EMS starts to export the generated electricity at time-step 70 (7 am) when the electricity export price is higher. The temperature of the lower part of the HWST starts to increase at time-step 80 (8 am) by the GSHP operation, after that the solar-thermal collector starts to charge the tank at around time-step 90 (9 am) followed by using the electric heating element at around time-step 100 (10 am) first with limited capacities. This brings the tank to a maximum temperature of 70 °C. However, the EMS is not pushing it towards a very high temperature in order to minimize the use of the low COP electric heating element thus trying to keep all parts of the tank at a closer range of temperatures. Battery charging is shifted to low export price times starting at time-step 120 (12 noon) and the EMS finds it feasible not to push it to a full-charge state.

In Figure 6.5, the EMS starts charging the battery at time-step 70 (7 am), even though it should take advantage of the high electricity price to export. This is because it expects low generation during the day based on the past 24 hours data. Accordingly, it is driving the battery to be fully charged, which stays so for the whole day because the demand is covered by the increased generation. After that, it starts alternatingly to run the electric heating element and export electricity. The HWST temperature starts to increase due to both the solar-thermal heat and the electric heating element operation pushing the top of the tank to reach 90 °C with a large difference between the top and other layers of the tank. It is clear that the inconsistent operation of the EMS with the generation is due to its dependency on poor forecasting of repetition of the past 24 hours data.

Table 6.1 indicates the net yearly results for the income for two cases using the RBC and using the model predictive controller (MPC). In Case 1, the energy export and import prices are equal, while in Case 2, the export price is lower than the import price. The MPC results are indicated using the two forecasting approaches; past 24 hours forecast and perfect forecast.

It is clear from the results that imports from the district heating were almost negligible in all cases. This is due to the high use of the GSHP, which has a high COP, making it cheaper than importing heat from the district heating.

In Case 1, the total annual income of the two MPC strategies with past 24 hours and perfect forecast are close. This indicates that using the imported energy or the onsite harvested energy are of similar values since the import and export prices are equal, which makes it possible to use the grid as a storage by importing and exporting larger amounts of energy according to the price fluctuations. On the other hand, the RBC appears to make much lower income due to its limited interaction with the grids due to its focus on the instantaneous needs.

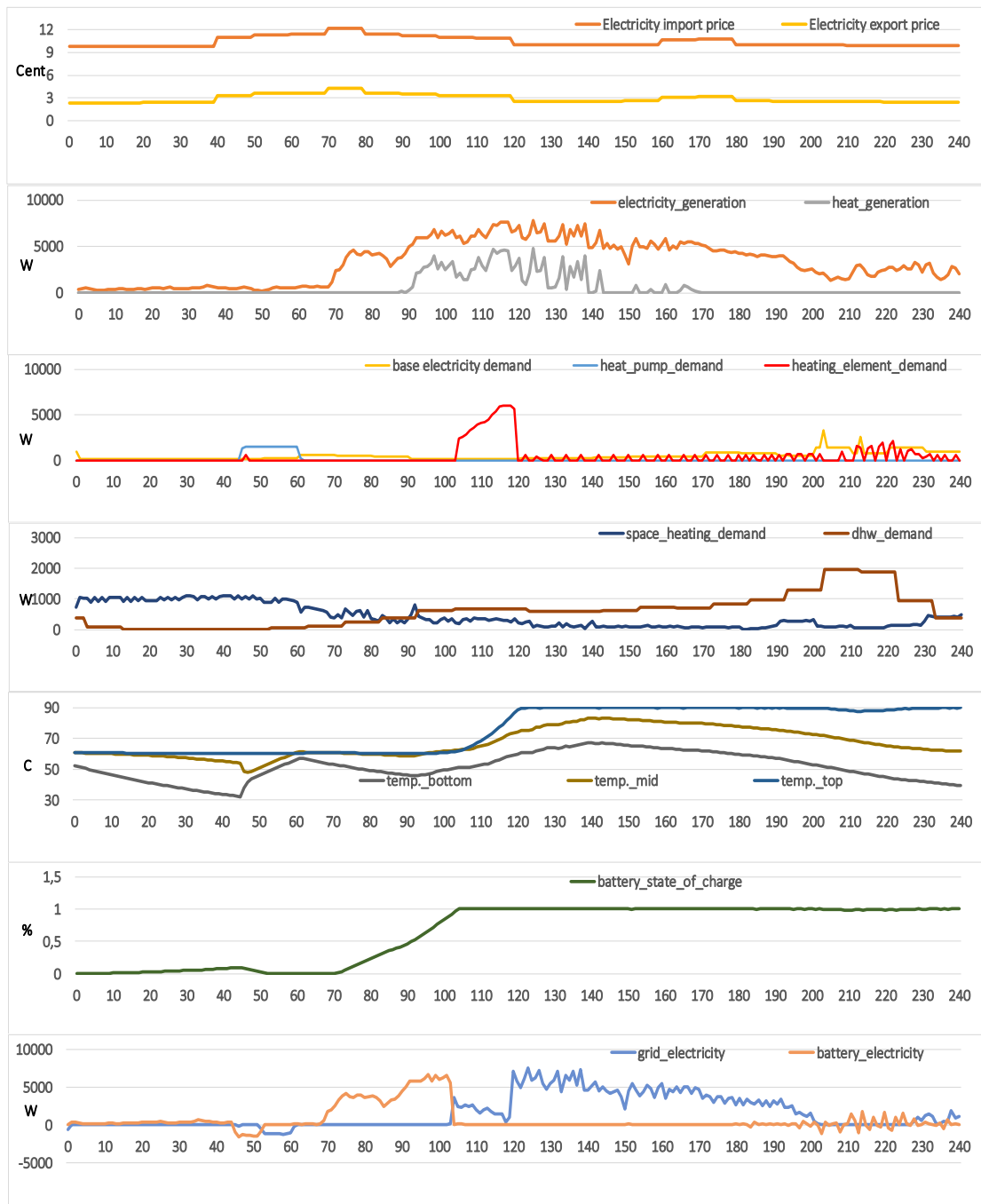


Figure 6.3 Rule-based controller behaviour on the 8<sup>th</sup> of April with 0.1 h time-step.

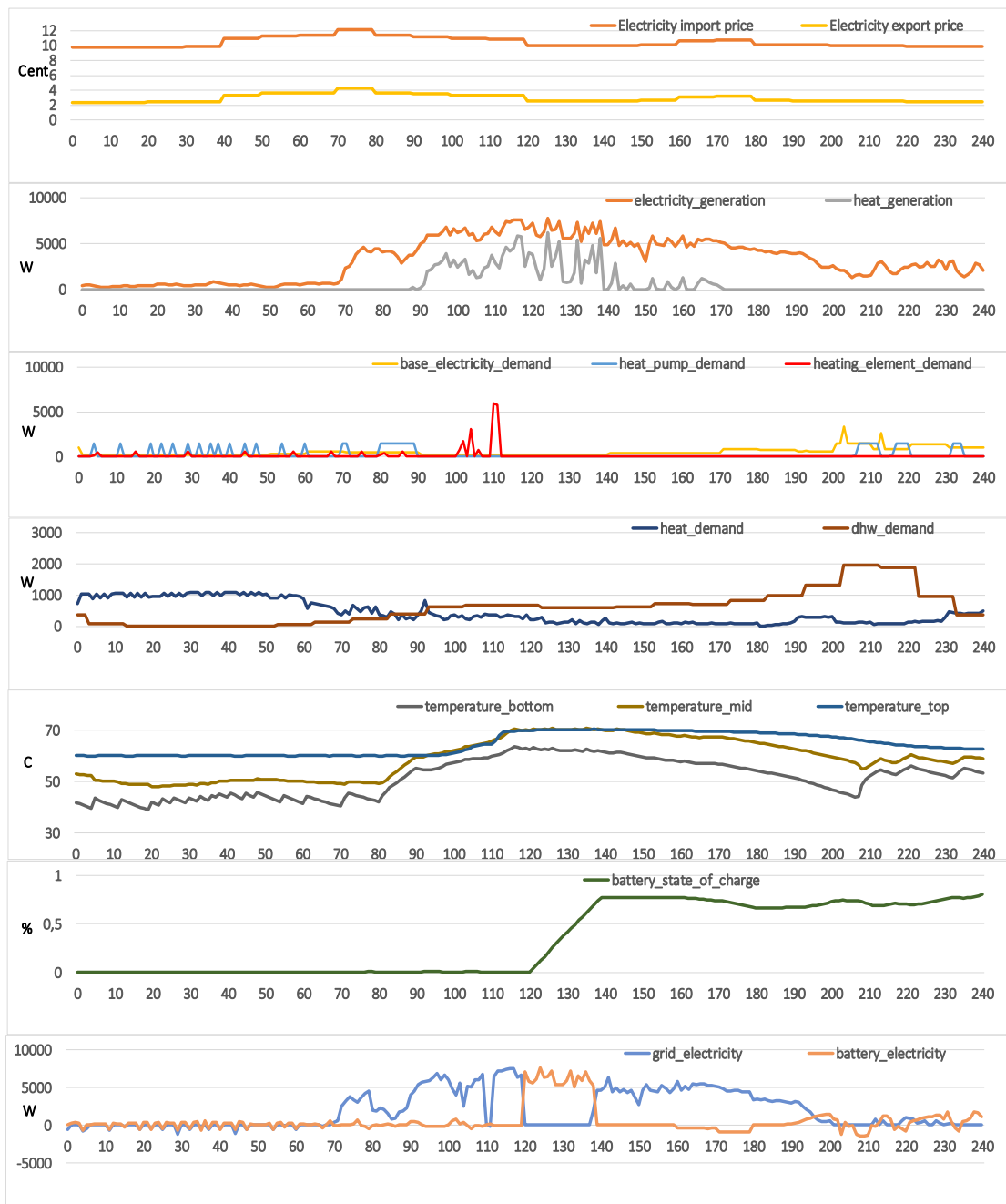


Figure 6,4 Model predictive controller behaviour on the 8<sup>th</sup> of April with 0.1 h time-step: Case 2 using the perfect forecast.

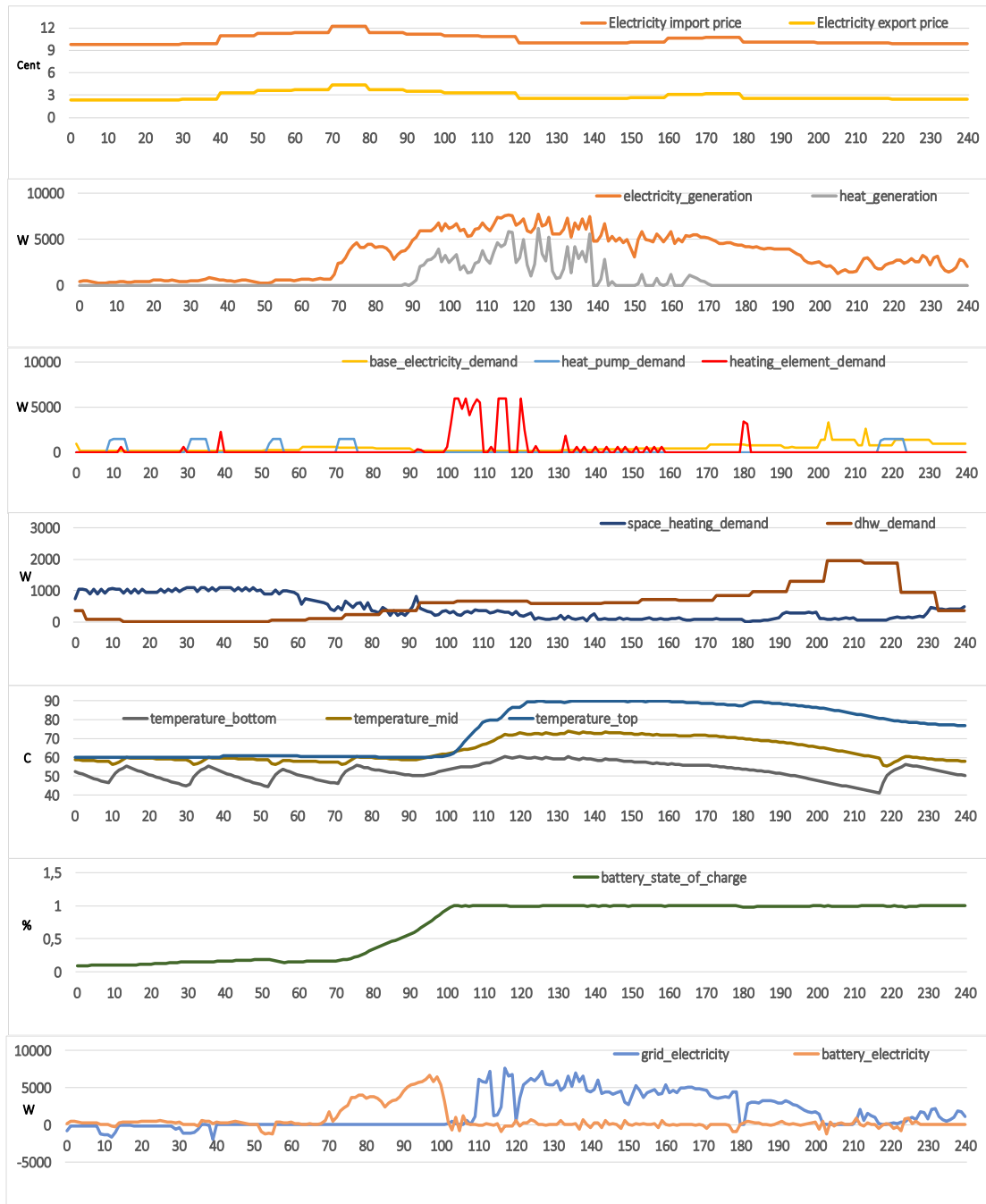


Figure 6.5 Model predictive controller behaviour on the 8<sup>th</sup> of April with 0.1 h time-step: Case 2 using the past 24 hours as forecast.

In Case 2, it can be noticed that the total income for the three control strategies shows negative values, which indicates that energy cost at the end of the year is higher than the income made of selling energy. Due to the lower export price, the system is interacting with the grid less compared to Case 1. It can be seen that the MPC with the perfect forecast makes better use of the flexibility sources in the building resulting in a better economic situation. The total results for the RBC case and the MPC with 24 hours forecasting are close, indicating that giving preference to energy

matching of the onsite harvested energy with the demand is a good strategy when there is lower export price, thus avoiding imports at a high price.

Income from the solar-thermal collector heat export to the district heating is close in each case and is not affected by the control strategy. This is due to the set temperature of 68 °C at the bottom of the tank to allow heat export.

Table 6.1 Net yearly income: Case 1 (equal energy import and export prices) and Case 2 (lower energy export prices).

		Income (€) Case-1			Income (€) Case-2		
		Rule-based (RBC)	MPC-Past 24h forecast	MPC-Perfect forecast	Rule-based (RBC)	MPC-Past 24h forecast	MPC-Perfect forecast
Electricity	Import	-221	-446	-435	-221	-272	-216
	Export	226	613	605	61	115	103
Heating	Import to space heating	0	-0.1	-0.1	0	-0.1	-0.1
	Import to DHW	0	-0.4	-0.6	0	-0.4	-0.2
	Export from solar-thermal	95	94	96	40	45	40
Total		99	260	265	-120	-113	-74
Improvement to RBC			161	166		7	46

The developed MPC method is shown to be fast and thus suitable for use in detailed simulation-optimization evaluations of multiple flexibility sources. Energy matching of onsite harvested energy with the demand is shown to be a suitable control method when the energy export price is lower than the import price. The MPC performance is shown to be affected by the quality of the forecasting data.

A description of the mathematical background of the developed MPC and its performance in the simulation environment is presented in details in (Ruusu et al., 2016) and (Ruusu et al., 2016). Description of the performance of a test facility that uses this developed MPC EMS in real-time operation is presented in Deliverable 6 - Test procedure and results. Description of that facility before integrating the EMS is presented in (Kilpeläinen et al., 2018).

## ACKNOWLEDGEMENTS

This work was carried out within the project “Advanced Local Energy Matching in Future Smart Hybrid Networks 2014-2018 decision no. 277680”, which was mainly funded by the Academy of Finland.

# 7 Model predictive control for carbon emissions reduction in residential cooling loads

Thibault Péan, Catalonia Institute for Energy Research, Spain

A model predictive control (MPC) strategy aiming at reducing the operational CO<sub>2</sub> emissions is tested on a residential building equipped with a reversible heat pump. Through a co-simulation study on a three days summer period, the performance of the controller is evaluated in cooling mode: it enables to save 19.1 % emissions compared to a standard thermostatic control. The control algorithm, its implementation and the development efforts are also discussed.

## 7.1 Building and system description

The building case-study is a residential flat of 110 m<sup>2</sup> net heated floor area, located in the Terrassa (Barcelona), Spain and inhabited by a family of four people. The 3D model, a photograph and the floor plan are shown in Figure 7.1. The building comprises 4 bedrooms, a living room, kitchen and a bathroom. It was built in 1991 and forms part of a multi-family-dwelling of 4 floors. A model of the flat was created and validated in TRNSYS (Ortiz et al., 2016), this model is used here, so the presented study consists only of simulation work. Furthermore, a refurbished version of the building is considered: a layer of 12 cm insulation is added within the external walls, bringing the U-value of these walls down to 0.20 W/(m<sup>2</sup>.K), compared to 0.60 W/(m<sup>2</sup>.K) before. The occupancy by the four family members is modelled stochastically.

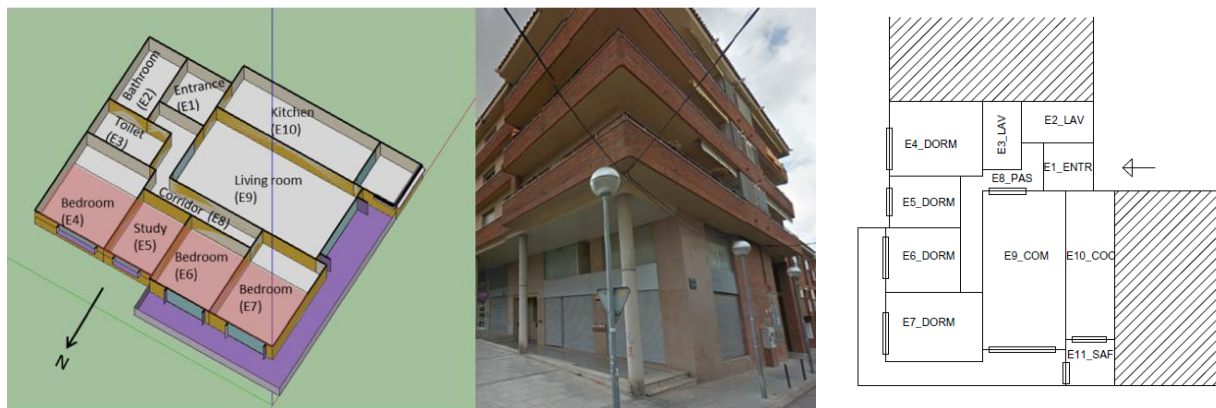


Figure 7.1 3D model, photograph, and floor plan of the studied building.

The building is conditioned by a circuit of Fan Coil Units (FCU), which are supplied by an air-to-water heat pump. The heat pump is reversible; thus, it can work in cooling mode in summer and heating mode in winter. Furthermore, the frequency of its compressor can be controlled in a certain range, thus it is a variable speed heat pump (VSHP). The indoor unit of the VSHP contains a 200 liters tank for storing domestic hot water (DHW).

The control strategies apply to the whole HVAC system. The commands are sent directly to the heat pump, ordering it to function either for space heating/cooling (SH/SC) or for DHW production, and at which supply temperature. When the heat pump is activated for SH/SC, the same commands are sent to the FCU so that they run in a synchronized way. Furthermore, the control strategies for heating and cooling apply to the overall apartment at once, there are no independent individual controls in the rooms.

## 7.2 Methodology: control strategies

A Model Predictive Control strategy is implemented in the building to control the heat pump and the FCU systems. The present study focuses on the cooling mode, therefore, only results from the summer season will be presented. The MPC control strategy intends to minimize the CO<sub>2</sub> emissions resulting from the electricity use of the heat pump system, hence aiming at reducing the impact of the HVAC systems use on the environment and climate change.

To this end, an external penalty signal is utilized: this signal represents the marginal CO<sub>2</sub> emissions of the electrical grid every hour. The marginal emissions factor (MEF) takes into account the merit order in which the plants are activated to supply the demand at a national scale (in Spain in the present case), and their respective emission factors. It represents in a more accurate way the savings that can occur after demand-side management or flexibility actions: these fluctuations will be absorbed by certain peak power plants for example, but the operation of the base power plants will not be affected, and this is thus reflected in the MEF. In the present case, a model of the marginal emissions factor for the Spanish grid was developed based on analysis of past data (Péan et al., 2018a). These raw data consisted of the hourly energy mix of Spain during one entire year (2016) and enabled to identify the CO<sub>2</sub> intensity of that grid, knowing the CO<sub>2</sub> emissions associated with each source of electricity.

The applied MPC strategy belongs to the class of indirect controls: it is provided with an external fluctuating signal, and will intend to shift the loads to where this penalty signal is the lowest. To achieve this objective, energy is stored in thermal form in the mass of the building and in the water tank for DHW.

The MPC optimization problem takes the form of Problem 1 shown hereafter. The model is a classical state-space model used to estimate the dynamics of the building envelope and was represented as a resistance-capacitance (RC) network with three states  $\mathbf{x} = [T_{int} \ T_w \ T_{TES}]^T$ , the temperatures in the inside zone, at the surface of the walls and in the Thermal Energy Storage (TES) tank. The MPC determines the controllable inputs  $\mathbf{u} = [Q_S \ Q_{TES}]^T$ , the thermal powers that the heat pump must deliver to the fan coils or the tank. As external inputs  $\mathbf{e} = [T_{amb} \ I_H \ Q_{occ} \ Q_{DHW}]^T$ , the outside temperature, the solar irradiation, the heat due to occupants and the DHW tappings are taken into account by the model (forecasted perfectly in the MPC framework). The model is also described in (Péan et al., 2018b).

---

**Problem 1 – Model Predictive Controller**


---

**Objective:**

$$\min_{u, \delta} [\alpha_\varepsilon J_\varepsilon + \alpha_{\Delta u} J_{\Delta u} + (1 - \alpha_\varepsilon - \alpha_{\Delta u}) J_{CO_2}]$$


---

**Subject to:**

$$\forall k \in \llbracket 1, N \rrbracket$$

**Model:**

$$\begin{cases} \mathbf{x}(k+1) = \mathbf{A} \cdot \mathbf{x}(k) + \mathbf{B}_u \cdot \mathbf{u}(k) + \mathbf{B}_e \cdot \mathbf{e}(k) \\ \mathbf{y}(k+1) = \mathbf{C} \cdot \mathbf{x}(k) \end{cases}$$

**Constraints on the inputs:**

$$\begin{cases} \delta_S(k) \cdot \underline{Q_{SC}} \leq Q_{SC}(k) \leq \delta_S(k) \cdot \overline{Q_S} & \text{with } [\underline{Q_{SC}}; \overline{Q_{SC}}] = [-8 \text{ kW}; -2.5 \text{ kW}] \\ \delta_{TES}(k) \cdot \underline{Q_{TES}} \leq Q_{TES}(k) \leq \delta_{TES}(k) \cdot \overline{Q_{TES}} & \text{with } [\underline{Q_{TES}}; \overline{Q_{TES}}] = [10 \text{ kW}; 10 \text{ kW}] \\ \delta_S(k) + \delta_{TES}(k) \leq 1 \end{cases}$$

**Constraints on the outputs:**

$$\begin{cases} T_{int}(k) \leq \overline{T_{int}}(k) + \varepsilon(k) & \text{with } \overline{T_{int}} = 26 \text{ }^\circ\text{C} & (\varepsilon \geq 0) \\ T_{TES} - \varepsilon(k) \leq T_{TES}(k) & \text{with } \overline{T_{TES}} = 50 \text{ }^\circ\text{C} & (\varepsilon \geq 0) \end{cases}$$


---

The cost function comprises three distinct objectives: a smoothing term  $J_{\Delta u}$ , a comfort term  $J_\varepsilon$ , and a CO<sub>2</sub> minimization term  $J_{CO_2}$ . The smoothing term penalizes too many consecutive changes in the control actions, to avoid oscillatory behavior of the systems. The comfort term penalizes excursions outside the hard comfort constraint ranges: upper bound of  $\overline{T_{int}} = 26 \text{ }^\circ\text{C}$  in the zone and lower bound of  $\overline{T_{TES}} = 50 \text{ }^\circ\text{C}$  in the tank. These hard constraints are softened with the  $\varepsilon$  slack variable which is included in the comfort objective  $J_\varepsilon$ . The actual flexibility objective is  $J_{CO_2}$ , it corresponds to the emissions due to the electricity use of the heat pump:

$$J_{CO_2} = \sum_{k=1}^N P_{el,HP}(k) \cdot MEF(k) \quad 7.1$$

The electricity consumption (in kWh) of the heat pump  $P_{el,HP}$  depends on its thermal power  $Q$ , and is determined through a model based on experimental tests data. The hourly MEF is derived from the model previously mentioned and is expressed in kgCO<sub>2</sub>/kWh. The whole cost function must be minimized over a time horizon of 24 hours, which enables to capture daily patterns.

The three objectives are weighted in the overall cost function by the coefficients  $\alpha_\varepsilon$  and  $\alpha_{\Delta u}$ . To determine appropriate values of the weighing coefficients, Pareto curves are plotted as shown in Figure 7.2. The points situated more in the hollow of the curve present the best balance between the different objectives. In the present case,  $\alpha_{\Delta u} = 0.01$  and  $\alpha_\varepsilon = 0.15$  were chosen. It should be noted that the choice of these coefficients can greatly affect the performance of the MPC controller, since this will determine whether it emphasizes more the flexibility while sacrificing the comfort of the occupants, or if it won't make any compromise on the comfort but then will not provide sufficient flexibility.

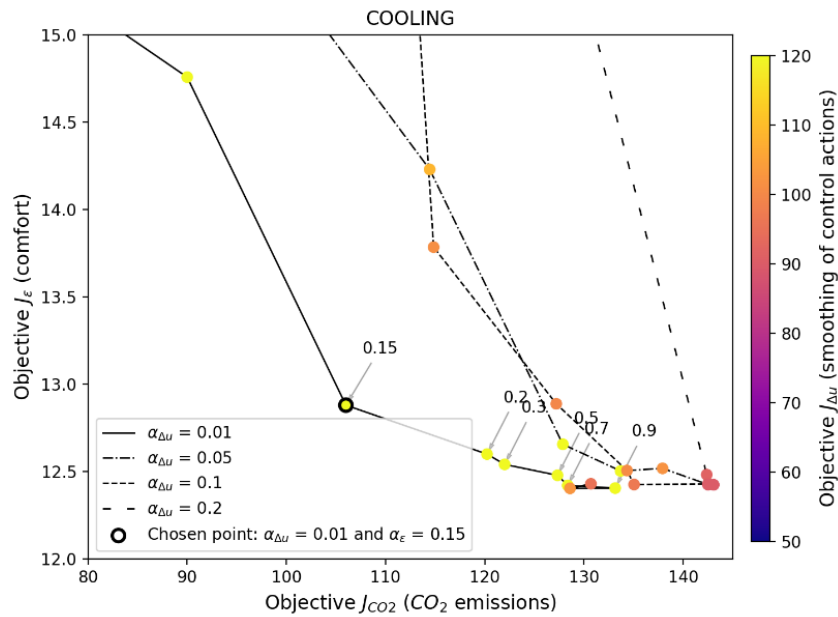


Figure 7.2 Pareto curves to find appropriate values of the weighting coefficients (Péan et al., 2019).

### 7.3 Implementation: control algorithms

The aforementioned control strategy is implemented in a co-simulation platform presented in Figure 7.3. The TRNSYS detailed model is used as the building on which the MPC controller can be tested. The controller is externalized in MATLAB to benefit from its stronger optimization features. The link between both software packages is realized with the Type155 of TRNSYS.

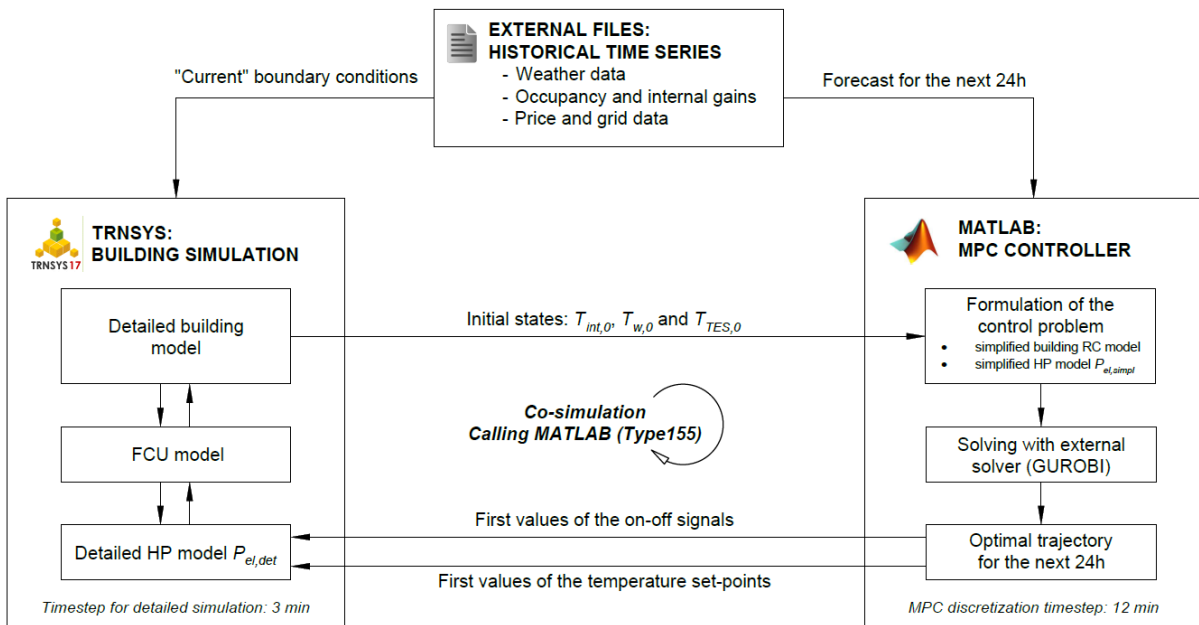


Figure 7.3 Co-simulation platform with TRNSYS and MATLAB (Péan et al., 2019).

The algorithm of the MPC is written in MATLAB code. To this end, the YALMIP tool is used to facilitate its formulation (Lofberg, 2004). YALMIP enables to declare the optimization variables (continuous or integer variables) and formulate the optimal control problem including the minimization objective and the constraints. This tool also facilitates the interface with different external solvers, and thus enables to solve many different types of optimization problems.

In the present case, both integer (switching binary variables) and continuous (thermal powers) variables are present within the optimal control problem. The presence of the integer variables complicates the optimization problem substantially. However, they enable to switch between DHW production and space cooling mode and to force a minimum level of power whenever the heat pump is switched on and are therefore indispensable. Because of the nature of the problem, MATLAB must resort to mixed-integer programming to solve it.

Once the problem is formulated with YALMIP, the GUROBI solver is called (Gurobi Optimization, 2018a). GUROBI utilizes a branch-and-bound algorithm (Gurobi Optimization, 2018b). Several options can be passed from MATLAB to the solver through YALMIP, like for example a time limit for the calculations, a maximum number of iterations, or the tolerance at which the convergence calculation will be stopped.

## 7.4 Results and conclusion

The MPC CO<sub>2</sub> minimization strategy is tested with the co-simulation platform on 3 selected days of summer 2016. Time series are presented in Figure 7.4, and summed indicators in Table 7.1, through a comparison with a standard thermostatic control case.

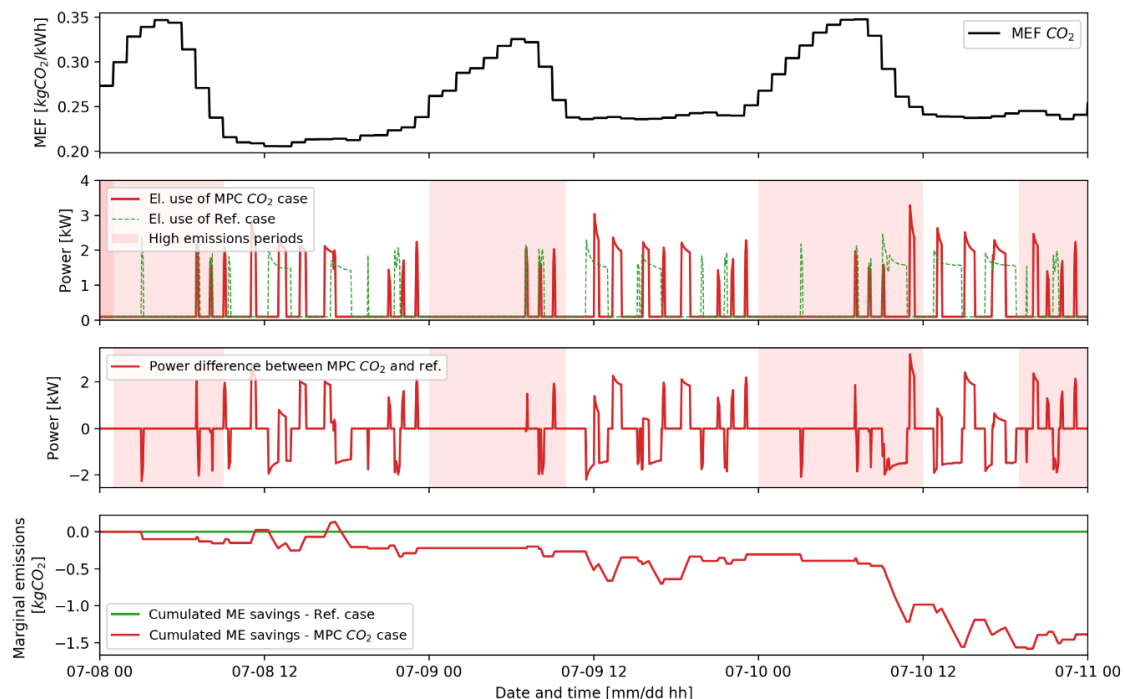


Figure 7.4 Time series of the MEF penalty signal (top), the electrical use of the heat pump in the reference and MPC CO<sub>2</sub> case (second), power difference between these two cases, and finally the cumulated ME savings (bottom) (Péan et al., 2019).

Table 7.1 Summary of the energy and emissions metrics of the MPC CO<sub>2</sub> case compared to the reference case with thermostat.

MPC objective case		MPC CO <sub>2</sub>
Thermal energy use compared to reference case	[kWh]	-15.35
	[%]	-18.8%
Electricity use variation compared to the reference case	[kWh]	-5.15
	[%]	-16.6%
Average CO <sub>2</sub> emissions variation compared to the reference case	[kgCO <sub>2</sub> ]	-1.22
	[%]	-16.8%
Marginal CO <sub>2</sub> emissions variation compared to the reference case	[kgCO <sub>2</sub> ]	-1.39
	[%]	-19.1%
Flexibility factor	[ - ]	0.34

A certain load shifting occurred towards the periods of lower emissions, although the reference case already used little energy in the high emissions periods so there was little room for improvement. The flexibility factor (Le Dréau and Heiselberg, 2016) is chosen as KPI for evaluating the load shifting: it is calculated with  $FF = \left( \int_{lp} P_{el} - \int_{hp} P_{el} \right) / \left( \int_{lp} P_{el} + \int_{hp} P_{el} \right)$ , where  $\int_{lp} P_{el}$  is the integral of the heat pump consumption during low-price periods (*hp* respectively for high price periods). *FF* should therefore ideally be 1 if all the energy is used in low emissions periods. In the present case, the flexibility factor was increased from 0.28 to 0.34. The amplitude of the load-shifting is thus rather small. The overall operation dictated by the MPC strategy resulted in 19.1 % savings in CO<sub>2</sub> marginal emissions. The MPC strategy lowers the delivered thermal energy to the building, leading to a small decrease of the occupants' comfort, as shown in Figure 7.5, however the acceptable range (Category III) is always maintained.

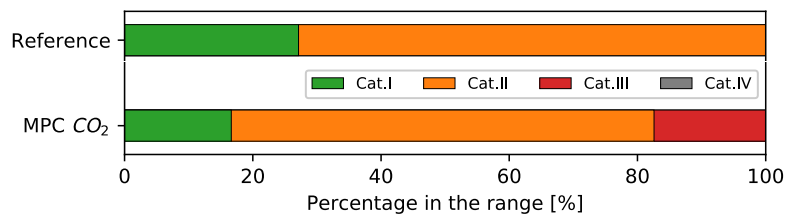


Figure 7.5 Percentage of times in the comfort ranges, as defined in the standard EN 15251 (CEN, 2007) by ranges of operative temperatures for the cooling season.

The achieved savings are significant, although they are mainly due to a reduction of the energy use, less so from the load shifting. In fact, the load shifting is rather limited in the present case and that might be due to the penalty signal used, as shown in the top graph of Figure 7.4: this signal does not present very large variations, and therefore does not differentiate clearly between periods of lower emissions from the periods of higher emissions. In the case of a price signal for instance, the clear discrepancy between day and night tariffs (e.g. 60 €/MWh at night and 120 €/MWh during the day, hence doubling the price) facilitates the task of the MPC by highlighting more clearly the periods of lower penalty. The MEF signal has been chosen because it presents larger variations than the

average emissions factor, but it might not be sufficient, and designing a new penalty signal based on the CO<sub>2</sub> emissions might yield better results.

The development and computational burdens of the MPC should also be discussed. Creating an MPC controller requires simplified models of the building and of the heat pump performance. These tasks require a lot of resources, since many adaptations are needed depending on the building typology, the HVAC systems in use, the season etc.. Fine-tuning all the parameters of the MPC is very important for the good performance of the controller, therefore this task cannot be eluded. This obstacle partly explains the still low penetration of MPC controllers for HVAC control in real buildings. Furthermore, in the present case the nature of the problem (mixed-integer programming) resulted in high solving times. This computational burden and the consequent constraints should be taken into account for real implementations. It is hoped that the constant improvement in computational performance will make this barrier less significant in the future.

This work features only simulation work and neglects the dynamics of the heat pump, i.e. if the MPC decides to supply heat during one hour with water at 50 °C, the current TRNSYS model will provide exactly that. In reality, the inertia and dynamics of both the building and the heat pump play an important role and create transient effects that the MPC ignores in its current form. Especially at start-up, the delays and the slow ramping before reaching the desired setpoint create important discrepancies between the plan anticipated by the MPC and the actual operation of the systems. These dynamic effects should be studied with real heat pump systems in laboratory or real-building setups. When implementing such controls with a real heat pump, the actual commands sent to the systems should be considered carefully: not all the parameters can be controlled directly, a lot of protection and local controllers operate the heat pump and its components at a lower control level, therefore the interaction with the higher level MPC is not always straightforward.

# 8 Investigation of the Energy Flexibility of a residential net-zero energy building involved with the dynamic operations of hybrid energy storages and various energy conversion strategies

Yuekuan Zhou and Sunliang Cao, The Hong Kong Polytechnic University, Hong Kong SAR, China

This section aims to quantitatively investigate the Energy Flexibility of a residential net-zero energy building (NZEB) in the cooling dominated region, Hong Kong. An interactive energy sharing network with various integrated systems was formulated and demonstrated through a building-vehicle energy system. The integrated systems include the on-site renewable system, hybrid thermal storage systems, a static battery, and a mobile battery of an electric vehicle. Different rule-based control strategies were proposed and contrasted in terms of the Energy Flexibility enhancement of the interactive energy sharing network. Moreover, to fully utilize the Energy Flexibility provided by the hybrid thermal storage systems, technical solutions were proposed, such as the excess renewable-thermal storage recharging strategy and the structural thermal mass of the building. Simulation results for different scenarios are presented to demonstrate and verify the effectiveness of the proposed technique.

## 8.1 Building and system description

The simulated single-family house is located at New Territory, a suburb in Hong Kong (22.3 °N, 114.2° E). Geometrical parameters of the simulated building are shown in Figure 8.1. The length and the width of the building are both 10 m. Each floor has the net floor area of 100 m<sup>2</sup>. The height of each floor is 3 m. There are four different thermal zones on each floor, including a living room, a bedroom, a kitchen and a washroom. The window-wall ratio is 30 %, which is common for residential buildings in Hong Kong (Ghisi et al. 2004). The annual cooling degree days (base temperature of 18 °C) and the annual solar radiation on a horizontal surface are 284 K and 1423.3 kWh/(m<sup>2</sup> a), respectively. Figure 8.1 shows the meteorological parameters in Hong Kong. The monthly average ambient temperature varies between 16 and 28.2 °C. The monthly solar radiation on a horizontal surface varies between 63.6 and 168 kWh/(m<sup>2</sup> mon). Moreover, compared to the monthly solar radiation, the monthly average wind speed (10 m above the ground) is more stable with the fluctuation range between 4.6 and 5.7 m/s, except for July with a magnitude of 3.6 m/s.

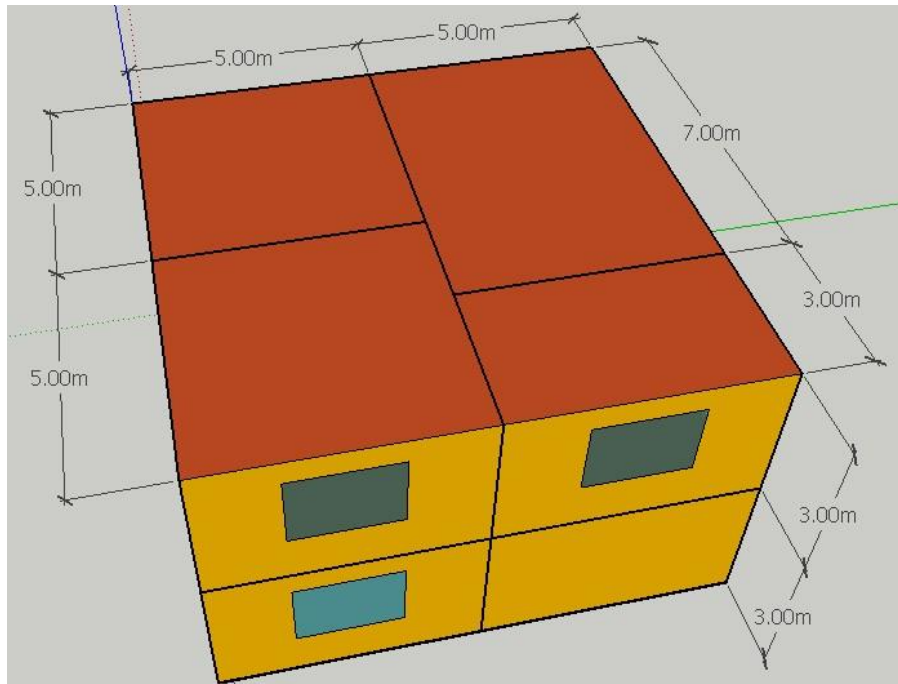


Figure 8.1 Geometrical parameters of the simulated single-family house.

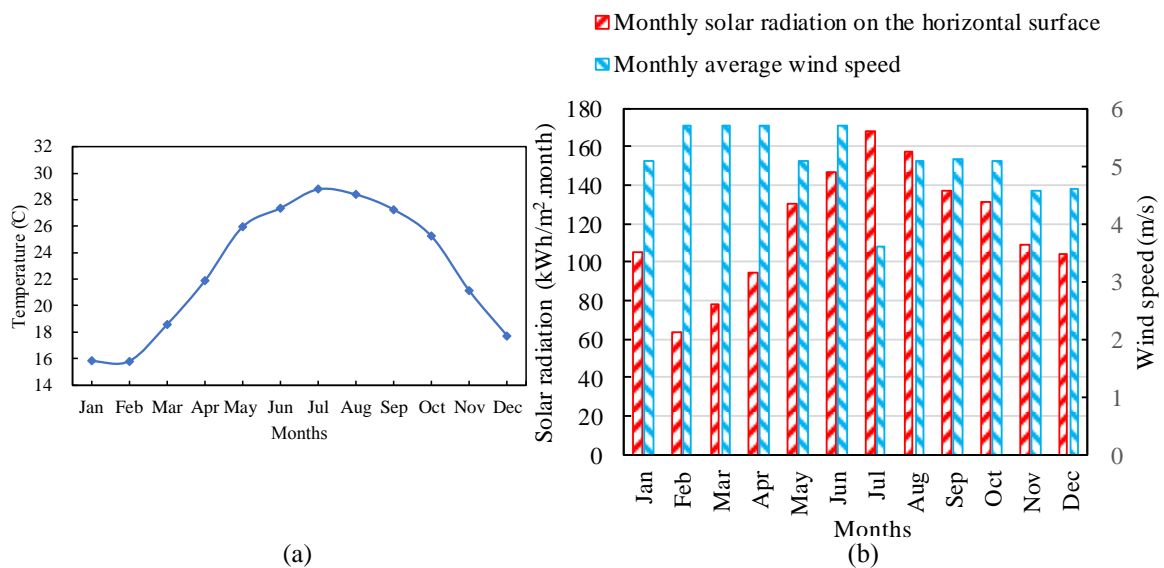


Figure 8.2 Meteorological parameters in Hong Kong: (a) The monthly average ambient temperature; (b) The monthly average wind speed and the monthly solar radiation on a horizontal surface.

### 8.1.1 Parameters for the building facade, the infiltration and internal gains

Table 8.1 lists the parameters of the building envelope according to (Burnett et al. 2004). The infiltration coefficient is calculated by the equivalent air change rate of 0.5 per hour (Burnett et al. 2004).

Table 8.1 Parameters of the building envelope (Burnett et al. 2004).

External Walls (front/inside)	Thickness (m)	Material	$\lambda$ (W/m K)	$\rho$ (kg/m <sup>3</sup> )	$C_p$ (J/kg K)	Absorptivity ( $\alpha$ )
Layer 1 (outside)	0.005	Mosaic tiles	1.5	2500	840	0.58
Layer 2	0.01	Cement/sand Plastering	0.72	1860	840	
Layer 3	0.1	Heavy concrete	2.16	2400	840	
Layer 4 (inside)	0.01	Gypsum plastering	0.38	1120	840	0.65
<b>Roofs (front/inside)</b>						
Layer 1	0.025	Concrete tiles	1.1	2100	920	0.65
Layer 2	0.02	Asphalt	1.115	2350	1200	
Layer 3	0.05	Cement/sand Screed	0.72	1860	840	
Layer 4	0.05	Expand Polystyrene	0.034	25	1380	
Layer 5	0.15	Heavy concrete	2.16	2400	840	
Layer 6	0.01	Gypsum plastering	0.38	1120	840	0.65
<b>Windows</b>						
Layer 1	0.006	Tinted glass	1.05	2500	840	0.65

The annual internal heat from the lighting and electrical appliances are 36.8 and 36.9 kWh/(m<sup>2</sup> a), respectively. There are 6 occupants in the single-family house. The average internal heat gain (including both the sensible and the latent) from each occupant is 126 W with respect to the metabolic rate of 1.2 MET and the clothing insulation of 0.6 Clo. The total heat gain of each zone is dependent on the occupants' schedule, which can be found in the reference (Burnett et al. 2004).

### 8.1.2 Building services system

The natural ventilation system is manually operated by opening windows unless the outdoor temperature is higher than 22 °C (Burnett et al. 2004). The air change rate of the mechanical ventilation is 5 ACH according to (HVAC 2012). The volume flow rate of the fresh air is 1 l/(m<sup>2</sup>s), which is within the range between 0.36 and 2.7 l/(m<sup>2</sup>s) as shown in the reference (Burnett et al. 2004). A total heat recovery system (rotatory wheel) is designed in the system for recovering of the cooling energy of the exhaust air to pre-cool the fresh air. The sensible and the latent efficiencies of the rotatory heat recovery system are 0.85 and 0.5, respectively. The desired supply air temperature is 18 °C in the system. Air source chillers are designed to cover both the air handling unit (AHU) cooling load and the space cooling (SC) load. The heating load, which is covered by the electric heater, is 5.3 kWh/(m<sup>2</sup>a). A solar thermal collector system is designed with a tilted angle, an azimuth angle and an area of 18°, 0° (facing directly southern) and 9 m<sup>2</sup>, respectively. The total number of occupants is six, and the specific daily DHW consumption is 0.12 m<sup>3</sup>/(person) (PRCMC 2002). Moreover, the AHU cooling storage tank (ACST) and the space cooling storage tank (SCST) are designed to cover the daily AHU cooling load and the daily space cooling load with the volume/height of 1.5 m<sup>3</sup>/1.15 m and 0.5 m<sup>3</sup>/0.84 m, respectively. The volume/height of the DHW tank is 1 m<sup>3</sup>/1.08 m. The heat transfer coefficient to the ambient of each tank is assumed to be 0.3 W/(m<sup>2</sup>K). To meet the building energy demand, both the AHU cooling chiller (called the normal AHU cooling chiller) and the SC cooling chiller (called the normal space cooling chiller) are designed to charge the ACST and

SCST, respectively. In addition, when the renewable generation is higher than the basic electric load, the surplus renewable electricity can be operated to charge the ACST (called the excess REe-ACST recharging strategy), or to charge the SCST (called the excess REe-SCST recharging strategy), or to charge the DHWT (called the excess REe-DHW recharging strategy). The control scope includes the indoor air set-point temperature of each thermal zone, the excess renewable-recharging thermal systems and the excess renewable-recharging battery systems. The water flows through the DHW tank before being heated by the auxiliary electric heater to the required temperature of 60 °C. The cooling system includes an AHU cooling chiller, an ACST, a space cooling (SC) chiller, a SCST and control pumps. Moreover, two excess renewable-recharging chillers are installed for recharging the ACST and the SCST with the assumed nominal COP of 2.1 and of 2.6 (considering the outlet temperature of chilled water at 1 °C and 9 °C), respectively. Table 8.2 lists the parameters of the cooling system. The nominal COPs of both normal chillers are assumed to be 3.6.

Table 8.2. Parameters of the thermal storage tanks, the heat transfer fluid and the devices.

	Normal AHU cooling chiller	Excess REe-ACST recharging chiller	Normal space cooling chiller	Excess REe-SCST recharging chiller	Excess REe-DHWT
	Nominal COP <sup>a</sup> : 3.6	Nominal COP <sup>b</sup> : 2.1	Nominal COP: 3.6 <sup>c</sup>	Nominal COP: 2.6 <sup>d</sup>	
Set-point temperature	7 °C	1 °C	15 °C	9 °C	60-100 °C
Heat transfer fluid	Water	20 vol% Ethylene Glycol	Water	Water	Water
Size of thermal storage tanks	1.5 m <sup>3</sup> , 1.15 m height		0.5 m <sup>3</sup> , 0.84 m height		1 m <sup>3</sup> volume, 1.08 m height

<sup>a</sup> nominal cooling conditions: Evaporator water inlet/outlet temperature 12/7 °C, external air temperature 35 °C;

<sup>b</sup> The assumed COP, nominal cooling conditions: leaving chilled water temperature of 0 °C, external air temperature of 35 °C;

<sup>c</sup> nominal cooling conditions: Evaporator water inlet/outlet temperature 12/7 °C, external air temperature 35 °C;

<sup>d</sup> The assumed COP, nominal cooling conditions: Evaporator water inlet/outlet temperature 12/7 °C, external air temperature of 35 °C.

### 8.1.3 The renewable system, the battery and the electric vehicle

There are two on-site renewable systems, including the building integrated photovoltaics (BIPVs) and the micro-wind turbine. The efficiency of the BIPV is 0.1427 under the provided reference condition: a reference temperature of 25 °C and a reference radiation of 1000 W/m<sup>2</sup>. The modelled private electric vehicle is the NISSAN LEAF (NISSAN LEAF Specs) with the nominal battery storage capacity of 24 kWh. The average daily travelling distance is 31.2 km according to the Hong Kong private transportation report (TCSFR 2011). The nominal storage capacity of the static battery is 24 kWh. The energy interaction between buildings and vehicles can decrease not only the emissions, but also the energy consumption of buildings and transportations (Zhou et al. 2019; Zhou and Cao, 2019c).

## 8.2 Methodology: control strategies

In terms of effectively managing the on-site surplus renewable energy (after covering the building-basic electric load) and covering the building energy demand with the higher Energy Flexibility, an energy control strategy has been proposed regarding different energy storages in the system. The principle for the energy management is peak load shaving and valley filling via the hybrid energy storages. As shown in Figure 8.3, the electricity generation from the hybrid renewable system,  $G_{REe}$ , is firstly used to cover the basic electric load. Afterwards, the surplus renewable energy,  $P_{Gen,surp 1}$ , is used to charge the electric vehicle before recharging the hybrid thermal storages. It should be noticed that, the excess renewable-recharging sequences of the hybrid thermal storages will be specifically discussed as shown in Table 8.4, Section, 8.4.1. The surplus renewable energy after recharging the hybrid thermal storages is used to charge the static battery before being exported to the electric grid. Whenever the basic electric load is higher than the renewable energy, the static battery is discharged before discharging the electric vehicle. The rest of the electric load is covered by importing electricity from the grid.

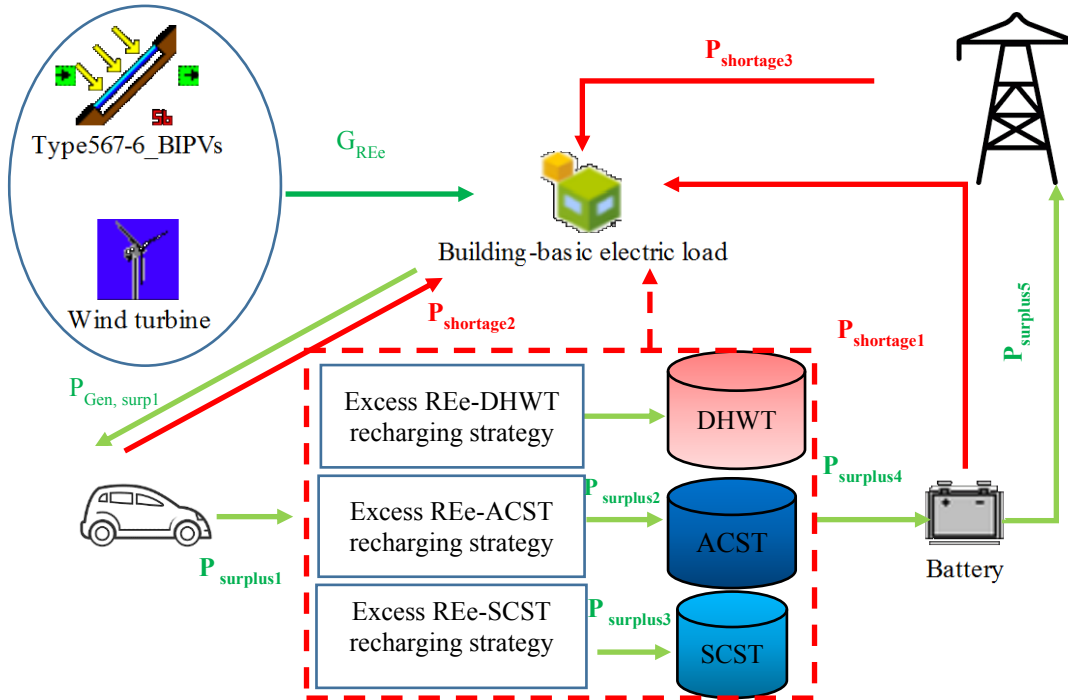


Figure 8.3 The schematic configuration and the energy control strategy. (Note: the green line indicates the flow of the surplus renewable electricity; the red solid line indicates the electricity flow during the renewable shortage period; the red dash line indicates the impact of the excess renewable-recharging strategies on the basic electric load. The energy flow in the figure only shows one case, and the excess renewable recharging strategy is case-dependent, as shown in Table 8.4, Section, 8.4.1.)

### 8.2.1 Demand responsive energy control strategy

In order to investigate the impact of different energy sources, i.e., renewable sources and static battery storage, on the building Energy Flexibility, two energy control strategies were proposed and compared: the “REe-to-demand control strategy (Control strategy 1)” and the “battery-to-demand control strategy (Control strategy 2)”. As shown in Figure 8.4, Control strategy 1 indicates that the basic electric load is firstly covered by the on-site renewable energy, and then it is covered by the electricity discharged from the battery. In the Control strategy 2, the battery is discharged to cover the basic electric load first, and then the remaining electric load is covered by the renewable energy. The remaining electric load shortage is covered by the electricity imported from the grid.

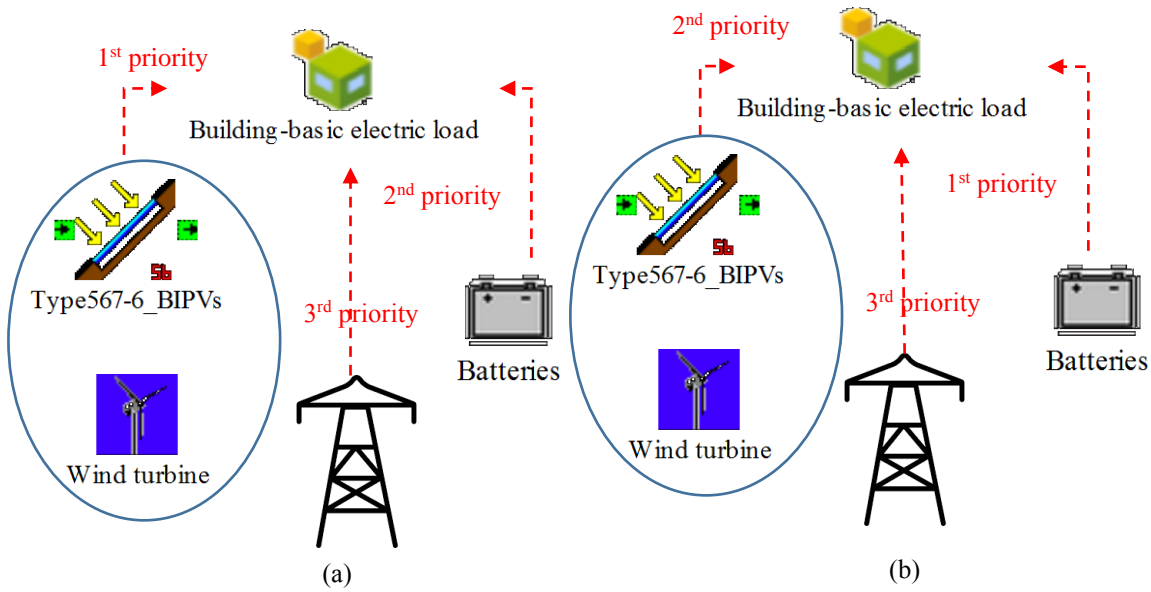


Figure 8.4 (a) The “REe-to-demand control strategy (Control strategy 1)”; (b) The “battery-to-demand control strategy (Control strategy 2)”.

### 8.2.2 Structural thermal mass storage

In addition to recharging the electrical storage, the on-site surplus renewable energy can also be managed to recharge the building thermal mass for the Energy Flexibility enhancement. When the on-site renewable electricity is higher than the basic electric load, i.e.,  $P_{surp}$  is greater than zero, the surplus on-site renewable electricity can be converted to the cooling energy and was then stored in the building facade by lowering the indoor air set-point temperature,  $T_{set,indoor}$ . When the on-site renewable electricity is lower than the basic electric load, the cooling energy in the building facade can be discharged to meet the indoor thermal comfort, reducing the operational time-duration of the chiller. The indoor air setpoint temperature is defined by Equation (1). The indoor thermal comfort range is between 18 and 26 °C.

$$T_{set,indoor}=24-\Delta T \times GT(P_{surp},0) \quad (1)$$

where  $\Delta T$  is the temperature difference deviating from the baseline of the indoor air set-point temperature.  $GT$  is the function as shown below.

$$GT(P_{\text{surp}}, 0) = \begin{cases} 1 & \text{when } P_{\text{surp}} > 0 \\ 0 & \text{when } P_{\text{surp}} \leq 0 \end{cases} \quad (2)$$

### 8.3 Implementation: control algorithms

Figure 8.5 demonstrates the energy flow chart of Control strategy 1. The renewable surplus/shortage period refers to the time-duration when the on-site renewable generation is higher/lower than the basic electric load. As shown in Figure 8.5, during the renewable shortage period, the basic electric load is covered by the electricity discharged from the static battery, and then the basic electric load is covered by the electricity discharged from the electric vehicle battery before being covered by the electricity imported from the grid. During the renewable surplus period, the surplus renewable electricity is used to recharge the electric vehicle (EV), the hybrid thermal storage systems and then to recharge the static battery before being exported to the grid. The overall efficiency of the regulator and the inverter is 95 %. The upper and the lower limitations of the fractional state of charge (FSOC<sub>battery</sub>) of the batteries are 0.3 and 0.9, respectively. The charging efficiency is assumed to be 90 %.

The energy flow of Control strategy 2 is shown in Figure 8.6. During the renewable surplus period, the surplus renewable electricity is used to charge the vehicles, the hybrid thermal storage systems and the static battery before being exported to the grid. During the renewable shortage period, the basic electric load is covered by the electricity discharged from the static battery and then from the electric vehicle battery before being covered by the electricity imported from the grid.

Table 8.3 summarizes the flexibility indicators proposed in (Zhou and Cao. 2019a). The proposed indicators include flexible power, flexible energy and the capability of the energy flexible building for shifting the flexible energy to the renewable surplus or the renewable shortage period.

### 8.4 Results and conclusion

As shown in Figure 8.7(a), compared to the “battery-to-demand control strategy (Control strategy 2)”, more flexible energy can be provided by the “REe-to-demand control strategy (Control strategy 1)”. For instance, compared to the flexible delayed energy,  $E_{\text{delayed},e}^+$  at 29.5 kWh/(m<sup>2</sup>a) for the case with the implementation of the Control strategy 2, the flexible delayed energy,  $E_{\text{delayed},e}^+$  is 30.3 kWh/(m<sup>2</sup>a) for the case with the implementation of the Control strategy 1. The inflexible energy ( $E_{\text{inflexible},e}^+$ ) includes both the electricity imported from the electric grid,  $E_{\text{imp},e}$ , and the delayed electricity from the battery during the REe surplus period,  $E_{\text{delayed},\text{battery}}^-$ . The inflexible energy ( $E_{\text{inflexible},e}^+$ ) is 60 kWh/(m<sup>2</sup>a) for the case with the implementation of the Control strategy 1, which is around 9 % less than the  $E_{\text{inflexible},e}^+$  for the case with the implementation of the Control strategy 2.

From the perspective of the flexibility factors, the Control strategy 1 is also found to be superior to Control strategy 2. For instance, compared to the Control strategy 2, for the case with the implementation of the Control strategy 1, the capability of an energy flexible building can be enhanced in terms of shifting the forced electricity from the renewable shortage period to the renewable surplus period and shifting the delayed electricity from the renewable surplus period to the renewable shortage period. Furthermore, the Control strategy 1 shows a higher on-site flexible electric load fraction, OFLe, of 54.9%, than the Control strategy 2 of 46.8%. This indicates that the

proportion of the basic electric load covered by the flexible electricity is much higher by adopting the Control strategy 1 than the Control strategy 2.

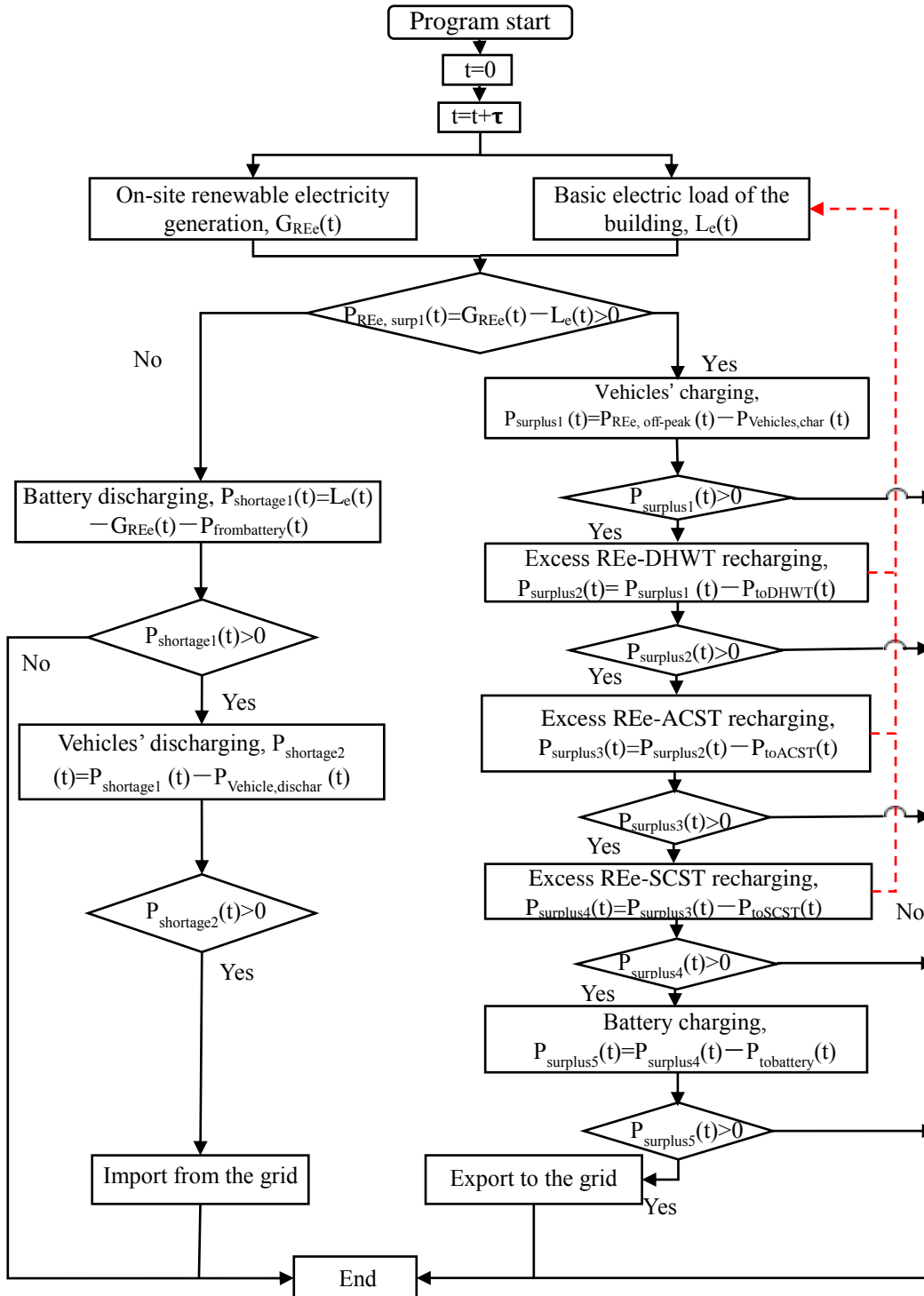


Figure 8.5 Energy flow of the “REe-to-demand control strategy” (Control strategy 1). (Note:  $\tau$  is the simulation time step, 0.125 h;  $P_{surplus1/2/3/4/5}$  and  $P_{shortage1/2}$  are the updated surplus renewable electricity and the updated basic electric load).

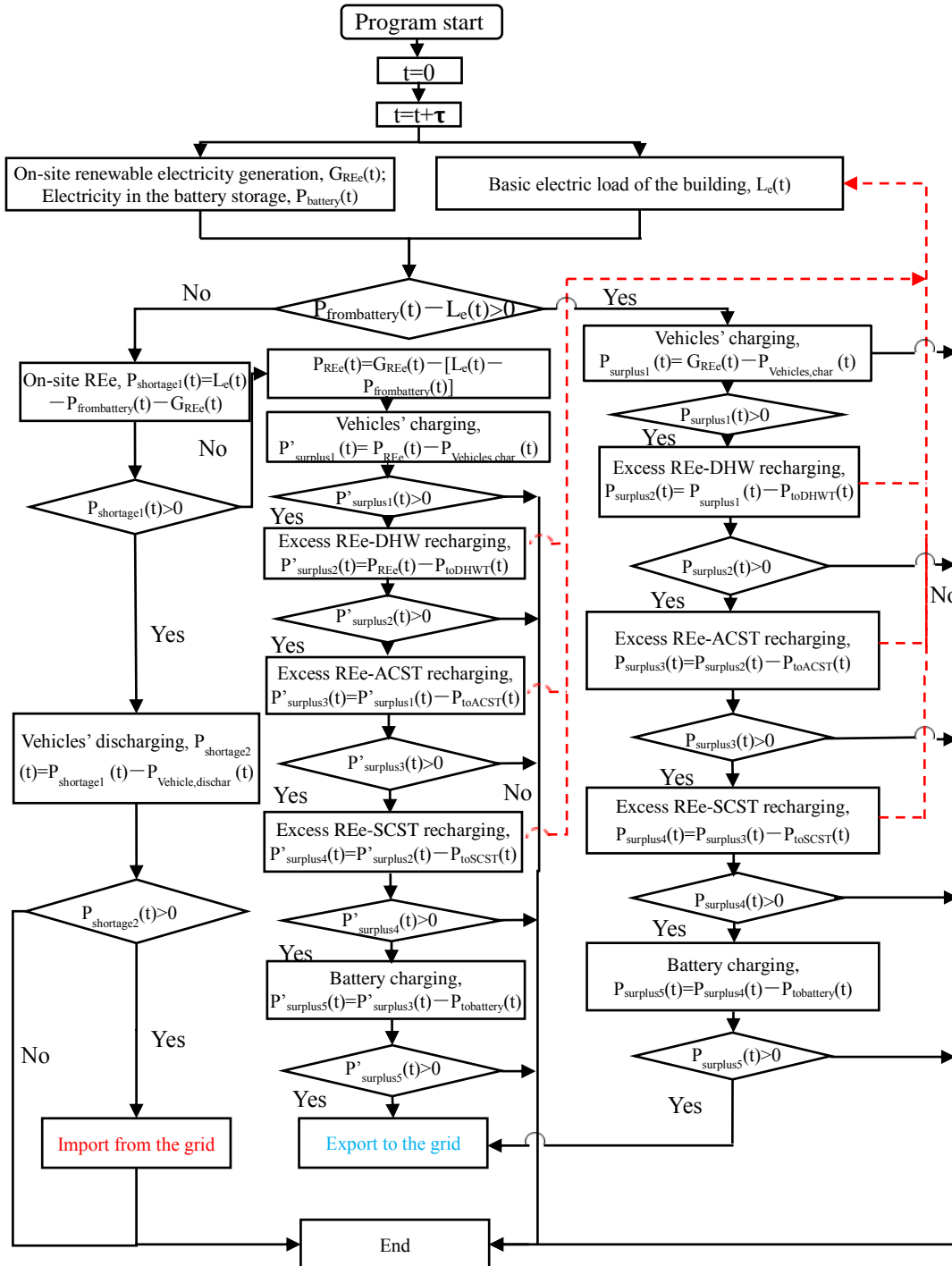
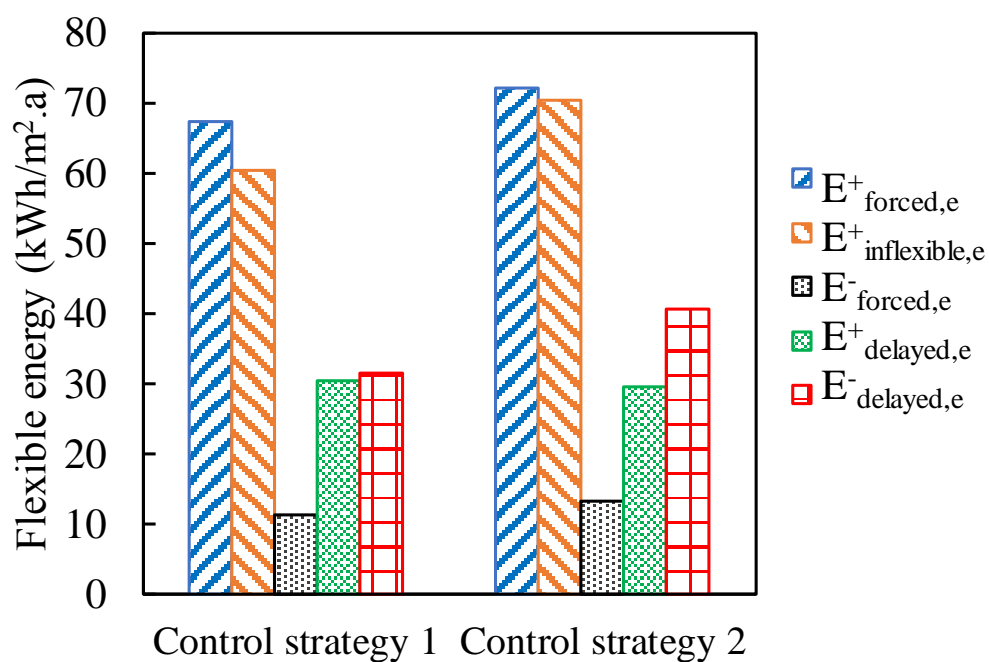


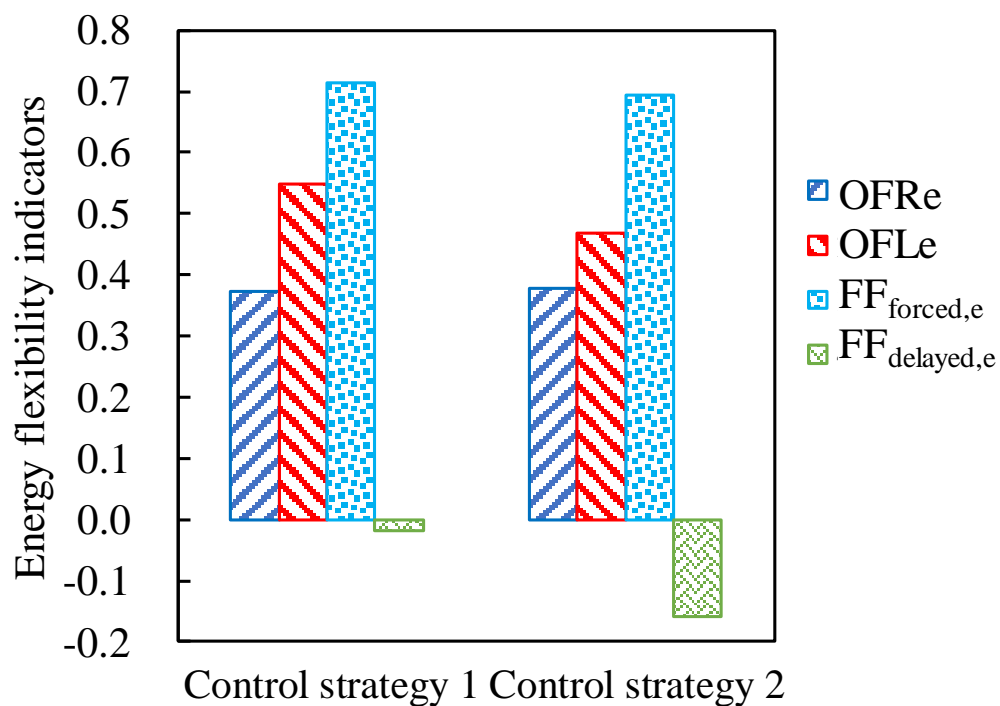
Figure 8.6 Energy flow chart for the “battery-to-demand strategy” (Control strategy 2). (Note:  $\tau$  is the simulation time step, 0.125 h;  $P_{REe}$  is the updated surplus renewable electricity after covering the basic electric load.  $P_{surplus1/2/3/4/5}$  and  $P_{shortage1/2}$  are the updated surplus renewable electricity when the battery can cover the basic electric load and the updated electric load.  $P'_{surplus1/2/3/4/5}$  is the updated surplus renewable electricity when the battery can't cover the basic electric load. The red dash line represents the impact of the excess renewable-recharging strategy on the basic electric load).

Table 8.3 Summary of the flexibility indicators (KPIs) from (Zhou and Cao. 2019a; Zhou and Cao. 2019b).

KPI	Equations	Remarks
Flexible time duration	$t_{\text{surp}} = \int_0^{t_{\text{end}}} \text{GT}[(G_{\text{REe}}(t) - L_e(t)), 0] \times dt$ $t_{\text{short}} = \int_0^{t_{\text{end}}} \text{GT}[(L_e(t) - G_{\text{REe}}(t)), 0] \times dt$	renewable energy, load
Flexible power	$P_{\text{forced,AC}} = \text{Max}[(C_{\text{chiller,normal,AC}} - L_{\text{cooling,AC}}), 0] + C_{\text{chiller,recharging,AC}}$ $P_{\text{delayed,AC}} = \text{Max}[(L_{\text{cooling,AC}} - C_{\text{chiller,normal,AC}}), 0]$ $P_{\text{forced,DHW}} = \text{Max}[(H_{\text{aux,DHW}} + H_{\text{STC}} - L_{\text{DHW}}), 0] + H_{\text{REe-DHW}}$ $P_{\text{delayed,DHW}} = \text{Max}[(L_{\text{DHW}} - H_{\text{aux,DHW}} - H_{\text{STC}}), 0]$ $P_{\text{forced,battery}} = P_{\text{charging,battery}}$ $P_{\text{delayed,battery}} = P_{\text{discharging,battery}}$	additional cooling/heating/electric power, forced power, shifted cooling/heating/electric load, delayed power (instantaneous value)
Flexible energy	$E_{\text{forced,e}}^+ = \sum E_{\text{forced}}^+ = \frac{E_{\text{forced,AC}}^+}{\text{COP}_{\text{AC}}} + \frac{E_{\text{forced,SC}}^+}{\text{COP}_{\text{SC}}} + E_{\text{forced,DHW}}^+ + E_{\text{forced,battery}}^+$ $E_{\text{forced,e}}^- = \sum E_{\text{forced}}^- = \frac{E_{\text{forced,AC}}^-}{\text{COP}_{\text{chiller,normal,AC}}} + \frac{E_{\text{forced,SC}}^-}{\text{COP}_{\text{chiller,normal,SC}}} + E_{\text{forced,DHW}}^- + E_{\text{forced,battery}}^-$ $E_{\text{delayed,e}}^+ = \sum E_{\text{delayed}}^+ = \frac{E_{\text{delayed,AC}}^+}{\text{COP}_{\text{chiller,normal,AC}}} + \frac{E_{\text{delayed,SC}}^+}{\text{COP}_{\text{chiller,normal,SC}}} + E_{\text{delayed,DHW}}^+ + E_{\text{delayed,battery}}^+$ $E_{\text{delayed,e}}^- = \sum E_{\text{delayed}}^- = \frac{E_{\text{delayed,AC}}^-}{\text{COP}_{\text{chiller,normal,AC}}} + \frac{E_{\text{delayed,SC}}^-}{\text{COP}_{\text{chiller,normal,SC}}} + E_{\text{delayed,DHW}}^- + E_{\text{delayed,battery}}^-$ $\text{OFRe} = \frac{E_{\text{forced,e}}^+}{\int_0^{t_{\text{end}}} \text{MAX}[(G_{\text{REe}}(t) - L_e(t)), 0] \times dt}$ $\text{OFLe} = 1 - \frac{E_{\text{inflexible,e}}}{\int_0^{t_{\text{end}}} L_e(t) \times dt} = 1 - \frac{E_{\text{imp,e}} + E_{\text{delayed,battery}}^-}{\int_0^{t_{\text{end}}} L_e(t) \times dt}$	additional cooling/heating/electric energy, forced energy, shifted cooling/heating/electric load, delayed energy (integrated value for a certain period)
Flexibility factor	$\text{FF}_{\text{forced,e}} = \frac{E_{\text{forced,e}}^+ - E_{\text{forced,e}}^-}{E_{\text{forced,e}}^+ + E_{\text{forced,e}}^-}$ $\text{FF}_{\text{delayed,e}} = \frac{E_{\text{delayed,e}}^+ - E_{\text{delayed,e}}^-}{E_{\text{delayed,e}}^+ + E_{\text{delayed,e}}^-}$	capability, exploiting the energy potential, shifting, forced energy, delayed energy, REe surplus period, REe shortage period (integrated value for a certain period)



(a)



(b)

Figure 8.7 The impact of energy control strategies on the (a) Flexible energy; (b) Energy flexibility indicators. (The system is supported by a 30-kW wind turbine.)

### 8.4.1 Excess renewable-recharging strategy for hybrid thermal storages

In terms of managing the on-site renewable energy, several case studies are defined as listed in Table 8.4. Case 1 is designed as the reference case for the comparative analysis. The impact of different combinations of thermal storage systems, as shown in the red dash line in Figure 8.3, on the Energy Flexibility of the hybrid energy system is investigated from Case 2 to Case 4 as listed in Table 8.3. For instance, in Case 3, the surplus renewable electricity is used to firstly recharge the ACST before recharging the DHW tank (DHWT). Furthermore, the Case 5 is designed to comparatively investigate the difference resulting from different recharging sequences of the hybrid thermal storage systems. In addition, the surplus REe-to-battery control strategy, Case 6, is designed to investigate the impact of the battery integration on the Energy Flexibility of the hybrid energy systems.

Table 8.4 Simulation cases for the hybrid thermal energy storages management.

Simulation groups	Control strategies
Case 1	Surplus REe-to-thermal recharging control strategy: No excess renewable-recharging strategy
Case 2	Surplus REe-to-thermal recharging control strategy: the excess REe-ACST recharging strategy
Case 3	Surplus REe-to-thermal recharging control strategy: the excess REe-ACST, and the excess REe-DHWT recharging strategies
Case 4	Surplus REe-to-thermal recharging control strategy: the excess REe-ACST, the excess REe-DHWT and then the excess REe-SCST recharging strategies
Case 5	Surplus REe-to-thermal recharging control strategy: the excess REe-DHWT, the excess REe-ACST, and then the excess REe-SCST recharging strategies
Case 6	Surplus REe-to-battery control strategy: the excess REe-DHWT, the excess REe-ACST, and then the excess REe-SCST recharging strategies

Several cases (as listed in Table 8.3) have been investigated with respect to different excess renewable-recharging strategies. As shown in Figure 8.8(a), several conclusions can be drawn.

- Compared to the Case 1, by implementing the excess REe-ACST recharging strategy (Case 2), the grid importation ( $E_{imp,a}$ ) decreases from 72.4 to 70.2 kWh/m<sup>2</sup>a by 3%, and the grid exportation ( $E_{exp,a}$ ) decreases from 24.4 to 20.3 kWh/m<sup>2</sup>a by 16.8%. Furthermore, the annual net equivalent CO<sub>2</sub> emission increases from 33.6 to 34.9 kg/m<sup>2</sup>a by 1.3 kg/m<sup>2</sup>a. Compared to the Case 2, by implementing the excess REe-DHWT recharging strategy (Case 3), the grid importation ( $E_{imp,a}$ ) decreases from 70.2 to 64.7 kWh/m<sup>2</sup>a by 7.8%, and the grid exportation ( $E_{exp,a}$ ) decreases from 20.3 to 12.1 kWh/m<sup>2</sup>a by 40.4%, respectively. Furthermore, the annual net equivalent CO<sub>2</sub> emission is increased from 34.9 to 36.8 kg/m<sup>2</sup>a by 1.9 kg/m<sup>2</sup>a.
- By changing the charging strategy from the surplus REe-to-thermal recharging control strategy (Case 5) to the surplus REe-to-battery control strategy (Case 6), the annual net equivalent CO<sub>2</sub> emission is decreased by 3.6 kg/m<sup>2</sup>a (from 36.4 to 32.8 kg/m<sup>2</sup>a).

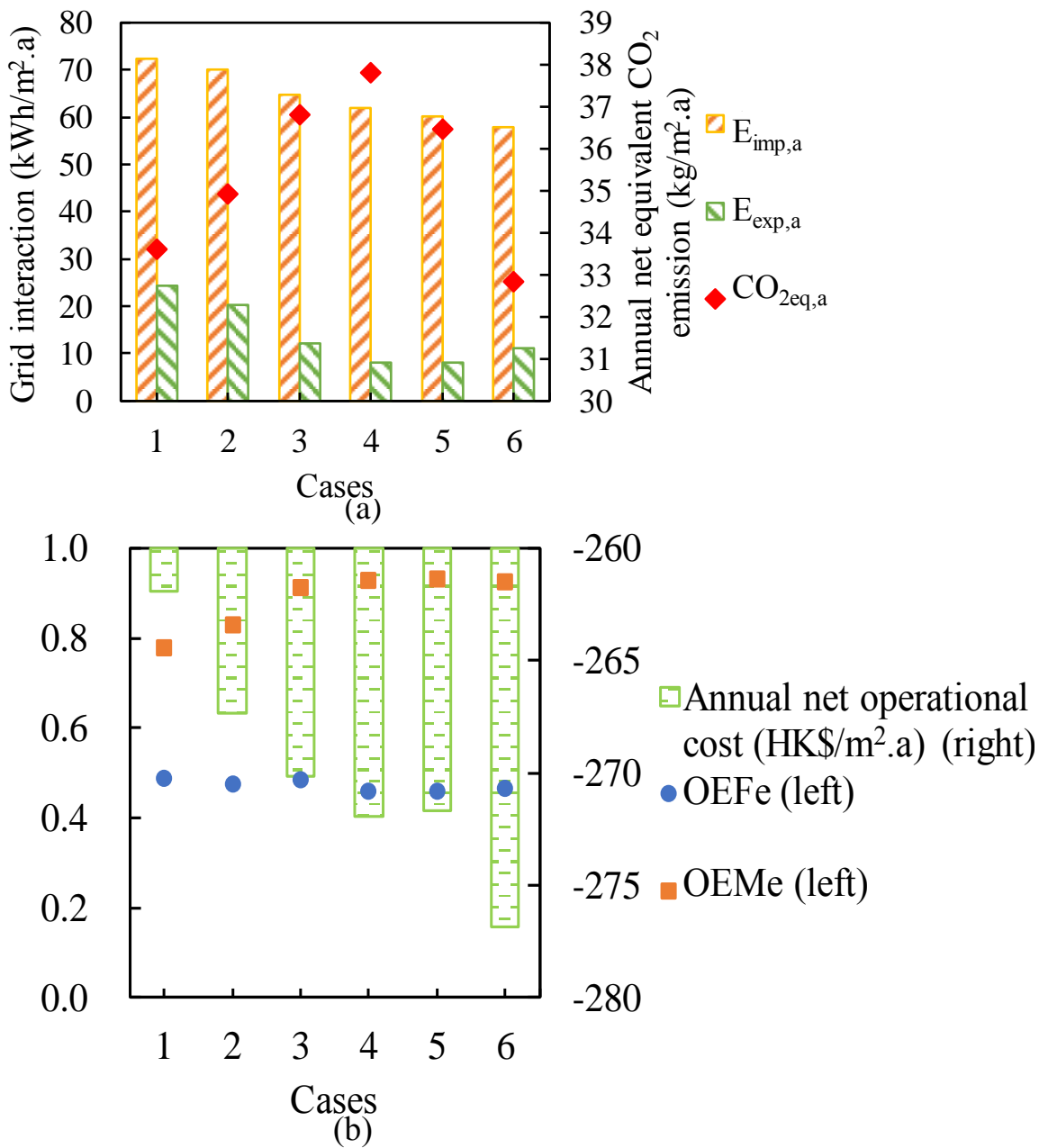


Figure 8.8 The effect of the excess renewable-recharging strategies on: (a) the grid interaction and the annual net equivalent CO<sub>2</sub> emission; (b) the annual net operational cost and the annual matching capability. (Note: the  $E_{imp,a}$ ,  $E_{exp,a}$  and  $CO_{2eq,a}$  refer to the annual grid importation, the annual grid exportation and the annual equivalent CO<sub>2</sub> emission. The OEF<sub>fe</sub> and OEM<sub>e</sub> refers to the on-site electricity fraction and the on-site electricity matching. The system is supported by a 15-kW wind turbine.)

Figure 8.8(b) shows the evolution of the annual net operational cost and the annual matching capability when implementing different excess renewable-recharging strategies. Several conclusions can be drawn as shown below.

- Compared to the Case 1, by implementing the excess renewable-recharging strategies in the Case 5, the annual OEM<sub>e</sub> increases from 0.78 to 0.93, whereas the annual OEF<sub>fe</sub> decreases

from 0.49 to 0.46. The reason is that, by adopting the excess renewable-recharging strategies, the grid exportation ( $E_{exp,a}$ ) decreases from 24.4 to 8.2 kWh/m<sup>2</sup>a, and the grid importation ( $E_{imp,a}$ ) decreases from 72.4 to 60.3 kWh/m<sup>2</sup>a. Furthermore, the basic electric load decreases from 152 to 128 kWh/m<sup>2</sup>a and the annual net operational cost decreases from -261.9 to -271.6 HK\$/m<sup>2</sup>a by 3.7%.

- There is a little difference when changing the charging strategy from the surplus REe-to-thermal recharging control strategy (Case 5) to the surplus REe-to-battery control strategy (Case 6). For instance, the annual net operational cost decreases from -271.7 to -276.9 HK\$/m<sup>2</sup>a, and the annual OEF<sub>e</sub> increases from 0.462 to 0.478.

### 8.4.2 The structural thermal mass storage

Figure 8.9 shows the impact of the structural thermal mass of the building façade on the Energy Flexibility. As shown in Figure 8.9, an increase of the temperature difference of indoor air set-point temperature ( $\Delta T$ ) from 0 to 6 °C (or the decrease of the indoor air setpoint temperature from 24 to 18 °C) will result in the increase of the  $E_{forced,e}^+$  from 43.1 to 72.4 kWh/m<sup>2</sup>a by 68%. This indicates that, 68% more flexible energy can be obtained by the surplus renewable energy. Meanwhile, the  $E_{delayed,e}^+$  increases from 31.5 to 43.1 kWh/m<sup>2</sup>a. The  $E_{forced,e}^-$  also increases from 13 to 37.2 kWh/m<sup>2</sup>a by 24.2 kWh/m<sup>2</sup>a. This indicates that, 24.2 kWh/m<sup>2</sup>a more inflexible energy can be resulted from the storage tank during the renewable shortage period. The reason is that by reducing the indoor set-point temperature, more cooling energy in the thermal storage tank is consumed for covering the increased cooling load. Therefore, more forced energy is required for charging the storage tank at the renewable shortage period. Meanwhile, the  $E_{delayed,e}^-$  does not monotonously increase with respect to the increase of the  $\Delta T$ . For instance, the  $E_{delayed,e}^-$  increases from 46.5 to 49.5 kWh/m<sup>2</sup>a by 6.5% when the  $\Delta T$  increases from 0 to 1 °C, and it decreases from 49.5 to 43.5 kWh/m<sup>2</sup>a by 12.1% when the  $\Delta T$  increases from 1 to 6 °C. The underlying reason is that, when the  $\Delta T$  increases from 0 to 1 °C, the designed excess renewable-recharging chiller can cover the cooling load, and the energy consumption of the normal chiller is not affected. The increase of the delayed energy at the renewable surplus period is due to the increase of the cooling load. However, with respect to the further increase of the  $\Delta T$  from 1 to 6 °C, the normal chiller is required to reduce the indoor temperature as the increase of the cooling load cannot be covered by the excess renewable-recharging chiller only. As a result, the delayed energy at the renewable surplus period is decreased due to the operation of the normal chiller.

Moreover, the proportion of the surplus renewable energy becoming the flexible energy, and the basic demand covered by the flexibility sources were also investigated in this part. With respect to the increase of the  $\Delta T$  from 0 to 6 °C, the OFRe increases from 0.38 to 0.82, indicating that more on-site surplus renewable energy can be the flexible energy by activating the thermal storage of the building façade. This is due to the increase of the  $E_{forced,e}^+$  from 43.1 to 72 kWh/m<sup>2</sup>.a. Meanwhile, the OFLe decreases from 0.81 to 0.41 with respect to the increase of the  $\Delta T$  from 0 to 6 °C. The reason is due to the increase of the  $E_{forced,e}^-$  from 13 to 37.5 kWh/m<sup>2</sup>.a. The  $FF_{delayed,e}$  increases from -0.19 to 0 when the  $\Delta T$  increases from 0 to 6 °C. This indicates that, by enlarging the temperature difference deviating from the baseline set-point temperature, the capability of flexibility sources can be enhanced in terms of shifting the delayed energy from the renewable surplus period to the renewable shortage period. Table 8.5 lists the impact of different energy control strategies on the flexibility indicators. It can be noticed that, compared to the “battery-to-demand control strategy”, the “REe-to-demand control strategy” shows more Energy Flexibility potentials. Moreover, the utilization

of the structural thermal mass storage can enhance the OFRe and the  $FF_{\text{delayed,e}}$ , whereas the OFLe and the  $FF_{\text{forced,e}}$  are decreased.

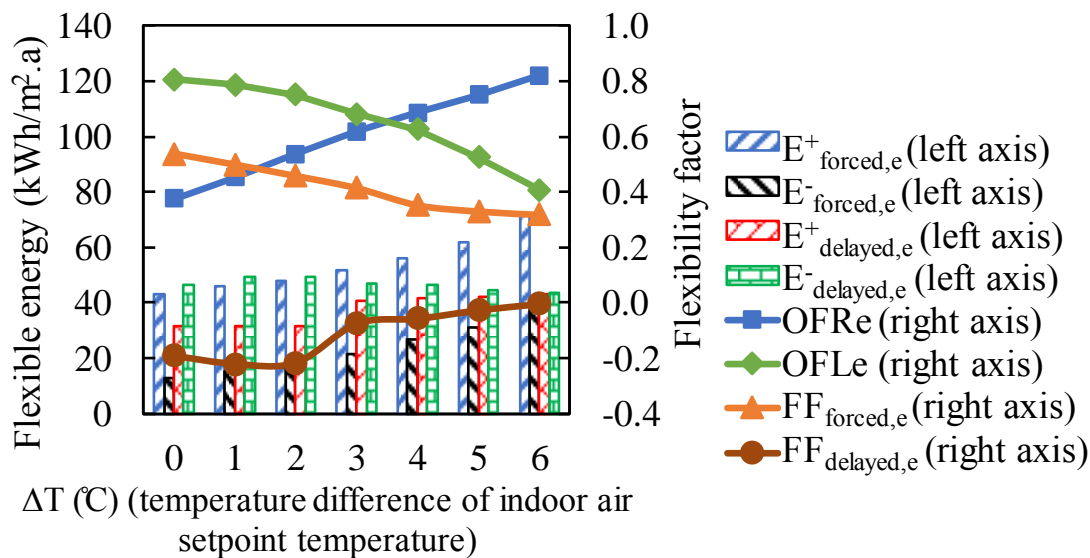


Figure 8.9 The impact of the temperature difference of indoor air set-point temperature ( $\Delta T$ ) on the flexible energy and the flexibility factors.

Table 8.5 Summary of the impact of energy control strategies on selected flexibility indicators.

Energy control strategies	Flexibility indicators			
<b>REe-to-demand control strategy</b>	Higher OFRe	Higher OFLe	Higher $FF_{\text{forced,e}}$	Higher $FF_{\text{delayed,e}}$
<b>Battery-to-demand control strategy</b>	Lower OFRe	Lower OFLe	Lower $FF_{\text{forced,e}}$	Lower $FF_{\text{delayed,e}}$
<b>Structural thermal mass storage</b>	Higher OFRe	Lower OFLe	Lower $FF_{\text{forced,e}}$	Higher $FF_{\text{delayed,e}}$

### 8.4.3. Conclusions

Based on the case study, the building Energy Flexibility of a building-vehicle energy system has been quantitatively investigated. The integrated building energy system includes the on-site renewable system, the hybrid energy storage systems, the battery storage, the electric vehicles' system and the electric grid. Two different energy control strategies have been formulated and contrasted. Several conclusions can be drawn as follows:

1) Compared to the “battery-to-demand control strategy”, by adopting the “REe-to-demand control strategy”, the proportion of the surplus renewable electricity which is the flexible forced electricity and the proportion of the basic electric load covered by the flexible electricity, can be increased. In addition, the capability of the energy flexible building can be enhanced in terms of shifting the forced electricity from the renewable shortage period to the renewable surplus period and shifting the delayed electricity from the renewable surplus period to the renewable shortage period;

2) By adopting the excess renewable-recharging strategies, the annual on-site electricity matching (OEME) increases from 0.78 to 0.93. Furthermore, with the implementation of the hybrid excess

renewable-recharging strategies as shown in Case 5, the annual net operational cost decreases from -262 to -271.7 HK\$/m<sup>2</sup>.a by 3.7%;

3) By activating the thermal storage of the building façade, more on-site surplus renewable energy can be the flexible energy. Moreover, by enlarging the temperature difference deviating from the baseline of the set-point temperature, the capability of flexibility sources can be enhanced in terms of shifting the delayed energy from the renewable surplus period to the renewable shortage period.

However, only the rule-based control strategy is implemented in this study and the impact of the time resolution on the building Energy Flexibility has not been discussed yet. Our future research works will be focused on the development of instantaneous Energy Flexibility indicators together with the model predictive control strategy, and the impact of the time resolution on the building Energy Flexibility.

# 9 Rule-based load shifting with heat pumps for single family houses

Young Jae Yu, Fraunhofer IEE, Germany

The study aims at increasing the load shifting potential of decentralized heat pumps by introducing a rule-based control (RBC) coupled with different thermal energy storages in a single-family house. The local residual load (energy demand not covered by renewable energy sources (RES)) is used as an external signal for the RBC and a flexibility strategy based on set-point modulation depending on the local residual load is applied to the heat pump control. Besides the analysis of the RBC, the study presents the impact of load shifting with RBC regarding energetic and economic aspects in comparison to the conventional heat pump operation (heat-driven) with heat pump blocking times (3x2 hours a day). During these blocking times, the grid operators can block the operation of heat pumps in order to avoid peak loads.

## 9.1 Building and system description

For the simulation study, a single-family house is modelled with multiple thermal zones using TRNSYS type 56 (University of Wisconsin, 2011). The building model has two floors with a total floor area of 160 m<sup>2</sup> and consists of 11 thermal zones representing a typical single-family house in Germany. The roof space and cellar are considered as unheated building parts. The building model is presented in Figure 9.1.



Figure 9.1 Perspective view and floor plan of the ground floor (left) and first floor (right) of the single family house.

The building model has a heavy weight construction consisting of brick walls and concrete floors. The heat transfer coefficients of the constructions are shown in Table 9.1. For the building, the hygienic ventilation is ensured by a mechanical ventilation system with heat recovery. The heat recovery unit preheats the airflow before the supply air enters the rooms 1, 2, 9, 8, 11 and 12 (see

Figure 9.1). Exhaust air is taken from rooms 5, 3, 10 and 13. The supply air flow rate is 50 l/s to the whole building and the heat recovery factor amounts to 0.8.

Table 9.1 Heat transfer coefficients of constructions (EnEV 2009, 2009).

Construction	U-value (W/(m <sup>2</sup> K))	Thermal insulation	Specific heat capacity (W/K)
External wall	0.28	10 cm external insulation	ca. 780
Top floor ceiling	0.20	Ceiling insulation	ca. 1,700
Cellar ceiling	1.12	Ceiling insulation	ca. 1,700
Window	1.3	Double thermal insulating glazing	-

The mechanical ventilation schedules and internal heat gains (occupants and household equipment) are based on occupancy schedules (see Figure 9.2). The daily occupancy schedules of individual room types are based on (Schneider, 2008), (Hartmann, 2010), (Feist, 1994) and (DIN V 4108-6, 2003).

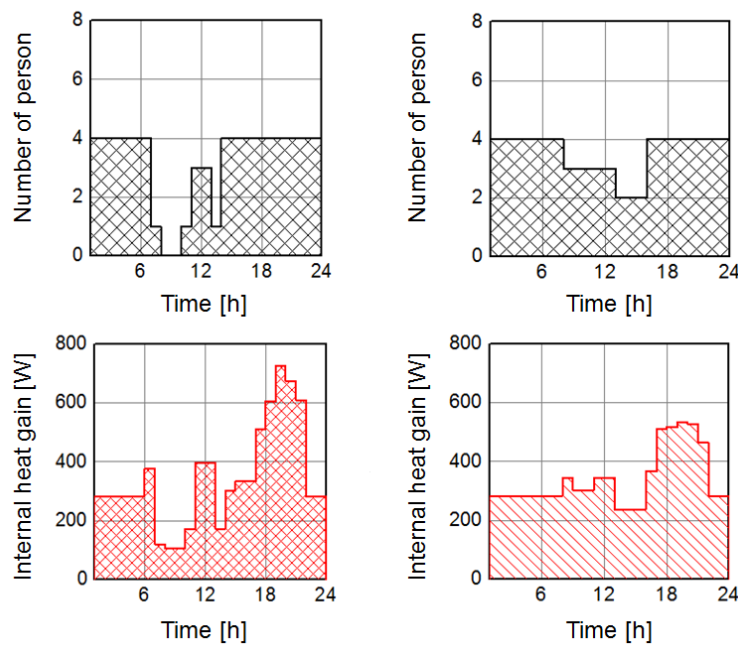


Figure 9.2 Daily occupancy schedule and internal heat gain (left: weekday, right: weekend)(Sources).

The single-family house is equipped with a ground source heat pump (GSHP). Figure 9.3 shows the schematic diagram of the heating system with a GSHP. The design heat-load calculation of the building model is based on DIN EN 12831 (DIN EN 12831, 2004), which determines the required heating capacity of heat pumps.

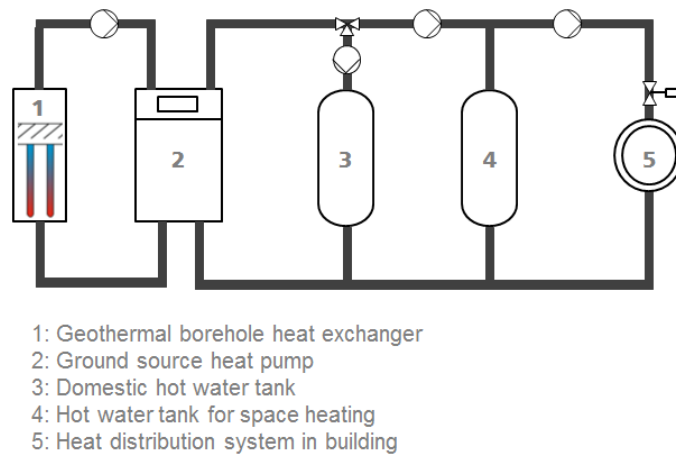


Figure 9.3 Schematic diagram of the heating system with GSHP.

In TRNSYS, the GSHP is modelled using manufacturer's supplied performance data (VIESSMANN, 2010) to ensure the accuracy of the results. Thereby, with the source and load side temperatures, the three-dimensional plots were interpolated for heating capacity and power draw. According to the data from the heat pump manufacturer, the rated heating capacity of the ground source heat pump is set to 6.2 kW, rated power draw is set to 1.4 kW and has a COP of 4.5 in the specified test condition (source inlet temperature of 0°C and load outlet temperature of 35 °C). The sizing of the ground source and the other implemented ground parameters are defined by GSHP catalog data (VIESSMANN, 2010). For the sizing of the ground source, it is assumed that the ground has a specific abstraction capacity of 50 W/m (VIESSMANN, 2010). As a result, the length of the geothermal heat exchanger amounts to 98 m. Besides the GSHP, a 300 liter domestic hot water (DHW) tank is implemented in the building model. Furthermore, a 1000 liter hot water storage tank for space heating is included in the system, which is typically used in practice to ensure the minimum operating time of the heat pump and to bridge blocking times. For the calculation of DHW, a 4-person based scheduled tap pattern (Jordan, 2003) is applied to the DHW-storage tank (see Figure 9.4). In the simulation, different heat distribution systems in the building have been investigated (low temperature radiator system, underfloor heating, wall heating and concrete core heating) in order to examine the flexibility potential by using building mass as thermal energy storage.

### 9.1.3 Local electricity supply system

The flexibility potential of the decentralized heat pump operation is investigated based on local electricity data from the city of Wolfhagen in Germany (Stadtwerke Wolfhagen, 2013). The city is one of the pioneers in renewable energy that has achieved 100% renewable energy supply on an annual basis since 2014. Wolfhagen is a small town of approx. 14,000 (2018) residents in an area of 112 km<sup>2</sup> located in the Kassel District of the Federal State of Hessen. Wolfhagen's 100% renewable strategy is essentially based on a newly installed wind farm with a rated capacity of 12 MW and a PV farm with a rated capacity of 12 MW. Due to fluctuating electricity feed-in, the electricity demand cannot be covered at all times and thus the rate of self-consumption amounts to round 60 percent. Figure 9.5 shows the estimated renewable energy feed-in, electricity demand and residual load of the city of Wolfhagen.

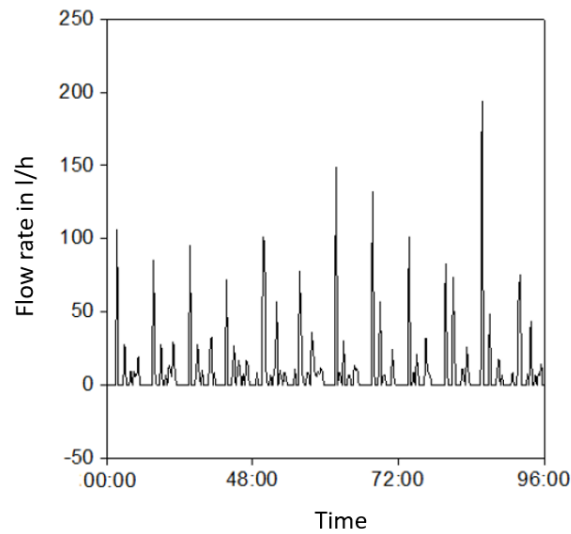


Figure 9.4 Exemplary tapping profile of 4-person during 4 days.

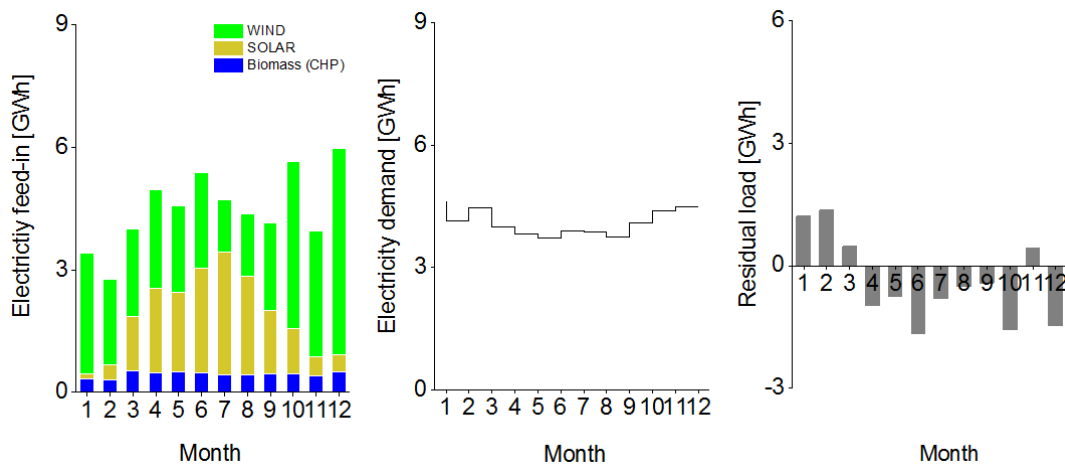


Figure 9.5 Monthly electricity feed-in, electricity demand and residual load in Wolfhagen in 2013 (Stadtwerke Wolfhagen, 2013).

A simple time-varying price signal is modelled based on the power demand and the electricity feed-in from renewable energy sources in Wolfhagen. In Figure 9.6, the electricity price signal for 48 hours in January is presented as an example. It is assumed that the local consumer can use surplus electricity with low or negative market prices. The price signal is converted into a digital signal of codes ( $\gamma_{elec}$ ) “1 (High tariff during positive residual load)” and “0 (Low tariff during negative residual load)” for the heat pump control.

$$\gamma_{elec} = 1 \text{ (high tariff), if renewable feed - in} < \text{demand (positive residual load)}$$

$$\gamma_{elec} = 0 \text{ (low tariff), if renewable feed - in} > \text{demand, (negative residual load)}$$

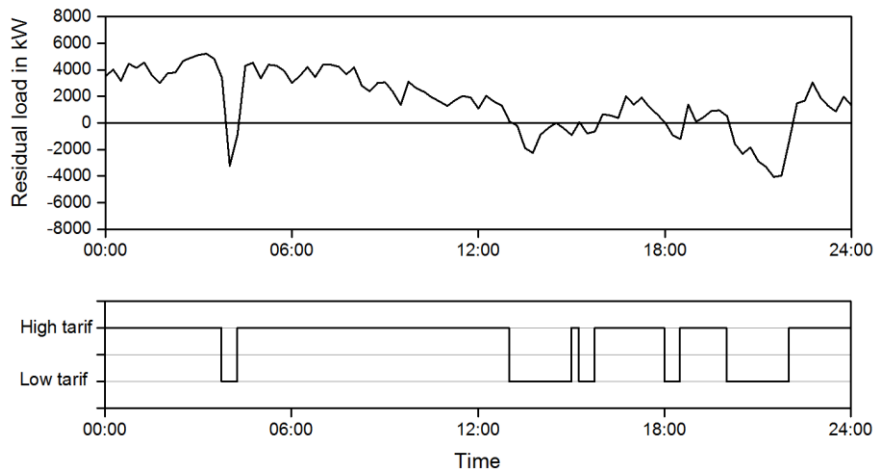


Figure 9.6 Electricity tariff depending on the residual load for 2 example days (Stadtwerke Wolfhagen, 2013).

## 9.2 Methodology: control strategies

The flexibility of buildings for space heating and domestic hot water (DHW) supply can be controlled in different manners. This study focuses on straightforward RBC, which aims at increasing the consumption of RE during peak periods with predefined rules. In general, RBC provides non-mathematical concepts and conditions into a control solution. Typically, there is a programmable fuzzy logic controller (e.g. thermostat) with a predefined control scheme that is executed based on the external data (electricity price signal) (Keshtkar, 2015). Figure 9.7 shows the schematic diagram of the RBC. As shown in Figure 9.7, the RBC continuously receives the information about the electricity price from the outside of the building to make decisions in order to adjust to new set-point temperatures of the thermal energy storage (TES), based on the new information received from the grid operator. In this study, thermal mass within the building, the hot water storage for space heating and the domestic hot water supply are regarded as available TES for the flexible operation of the electric heat pump.

Based on the information about the electricity price signal, a new set-point temperature for space heating and hot water supply is defined by switching the heat pump operation from heat-driven to grid-driven operation. The heat-driven heat pump control supplies the required thermal energy for space heating and domestic hot water with the defined set-point temperatures. In comparison, the grid-driven heat pump control manipulates the defined set-point temperatures depending on an external signal in order to charge/deplete the thermal energy storage while maintaining acceptable temperature levels for the occupants. The use of thermal mass in the building as TES during the grid-driven control is very limited due to the thermal comfort of occupants. In comparison, the set-point temperature of external (outside of thermally conditioned zones) thermal energy storages, such as hot water storage for space heating and domestic hot water supply, can be modified depending on the price signal without affecting user comfort, since the control of the hydraulic circuit within the building is separated from the control unit of the heat pump supply temperature. In this case, it is important to maintain the supply temperature below approx. 60 °C (maximum supply temperature of small size heat pumps) (VIESSMANN, 2010).

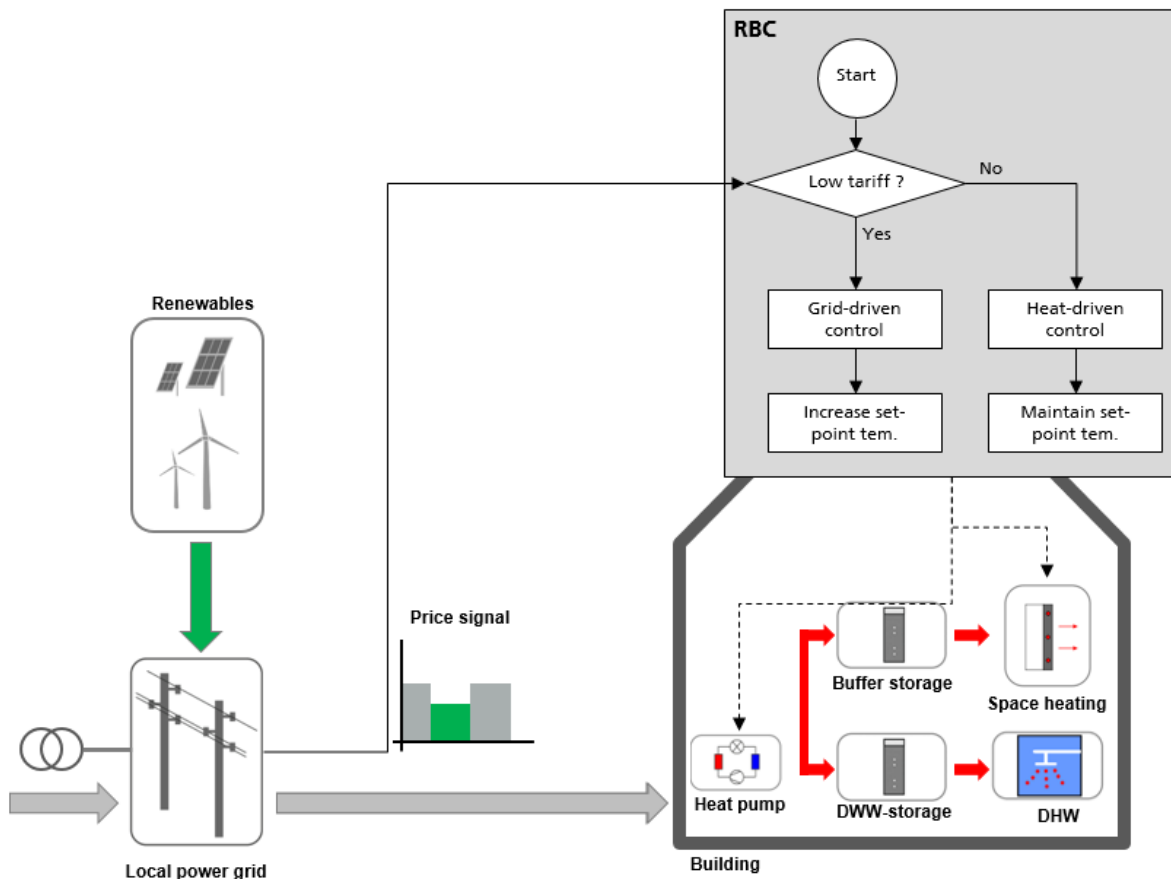


Figure 9.7 Schematic diagram of the RBC.

### 9.3 Implementation: control algorithms

As explained in the former section, the heat pump is operated based on a RBC, which decides the operating mode of the heat pump. The RBC design methodology is illustrated in Figure 9.8.

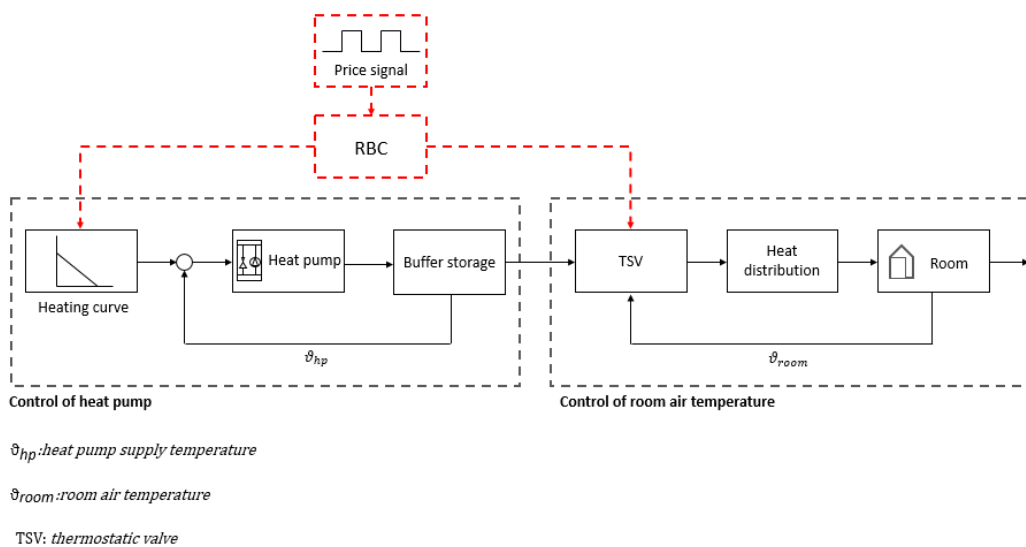


Figure 9.8 Architecture of RBC.

During heat pump operation, temperatures of different TESs, such as building mass and buffer storage for space heating and domestic hot water supply, can be modified by using a RBC depending on an external signal (electricity price). As shown in Figure 9.8, the control of the room air temperature and the supply temperature of the heat pump is controlled separately, since the heat pump system and the heat distribution system are usually hydraulically separated from each other by using a buffer storage. This separation especially allows for a flexible operation of the heat pump for load shifting by using the buffer storage, independent of the room air temperature control. Mostly, an on-off controlled heat pump is operated using a hysteresis of the supply temperature. The set-point temperature is defined by a heating curve depending on outside temperature. Thereby, the hysteresis determines the length and number of operating cycles of the heat pump (Huchtemann, 2015). Whereas a constant hysteresis (heat-driven control) leads to relatively short cycling with low heat loads (at low supply temperatures) and delivers exactly the required heat demand. In comparison, the grid-driven control in RBC increases the set-point temperature by shifting the heating curve up in order to extend operation cycles and overload the TES during low tariff periods. In this case the buffer storage can be used as TES without affecting user comfort due to the separated control of the room air temperature. Principally, it is possible to integrate the building mass (underfloor heating, wall heating and concrete core heating) as TES during the grid-driven control in order to increase the heat storage capacity, if the occupants accept a certain temperature fluctuation within the building. In comparison to buffer storage for space heating, DHW storages are usually integrated into the heat pump system by an additional loading circuit that is connected to the heat pump by using a three-way valve. For the utilization of DHW storage as TES for load shifting, the set-point temperature of the domestic hot water should be increased by using a RBC. Since the supply temperature of the heat pump during DHW supply varies between 50 – 55 °C, the temperature increase of the DHW storage during load shifting is quite limited.

The explained modification of temperatures in the TESs with a RBC enables charging TES during low price periods and discharging the stored thermal energy during following high price periods. Figure 9.9 shows an example of the heat pump operation with a traditional heat-driven control compared with the RBC control during five winter days. In this example, an underfloor heating is utilized as heat distribution system in the building and the heat pump is coupled with a 1000 liter buffer storage for space heating and a 300 liter DHW storage.

By using the RBC, the intention is to increase the supply temperature for the DHW storage by 5 Kelvin and the supply temperature of the space heating by 20 Kelvin. Additionally, the room air set-point temperature is increased by 2 Kelvin. The reduction of the room temperature is not considered here due to the thermal comfort. The comparison of COP profiles of both variations shows different operating characteristics of the heat pump. It is clearly seen that the operating cycle of the heat pump with the RBC during low tariff periods is significantly longer than the heat driven heat pump operation. However, the heat pump operation with the RBC decreases COP due to the higher supply temperature and long-term operating cycles. This leads to increased energy demand of the heat pump operation. In order to analyze if this kind of additional energy demand is acceptable from an energetic and economic point of view, the load shifting of the heat pump is evaluated further in the following section.

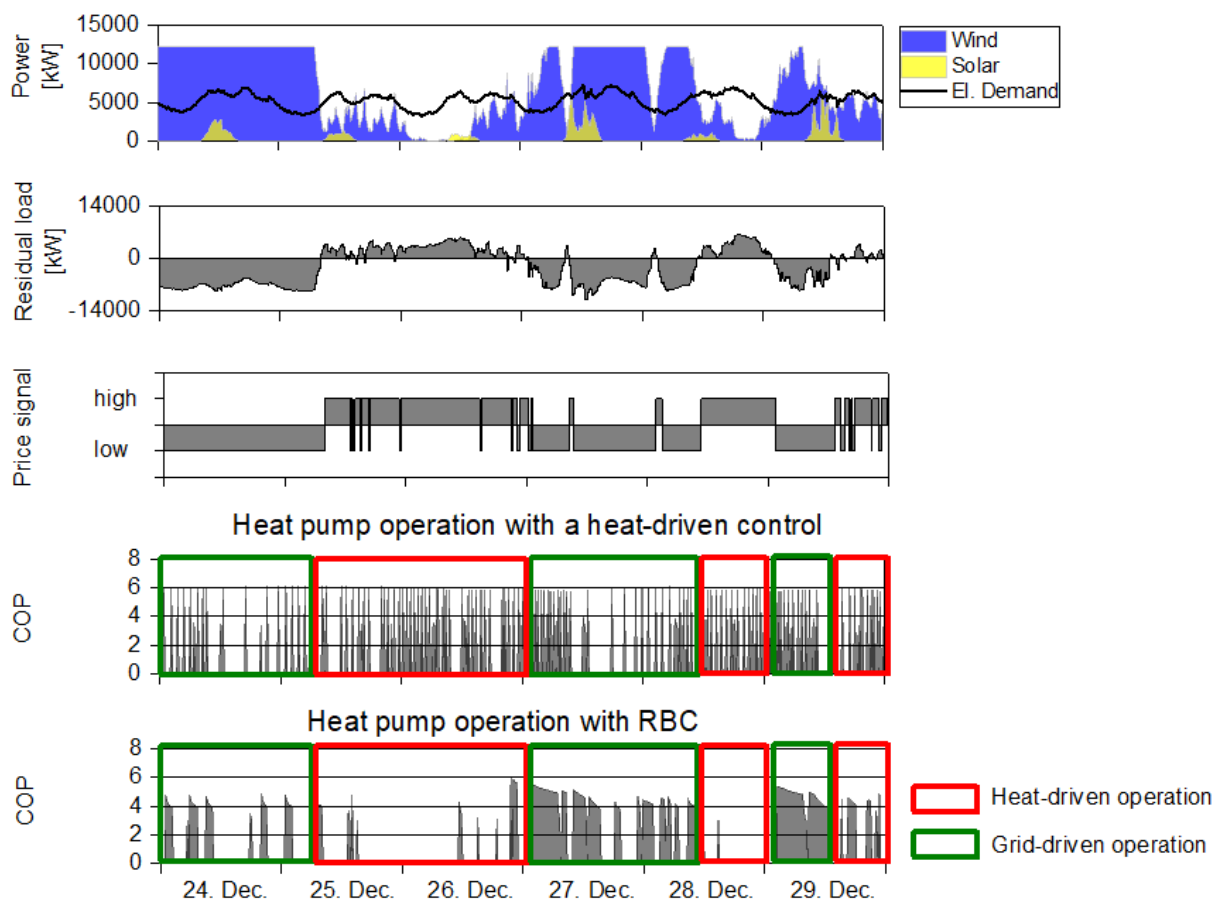


Figure 9.9 Comparison between a traditional heat-driven heat pump operation and a heat pump operation with external price signal based RBC for five winter days.

## 9.4 Results and conclusion

In order to gain better insight in the potential of load shifting with the heat pump, the theoretical potential for the RBC using different TES within the building is evaluated in regard to different aspects in this section. To do this, the heat pump operation using the RBC is compared with the conventional heat pump operation (heat-driven) using heat pump blocking times (3x2 hours a day: 11 am -1 pm and 6 pm - 8 pm). The investigated operating variations are described in Table 9.2.

Figure compares the electricity demand of the control strategies investigated. Generally, increased use of surplus electricity for space heating and DHW-supply can be achieved through load shifting with the RBC. Especially, the RBC using the buffer storage as TES (Variation 2) enables to shift the load from high tariff periods to low tariff periods for a total of 234 kWh/a, which corresponds to around 10 % of the annual electricity demand of the heat pump. However, the heat pump operation has an additional electricity demand of 378 kWh/a (Increase of electricity demand around 10 %) due to the reduced coefficient of performance (COP) and heat losses of the TES. In comparison to Variation 2, the additional utilization of the DHW storage during load shifting (Variation 3) has a marginal influence on the electricity demand, since the DHW storage is already operating at a high temperature level and has limited storage volume. In comparison, the utilization of the thermal building mass (Variation 4) increases the potential of load shifting significantly. The electricity

demand of around 570 kWh/a, corresponding to around 30 % of the annual electricity demand, can be shifted over a year by using RBC. However, the heat pump operation in Variation 4 increases the additional electricity demand of the heat pump as well. The expected additional electricity demand amounts to 591 kWh/a (Increase of electricity demand around 28 %).

Table 9.2 Variation of the control strategies.

Variation	Heat pump control	Thermal energy storage for load shifting
Variation 1 (Reference case)	Heat-driven control with blocking times (conventional)	1000 liter buffer storage for space heating as TES
Variation 2	RBC (heat-driven + grid-driven)	1000 liter buffer storage for space heating as TES
Variation 3	RBC (heat-driven + grid-driven)	1000 liter buffer storage for space heating and 300 liter DHW storage as TES
Variation 4	RBC (heat-driven + grid-driven)	1000 liter buffer storage for space heating, 300 liter DHW storage and thermal mass with buildings as TES

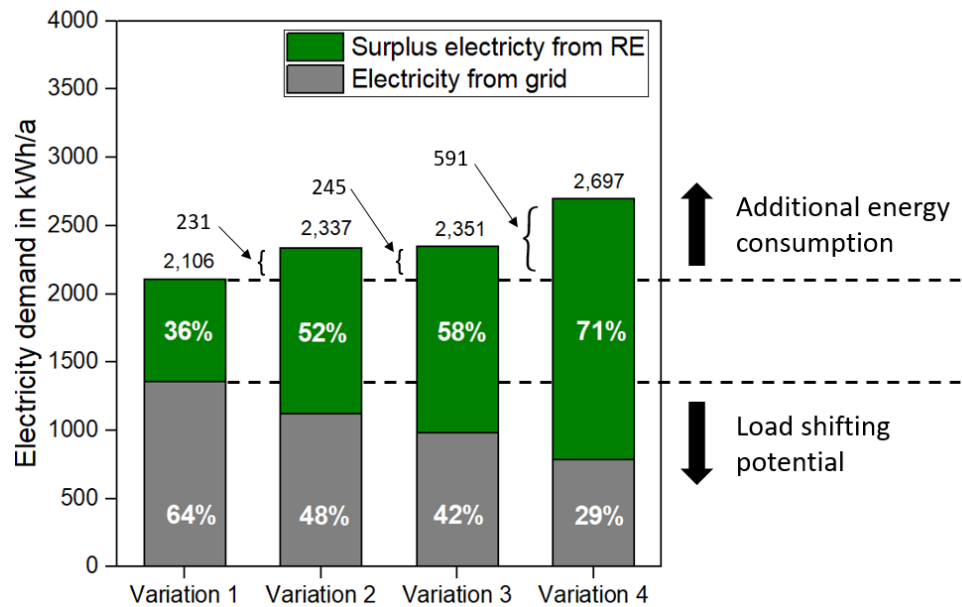


Figure 9.10 Electricity demand of the heat pump.

Figure 9.11 depicts the annual COP distributions of the heat pump with the four control strategies, which are described in Table 9.2. It is clearly seen that the increased supply temperature of the heat pump during the load shifting reduces the COP and consequently the seasonal performance factor (SPF) of the heat pump, which represents the efficiency of the heat pump operation.

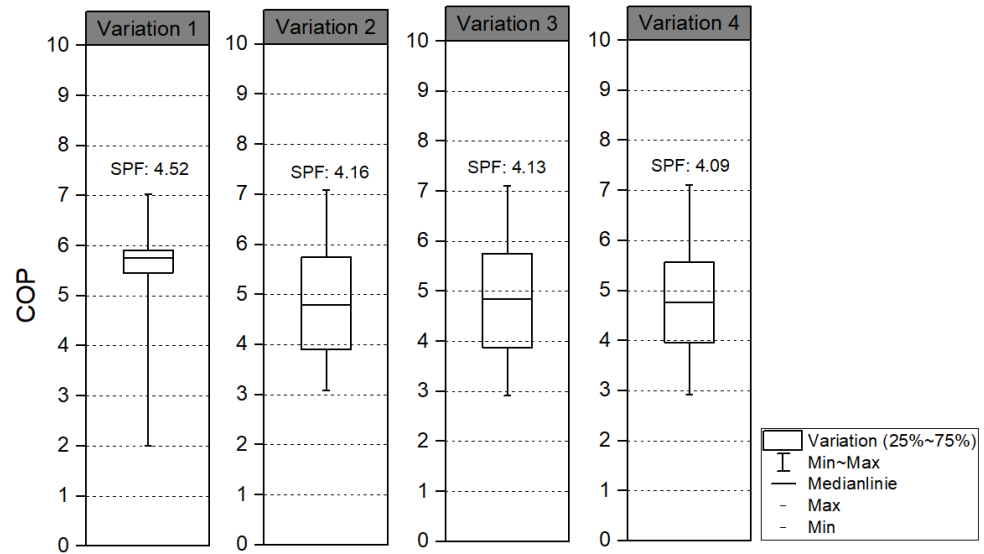


Figure 9.11 The annual COP distribution and SPF.

In comparison to SPF, this study evaluates the primary energy ratio (PER) since the extension of system boundaries from the final energy input (heat pump) to the primary energy input can describe further performance figures related to efficient primary energy usage or renewable energy usage. PER is defined as the ratio of the useful energy output (thermal energy for space heating and DHW supply) to the primary energy input. Primary energy input can be defined either as total energy (renewable and non-renewable) or non-renewable, only. For this study PER is calculated as:

$$PER = \frac{\int (\dot{Q}_{Heat} + \dot{Q}_{DHW}) \cdot dt}{\int E_p \cdot dt}$$

$\dot{Q}_{Heat}$  : Heat demand for space heating

$\dot{Q}_{DHW}$  : Heat demand for DHW-supply

$E_p$  : Primary energy demand (electricity from non-renewable sources)

For the calculation of PER, it is theoretically assumed that local surplus electricity production from wind and PV farms is regarded as renewable energy and has a primary energy factor of 0. Non-renewable electricity has a primary energy factor (PEF) of 2.6 (EnEV 2009, 2009). Figure 9.12 shows the primary energy demand and PER of the heat pump with the different operation strategies. In comparison to SPF, the primary energy demand of the heat pump decreases by using a RBC and the corresponding PER increases by using TES. For example, the primary energy demand (electricity) can be reduced by around 1500 kWh/a and PER increases from 2.7 to 5.4 by a maximum integration of available TES (Variation 4).

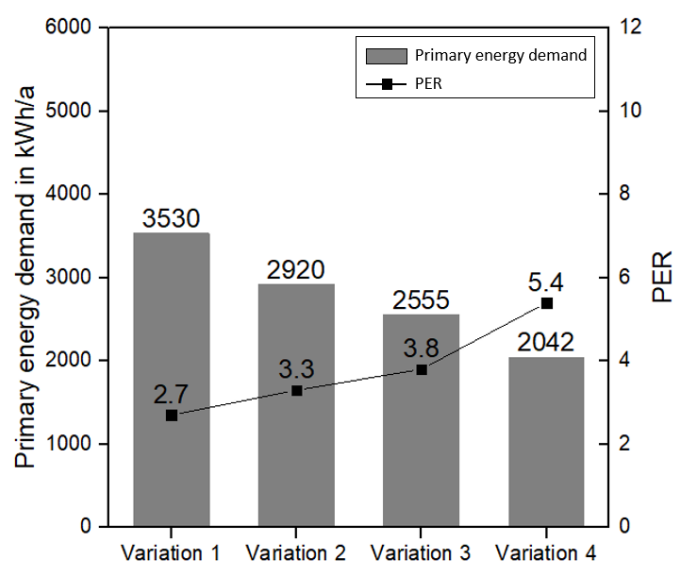


Figure 9.12 Primary energy demand and PER of the heat pump.

In addition to the energetic aspects, the economic aspects of load shifting with RBC are analyzed with different electricity tariff scenarios based on (Weiß, 2013), (Büchner et al., 2017) and (Fraunhofer IWES et al., 2014). The tariff scenarios are based on low and high tariff systems regarding the local residual load (see Figure 9.13). In tariff scenario 1 and 2, the low tariff varies depending on different assumptions for example relief of German Renewable Energies act-surcharge, taxes and network charges for surplus electricity in Germany (Büchner et al., 2017), (Fraunhofer IWES et al., 2014). Additionally, Tariff Scenario 3 considers a case in which energy suppliers provide customers surplus electricity for free, in order to avoid urgent grid congestions. Table 9.3 summarizes the electricity tariff scenarios with specific assumptions.

Table 9.3 Electricity tariff scenarios for the heat pump operation.

Variation	High tariff	Low tariff	Assumption
Reference (conventional tariff for heat pumps)	26.07 Eurocent/kwh	21.02 Eurocent/kwh	-
Tariff Scenario 1	26.07 Eurocent/kwh	14.07 Eurocent/kwh	Relief of EEG-surcharge and taxes for surplus electricity
Tariff Scenario 2	26.07 Eurocent/kwh	7.12 Eurocent/kwh	Relief of EEG-surcharge, taxes and network charge for surplus electricity
Tariff Scenario 3	26,07 Eurocent/kwh	0 Eurocent/kwh	Surplus electricity is available for free

The results of this study show that the load shifting with RBC can reduce the operating costs and give significant economic values to electricity customers with heat pumps, if surplus electricity is available at lower prices. Figure 9.13 shows the savings potential of the operating cost with different heat pump operation strategies in comparison to the heat-driven heat pump operation (Variation 1). Generally, load shifting with the current tariffs increases the operating costs for the heat pump operation. This is due to the fact that the additional electricity demand during load shifting

cannot be compensated with the current electricity price system. This effect can be seen more clearly in Variation 4 by using building mass as TES, since the building has higher heat losses through building envelope compared to hot water storage tanks. From the price difference between high and low tariffs of around 0.12 €/kWh (Tariff Scenario 1), the load shifting with RBC starts to reduce the operating costs. In Tariff Scenario 1, the saving of operating costs is less than 60 €/a. By reducing the electricity price during surplus electricity production, the saving potential of the heat pump operating costs increases significantly. In Tariff Scenario 2, the saving potential of the operating cost ranges between 130 and 170 €/a depending on the use of TES. The utilization of the building mass as TES only has a significant influence on the operating cost saving, if the surplus electricity is delivered with a very low price or for free, as shown in Tariff Scenario 3. In Tariff Scenario 3, the operating costs of the heat pump can be reduced by up to around 310 €/a, which corresponds to 60 % of the operating costs in the reference tariff.

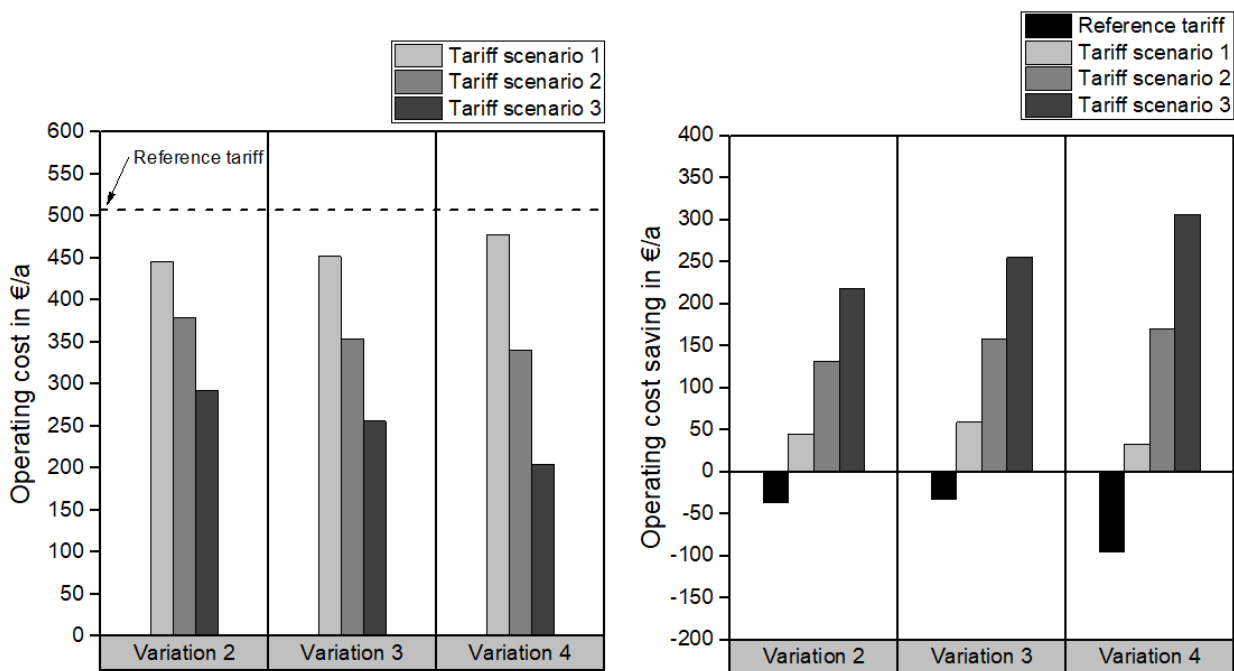


Figure 9.13 Operating cost savings potentials.

In this study, a straightforward RBC is implemented into a heat pump system of a single-family house by using electricity data of a small city in Germany. Thereby, the RBC uses different TES in the building such as, building mass, buffer storage for the space heating and DHW-storage. The operation of the heat pump with a RBC is evaluated regarding energetic and economic aspects. From an energetic point of view, the load shifting of the heat pump with RBC provides disadvantages such as additional electricity demand and reduced COP and SPF of the heat pump, if the energy balance boundary is limited to final energy use. The expansion of the system boundary from final energy to primary energy can enable evaluation of the surplus electricity utilization for load shifting on the overall power network, regarding the energy chain from generation to consumption. For this reason, the heat pump operation should be evaluated for the future energy systems, with a high share of renewable energy sources, using PER besides SPF. From a societal economic point of view, the heat pump operation with RBC for load shifting provides a savings potential of the operating costs if the price difference between low and high tariffs is higher than 0.12 €/kWh. The utilization of the building mass can enable economic benefits, if the surplus electricity price is very low or delivered for free, in order to avoid urgent grid congestions.

# 10 Predictive rule-based control to perform heating demand response in Norwegian residential buildings

John Clauß, Norwegian University of Science and Technology (NTNU), Norway

Four demand response strategies for heating a Norwegian single-family house are investigated in this study. The study is performed for two building insulation levels. Two demand response strategies are based on the electricity spot price, whereas the two other strategies use the average CO<sub>2</sub>eq. intensity of the electricity mix as a control signal. The demand response measures are implemented into predictive rule-based controls that vary the temperature setpoints for space heating and domestic hot water heating depending on the control signals. The predictive rule-based controls are implemented into the building performance simulation tool IDA ICE. Results show that, in Norway, price-based controls typically lead to increased annual emissions because operation is shifted towards nighttime, when Norway usually imports carbon-intensive electricity from the continental European power grid. Furthermore, it is challenging to achieve cost and emissions savings in the investigated Norwegian bidding zone because there are only limited daily fluctuations in the spot price and the CO<sub>2</sub>eq. intensity of the electricity mix.

## 10.1 Building and system description

The building used in this study is a single-family detached house. The building geometry is based on the ZEB LivingLab (Goia, Finocchiaro and Gustavsen, 2015) which is located in Trondheim.. The two building insulation levels investigated comply with the Norwegian building standards from 2010, TEK10, and with the Passive House Standard for residential buildings NS3700, PH. The building has a floor area of 105 m<sup>2</sup> (see the floor plan in Figure 10.1). A brief overview of the building properties is presented in Table 10.1. A model of the building is created in the building performance simulation tool IDA ICE Version 4.8 (EQUA, 2015).

Electric radiators are used for space heating (SH). This is the most common SH system in Norwegian houses (Brattebø et al., 2014). There is one electric radiator in each room with a power equal to the nominal SH power of the room at the design outdoor temperature of -19 °C. Domestic hot water (DHW) is produced in a storage tank, which is equipped with an electric resistance heater with a capacity of 3 kW.

The water storage tank is divided into four horizontal layers to account for stratification effects. The DHW storage volume is 214 liters and is calculated by:

$$V_{\text{DHW}} = S * 65 * n_{\text{people}}^{0.7} \quad [\text{liters}] \quad (1)$$

S is the safety margin and n<sub>people</sub> the number of occupants. S is set to 125 % for a low number of people (Fischer et al., 2017). The charging of the DHW storage tank is controlled by two temperature sensors that are installed at the bottom and at the top of the tank. Regarding the operation principle, the electric resistance heater starts heating as soon as the temperature in the upper part of the tank drops below the setpoint and continues until the setpoint for the temperature sensor in the lower part

of the tank is reached. Daily profiles for DHW use and internal heat gains from electrical appliances, occupants and lighting are implemented according to the Norwegian technical standard, SN/TS 3031:2016 (SN/TS3031:2016, 2016). Schedules for occupancy and lighting are taken from prEN16798-1 and ISO/FDIS 17772-1 standards (Ahmed et al., 2017; ISO17772-1, 2017).

Table 10.1 Building envelope properties and energy system characteristics of the case study building (EW – external wall, IW – internal wall, HR – heat recovery,  $U_{Total}$  is the total U-value of the windows including the glazing and the frame, AHU – Air handling unit, ER – Electric radiator) (Clauß, Stinner, Sartori, et al., 2019).

Building	Building envelope				Thermal bridges	Infiltration	Windows	AHU	HDS	SH needs
	$U_{EW}$	$U_{IW}$	$U_{Roof}$	$U_{Floor}$			$U_{Total}$	$\eta_{HR}$	ER	
	W/(m <sup>2</sup> K)				W/(mK)	ACH	W/(m <sup>2</sup> K)	%	W/m <sup>2</sup>	kWh/m <sup>2</sup>
PH	0.10	0.34	0.09	0.09	0.03	0.60	0.80	85	40	34
TEK10	0.16	0.34	0.18	0.18	0.03	2.5	1.2	70	78	91

The Energy Flexibility potential of four different predictive rule-based controls (PRBC) is evaluated; two strategies are based on the electricity spot price and two scenarios are based on the average CO<sub>2</sub>eq. intensity of the grid electricity mix. The reference scenario, termed BAU (for business as usual), applies constant (reference) temperature setpoints ((R)TSP) for DHW (50 °C) and SH (21 °C). The bathroom TSP is 24 °C. All doors are closed at all times. The demand response (DR) strategies are applied to the common rooms (meaning both Living Rooms). The study is performed for the year 2015. Weather data is retrieved from (OpenStreetMap, 2017) and hourly day-ahead spot prices for each bidding zone are taken from NordPool (Nord Pool Spot, 2016). The spot price is used as an input signal for the price-based control and to calculate the heating costs. An electricity fee for the use of the distribution grid is not considered in the cost evaluation. The hourly average CO<sub>2</sub>eq. intensity of the electricity mix is calculated based on the methodology introduced in (Clauß et al., 2018).

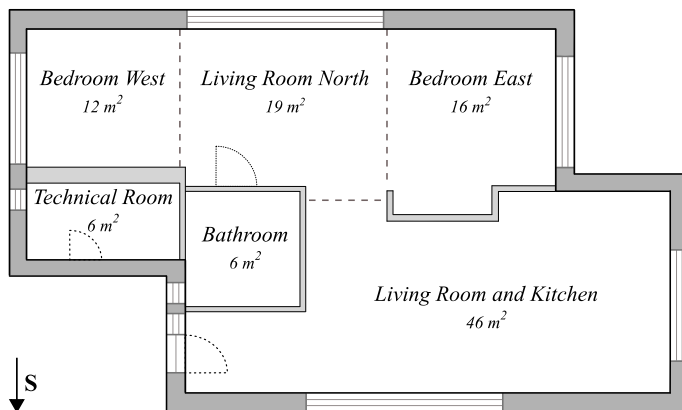


Figure 10.1 Floor plan of the studied building (Clauß, Stinner, Sartori, et al., 2019).

## 10.2 Methodology: control strategies

The DR strategies are implemented into PRBCs. The TSPs for SH and DHW heating are varied depending on the penalty signal. The main objective of the controls is shifting loads away from peak hours. At the same time, the control strategies aim at reducing costs and/or carbon emissions. Thermal energy storages, here the building thermal mass and a water storage tank, are activated by changing the respective TSPs depending on the penalty signal. The TSPs for SH are either increased by 3 K (24 °C), or decreased by 1 K (20 °C). For DHW, the TSPs can be increased by 10 K (60 °C) or decreased by 5 K (45 °C).

The penalty signal for the CO<sub>2</sub>eq.-based controls is determined based on two principles. CSC-a, aims at operating the energy system in times of lowest CO<sub>2</sub>eq. intensities, whereas CSC-b rather charges the storages just before high-carbon periods in order to avoid the energy use during these critical periods. Both principles for the determination of the control signal are illustrated in Figure 10.2. For Norway, principle CSC-a may, in practice, lead to extended periods with high TSPs because hourly CO<sub>2</sub>eq. intensities are typically low during daytime (Clauß et al., 2018). Thus, an unnecessary increase in annual energy use for heating may occur. Applying CSC-b, the TSPs are increased for shorter time periods compared to CSC-a, thus improving the energy efficiency.

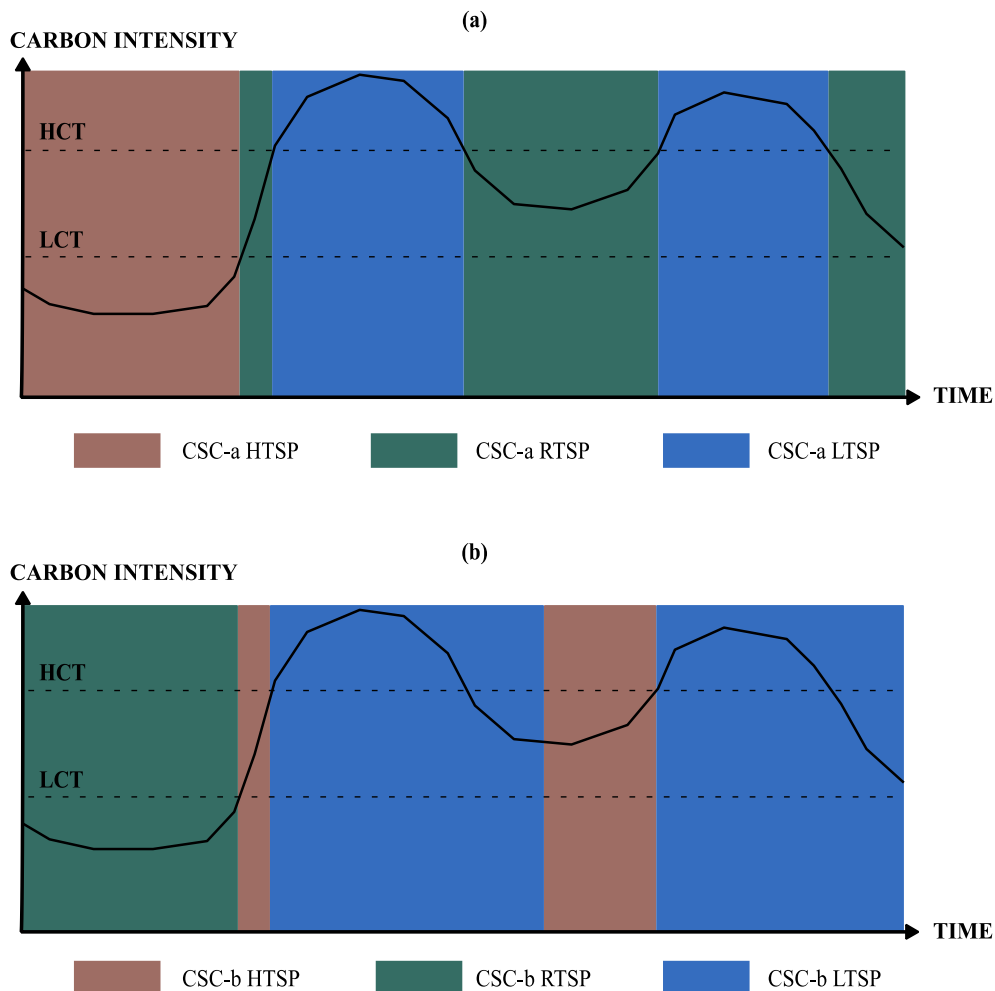


Figure 10.2 Principle of the determination of the carbon-based control signal according to (a) CSC-a and (b) CSC-b (HTSP is high temperature setpoints, RTSP is reference temperature set-points, LTSP is low temperature setpoints) (Clauß, Stinner, Solli, et al., 2019).

The penalty signal can be divided into three segments. The PRBCs use a 24-hour sliding horizon to determine a high- CO<sub>2</sub>eq. intensity threshold (HCT) and low- CO<sub>2</sub>eq. intensity threshold (LCT). The current CO<sub>2</sub>eq. intensity (CI) is compared to these thresholds at each hour. Taking C<sub>l</sub>max and C<sub>l</sub>min as the maximum and minimum intensities for the next 24h, LCT has been selected to C<sub>l</sub>min + 0.3 (C<sub>l</sub>max-C<sub>l</sub>min) and HCT to C<sub>l</sub>min + 0.7 (C<sub>l</sub>max-C<sub>l</sub>min). For CSC-a, the TSPs are increased, if the CO<sub>2</sub>eq. intensity of the current hour is below the LCT and the setpoints are decreased to delay the start of the heating, if the CO<sub>2</sub>eq. intensity is above the HCT. If the CO<sub>2</sub>eq. intensity of the current hour is between the LCT and HCT, the TSPs remain equal to the reference scenario. For CSC-b, the control signal is also determined based on the three price segments, as defined for CSC-a, but, additionally, the control considers if the current CO<sub>2</sub>eq. intensity is increasing or decreasing with time. TSPs are increased, if the current CO<sub>2</sub>eq. intensity is between the LCT and HCT and the CO<sub>2</sub>eq. intensity is increasing in the next two hours (Clauß, Stinner, Solli, et al., 2019).

Price-based control signals, hereafter called CSP-a and CSP-b, are also determined similar to CSC-a and CSC-b, to also investigate DR measures based on the electricity spot price in the bidding zone (BZ). It is interesting to investigate CO<sub>2</sub>-based and price-based controls because the electricity spot price and the average CO<sub>2</sub>eq. intensity of the electricity mix are opposing. This is shown in Figure 10.3.

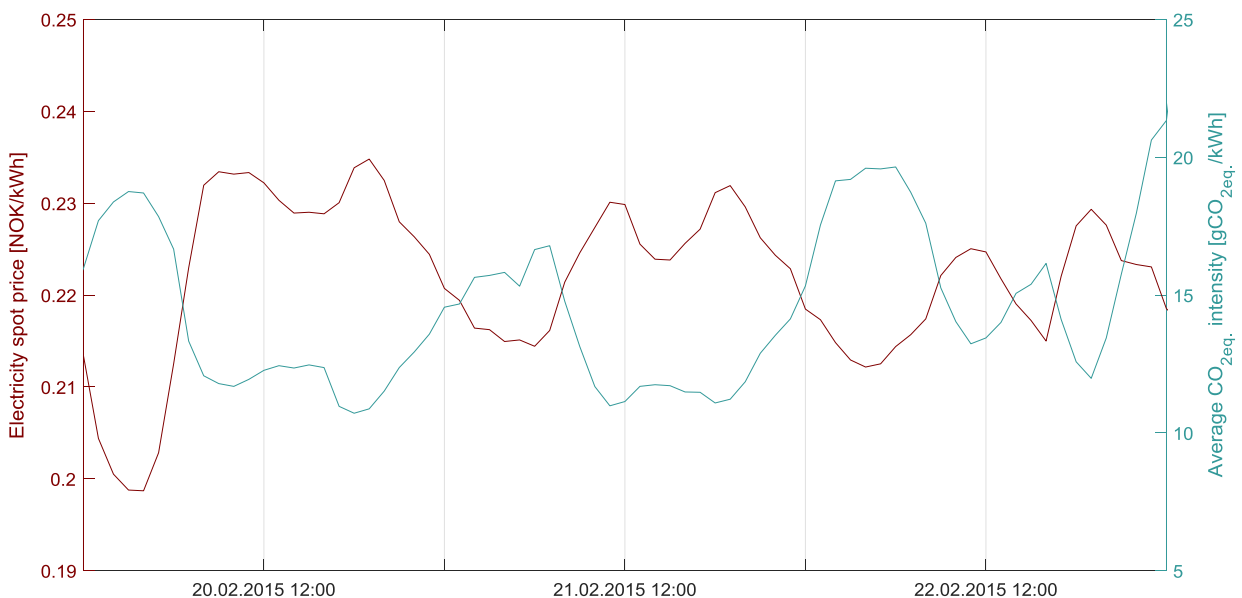


Figure 10.3 Spot price (Nord Pool Spot, 2016) and average CO<sub>2</sub>eq. intensity (Clauß *et al.*, 2018) in bidding zone NO3 during an exemplary period in 2015.

### 10.3 Implementation: control algorithms

The control principles are implemented into predictive rule-based control strategies. Figure 10.4 illustrates the principle of the CSC-b control strategy for the TEK10 building during 48h of the heating season in the Norwegian bidding zone NO3 as an example. Figure 10.4(a) presents the CO<sub>2</sub>eq. intensity as well as the low-carbon and high-carbon thresholds. Figure 10.4(b) shows the start and stop TSPs for the DHW hysteresis control as well as two temperatures in the DHW tank. The TSPs fluctuate based on the CO<sub>2</sub>eq. intensity signal. Also the TSPs for SH vary depending on the control signal, shown in Figure 10.4(c). It can be seen from Figure 10.4(d) that the operation of the electric

resistance heater for DHW heating depends on the CO<sub>2eq.</sub> intensity signal and the temperature hysteresis.

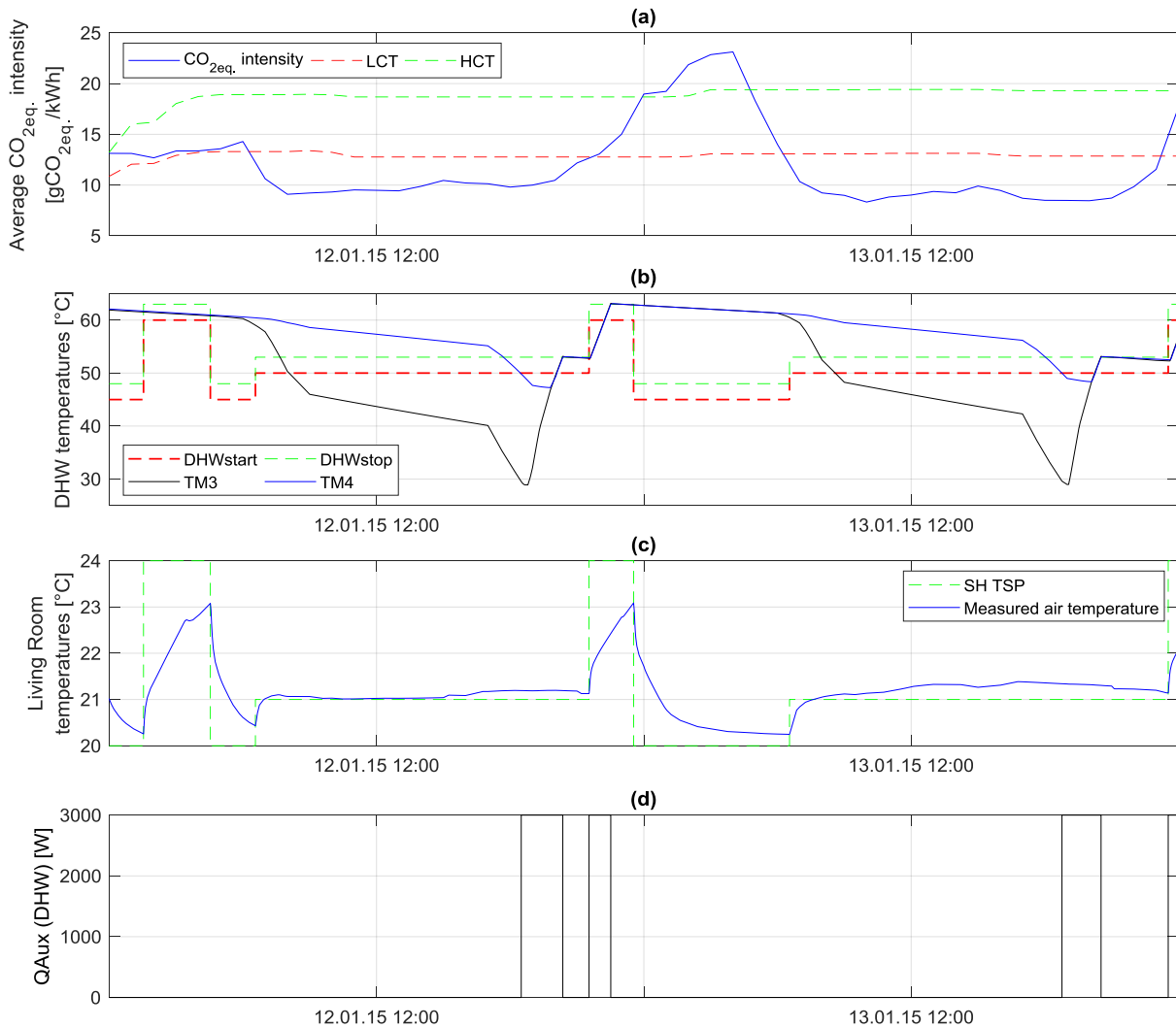


Figure 10.4 Illustration of the control principle for NO<sub>3</sub> for TEK10 case CSC-b during a 48h period (LCT is Low-carbon threshold, HCT is High-carbon threshold, DHWstart and DHWstop are the start and stop temperatures for DHW, TM<sub>x</sub> are two temperatures in the water tank).

## 10.4 Results and conclusion

Table summarizes energy use, costs and emissions for the investigated DR strategies for both building insulation levels. The relative difference for annual electricity use for heating compared to the reference case (BAU) is calculated by

$$EI. = (EI._{CS}/EI._{BAU}) * 100 - 100 \quad [\%] \quad (2)$$

where CS is Control Strategy, EI. is Electricity. The same equation can be used to determine the relative differences for the total annual carbon emissions and costs.

Table 10.2 shows that electricity use increases for all four control strategies. It can be seen that the CO<sub>2</sub>eq.-based and price-based control strategies lead to contradictory results: if the aim is to reduce emissions (CSC-a and CSC-b), costs are increased and if the aim is to reduce costs (CSP-a and CSP-b), emissions are increased significantly. This is due to the typical daily profile for the Norwegian spot prices and CO<sub>2</sub>eq. intensities, because CO<sub>2</sub>eq. intensities are low, when spot prices are high and vice versa (Clauß et al., 2018; Clauß, Stinner, Sartori, et al., 2019). Therefore, a trade-off between the objectives has to be made to satisfy both aims. Similar trends for annual costs and emissions are visible for both building insulation levels.

More specifically, regarding the CO<sub>2</sub>eq.-based control strategies, the CO<sub>2</sub>eq. emissions are increased slightly (3 % and 2 % for the two insulation levels), while costs are increased by up to 14 % and 13 % for the PH and TEK10 respectively with the control strategy CSC-a. This results from increased temperature setpoints during grid peak hours because the CO<sub>2</sub>eq. intensity is usually lowest during these periods. For CSC-b, the temperature setpoints are increased just after grid peak hours, when the CO<sub>2</sub>eq. intensities are increasing. On an annual perspective this strategy leads to increased CO<sub>2</sub> emissions, but to lower cost increases compared to CSC-a, also because the energy use increases less for CSC-b than for CSC-a.

Regarding the price-based control strategies, both strategies lead to slightly increased costs (2 %) for both building insulation levels even though for CSP-a the energy use is increased by 10 % and 12 % for TEK10 and PH respectively, whereas it is increased by only 5 % and 7 % for CSP-b. The energy use is higher for CSP-a compared to CSP-b because the temperature setpoints are increased for longer time periods (usually several hours during the night). CSP-b increases the temperature setpoints just before each peak period to make sure that the thermal storages are charged just before peak hours. This means that CSP-a makes use of the lowest spot prices, whereas CSP-b does not, hence costs increase by 2 % for both cases even though the energy use increases more for CSP-a than for CSP-b. Furthermore, it is shown that CSP-a increases total CO<sub>2</sub>eq. emissions by 19 % for the TEK10 building and by 26 % for the PH building. This is again due to the fact that CO<sub>2</sub>eq. intensities in NO3 are usually low when spot prices are high (see Figure 10.3). Compared to CSP-a, total CO<sub>2</sub>eq. emissions are increased less for CSP-b because temperature setpoints are increased during periods with increasing spot prices. During the same periods, CO<sub>2</sub>eq. intensities are decreasing, thus leading to lower total CO<sub>2</sub>eq. emissions.

Table 10.2 Energy use, annual costs and emissions relative to the reference case for the investigated cases.

	BAU			CSC-a			CSC-b			CSP-a			CSP-b		
	E <sub>Use</sub>	CO <sub>2</sub>	\$	E <sub>Use</sub>	CO <sub>2</sub>	\$	E <sub>Use</sub>	CO <sub>2</sub>	\$	E <sub>Use</sub>	CO <sub>2</sub>	\$	E <sub>Use</sub>	CO <sub>2</sub>	\$
	kWh	kg	NOK	%	[%]	[%]	[%]	[%]	[%]	[%]	[%]	[%]	[%]	[%]	[%]
PH	7543	86	1622	+12	+3	+14	+7	+8	+3	+12	+26	+2	+7	+11	+2
TEK10	13512	159	2872	+11	+2	+13	+5	+4	+3	+10	+19	+2	+5	+8	+2

It should be investigated whether savings could be increased with advanced controls such as model-predictive control. Furthermore, the potential emission and cost savings would be stronger in locations with higher daily fluctuations of the spot price and average CO<sub>2</sub>eq. intensity. For bidding zone NO3, the potential savings are outweighed by the increased electricity use for heating, independent of the building insulation level.

# 11 CO<sub>2</sub>-aware heating of indoor swimming

Rune Grønberg Junker, Department of Applied Mathematics and Computer Science, Technical University of Denmark

In this study, an economic model predictive control was used to control the heating of indoor swimming pools. The objective was to minimize the CO<sub>2</sub> emission caused by the power plants producing the electricity used by the heat pumps of the swimming pools. The case study showed how flexibility can successfully be utilized by simply having varying penalty signals describing the cost of consumption in time.

## 11.1 Building and system description

This case study is based on indoor swimming pools located in Danish summer houses. The swimming pools are heated by air-to-water heat pumps, which are controlled to activate the Energy Flexibility associated with the thermal inertia of the water in the swimming pools. A total of 30 houses are controlled, 17 of them being located in Blåvand and 13 in Blokhus (both at the coast of the North sea). To simplify the setup and protect the hardware, the heat pumps are activated through temperature setpoints for the pool water. These are set higher than the current water temperature to turn the heat pumps on and vice versa to switch them off. The air temperature is not controlled in this project, but it is left as is, with standard thermostatically controlled heating. The summer houses are rented out on weekly basis, so the test period includes both periods without any residents using the pool and periods where it is used. When the summer houses are not rented out, the temperature of the pools is reduced to limit energy consumption. Since the heat loss of the swimming pools depends on the ambient temperature, the power consumption does as well. Thus, the varying weather conditions and occupancy of the summer houses impact the heating of the swimming pool, and thus also the available Energy Flexibility. The size and shape, and thus also the thermal properties, of the swimming pools is vastly different for each of the summer houses. Most of the swimming pools are equipped with heat pumps, however, again many different sizes and types are used. Furthermore, a few of the swimming pools are heated by electric boilers. The differences between swimming pools and heating equipment is not assumed to be known by the controller. Thus, individual models used for each of the summer houses are estimated adaptively by RLS (Madsen, 2007).

## 11.2 Methodology: control strategies

Swimming pools are filled with large amounts of water, which implies large heat capacities. This means that a lot of energy can be stored in the water by a small increase of the temperature level. Conversely, heating of the swimming pools can be reduced without an immediate large drop in water temperature. For example, a swimming pool of 1.5 m depth and a surface area of 16 m<sup>2</sup> has a total of 24 tons of water, amounting to a heat capacity of 100,464 KW/K. If the temperature can be tolerated to change within  $\pm 1$  K, then the swimming pools present approximately 200 MWh of Energy Flexibility. However, heat pumps are designed to be turned on and off infrequently, and thus

these systems are not ideal for ancillary services for voltage and frequency control, where up and down regulation changes frequently.

The swimming pools are controlled through indirect control. This is made possible by equipping each swimming pool with an Economic Model Predictive Controller (E-MPC) as described in (Zemtsov, et al., 2017), that schedules the heating of the pool such as to keep the temperature within comfort boundaries as cheaply as possible. To utilize the Energy Flexibility, varying penalties can be sent to the E-MPC, according to which it will minimize the operational costs. For this pilot, first the CO<sub>2</sub>-intensity was used as penalty signal, and later the prices from the Danish regulation market. Thus, it was first used to minimize CO<sub>2</sub> emission, and later to improve grid balancing.

### 11.3 Implementation: control algorithms

E-MPC are used to control the temperature of the swimming pools according to penalty signals. The optimization problem solved by the controllers is given by:

$$\begin{aligned} \min \sum_{k=0}^N & \lambda_{t+k} u_{t+k} + \lambda^A |u_{t+k} - u_{t+k-1}| + \lambda^T s_{t+k} \\ \text{s.t. } \forall k \in & \{k, k+1, \dots, N\} \\ & u_{t+k} \in \{0, 1\}, s_{t+k} \geq 0, \\ & T_{t+k+1} = AT_{t+k} + Bu_{t+k}, \\ & T_{t+k} \geq T_{min} - s_{t+k}, \\ & T_{t+k} \leq T_{max} + s_{t+k}. \end{aligned}$$

where subscripts refer to time steps,  $\lambda_t$  is the forecast electricity price,  $\lambda^A$  is the cost of turning the heat pumps on and off,  $\lambda^T$  is the penalty for each K the swimming pool is out of the comfort limits.  $u_t$  is the state of the heat pump, 1 for on and 0 for off. The temperature limits are given by  $T_{min}$  and  $T_{max}$ .

The cost related to turning the heat pump on and off is due to fatigue on the heat pump, which should be limited.  $A$  and  $B$  are the system matrices describing how the temperature is expected to evolve over time, for given heating schedules. For the swimming pools it is found that using a first order autoregressive model is sufficient to describe the heat dynamics. This means that  $A$  and  $B$  are simply scalars. The case study deals with several summer houses, all with similar but different heat dynamics, due to their varying shapes, sizes and heating equipment. Thus, the numerical values of  $A$  and  $B$  are estimated individually for each summer house. Furthermore, to accommodate the changing weather conditions and their effect on the swimming pools, the parameter estimates are allowed to change in time. This is incorporated by using recursive least squares (RLS) (Madsen, 2007), to re-estimate the model parameters at every time step. Also, the energy consumption is reduced when the summer houses are not booked, by lowering the temperature requirements in these periods. For the controller this is simply achieved by varying  $T_{min}$  and  $T_{max}$ .

The controller is designed to be indifferent about the temperature as long as it is within the comfort interval. This is seen from the objective function that only consists of two terms related to the cost of running the heating, and a third term that penalizes the controller if it leaves the comfort interval.

This is in contrast to other approaches where the temperature is kept close to some value with deviations being accepted if the penalty signal warrants it. These are two different philosophies, where on the one hand temperature deviations are assumed to only impact the comfort significantly if they last for long enough, and on the other hand relatively large temperature deviations are considered unacceptable no matter how short, but small temperature deviations are considered acceptable, no matter how long. The approach taken here is in the category of the latter.

Since the heat dynamics of swimming pools are very slow, the control horizon has to be long. In this project a control horizon of 24 hours is chosen, since longer horizons are computationally infeasible when operating in a 5 min. resolution. However, this horizon is too short to ensure that the swimming pools has enough time to get heated, when the temperature is to be increased prior to guests arriving in the summer houses. To combat this limitation without increasing the control horizon, the temperature limits are continuously increased 24 hours before the arrival of new guests, so that the controller sees the increased temperature limits 48 hours in advance, and thus has enough time to heat the pool.

## 11.4 Results and conclusion

The agile implementation of the setup, where setpoints are sent to control the pool, with the actuation being carried out by the default hardware, meant that sometimes the heating would not start or stop, even though the controller asked for it. This can be seen in Figure 11.1 that shows box plots of the power demand of summer house P32359, when the E-MPC did and did not call for heat. It is evident that usually the electricity consumption is much larger when the controller calls for heat, indicating that the control works. However, there are many instances where the E-MPC is calling for heat, but the power demand stays at almost zero, meaning that actually the heating is not on. Of course, the power demand of the remaining parts of the summer house is also included, which is not controlled, and thus this is seen as noise.

Following the approach described in (Junker, et al., 2018) the Flexibility Function shown in Figure 11.2 will be used to evaluate the flexibility of the swimming pools. This shows the expected change in power consumption if the penalty signal is a step increase of  $1 \text{ DKK/kWh} \approx 1/7.5 \text{ EUR/kWh}$ . It is evident how the very slow dynamics of the pool on the one hand enables it to move a lot of flexibility for a long time, we get  $A = 21 \text{ kWh}$  and  $\beta = 19 \text{ h}$ . On the other hand, the maximum effect is relatively low, corresponding to  $\Delta = -2 \text{ W}$ , which is small, and the change in demand takes effect slowly, with  $\alpha = 12 \text{ h}$ . Lastly, there is only a small rebound effect, with  $B = 3.5 \text{ kWh}$ .

The objective with regard to the temperature of the pool is to keep it within comfort boundaries. This, combined with the fact that the controller is deterministic in the sense that it believes forecasts to be accurate, means that it will operate the temperature very close to the lower temperature boundary in order to reduce energy consumption. This means that it is usually not ready to reduce power consumption, in case of a non-anticipated increase in penalty, since this would result in the temperature dropping below the lower temperature limit. As a consequence, the controller is not good for providing flexibility, if the need for this is not anticipated hours in advance. The very nature of the regulation market means that up and down regulation is usually not anticipated, and so this is not an ideal way of designing controllers for this market. On the other hand, this kind of deterministic controller works well for foreseeable problems, such as peak demands in the morning and afternoon, since the increased cost associated with these can be forecasted with high accuracy. Thus, this flexibility should be bid into the wholesale market, rather than the regulation market. The slow response observed for the flexibility function in Figure 11.2 is a result of the MPC limiting the fatigue

on the heat pump, resulting in the response to penalty changes not being instantaneous. Similarly, the lack of a rebound effect can be linked to the fact that the MPC does not try to bring back the temperature to what it was prior to a large change in penalty.

It is found that the Energy Flexibility varies in time, partly due to weather conditions, but even more so due to occupancy of the summer houses. Here, the summer houses are always in one of the 4 states:

- 1) Booked.
- 2) Available.
- 3) Transitioning from Available to Booked.
- 4) Transitioning from Booked to Available.

To save energy, the temperature of the pool is decreased when the summer house is available. However, the temperature can vary a bit no matter whether the summer house is booked or not, so there is Energy Flexibility available in both cases. On the other hand, when the summer house is approaching a time where it is Booked, the temperature of the swimming pool has to be increased, and during this time there is almost no flexibility available, since the heating has to be turned on almost constantly for two days. Similarly, when a period in which the summer house was booked comes to an end and is followed by a period of being available, the temperature of the swimming pool is much higher than what it is required to be, and thus almost no heating is required for several days. This severely limits the Energy Flexibility, since it is usually cheaper to simply leave the heating off. The length of the transitions depends on the swimming pools, but usually takes between two and four days. This means that if the summer house is Available for one week in between two periods of being booked, all or almost all of the Available week is made up of transitioning periods with little to no Energy Flexibility.

An example of this is shown in Figure 11.3, that shows the temperature of one of the swimming pools during operation where it became Available, but the temperature only barely reached the Available steady state before the heating had to resume heating to meet the temperature requirements of being warm for a booked period. For this particular swimming pool, it took approximately 7 days of almost no heating to reach the lower temperature boundary. In fact, two events where the heating was switched on are seen, showing that some Energy Flexibility was still present. After the lower temperature is reached, the heat is turned on again, and it takes around 1.5 days to reheat the swimming pool, during which the heating is never turned off.

The effectiveness of the control is estimated based on one of the summer houses, D7811 during the three first weeks of October 2017. This period is shown in Figure 11.4, where the top plot shows the temperature of the swimming pool in blue, and the heating (1 for on and 0 for off) in red. The bottom plot displays the CO<sub>2</sub>-intensity for the same period. Inspecting the figure reveals that indeed the pool is mostly heated during periods with low CO<sub>2</sub>-intensity. In fact, the average CO<sub>2</sub>-intensity during the periods where the pool is heated equaled 202 g CO<sub>2</sub>/kWh, while the overall average is 223 g CO<sub>2</sub>/kWh. Thus, assuming that the total amount of required energy is not influenced by the controller, it manages to reduce the CO<sub>2</sub>-emissions by 9.6 %. Considering the limited budget used for the installations, and the technical issues related to this, 9.6 % is considered a success.

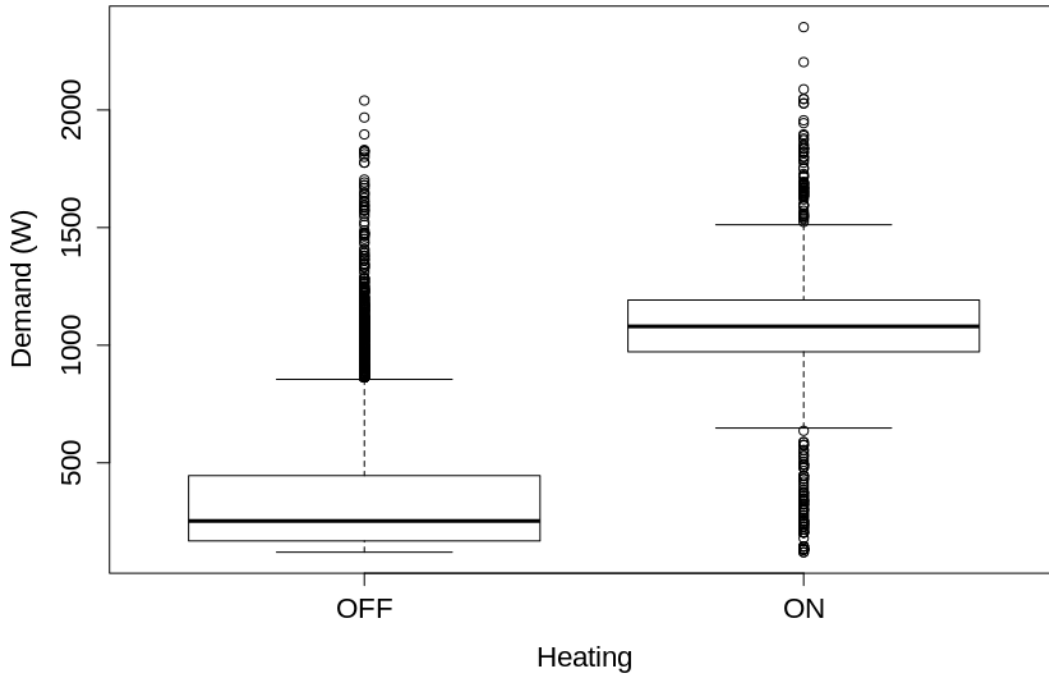


Figure 11.1 Demand when E-MPC is and is not calling for heating.

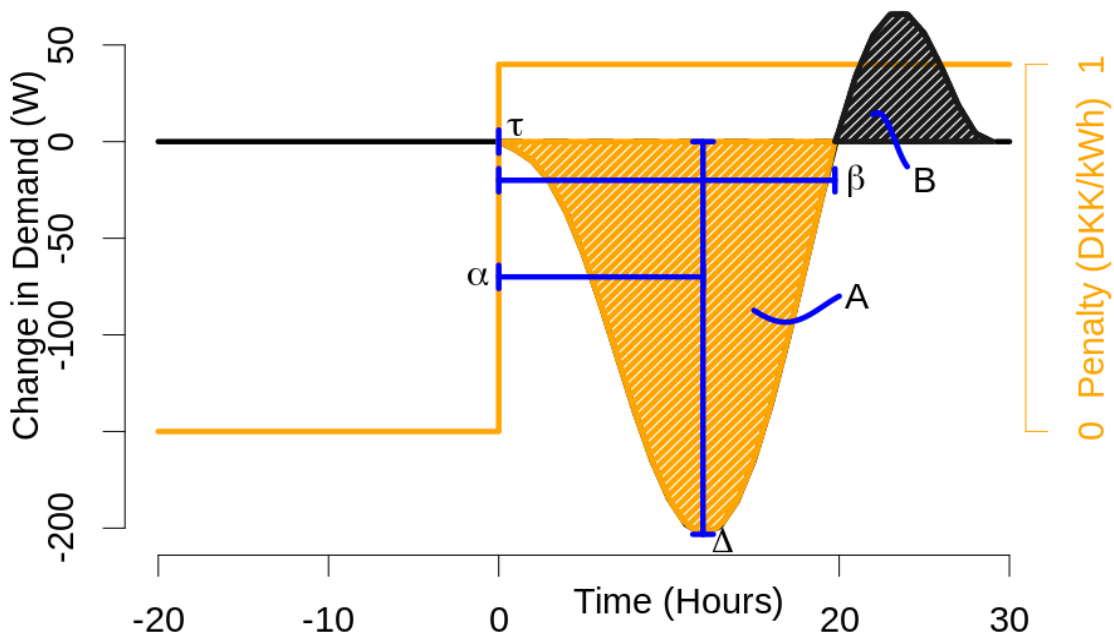


Figure 11.2 Flexibility function estimated from Danish summer houses with indoor swimming pools controlled by E-MPCs.

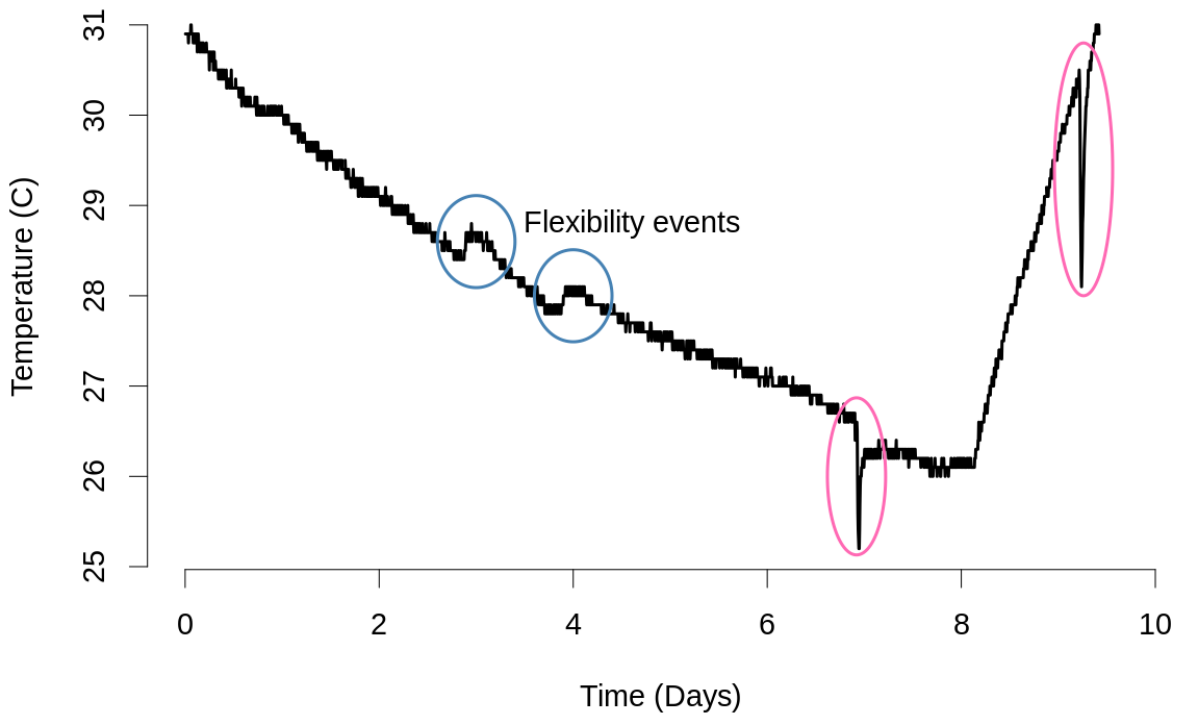


Figure 11.3 The temperature of a swimming pool during a period just after the summer house became Available and before it was Booked again. The blue circles show the only two events where flexibility is used to change the heating schedule. The temperature drops within the pink ellipsoids are sensor errors.



Figure 11.4 The effectiveness of the control during the three first weeks of October 2017

# 12 Economic model predictive control for demand flexibility of a residential building

Christian Finck, Eindhoven University of Technology, Netherlands

In this study, an economic model predictive control (EMPC) is validated and tested to optimize demand flexibility (Finck, et al., 2019). The operational costs of energy usage are associated with demand flexibility, which is represented by three flexibility indicators: flexibility factor, supply cover factor, and load cover factor. The results from a day-long test show that these flexibility indicators are maximized when the EMPC controller's demand flexibility is compared to that of a conventional proportional-integral (PI) controller. The EMPC framework for demand flexibility can be used to regulate use of on-site energy harvest, grid draw and grid feed-in and can thus serve as a basis for overall optimization of the operation of heating systems to achieve greater demand flexibility.

## 12.1 Building and system description

A Dutch residential building is used as a testbed to conduct the experimental case study. During the test period, two persons lived in the dwelling. The dwelling is located in the city of Utrecht, the Netherlands, representing a typical old row house from 1910. The dwelling has an overall floor area of 75 m<sup>2</sup> spread across three floors (kitchen on first floor, living room on second, and bedroom on third). During cold periods, when heating is required, the room temperature is controlled by one thermostat located on the second floor. The annual heating energy usage is about 0.47 GJ/m<sup>2</sup>, which was delivered by a gas-fired condensing boiler. A detailed description of the building and the heating system can be found in (Finck, et al., 2019).

## 12.2 Methodology: control strategy

For the modelling of the heating system and the building, artificial neural network (ANN) models are identified from measurements. The ANN models are validated and implemented in the MPC framework. The validation of the ANN-MPC is conducted based on heating consumption. The MPC is modified to EMPC, and photovoltaic (PV) panels are virtually installed on the building to simulate on-site electricity generation (Figure 12.1). Additionally, a heat pump (HP) is virtually installed to simulate energy conversion from electricity to heating power. The virtual models of the PV panels and the HP are implemented in the EMPC. Thus, the EMPC is simulated and tested with the energy system, including PV panels providing power that can be directly used by a heat pump (HP) or can be fed to the power grid (Finck, et al., 2019).

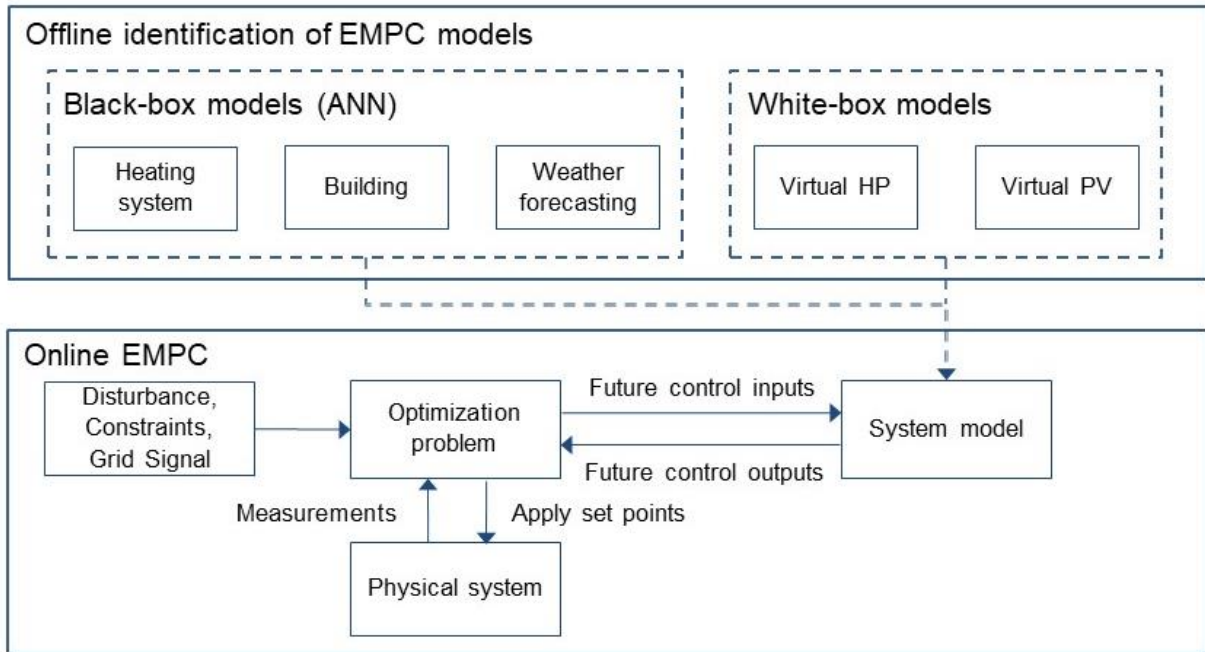


Figure 12.1 Methodological framework of the economic model predictive control (EMPC) controller (Finck, et al., 2019).

### 12.3 Implementation: control algorithm

The EMPC is implemented enabling real-time control with hourly time steps. A receding horizon of 12 hours is used for the EMPC to regulate the room temperature setpoints. Real-time measurements serve as hourly starting points. The controller implements openings of windows, openings of curtains, and upper and lower comfort bounds, which are based on occupants' preferences (Finck, et al., 2019).

Dynamic programming (DP) is used as optimization strategy and carried out in MATLAB. The DP algorithm handles the optimization with sufficiently short computational times of less than 30 min, because there is only one control variable, which is the average room temperature of the living room. During the computation of the optimization at each control time step, first the duration of computation is estimated, then the simulation is run to predict 12 hours ahead.

To investigate the optimization of costs of energy usage associated with demand flexibility, the EMPC assumes (1) the costs of consuming electricity from the grid, (2) the costs of consuming electricity from on-site PV power generation, and (3) the costs of delivering electricity from on-site PV power generation to the grid. Thus, the EMPC incorporates the costs of export of electricity and the costs of electricity consumption in one objective function.

$$\begin{aligned} \min J_{EMPC} = & \sum_{t=1}^N (C_{el.cons.grid}(t) Q_{el.cons.HP-grid}(t) \Delta t) + \sum_{t=1}^N (C_{el.cons.PV}(t) Q_{el.cons.HP-PV}(t) \Delta t) \\ & + \sum_{t=1}^N (C_{el.feed\ in\ grid}(t) Q_{el.PV\ grid}(t) \Delta t); \quad N = 12\ h; \quad \Delta t = 1\ h, \end{aligned}$$

where  $C_{el.cons.grid}$  is the price of electricity consumption from the grid,  $C_{el.cons.PV}$  is the price of electricity consumption from on-site PV generation, and  $C_{el.feed\ in\ grid}$  is the price of electricity exported to the power grid (Finck, et al., 2019).

Accordingly, the most common indicators representing demand flexibility – the flexibility factor, supply cover factor, and load cover factor (C, et al., 2018) (J, et al., 2017) – can be maximized while using an EMPC implementation that minimizes the total costs of energy usage. The flexibility factor  $FF$ , supply cover factor  $\gamma_{supply}$ , and load cover factor  $\gamma_{load}$  are defined as follows

$$FF = \frac{\int_{t_{low\ price\ start}}^{t_{low\ price\ end}} Q_{heating} dt - \int_{t_{high\ price\ start}}^{t_{high\ price\ end}} Q_{heating} dt}{\int_{t_{low\ price\ start}}^{t_{low\ price\ end}} Q_{heating} dt + \int_{t_{high\ price\ start}}^{t_{high\ price\ end}} Q_{heating} dt},$$

with  $-1 \leq FF \leq 1$ ,

$$\gamma_{supply} = \frac{\sum_{t=1}^N Q_{el.cons.HP-PV}}{\sum_{t=1}^N Q_{el.gen.PV}},$$

with  $0 \leq \gamma_{supply} \leq 1$ ,

$$\gamma_{load} = \frac{\sum_{t=1}^N Q_{el.cons.HP-PV}}{\sum_{t=1}^N Q_{el.cons.HP}},$$

with  $0 \leq \gamma_{load} \leq 1$ .

A reference case was simulated to evaluate the results of EMPC1 and EMPC2. A 24-h period was simulated using a traditional PI controller according to

$$T_{room,set,ref} = \begin{cases} T_{room,set,ref} = 18 & \text{if } t \in (0:00, 8:00) \\ T_{room,set,ref} = 20 & \text{if } t \in (8:00, 24:00) \end{cases}.$$

## 12.4 Results and conclusion

During the test day, hourly predictions of the ambient temperature are retrieved from local weather stations. Global and horizontal solar radiation is calculated based on the developed forecasting model. The EMPC results are illustrated below, and measured data are compared to predicted data (Finck, et al., 2019).

The EMPC, designed to maximize the flexibility factor, the supply cover factor, and the load cover factor, is implemented and tested. Figure 12.2 shows the results of the weather forecasting and measurement data

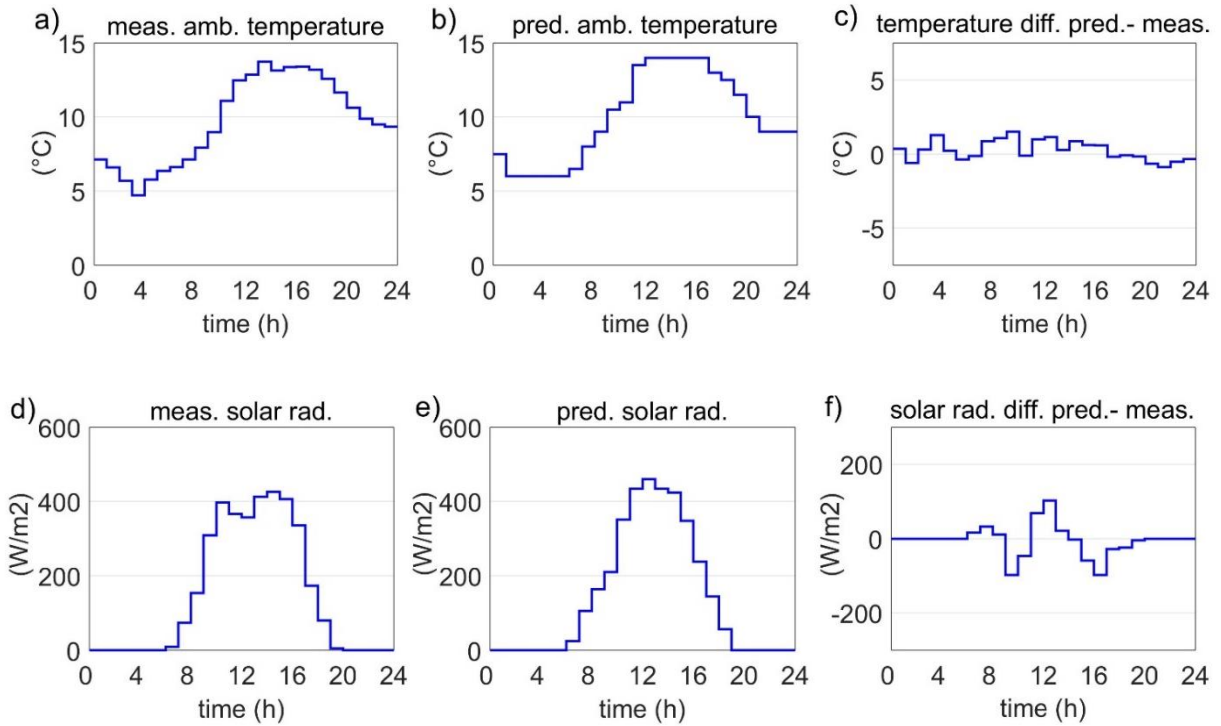


Figure 12.2 EMPC; hourly ambient temperature a) measured, b) predicted, and c) difference; hourly global and horizontal solar radiation d) measured, e) predicted, and f) difference (Finck, et al., 2019).

A prediction performance is calculated for the ambient temperature of RMSE = 0.71, MAE = 0.58, MAPE = 0.06, R2 = 0.94, and G = 0.76 and for hourly solar radiation of RMSE = 42, MAE = 25, MAPE = 0.25, R2 = 0.95, and G = 0.76 (Finck, et al., 2019).

In addition to electricity prices ( $C_{el.cons.grid}(t)$ ) from Amsterdam Power Exchange market, the EMPC requires the determination of the price of electricity consumed from PV generation ( $C_{el.cons.PV}$ ) and the price of electricity exported to the power grid ( $C_{el.feed\ in\ grid}$ ). For the test day, the electricity prices are assumed according to

$$C_{el.feed\ in\ grid}(t) = -C_{el.cons.grid}(t) \quad (2)$$

and

$$C_{el.cons.PV}(t) = -5 \left( C_{el.cons.grid}(t) \right) \quad (3)$$

The results of the control decisions of the EMPC are shown in Figure 12.3. A prediction performance is calculated for the room temperature of RMSE = 0.27, MAE = 0.18, MAPE = 0.01, R2 = 0.93, and G = 0.73 and for heating demand of RMSE = 0.19, MAE = 0.10, MAPE = 0.28, R2 = 0.99, and G = 0.89. During low-price periods (APX price), the HP provides heating to the building (5:00 – 6:00). Between 15:00 and 17:00 the optimal temperature setpoint is raised to 22 °C. During this time slot, the APX prices are relatively low and PV power generation is relatively high compared to the daily average. Using the EMPC results in an increases of the flexibility factor from -0.88 to 0.67, the supply cover factor from 0.04 to 0.13, and the load cover factor from 0.07 to 0.16, as shown in Table 12.1.

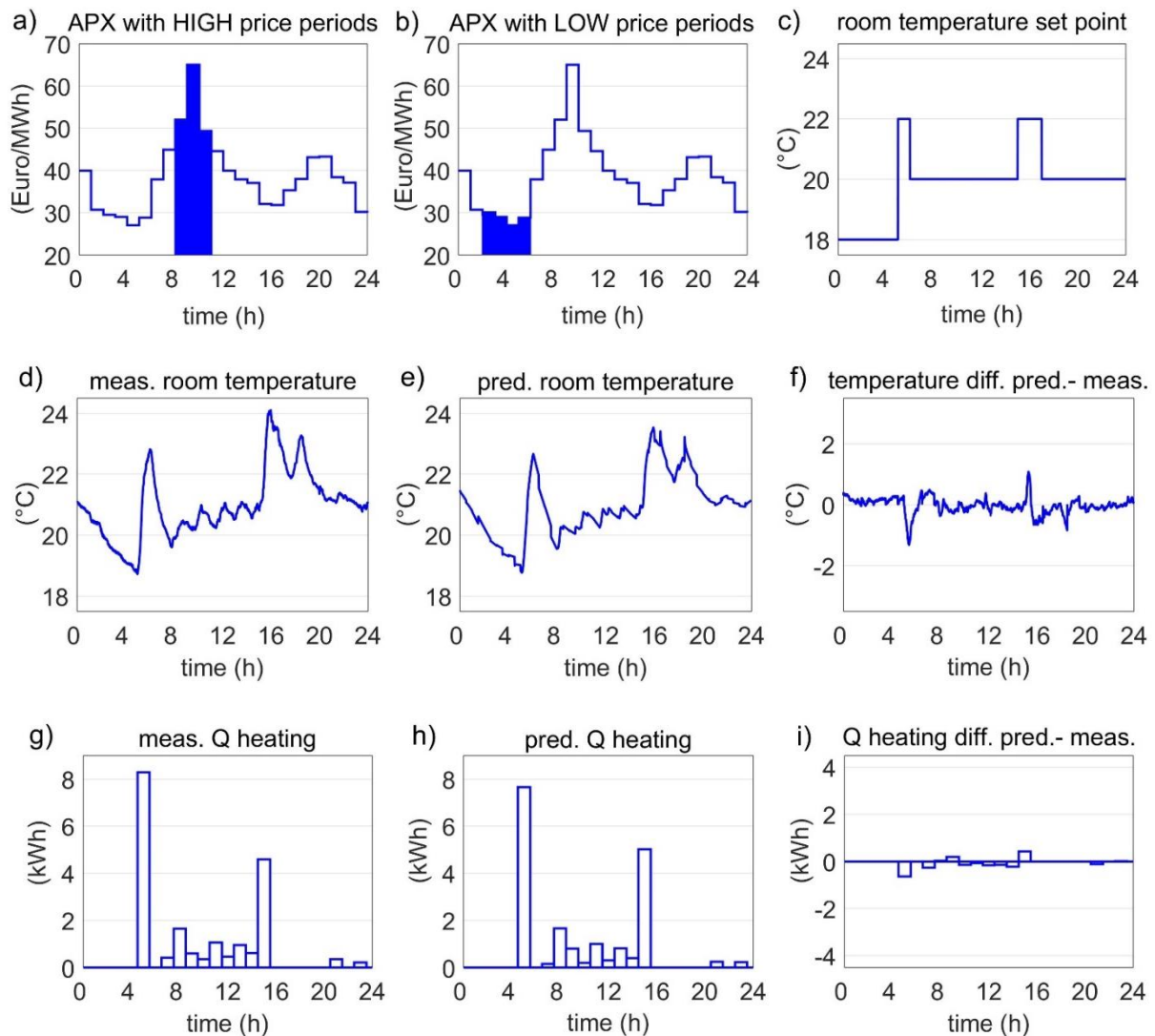


Figure 12.3. EMPC; Hourly Amsterdam Power Exchange (APX) electricity prices including a) high-price periods and b) low-price periods; c) hourly room temperature setpoints; room temperature d) measured, e) predicted, and f) difference; heating demand g) measured, h) predicted, and i) difference (Finck, et al., 2019).

An experimental case study of an MPC implemented in a residential building is presented. An ANN-MPC approach is used to represent the dynamical behavior of the heating system and the building. Another ANN model is developed for weather forecasting to obtain global, horizontal solar radiation. All ANN models and the ANN-MPC are validated and tested, showing good prediction performance. The application of ANN models can be recommended for future identification of the dynamics of buildings and heating systems and for weather forecasting. The application of ANN-MPC can be recommended as a generic approach for optimal control of energy usage in energy systems in residential buildings. As a next step, it is important to adapt this generic methodology to other residential buildings. Further experimental case studies are required that compare MPC implementations, including performance evaluation of conventional and flexibility indicators.

Table 12.1 Summary results for EMPC (Finck, et al., 2019).

Results	MPC predicted	MPC measured	Reference case
$J$ (Euro cent)	13.69	13.85	14.28
$Q_{heating}$ (kWh)	19.53	19.33	16.13
$Q_{el.cons.HP-grid}$ (kWh)	4.05	4.25	3.61
$Q_{el.cons.HP-PV}$ (kWh)	0.81	0.82	0.28
$Q_{el.gen.PV}$ (kWh)	7.15	6.56	6.56
$COP$ (-)	4.02	3.76	4.15
$FF$ (-)	0.68	0.67	-0.88
$\gamma_{supply}$ (-)	0.11	0.13	0.04
$\gamma_{load}$ (-)	0.17	0.16	0.07

An EMPC approach is introduced to optimize demand flexibility. For this approach, operational costs of energy usage are associated with demand flexibility, which is represented by the flexibility indicators: flexibility factor, supply cover factor, and load cover factor. The operational costs are (1) the costs of consuming electricity from the grid, (2) the costs of consuming electricity from on-site PV power generation, and (3) the costs of delivering electricity from on-site PV power generation to the grid. By taking into account the operational costs of energy usage, one objective function can be created, and demand flexibility can be optimized. As an example, assuming positive prices for electricity consumption from the grid, negative prices for electricity consumption from on-site PV generation, and negative prices for grid feed-in from on-site PV power generation result in an increase of the flexibility factor, the supply cover factor (self-consumption), and the load cover factor (self-generation). This generic approach offers the possibility to regulate on-site generation, grid consumption, and grid feed-in. The methodology can be adapted to flexibility indicators which are associated with the costs of energy usage.

# 13 Implementation of demand response strategies in a multi-purpose commercial building

Despoina Christantoni and Donal P. Finn, University College Dublin (UCD), Ireland

Exploiting demand-side flexibility may increase the overall capacity of power systems to handle variable renewables and help reduce overall system costs. In such scenarios, Energy Flexibility by means of demand response can be utilised to provide the necessary flexibility to the grid. To date, there has been considerable work done on commercial building participation in price-based demand response schemes, but less has been done on the investigation of the capabilities of commercial buildings to provide demand response under different and non-predictable utility / aggregator requests. The main objective of the present study is to develop a demand response strategy selection scheme for commercial buildings, which employs the appropriate strategies as a response to varying utility / aggregator requests while maintaining occupant comfort. A building energy simulation model of a multi-purpose commercial building is developed to act as a virtual test bed environment to examine the potential of different demand response strategies. The building is modelled using EnergyPlus and validated at 15-minute intervals. The Energy Management System feature in EnergyPlus is used to emulate various demand response measures, targeting heating, ventilation and air conditioning equipment, which are evaluated based on their ability to shift or curtail building electrical power demand as well as their effect on occupant comfort. Results indicate that reductions of up to 15 % in electrical power demand when targeting centralised loads (i.e., chiller) are possible.

## 13.1 Building and system description

The Student Learning Leisure and Sports Facility (SLLS) building, located in University College Dublin (UCD) in Ireland, is selected as the testbed site for this research. It was constructed in 2012 and is comprehensively monitored, with a variety of HVAC equipment and systems that are typically found in the commercial building sector. It contains multiple zones with different occupancy and usage patterns with associated HVAC equipment which can be utilised in the case of a demand response (DR) event. The SLLS building has 11,000 m<sup>2</sup> floor area and consists of three floors. It contains a gym, a 50 m x 25 m swimming pool with related ancillary areas, including a wellness suite and additional facilities such as a fitness centre with associated aerobics and dance studios, a debating chamber, a drama theatre, a multimedia centre, seminar rooms, a student media studio, health facilities, offices, shops and a cafe space. Additionally, it contains spaces dominated by different loads and occupancy patterns which facilitate the evaluation of different DR strategies for different loads and zones. For example, the swimming pool and fitness centre exhibit large occupancy fluctuations on an hour-to-hour basis, while the offices have almost constant occupancy during their operational hours.

The SLLS building is equipped with data monitoring facilities, thereby, from the beginning of its operation, building energy management system (BEMS) data is archived at fifteen-minute intervals. Not only is total electricity and gas consumption monitored, but there also are sub-meters for individual HVAC components (such as boilers, combined heat and power (CHP) units, chiller).

Pressure, humidity, temperature and CO<sub>2</sub> concentration levels are measured at different points of the HVAC systems. In 2014, the total electricity consumption was 2.7 GWh, of which 1.2 GWh was imported from the grid while the rest was provided by CHP units, which consumed 7.5 GWh of gas. In the same year, building electricity intensity was 244.5 kWh/m<sup>2</sup>/yr. For centers with a leisure pool, the typical electricity consumption is 258 kWh/m<sup>2</sup>/yr, whereas UCD Fitness Centre (a special high-intensity gym zone within the building) consumes 194 kWh/m<sup>2</sup>/yr (BRECSU 1999). In order to investigate the capabilities of the different HVAC systems and zones to provide DR and assess its impact on occupant comfort, focus is placed on the development of a detailed physical model (white-box). EnergyPlus, particularly, was selected as the modelling software since it is widely used, enables the development of DR routines which overwrite the scheduled operation in the case of a DR event and can easily be coupled with other software enabling the development of control schemes. Figure 13.1 depicts the ground floor plan and the defined thermal zones for the SLLS model.

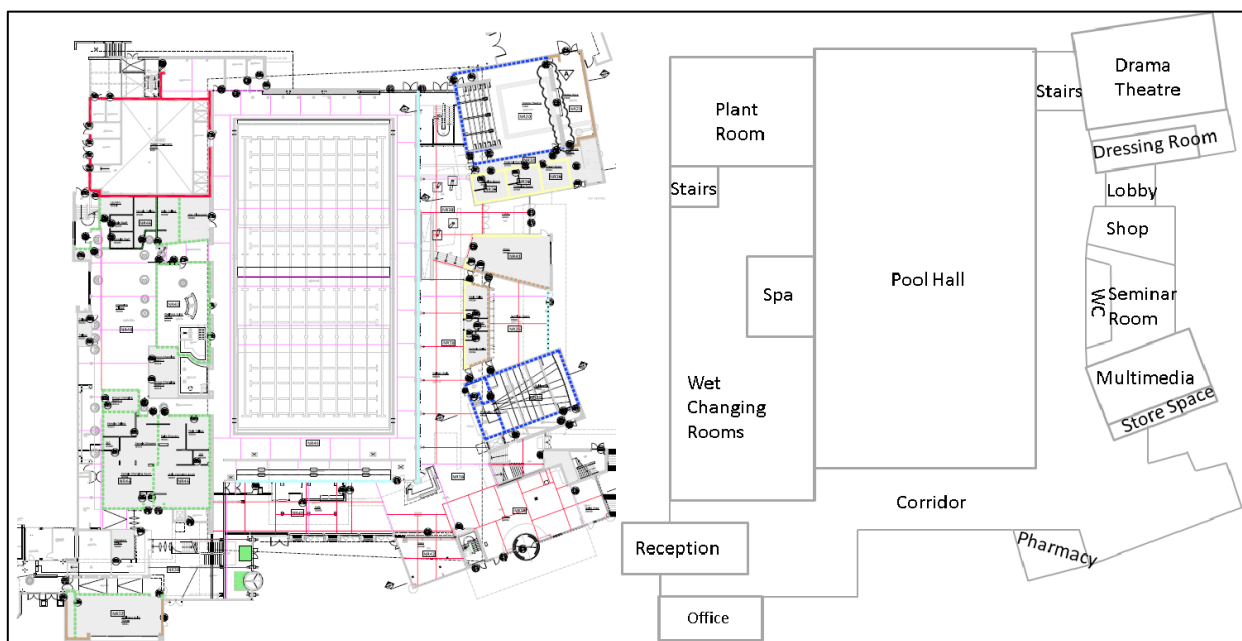


Figure 13.1 Ground floor plan (left) and the defined thermal zones (right).

The completed building model, which consists of sixty-four zones, is shown in Figure 13.2. The building has a considerable area of windows, all framed and double glazed. The overall window to wall ratio is 37 %, while this percentage reaches 59 % for the south facing part of the building. External windows are present in all offices and common areas such as corridors and halls, allowing natural light to enter the building. The swimming pool zone has the most internal and external windows to utilize natural light.

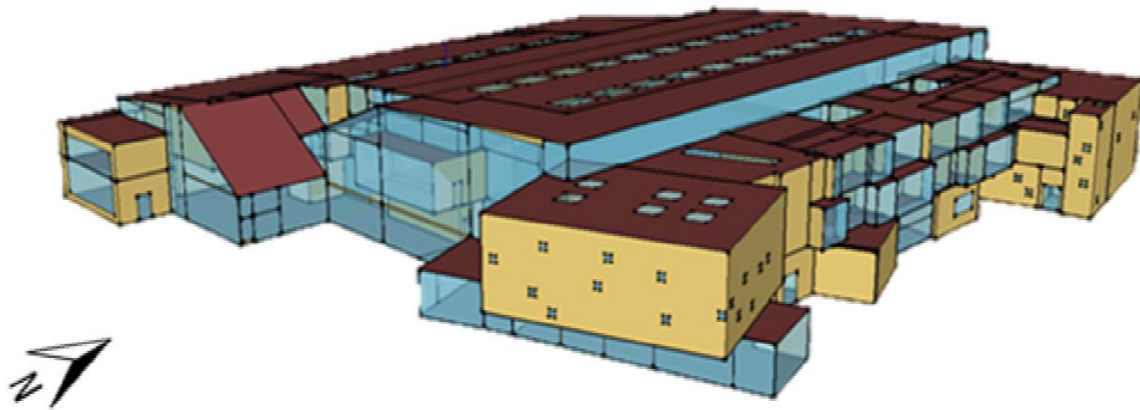


Figure 13.2 EnergyPlus model of the Student Learning Leisure and Sports (SLLS building).

In total, 138 different construction materials were defined, composing 88 different fabric constructions. The U-values for key building elements are given in Table 13.1.

Table 13.1 Building element U-value.

Building Element	U-value (W/(m <sup>2</sup> K))
External Walls	0.22
Roof	0.14
External Glazing	1.48
Internal Glazing	2.52

The swimming pool operates daily from 06:00 to 23:00 and from 08:00 to 18:00 on weekends. Its occupancy schedule is created based on measured hourly data, with 70 occupants being the maximum allowed and hence recorded data value. Lighting and electric equipment peak power density values for the swimming pool area are 16 W/m<sup>2</sup> and 2 W/m<sup>2</sup>, respectively. The lighting schedule is independent of the outdoor conditions and only depends on the number of occupants in the zone. Accordingly, the lighting level is kept at 20 % of its peak density level during unoccupied hours, acting as access lighting. During low occupancy periods, lighting level is kept at 60 % of its peak density reaching 100 % during full occupancy periods. Higher occupancy values exist in the early morning and evening hours. The schedules for the SLLS office zones is in operation from 07:00 to 20:00 daily, are given in Figure 13.3. Lighting and electric equipment peak power density values for the Fitness Centre are 12 W/m<sup>2</sup> and 10 W/m<sup>2</sup>, respectively. Based on building data, a value of 13.28 m<sup>2</sup> per person is used to describe the maximum number of occupants in the office zones. In addition, a constant infiltration rate of 5 m<sup>3</sup>/(m<sup>2</sup>hr) at 50 Pa is set for all perimeter zones. This value is in accordance with the Irish regulations for acceptable limits of infiltration rates.

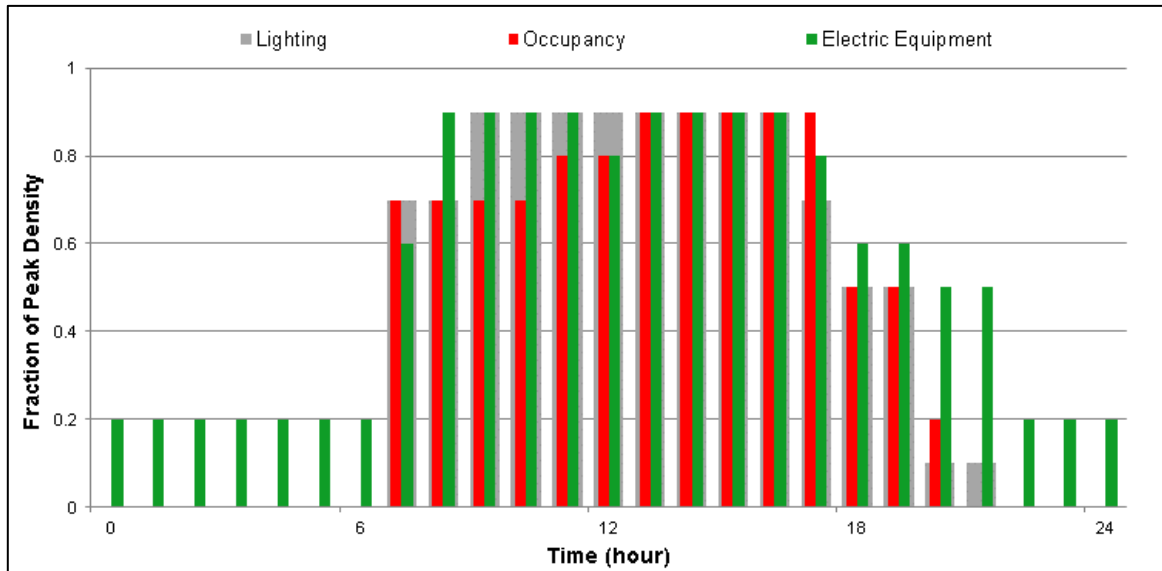


Figure 13.3 Occupancy, lighting and electric equipment weekday schedules for the offices zones.

The building electrical and space conditioning requirements are provided by two CHP units (506 kW thermal and 400 kW electrical output), two gas boilers (nominal in total 1,146 kW) and an air-cooled water chiller (nominal 865 kW). Moreover, heat is also provided by the campus district heating installation (500 kW). The space conditioning delivery equipment consists of Air Handling Units (AHUs) with heat recovery, Fan Coil Units (FCUs), underfloor heating and baseboard heaters. All the delivery equipment is weather compensated utilizing an outdoor temperature sensor, indoor temperature sensors, heating flow temperature sensors and heating temperature sensors. Boilers, CHP units and district heat are connected, via individual pumps, to a primary heating circuit. Seven secondary heating circuits are provided with hot water by the primary. These circuits cover the needs of the low temperature hot water calorifiers, the pool water heat exchangers, the AHU heating coils, the FCU heating coils, the underfloor heating circuit and the radiators. All of these comprise the supply heating circuit. The air-cooled chiller with its individual pump constitutes the chilled primary circuit. This circuit provides chilled water to all AHUs and FCU cooling coils. The heating circuit is modelled with two water loops, a heating and a heat recovery loop. A key component of the heating circuit is a water tank, modelled as a water heater mixed tank of 10 m<sup>3</sup> volume, that links the two loops. The heat recovery loop consists of the boilers, the CHP units and the district heat installation from the campus, which supply the water tank with hot water. The heating loop includes the AHU and FCU heating coils, the calorifiers and pool water, which are supplied with hot water from the tank.

The boiler nominal capacity, efficiency, design water flow rate, and design water outlet temperature are 1146 kW, 0.93, 0.024 m<sup>3</sup>/s, and 85 °C, respectively. The maximum electric power (kW), thermal efficiency, and electrical efficiency of the CHP units are 800 kW, 0.47, and 0.373, respectively. Regarding the cooling operation, only one loop is utilized in EnergyPlus, where the chiller and its circulation pump constitute the supply side, and the AHU and the FCU cooling coils form the demand side. The air-cooled electric chiller has a nominal capacity of 865 kW, reference COP of 3.1, and a reference supply chilled water temperature of 6 °C.

Baseboard heaters are installed in thirty-five zones within the building, either as the only (mainly in some office zones) or as a complementary heating system (in zones that are heated with an AHU or underfloor heating). The total floor surface area of all thirty-five zones is 3240 m<sup>2</sup>.

Underfloor heating is installed in all changing facilities within the building (for the pool and the Fitness Centre) and the main corridor on the ground floor of the building which also operates as an open space. The total floor surface area is 2753 m<sup>2</sup> and the total length of the hydronic piping is almost 1740 m.

Fan Coil Units (FCUs), with ceiling mounted supply and extract grilles, are installed in the ground floor administration and manager offices (reception), the first-floor newspaper office, the TV suite, the radio pod, the two meeting rooms and the fitness center. All FCUs in the building are equipped with fans, which are cycled on and off to meet the heating or cooling demand. Air loops along with zone equipment form the entire forced air heating and cooling system (air side). Constant Air Volume (CAV) units which operate continuously based on a time schedule or Variable Air Volume (VAV) units which vary the air flow rate to meet the demand. There are eight AHUs located in three plant rooms throughout the SLLS building.

Weather data based on a Typical Meteorological Year (TMY) weather file for Dublin is used. This data contains typical weather / climate data that is based on historical Actual Meteorological Year (AMY) weather / climate data and was downloaded from the U.S. Department of Energy.

## **13.2 Methodology: control strategies**

Following the development of the building energy simulation model, building load analysis is conducted to determine the building energy usage breakdown and seasonality of the different loads associated with the various HVAC systems. Following the load analysis, targeted DR strategies are designed. Chiller, fans and thermal mass of the building are considered in the formulation of the DR strategies. The Energy Management System (EMS) feature in EnergyPlus is used to develop control routines, which are capable of overwriting the scheduled operation of the HVAC systems in order to emulate DR strategies. Subsequently, DR signals are used to initiate the DR strategies, demonstrating different utility / aggregator requirements.

In order to evaluate the capabilities of different HVAC systems to provide DR under different external and internal conditions, such as weather conditions and operational schedules, a number of DR signals are created. These signals contain three data points: the advance time, the time of activation for the DR action, and the duration of the DR action. The signals are utilized to investigate the capabilities and limitations of the various DR strategies to provide load reduction / shifting for different requests (activation time, event duration and season). The duration of a DR event is usually between 30 minutes and 2 hours (Kiliccotte 2010). Events of between 30 minutes and 2 hours are evaluated, as well as extended duration events of 3, 4, 6 and 8 hours in order to evaluate the building for longer periods. Moreover, four different activation times are considered in order to examine the capability of the building to provide DR at different times of the day (morning, noon, afternoon and evening). Namely, DR is requested at 09:00, 12:00, 16:00 and 18:00, in both winter and summer. At these times, the building zones experience different operational schedules and occupancy conditions. The sequence of the basic steps followed in this research is presented as follows: 1. Model development: development of an EnergyPlus model to be used as a DR testbed, 2. Load analysis: conduct thermal load analysis to identify the important energy end-use categories, 3. Demand response strategy development: develop DR strategies targeting building HVAC systems, 4. Demand response strategy assessment: create a repository of DR strategies based on simulated results for a representative winter and summer weekday for different activation times and event durations, and 5. Demand response strategy selection scheme: a DR selection scheme which identifies the "best" strategy from the DR repository which meets the utility/aggregator requirements. The selection

scheme is also updated to be executed with simulated data under real conditions in order to eliminate uncertainties derived from weather conditions or occupancy. Only steps 1 to 3 are described in the current summary. A schematic representation of the overall research methodology is given in Figure 13.4.

In order to investigate the different DR events based on event duration, event commencement time, event advance time, the parametric feature in EnergyPlus is utilized to automate and simplify this process. The evaluation of the DR strategies is based on their impact on electricity pattern modifications as well as on occupant comfort. The performance of each strategy is determined by comparing its outputs against the baseline case where no DR action is applied. The change in the building electrical power demand and the influence on occupant comfort are the two main variables that are considered. As the DR strategies under investigation target the HVAC systems, they only affect thermal comfort and air quality; thus, occupant comfort assessment records depend on these values. Thermal comfort is assessed using the 7-point predicted mean vote (PMV) index of the Fanger thermal comfort model (ASHRAE, 2017). In general, an acceptable PMV-index values lies between -1 (slightly cool) and +1 (slightly warm), since it is not possible to satisfy all individuals in a large group sharing a collective climate. Regarding air quality, the threshold value for the CO<sub>2</sub> concentration in a zone is 1000 parts per million (ppm).

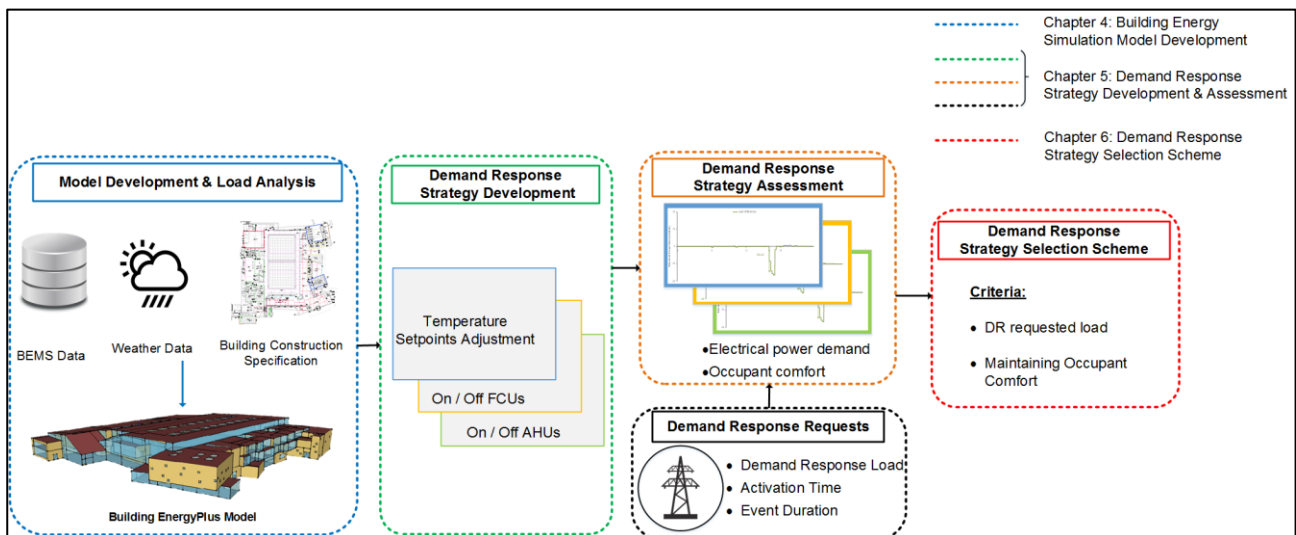


Figure 13.4 Overall methodology diagram.

### 13.3 Implementation: control algorithms

A wide range of DR strategies targeting building HVAC systems are developed and accessed, based on their modification of electricity consumption patterns and effect on occupant comfort. These DR strategies are as follows:

- 1) Plant equipment (chiller) water temperature increase to target the chiller load;
- 2) Delivery equipment (fans) on/off control strategy and decreasing the supply air flow rate of variable air volume (VAV) unit;
- 3) Zone air temperature setpoint modification.

The DR strategy selections scheme is developed based on case-based reasoning (CBR) techniques which is implemented using MATLAB. The main objective of the selection scheme is to identify the optimal DR measures that should be implemented to meet the utility / aggregator requests with the lowest impact on occupant comfort. Moreover, the scheme is developed not only to be extensible to additional DR measures inclusion but also to be easily applicable to other buildings as well. The initial scheme, where the strategy selection is made based on historical simulated data, is updated and through the Building Controls Virtual Test Bed (BCVTB) feature coupled with the building energy simulation model to provide the DR strategy selection scheme with real-time data. The DR strategy selection scheme based on historical simulated data consists of four different parts: data retrieval, possible strategy combinations formulation, identification of accepted combinations and final selection. All these steps are applied on retrieved data from a synthetic database (DR repository). The purpose of this scheme is to identify an "ideal" DR strategy from a number of similar simulated results, field tests or outputs from recorded events.

The first part of the selection scheme, data retrieval, is then replaced and real-time simulation results are created for each DR event. Namely, the DR strategies can be updated with current weather and occupancy conditions in order to eliminate uncertainties derived from the model. This updated scheme enables zones to be included or excluded from the DR measures, taking into account their operational schedules which may differ from the simulated ones.

## 13.4 Results

In this section the influence of different DR strategies on the plant equipment (chiller) is investigated. The increase in chilled water temperature can reduce chiller electrical power demand. Using this strategy, DR reduction, and energy savings can be achieved without significant impact on occupant comfort. As shown in Figure 13.5, the chilled water temperature (CWT) strategy in winter is capable of providing a maximum load reduction of 17.6 kW (4.5% of peak electrical demand of approximately 400 kW) for the duration of the DR event. The total electricity reduction is 15.8, 32.8 and 66.9 kWh for the one, two- and four-hour events, respectively. As observed in Figure 13.5, rebound effects for the one- and two-hour duration events occur only when the CWT is set back to its schedule value of 6 °C (two hours after the end of the DR events). On the other hand, for the four-hour duration event, two rebound spikes are recorded at 17:00 and 18:00 when the CWT setpoint is decreased to 8 °C and 6 °C, respectively. Rebound electricity consumption values of 19.5, 24.9 and 34.8 kWh are estimated for the one, two- and four-hour duration events, respectively. As shown, events of longer duration cause higher rebound electricity consumption. Nevertheless, when the strategy is applied for a four-hour period at midday in summer, it is only capable of a load reduction for a limited period of time (2.5 hours), as shown in Figure 13.6. For the summer period, the load reduction during the events is higher. The maximum recorded load reduction over the duration of the events is 52.4 kW (11% of peak electrical demand of approximately 450 kW) and the total energy reduction is 50.2, 101.4 and 113.2 kWh for the one, two- and four-hour events, respectively. After the DR event, significant rebound peaks are recorded as well (maximum load increase of up to 82.4 kW), which increases with the duration of the event.

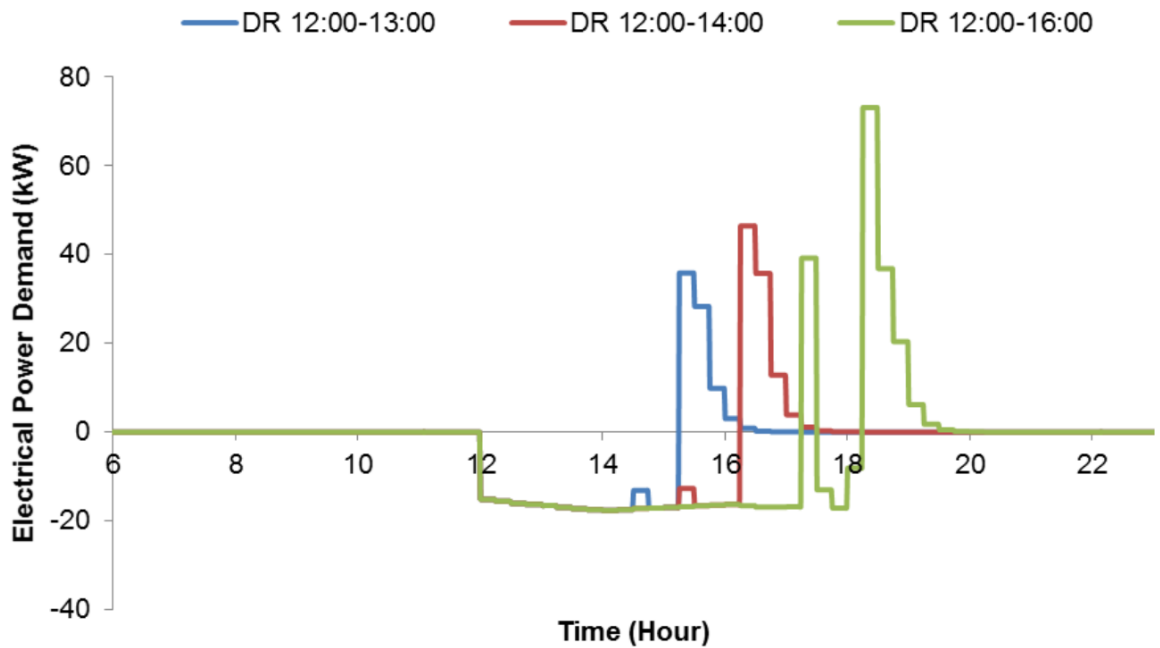


Figure 13.5 Difference in building electrical load demand for the CWT strategy for 20<sup>th</sup> January in 15-minute intervals (Christantoni et al., 2016).

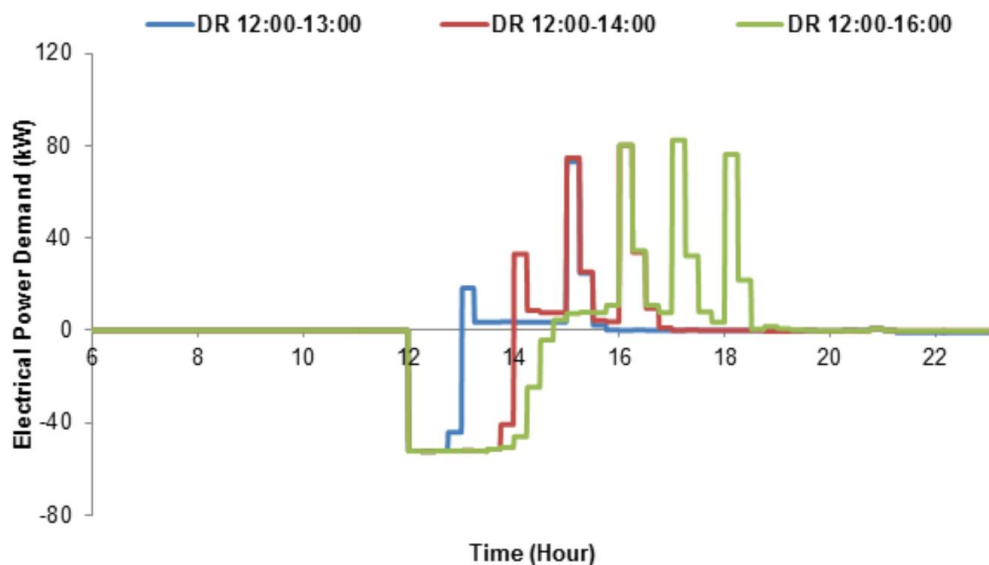


Figure 13.6 Difference in building electrical load demand for the CWT strategy for 10<sup>th</sup> July in 15-minute intervals.

Figure 13.7 shows the chiller electrical power demand when no DR measure is applied and in the case of the four-hour duration event, alongside the temperature of the water leaving the chiller. The CWT setpoint is 6 °C until noon, when the DR event starts. At this time, the setpoint is set to 12 °C. As long as the CWT is below the new setpoint (12 °C), the chiller electrical power demand is equal to zero. When the CWT reaches the 12 °C setpoint at 13:45, the chiller electrical power demand is slightly higher in comparison with the reference case. Namely, the average electrical power demand

in the reference case between 14:30 and 16:00 is 48.6 kW, whereas in the four-hour event case this value is equal to 54.2 kW. Following the DR event, three spikes are recorded in conjunction with the decrease of the CWT setpoint.

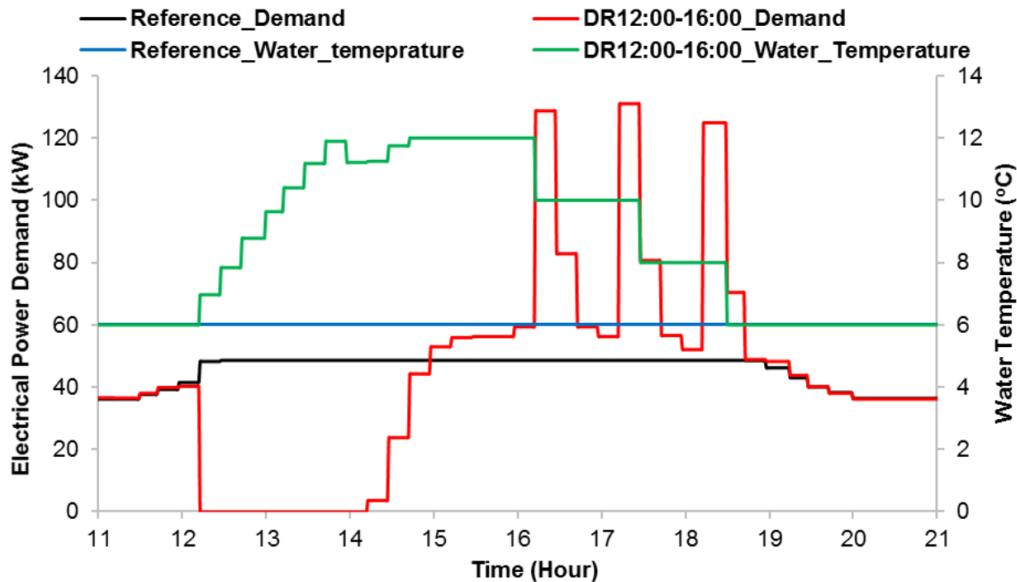


Figure 13.7 Chiller electrical power demand and CWT for the four-hour duration event and the reference case for 10<sup>th</sup> July at 15-minute intervals (Christantoni et al., 2016).

Regarding the occupant comfort assessment in all the conditioned zones of the SLLS building, little difference is recorded between the reference case and the events for the zone mean air temperature and the PMV-index values (to within 0.1°C) in both winter and summer time. Additionally, delivery equipment (fan on/off control strategy) in the office zones are considered. A fitness center, with a high design fan capacity, is not a common feature in typical commercial buildings, except hotels. For this reason, the on / off control strategy is also implemented in another group of zones (two meeting rooms, three offices, one radio station studio and two retail units) that are more germane of commercial buildings and are conditioned exclusively by FCUs. A FCU is assigned to each zone, providing heating or cooling.

The fan nominal electrical capacity for Meeting Room 1, Meeting Room 2, Reception Shop, Pharmacy, Newspaper Office, Library, and Radio Station Studio are 0.7, 0.5, 1, 1.1, 2.1, 0.2, 0.5, and 0.5 kW, respectively. Both space conditioning and ventilation for these zones are provided from the FCUs, where the total fan electrical capacity is 6.6 kW. The FCUs are divided into two groups and are in turn cycled on/off at 30-minute intervals, in order to reduce the impact on the zone air temperature and, therefore, occupant comfort, while implementing the DR strategy. The first group consists of the pharmacy, newspaper, library and radio station studio FCUs. The remaining FCUs, constitute the second group. Both groups are selected to have the same value of fan rated electric power. The difference in electrical power demand for each of the three events and the reference case for winter is given Figure 13.8. The maximum recorded load reduction is 3.99 kW, whereas the electricity reduction during the one, two- and four-hour duration events is 3.9, 7.6 and 14.9 kWh, respectively.

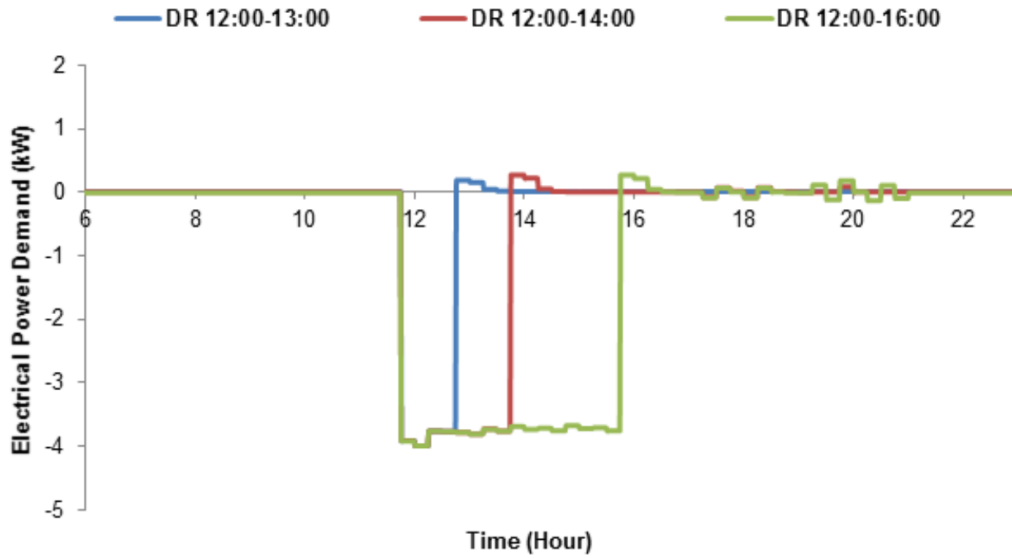


Figure 13.8 Difference in building electrical load demand for the office zones on / off fan control strategy for 20<sup>th</sup> January in 15-minute intervals (Christantoni et al., 2016).

In the SLLS building, some of the zones require, due to their usage and thermal characteristics, cooling at certain periods of the day, even during the winter. Figure 13.9, for example, shows the heating and cooling power demand for the day of the event in two zones, the pharmacy which is located on the ground floor and the meeting room on the second floor (Meeting 2). The pharmacy operates daily from 07:00 to 18:00 and the meeting room from 08:00 to 20:00. As observed, the meeting room requires heating at the beginning of its operation (08:00-10:15) and afterwards (11:00-22:00) there is a cooling demand (Figure 13.9). On the contrary, FCUs serving the pharmacy zone are required to provide heating throughout its operation. Cooling loads occurring during the winter period are either met by cycling outdoor air into the zones or by using cooling coils. At the time of the event, the FCUs in the two meeting rooms, the reception and library zones are used to address the cooling loads. Consequently, an interruption to FCU operation results in an increase of the air temperature in these zones during the DR event. For the remaining zones, the FCUs are utilized to meet the heating loads.

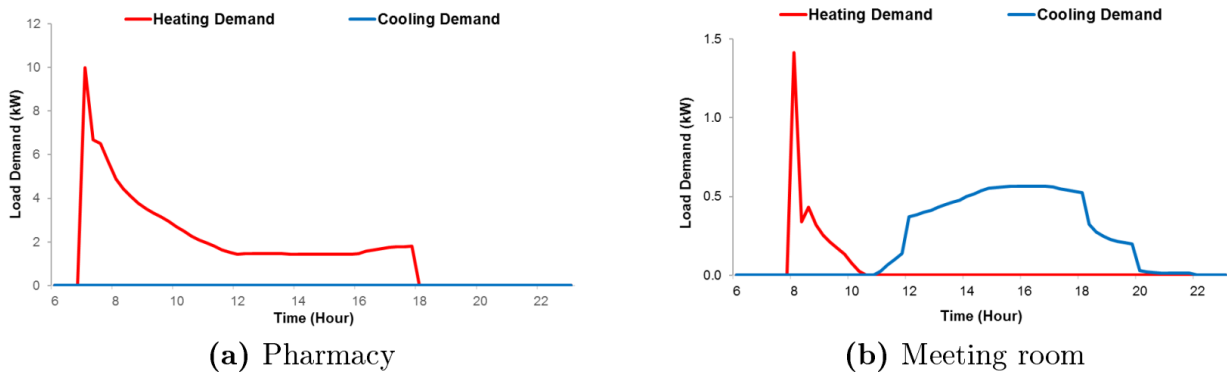


Figure 13.9 Heating and cooling demand for the pharmacy and meeting room zones for the 20<sup>th</sup> of January.

The minimum recorded values for the zone air temperature and PMV-index for these zones are given in Table 13.2. As shown in Table 13.2, the PMV-index values in all cases are within the acceptable limits of occupant comfort. However, in some of them, the values are close to the lower limits and in the case of longer duration events, these values may be exceeded.

Table 13.2 Minimum recorded values for the mean air temperature, maximum values for CO<sub>2</sub> concentration levels and minimum PMV-index values for office FCUs on / off control strategy for the DR events for 20th January (Figure 13.8).

Zone	Air Temperature (°C)			CO <sub>2</sub> Concentration (ppm)			PMV-index		
	S0D1	S0D2	S0D4	S0D1	S0D2	S0D4	S0D1	S0D2	S0D4
Shop	20.8	20.8	20.8	532.6	575.4	649.6	-0.5	-0.5	-0.5
Pharmacy	19.2	19.2	19.0	478.0	504.5	560.7	-0.8	-0.8	-0.9
Newspaper Office	20.7	20.5	20.4	682.0	761.0	857.7	-0.5	-0.5	-0.5
Radio	21.4	21.4	21.4	636.2	657.3	667.5	0.1	0.1	0.1

The CO<sub>2</sub> concentration levels increase in all cases, as the FCUs are used for ventilation purposes and an interruption to their operation results in limiting outdoor air provision.

Figure 13.10 shows the variation in building electrical load demand for each of the three events in summer. The maximum electrical power demand reduction recorded in any one-time interval (15 minutes) is 6.4 kW. The electricity consumption is decreased by 4.5, 8.8 and 16.9 kWh for the one, two- and four-hour duration events, respectively. It can also be observed that a significant rebound effect is only evident after the four-hour duration event. For the remaining events, a lower reduction in building electrical power demand is recorded.

During the summer period, all the office zones in the SLLS building conditioned by FCUs require cooling. Table 13.3 gives the maximum recorded values for the zone mean air temperature, PMV-index value and CO<sub>2</sub> concentration levels for these zones. The highest mean air temperature is recorded for the pharmacy, which is located on the ground floor and has external windows on three of the four of its walls. As a result, it has the highest solar heat gains in comparison with the other zones, which contributes to the zone air high temperature. The variation in the zone maximum temperatures for the remainder of the zones is mainly due to the various internal heat gains. In contrast with the results obtained for winter, during the summer period, some of the zones (meeting 1, pharmacy and library) exceeded the occupant comfort limits, mainly for the two- and four-hour duration events. In the same zones, the CO<sub>2</sub> concentration levels exceed the threshold limit of 1000 ppm as well. For the remainder of the zones, CO<sub>2</sub> concentration levels increase with the duration of the events, however they are maintained below the limits. The predicted electricity reduction in summer (4.5, 8.8 and 16.9 kWh) is greater in comparison with the reduction during winter (3.9, 7.6, 14.9 kWh), especially for the two- and four-hour duration events. That is due to the fact that in summer, when greater outdoor temperatures occur, cooling is provided to the zones using the cooling coils which are supplied with chilled water from the chiller.

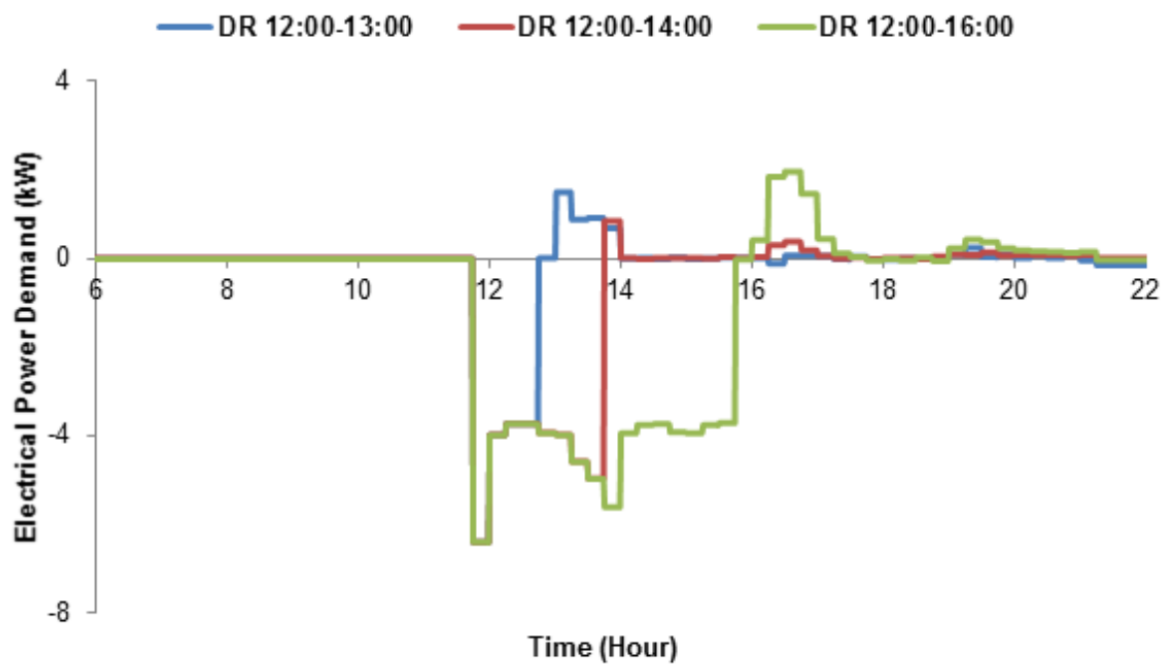


Figure 13.10 Difference in building electrical load demand for the office zones on/off fan control strategy for 10<sup>th</sup> July in 15-minute intervals (Christantoni et al., 2016).

Table 13.3 Maximum recorded values for the mean air temperature, CO<sub>2</sub> concentration levels and PMV-index values for office FCUs on / off control strategy throughout the DR events for 10th July.

Zone	Air Temperature (°C)			CO <sub>2</sub> Concentration (ppm)			PMV-index		
	S0D1	S0D2	S0D4	S0D1	S0D2	S0D4	S0D1	S0D2	S0D4
Meeting 1	27.8	28.5	28.7	859.0	1100.6	1386.0	0.2	0.9	1.0
Meeting 2	26.8	27.4	27.8	582.4	725.4	891.5	0.1	0.5	0.7
Reception	25.5	25.9	26.4	910.2	1059.9	1241.3	-0.1	0.0	0.2
Shop	26.2	26.4	26.7	538.3	583.9	667.9	0.1	0.2	0.3
Pharmacy	27.2	28.8	30.9	480.8	508.7	570.3	0.9	1.4	2.1
Newspaper Office	24.3	24.5	24.8	681.5	761.5	860	-0.4	-0.3	-0.2
Library	27.6	28.3	29.0	1014.9	1217.6	1379.6	0.7	1.0	1.2
Radio station studio	25.6	25.9	26.6	724.3	766.4	815.3	-0.4	0.3	0.5

Thus, a limitation in the cooling load demand leads to a lower electricity consumption from the chiller as well. In general, the strategy does not affect occupant comfort in the zones during the one-hour event (recorded PMV-index values are within the threshold limits for both winter and summer). However, for longer duration events, especially during the summer, some of the zones may exhibit occupant comfort limits (pharmacy and library). On the other hand, since FCU fans use on / off fans, which are cycled on or off in order to maintain the setpoint temperature in the zones, in some cases indoor air quality is more likely to be exceeded (Meeting 1, reception and library). Finally, a noticeable rebound effect is only evident after the four-hour event in summer, when a two-hour rebound period follows the DR event. The electricity consumption increase during that period is 3.3 kWh, notably lower than the 16.9 kWh reduction throughout the event (equivalent to a 5.1 DR ratio). In all other cases, as the zones are partially conditioned throughout the duration of the events, rebound effects are negligible. The maximum electrical power demand reduction recorded in one-time interval is 4.2 and 6.1 kW for winter and summer, respectively. These values are low compared with the total building electrical power demand of almost 350 kW. However, this reduction is likely to be proportionally larger in other office only type buildings, where office zones conditioned by FCUs occupy a larger portion of the building. In the SLLS building, this group of zones occupies just 3 % (234 m<sup>2</sup>) of the total floor area.

## 13.5 Conclusions

An evaluation of the capabilities of different demand response strategies to maintain occupant indoor thermal comfort while simultaneously meeting utility/aggregator requirements regarding the immediacy and the duration of the load reduction is presented. The chilled water temperature (CWT) increase strategy proves to have the largest DR potential. Namely, it can provide up to 14.1 % load reduction in summer, when most of the analyzed zones require cooling, without any significant effect on occupant comfort. This decrease is lower during winter (4.5 %). However, simulation results reveal that when there is a considerable cooling demand in the building, the strategy is capable of providing a load reduction only for a limited duration. Specifically, for summer events commencing at noon and of a duration longer than 2.5 hours, the electrical power demand is increased in comparison with the base case. Delivery equipment on/off control constitutes also a significant DR load, but it requires careful planning to ensure occupant comfort in zones is maintained, especially where considerable heat gains occur. In addition, it is observed that longer duration demand response events are more likely to disrupt occupant comfort. Eventually, the results show that even for temperate climate conditions, as exhibited in Ireland, there is a considerable DR potential in the commercial building sector, which can be utilized to provide additional flexibility to electricity end-use demand profiles, thereby improving the renewable energy system integration.

# 14 Experimental assessment of Energy Flexibility potential of a zone with radiant floor heating system

Ali Saberi Derakhtenjani, Jose Agustin Candanedo and Andreas Athienitis, Center for zero energy building studies (CZEBS), Concordia University, Montreal, Canada

This study illustrates the potential to provide Energy Flexibility of a radiant floor embedded in a concrete slab. The study is carried out in an experimental room designed to simulate the conditions of an office space near a window. This room –denominated “perimeter zone test cell” (PZTC)– has a radiant floor heating system. The PZTC is located inside a controlled environment. The EC provides the desired exterior conditions. The temperature inside the PZTC is controlled with a thermostat that adjusts the heating power delivered from the pipes to the slab. Relatively small adjustments of the zone air temperature setpoint result in significant changes in the heating load, and thus provide a certain Energy Flexibility potential. This flexibility, along with applicable strategies in response to a specific price signal profile, are discussed below.

## 14.1 Building and system description

The case study is conducted in the perimeter zone test cell (PZTC) located at Concordia University’s solar simulator/environmental chamber (SSEC) laboratory. The temperature of the SSEC can be controlled within a wide range (between -40 °C and +50 °C) and, thus, allows for a great deal of flexibility in terms of testing conditions. Figure 14.1 shows the schematic of the SSEC, perimeter zone, radiant floor system and the mechanical room.

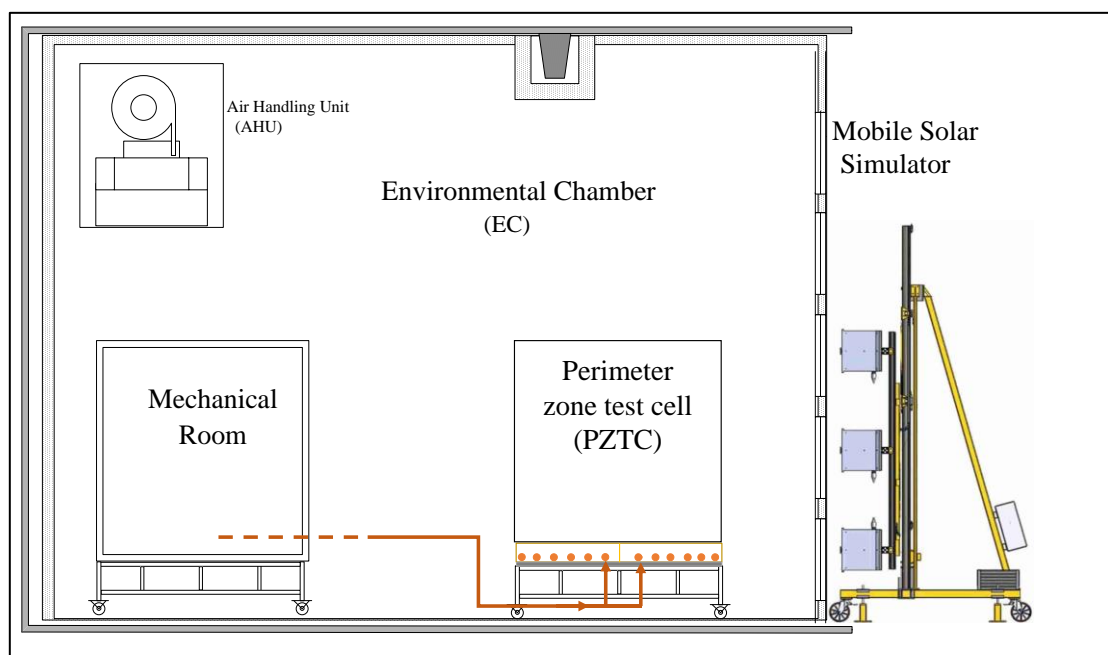


Figure 14.1 Schematic of SSEC with PZTC and radiant floor.

The PZTC is a 3 m×3 m×3 m office placed inside the environmental chamber and it has a radiant floor heating system. The side and back walls and ceiling consist of 4 in (10cm) insulation having the R-value of R32 (RSI 5,64). The front wall is a BIPV/T façade with an approximately R5 (RSI 0,88) thermal resistance. The floor is made of an 8 cm thick concrete with insulation at the bottom. The pipes of the radiant floor system are made of conventional cross-linked polyethylene (PEX), and they have an external diameter of 1.75 cm. The pipes are installed in a “foam matrix” of insulating material that also facilitates keeping them in place. The pipes have an approximate separation of 15 cm between them. A mechanical room provides controlled flow rate of fluid (propylene-glycol and water mixture) for the radiant floor. The floor is divided into two slabs as shown in Figure 14.2. The schematic in Figure 14.3 shows the total concrete slab thickness as well as the pipe diameter.

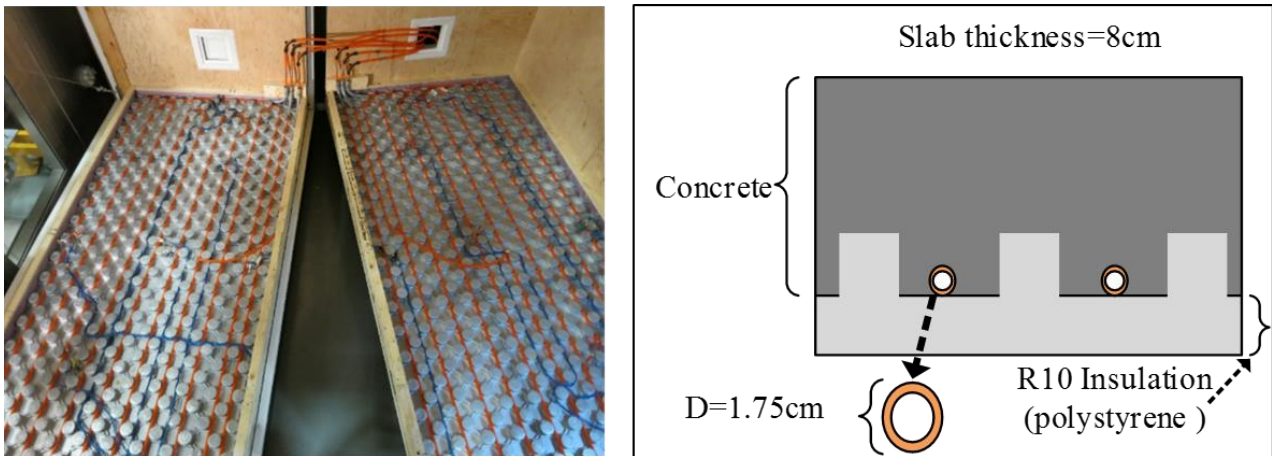


Figure 14.2 Radiant floor pipes (before pouring the concrete) and the schematic.

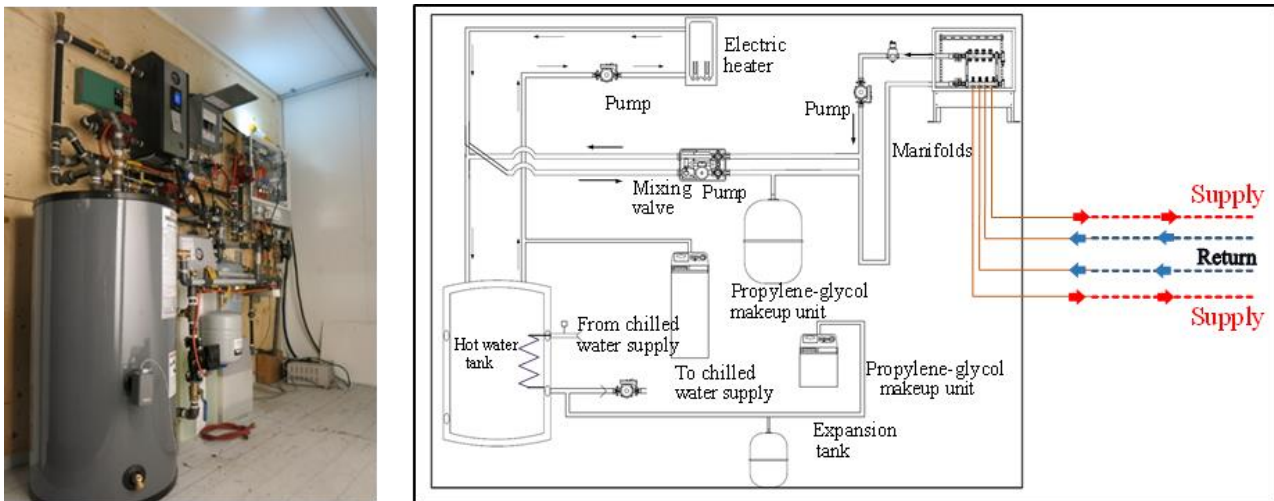


Figure 14.3 Mechanical room and its schematic.

A number of studies were carried out on the thermal characterization of the facility’s radiant floor system itself when exposed to exterior conditions (Candanedo et al. (2018), Saberi et al. (2018)). These studies were done before installing the front wall of the PZTC and only the radiant floor was studied and not the PZTC. The study that is presented in this document is the first experimental study on the PZTC and its Energy Flexibility.

## 14.2 Methodology: control strategies and implementation

This is a simple control case study using a zone thermostat. The thermostat controls the room air and floor temperature for a hydronic heating zone using Pulse Width Modulation (PWM) technology to control the flowrate. A slab sensor is included with the thermostat to measure floor temperature to protect the floor from overheating and enhance comfort. In the experiment, the maximum allowable floor temperature is set to be 29 °C based on the ASHRAE standard 55.

The control of the system is based on an assumed price signal. Therefore, it is investigated how much flexibility can be obtained by modulating the air temperature setpoint from the baseline room air temperature (22 °C) to the comfort limits of the zone (20 °C and 24 °C). The increasing/decreasing of the setpoint is done manually by entering the room and increasing the temperature on the thermostat, waiting for the desired period (about 6 hours) after which the temperature is returned to the baseline again manually – see Figure 14.4. Both setpoint increase and decrease from the baseline are considered to examine the upward and downward flexibility of the system.

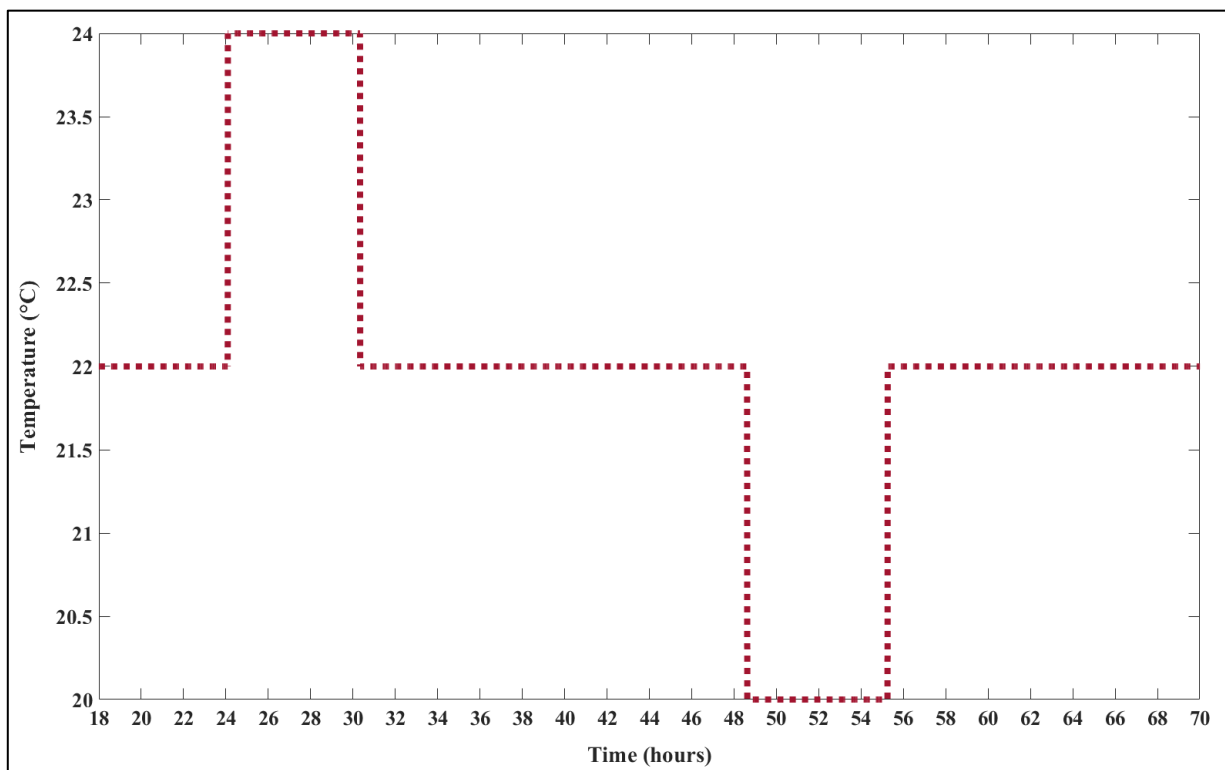


Figure 14.4 Implemented control strategy (zone air setpoint).

## 14.3 Control algorithms

The control strategy is based on simple increasing and decreasing of the zone temperature by means of the zone thermostat. The thermostat works based on pulse-width modulation of system flowrate. This type of control is briefly described in the following.

A Pulse Width Modulation (PWM) Signal is a method for generating an analog signal using a digital source. A PWM signal consists of two main components that define its behavior: a duty cycle and a

frequency. The duty cycle describes the amount of time the signal is in a high (on) state as a percentage of the total time it takes to complete one cycle. When a digital signal is on half of the time and off the other half of the time, the digital signal has a duty cycle of 50 % and resembles a "square" wave. When a digital signal spends more time in the on state than the off state, it has a duty cycle of > 50 %. When a digital signal spends more time in the off state than the on state, it has a duty cycle of < 50 %. Figure 14.5 illustrates these three scenarios.

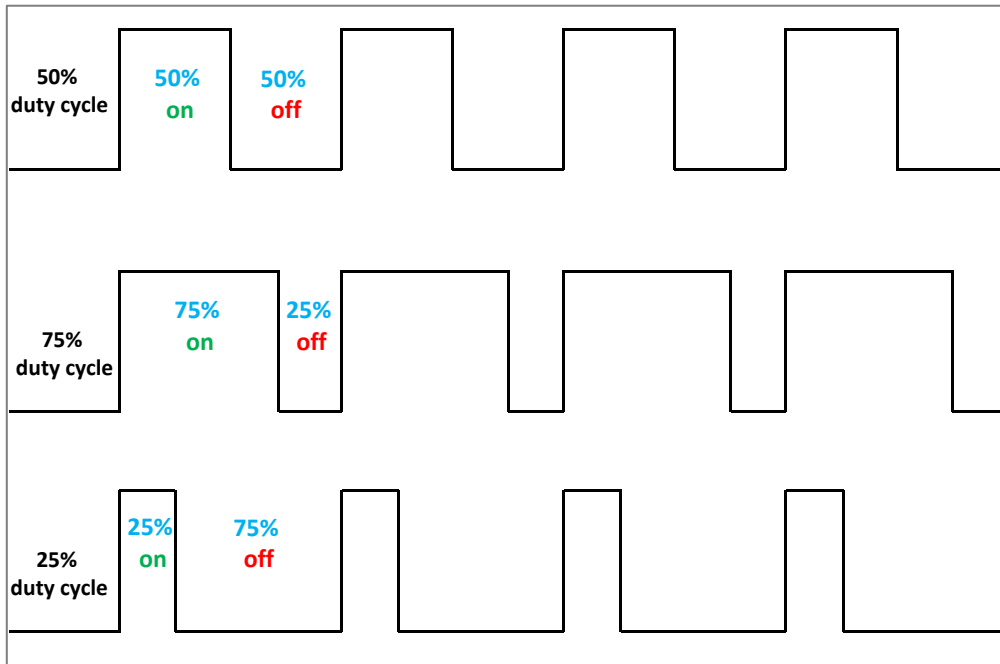


Figure 14.5 Examples of 50 %, 75 %, and 25 % duty cycles.

The frequency determines how fast the PWM completes a cycle (i.e. 1000 Hz would be 1000 cycles per second), and therefore how fast it switches between high and low states. By cycling a digital signal off and on at a fast-enough rate, and with a certain duty cycle, the output will appear to behave like a constant voltage analog signal when providing power to devices. The main advantage of PWM is that power loss in the switching devices is very low. When a switch is off there is practically no current, and when it is on and power is being transferred to the load, there is almost no voltage drop across the switch. Power loss, being the product of voltage and current, is thus in both cases close to zero. PWM also works well with digital controls, which, because of their on/off nature, can easily set the needed duty cycle.

## 14.4 Results and conclusion

Figure 14.6 shows the system flowrate (the moving-window-mean value) before and during the active demand response (ADR) event (12-18 hours and 37-43 hours), when the zone air temperature is modulated accordingly. As it can be observed from Figure 14.6, before hour 12 there is a steadier on/off to the system flowrate through pulse-width modulation in order to keep the zone temperature at 22 °C. Then, between hours of 12 and 18 when the temperature is set to be increased to 24 °C the controller keeps the flowrate near maximum (1 gpm) and keeps the flow running for a much longer period until the surface temperature gets really hot around the hour of 14.5 (see Figure 14.9) so the flow is stopped for about 1.5 hours. The flow is started again for another 1.5 hours (16-17.5

hours) and stopped at hour 18 when the setpoint is reduced to 22 °C from 24 °C. After 18 h it is observed that there is no heating power to the system for more than 4 hours. Therefore, it can be stated that this strategy gives a 4 hours power shifting capacity compared to the baseline heating power profile (constant 22 °C zone temperature).

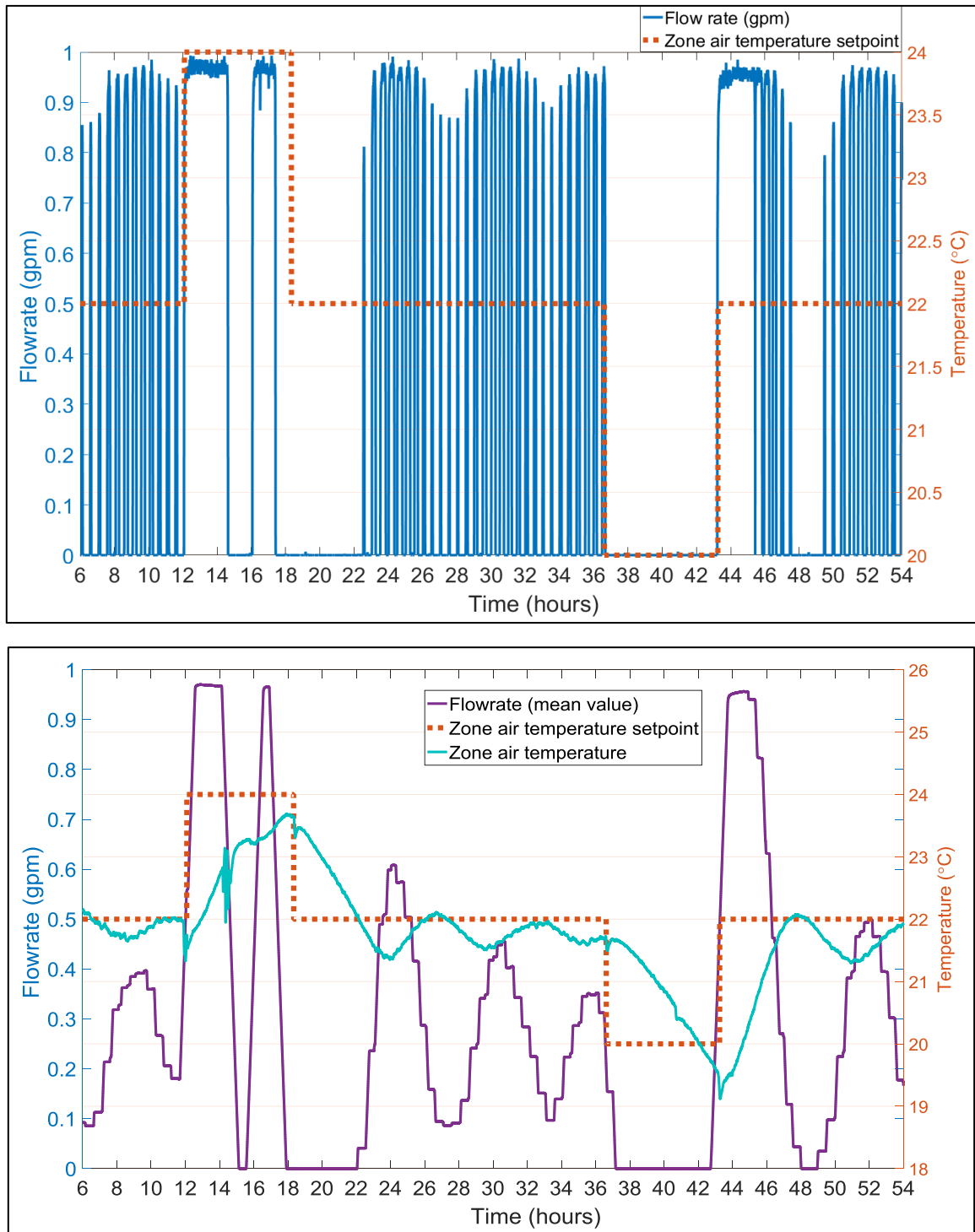


Figure 14.6 Radiant floor System flowrate actual measurement (top), moving-window mean value vs room setpoint modulations (bottom).

Heating power to the radiant floor is calculated by using the flowrate ( $\dot{m}$ ), supply and return temperatures difference ( $\Delta T$ ) as:

$$Q = \dot{m} \times C_p \times \Delta T$$

For the ADR events, hours 12 to 18 and 37 to 43, the flexibility of the system is calculated. As shown in Figure 14.7, the upward flexibility is equal to 195 Wh/m<sup>2</sup> and the downward flexibility is 237 Wh/m<sup>2</sup>. Also, an increase of 125 W in the heating power in the rebound effect of the downward flexibility (hour 43) compared to the one for the upward flexibility (hour 12) can be observed. This increase in heating power is due to the fact that at hour 43 no heat has been injected into the system for 6 hours. Therefore, a higher spike in the heating power compared to hour 12 is observed.

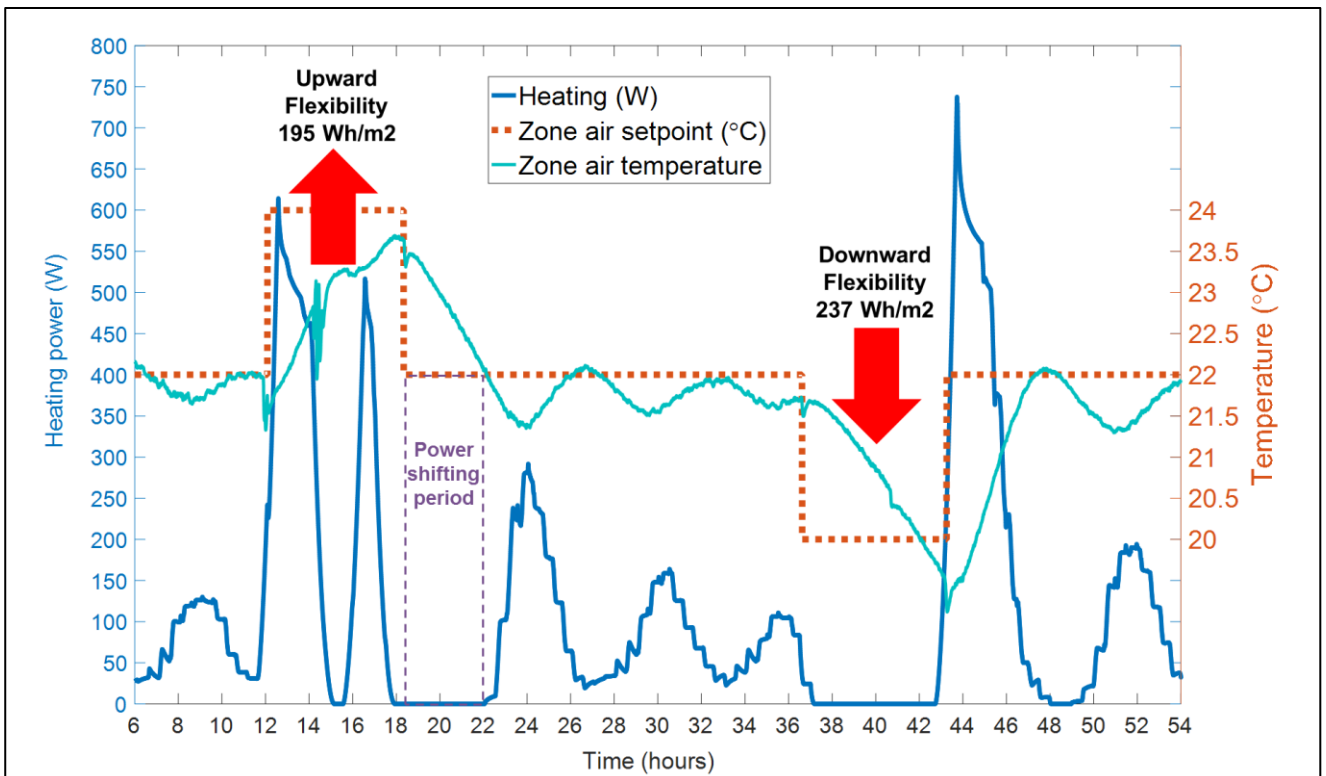


Figure 14.7 Heating power of the radiant floor system and the upward/downward flexibility calculation.

This setpoint modulation strategy described above can be defined and applied to a price signal as shown in Figure 14.8. Therefore, when there is a high price signal for a certain period of time in the forecast, the zone setpoint can be increased by 2 K for a certain period and then get back to the normal operating condition. It is observed that with this strategy the system offers about four hours of power shifting potential. Also, with the downward flexibility it will be possible to decrease the rebound effect by using a ramp profile or other transition paths for which a programmable thermostat is required, however.

Figure 14.9 shows the radiant floor surface temperature as well as the zone operative temperature and the exterior temperature conditioned by the environmental chamber. It is observed that the operative temperature is within the comfort limits almost all the time. Also, it can be observed that when the floor temperature reaches the 29 °C limit (around hours of 15), the controller shuts down the heat input by turning off the flowrate for the radiant floor.

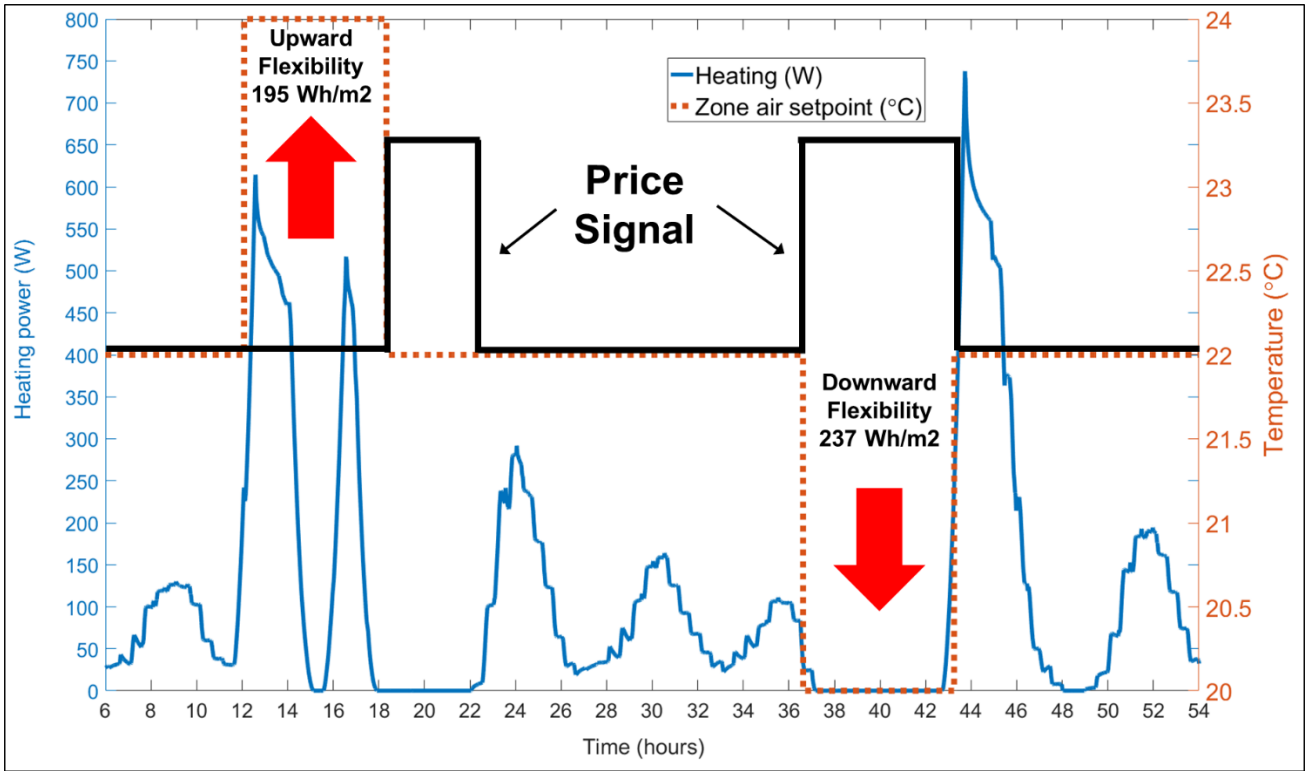


Figure 14.8 Price signal..

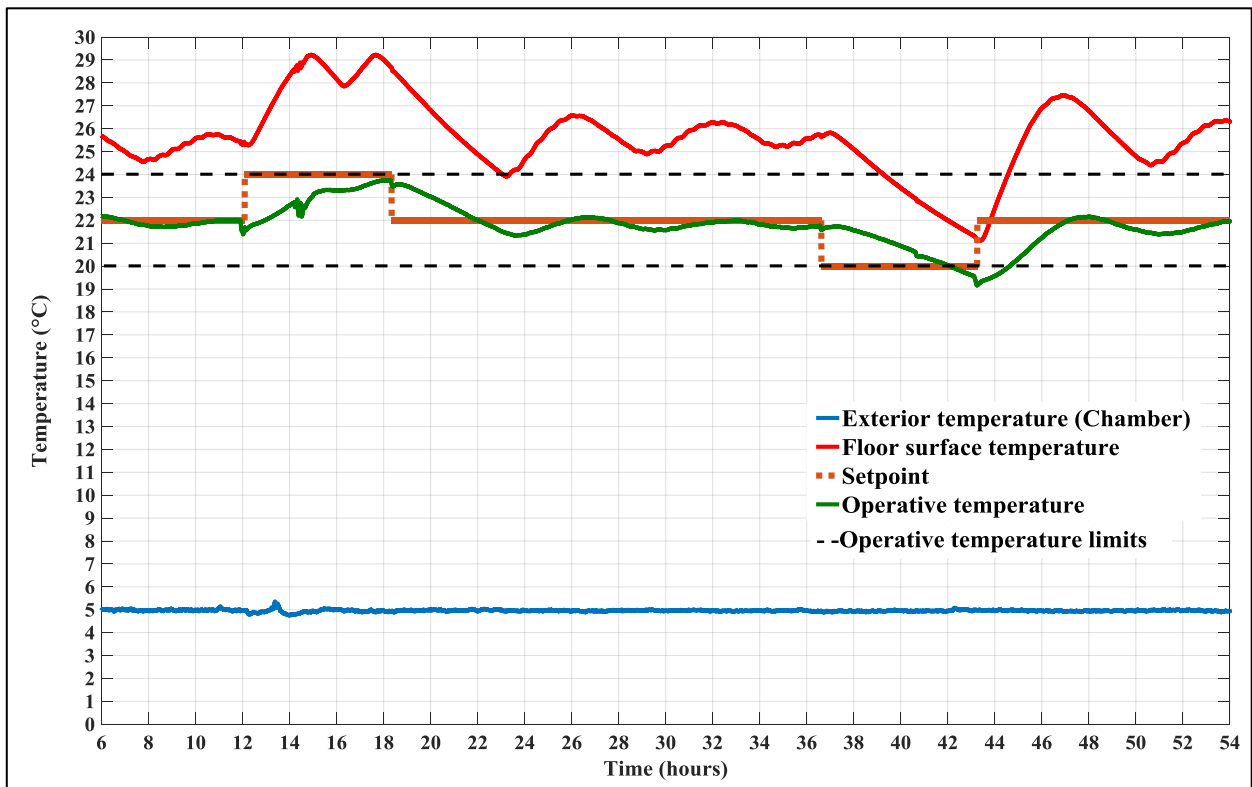


Figure 14.9 Floor surface and operative temperatures.

### **1.4.1. Conclusion**

This report presented an experimental evaluation of Energy Flexibility potential of a radiant floor heating system. It was observed that by modulating the zone air temperature setpoint certain flexibility in energy consumption and power shifting can be obtained for the thermal zone. This flexibility can be utilized especially during the peak power periods to minimize the power (or energy) consumption of the thermal zone.

# 15 Aggregation of Energy Flexibility of commercial buildings

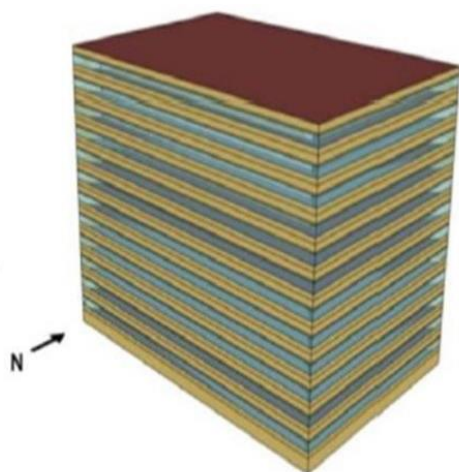
Anjukan Kathirgamanathan, Killian Murphy, Mattia De Rosa, Mohammad Saffari, Eleni Mangina and Donal Finn, University College Dublin

In this study, demand response is applied through direct control to an EnergyPlus archetype simulation model of a large office building. Several demand response strategies are considered, including chiller water modulation, global setpoint modulation, fan mass flow rate modulation and the use of an electric battery. The study is motivated by whether the available electrical Energy Flexibility of the various strategies can be simply summed together and how multiple strategies interact. Results show that in some cases certain demand response (DR) strategies interact with each other and, therefore, cannot be considered in isolation, they must be simulated together. In this study, the adopted rule-based control is non-predictive and is unable to harness the Energy Flexibility of the thermal mass of the building fully to provide Energy Flexibility whilst meeting thermal comfort constraints.

## 15.1 Building and system description

This study uses a virtual test bed building simulated in EnergyPlus, a whole building energy simulation program. A virtual DR test bed building is used instead of a real case-study building in this case, as this allows various DR technologies to be implemented and studied in parallel. The testbed building is a US-DOE (United States Department of Energy) commercial building archetype model (Deru et al., 2011). The 'Large Office' building (illustrated in Figure 15.1) is specifically selected, as many of the DR strategies implemented in this study are relevant to large office buildings. The version with "new construction", which complies with the minimum requirements of ASHRAE Standard 90.1-2004, is selected for climate zone 4C. The weather data used is that of Dublin, Ireland, the location of the virtual test bed. The large office has a floor area of 46,320 m<sup>2</sup> over 12 floors (plus a basement). The building operates from 6.00 am to midnight on weekdays and 6.00 am to 5.00 pm on Saturdays (with no occupancy on Sundays). The building has a 'Mass Wall' (continuous insulation) wall type based on ASHRAE Standard 90.1-2004 with a U-Value of 0.857 W/(m<sup>2</sup> K) (Deru et al., 2011).

This building uses a gas boiler for heating (1,766 kW), two water-cooled electric chillers for cooling (1,343 kW) and a multi zone variable air volume system for air distribution as illustrated in Figure 15.2. The archetype model is modified to add a lithium ion battery to provide a means for electricity storage and a solar PV panel for local electricity generation. The battery is sized to have a 1.5 MWh storage capacity (for a two-hour duration) with 500 kW discharge. The PV array is sized to have a rated power output of 200 kWp. The fraction of the roof with active solar cells assumed to be 46 % with a solar cell efficiency of 20 % based on (Gagnon et al., 2016).



Floor Area	46,320 m <sup>2</sup>
No. of Floors	12
Wall U-value	0.857 W/(m <sup>2</sup> K)
Heating	Gas Boiler (1,766 kW)
Cooling	Two water-cooled chillers (1,343 kW)
Air Distribution	Multizone variable air volume (MZ VAV)
Solar PV	200 kWp output
Electric Battery	1.5 MWh storage/ 500 kW discharge

Figure 15.1 'Large Office' US-DOE Archetype Model in EnergyPlus.

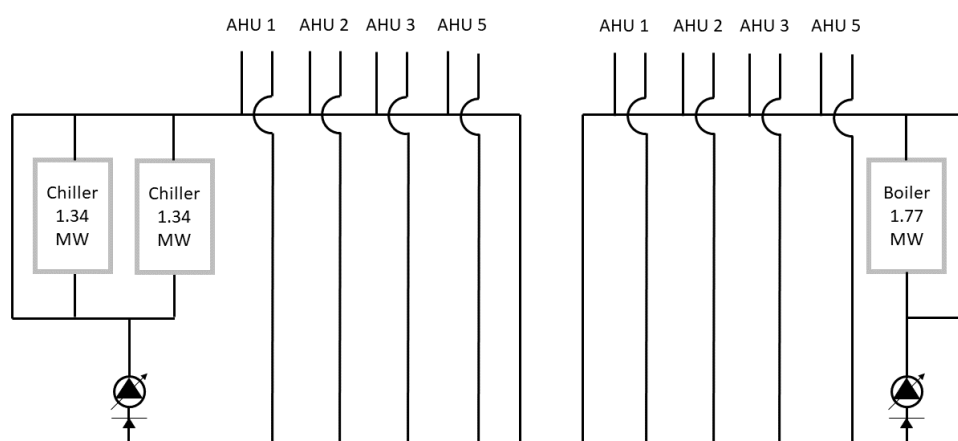


Figure 15.2 Hydraulic scheme of the HVAC system including chillers, air handling units (AHU) and a boiler of the 'Large Office' US-DOE Archetype Model.

A simulation time-step of 15 minutes is selected, as this is an appropriate compromise between modelling the fast-dynamics and the data-burden from simulating short time steps over large prediction horizons (Sturzenegger et al., 2016). The control scope of this case study includes the entire cooling system (plant side and air side), and the battery system.

## 15.2 Research aim

Given that a commercial building is capable of providing Energy Flexibility through a range of mechanisms (described in the next section), it is of interest whether the total available Energy Flexibility can be simply summed and the question arises of what the optimal strategy or set of

strategies is for a given demand response event. The research questions addressed in this study are “Can a suitable framework be identified that considers the various demand response strategies are available in a commercial building? Can the various demand response strategies be aggregated to calculate the total flexibility that a building can offer?” The work and results presented here are based on the work carried out by (Kathirgamanathan et al., 2018).

## 15.3 Methodology

The overall methodology is given below:

1. Build a white-box virtual DR testbed model using EnergyPlus.
2. Using this virtual DR testbed model to analyze potential for demand response strategies (applied for hourly durations) initially for the summer design day case.
3. Quantify the flexibility for these strategies individually and aggregate at hourly intervals using enhanced flexibility indicators.
4. Create a daily flexibility profile featuring the various demand response strategies (assuming independent DR events at every hour and that there is only one DR event in a day for use of the profile). Only down-flexibility results are presented in this study.

### 15.3.1 Demand response strategies

Demand response is applied through the use of four different strategies for a summer design day to achieve load shifting. The four demand response strategies are detailed below. The first three strategies take advantage of the building thermal mass as a passive form of storage with the last strategy using the electric battery for active storage. In this study, the PV is not considered as a DR strategy. However, as it reduces the imported power, it is considered for comparison purposes. In all cases, DR events of a duration of one hour are considered.

#### **Global Setpoint Adjustment (GSA)**

The first strategy involves adjusting the global setpoint temperature (of the zonal air temperature), thus shifting the cooling load. There is a strong correlation between the cooling setpoint temperature and the cooling load, making this an effective strategy. For simplification, zone pre-conditioning is not considered. Operative temperature drift values given in ASHRAE 2004b Standard 55 (Thermal Environmental Conditions for Human Occupancy, 2004) are used in this study for temperature adjustment limits.

#### **Chiller Water Temperature (CWT)**

This strategy involves modulating the chilled water temperature setpoint in the chiller supply loop. The chilled water setpoint temperature is increased from 6 °C to 12 °C during the demand response period, thus decreasing the chiller load. For this strategy, the air flow rates are locked to the reference values to prevent compensation by the air handling units (AHU) during the demand response event.

#### **Fan Modulation (Fan)**

The third strategy is to modulate the fan mass flow rate (or fan speed) and in this case, the flow rate is modulated to 20 % of the reference value. The mass flow rates of the cooling loop are also modulated to prevent compensation. For this strategy, however, minimum ventilation requirements need to be satisfied.

### **Electric Battery (Bat)**

The fourth and final strategy involves the battery to shift consumption from the grid (active electric storage). Note that in this research, the PV and battery are considered as separate systems although future work will consider them as a coupled system providing Energy Flexibility with the battery only charging from the PV output. In this case study, only the provision of down flexibility (a reduction in the power imported from the grid compared to the reference) is considered.

#### **15.3.2 Flexibility indicators**

To quantify the amount of flexibility available, the “Available Electrical Energy Flexibility” or *AEEF* is defined as follows:

$$AEEF = \int_j^{l_{DR}} |P_j^{flex} - P_j^{ref}| dt \quad (15.1)$$

where  $l_{DR}$  is the duration of the demand response event,  $P_j^{flex}$  is the power consumption during the demand response event and  $P_j^{ref}$  is the power consumption in the reference control case. This indicator is based on (Reynders, 2015) with the key difference being that the difference in power consumption is used rather than the thermal heating or cooling loads.

As the thermal mass of the building is essentially used as a form of energy storage when applying demand shifting through the demand response strategies used in this study, a storage efficiency ( $\eta_{AEEF}$ ) is defined next. This is defined differently based on whether up-flexibility or down-flexibility is considered. For down-flexibility, a rebound effect is expected following the period of demand response and hence the efficiency is a measure of the magnitude of the rebound effect over the amount of energy shifted. For down-flexibility, the efficiency is defined as:

$$\eta_{AEEF} (down - flex) = 1 - \frac{\int_0^{hor} (P^{flex} - P^{ref})^+ dt}{\left| \int_0^{hor} (P^{flex} - P^{ref})^- dt \right|} \quad (15.2)$$

For up-flexibility, the definition is as follows:

$$\eta_{AEEF} (up - flex) = \frac{\left| \int_0^{hor} (P^{flex} - P^{ref})^- dt \right|}{\int_0^{hor} (P^{flex} - P^{ref})^+ dt} \quad (15.3)$$

For the Energy Flexibility provided by batteries, equation (3) is applicable to both down and up flexibility. For more information on the derivation and implementation of these Energy Flexibility indicators, refer to (Kathirgamanathan et al., 2018).

## **15.4 Implementation: control algorithms**

The reference control strategy employed by this building is rule-based control (RBC). The temperature of the zones is controlled through a dual setpoint thermostat, one for cooling and one

for heating. This is achieved through a combination of low-level and high-level control objects. Low-level controls are meant to simulate certain closed-loop hardware controls that have very specific functions to perform. An example includes the ZONE CONTROL:THERMOSTATIC object which provides basic thermostatic control for zone heating and cooling. On the contrary, high-level controls control the operation of large parts of the system and can coordinate control of the air system and the plant system. Examples of high-level controls include setpoint managers and system availability managers. High-level control decisions are simulated once per system time step. Control decisions are made based on the conditions in the previous time step. Demand response actions are simulated through the use of the Energy Management System (EMS) module of EnergyPlus using the EnergyPlus runtime language (ERL). See Figure 15.3 and (Ellis, Torcellini and Crawley, 2007) for further details. This case study uses a form of direct load control for demand response.

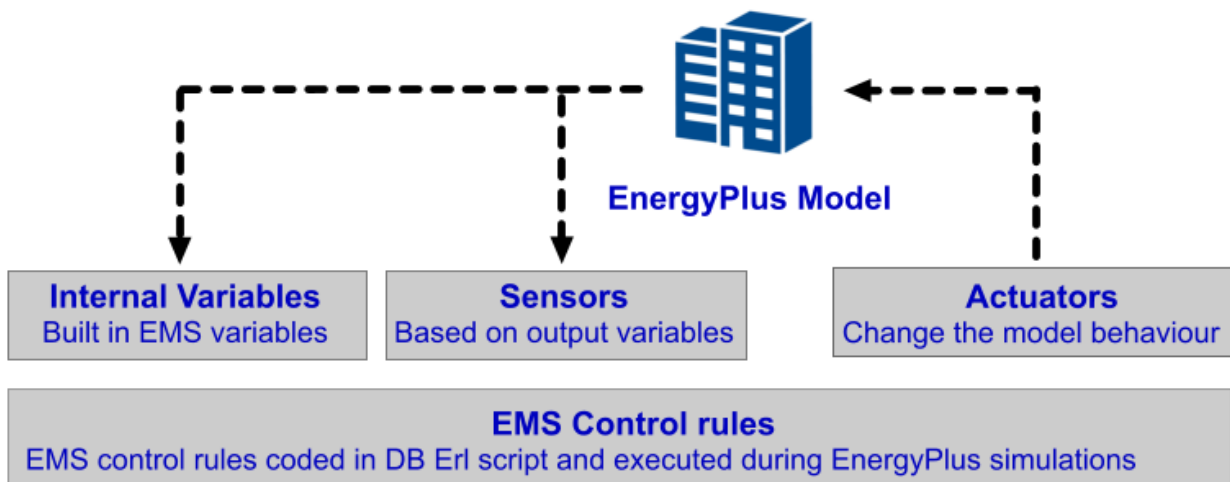


Figure 15.3 Overview of Energy Management System in EnergyPlus (DesignBuilder, 2012.).

The EMS is used to apply DR actions at every hour of the day for the summer design day for each strategy – i.e. one simulation for each DR event. Actuator objects are used to modulate the control variables such as cooling setpoint for the GSA strategy, cooling loop setpoint for the CWT strategy, fan flow rate setpoint for the fan modulation strategy and battery discharge rate for the battery strategy. The performance of each strategy is quantified by comparing the total power demand and occupant comfort (through the zonal Fanger Predicted Mean Vote (PMV)) against the reference case where no DR is applied. A PMV value of between -1 and 1 is considered to be acceptable thermal comfort. Note that the reference scenario is not optimal with regards to energy demand or cost as is commonly found in many studies and other case studies.

## 15.5 Results and conclusion

The daily profiles of the available electrical Energy Flexibility for all the DR strategies is shown in Figure 15.4 as a carpet plot. As this figure shows, the available electrical Energy Flexibility is limited during the unoccupied hours due to the lower total building power demand. DR strategies modulating the HVAC system are only able to provide Energy Flexibility during the occupied hours when the chiller and fan are operating. The battery provides the largest quantity of Energy Flexibility, i.e. a consistent amount of 460 kWh. The efficiency of the DR strategies is illustrated next in Figure 15.5 similarly in a carpet plot. Again, the battery efficiency is constant around a value of 60-70 % and is due to a combination of charging, discharging and inverter losses. The efficiency of the fan strategy

dips during the middle of the day when a larger rebound is to be expected given the higher internal and solar gains during this period. Given both the quantity and efficiency of a certain DR action, a priority list can be constructed for every hour of the day ranking the strategies, allowing a building operator to act given a demand response event. Where the Energy Flexibility requested is greater than the amount able to be provided by any individual strategy, a combination may have to be used and this is investigated below.

Generally, a rebound effect is to be expected following a demand response event as the systems have to recover to the steady state operating conditions. However, given that the reference control is rule-based, there are some cases with the DR strategies studied where either no rebound effect is seen following the DR event or even where further load reductions occur following the DR event (e.g. Figure 15.6). This leads to an efficiency of greater than 100% in certain cases. This behaviour is not expected with optimal energy control as the reference case.

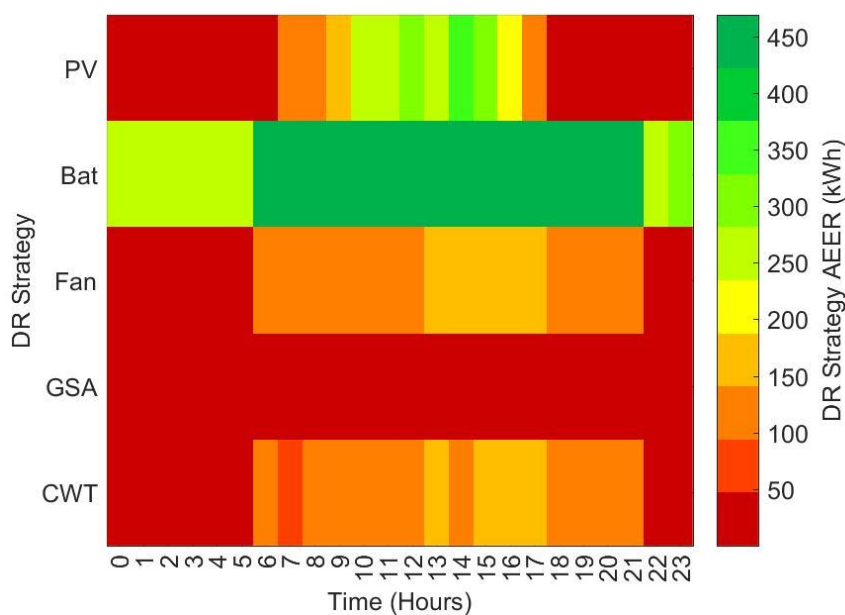


Figure 15.4 Available Electrical Energy Flexibility for all DR strategies for summer design day.

The chilled water temperature and global setpoint strategies are capable of being combined together. The combined available electrical Energy Flexibility (CWT + GSA (2) - through simulation) is compared with the summation of the individual flexibility values (CWT + GSA (1)) from each of the respective strategies in Figure 15.7. Results show that the simple summation of the available electrical Energy Flexibility is not the same as the case when they are applied together in the simulation.

The maximal Energy Flexibility is achieved in this building through a combination of the battery, modulating the fan and the output from the PV. This is illustrated in Figure for the summer design day. The building is capable of delivering almost 1000 kWh of Energy Flexibility to the grid between 3.00 pm and 4.00 pm. Note that this is highly sensitive to the control scheme used in the reference case and the results would be expected to be different if the reference scheme was an energy optimal model predictive control for example.

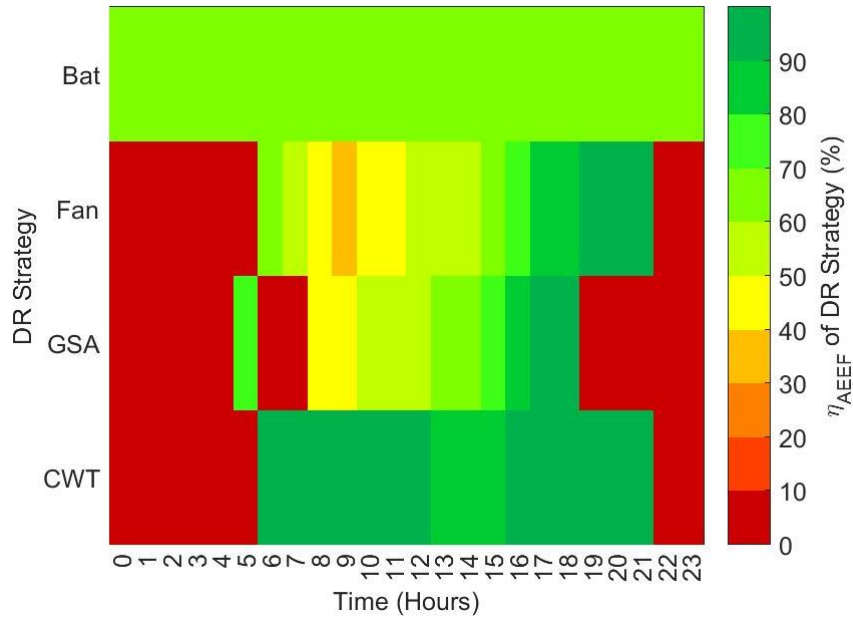


Figure 15.5  $\eta_{AEEF}$  – all DR Strategies (Down Flex) – Daily Profile.

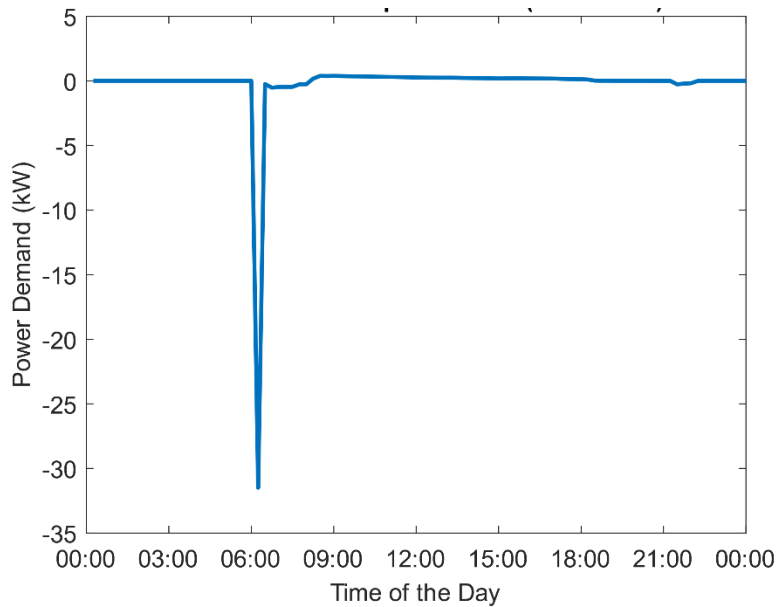
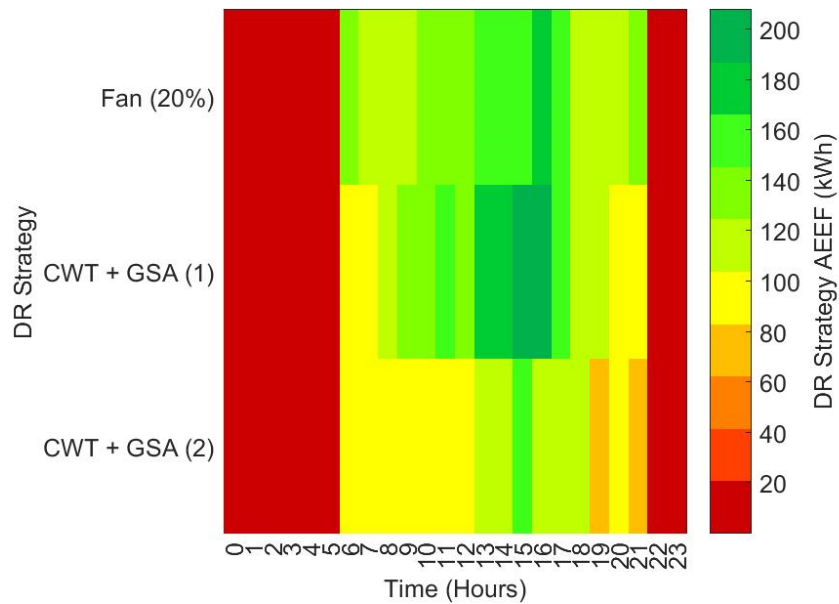


Figure 15.6 Difference in the power demand with the reference case for global setpoint adjustment DR strategy with DR event at 6 am.

In conclusion, the methodology presented in this case study is able to capture the Energy Flexibility available from various demand response strategies available in a building, both individually and in aggregation. A limitation is that comfort constraints are not implicit in the control formulation and these have to be accounted for manually, e.g. through the experience of a building operator. A further limitation is that the profiles presented are only applicable in the case of one DR event during a 24-hour period. The provision of Energy Flexibility would affect the available Energy Flexibility in the following hours. Generally, given that a predictive control scheme (such as MPC) is capable of taking full advantage of the thermal mass of the building as well as respecting constraints, it is expected that this should give a more complete picture of the Energy Flexibility available and the associated

cost in a given building. The methodology used in this study can be extended to obtain a profile of the available Energy Flexibility and associated efficiency over a longer period as required for operation or even a year for early-stage Energy Flexibility assessment of a building



Note: CWT + GSA (1) – individual sum (mutually exclusive)

CWT + GSA (2) – combined simulation (mutually inclusive)

Figure 15.7 Aggregation of CWT & GSA DR Strategies & Comparison with Fan Modulation DR Strategy.

## 15.6 Conclusion

The results and lessons learned from the case studies are very specific for each case. The results from investigations apply different boundary conditions (weather, energy prices, etc.) and constraints (use of buildings, comfort range, etc.) so the results may differ between the examples or even contradict in some cases.

Since buildings are unpredictable consumers of electrical energy, optimal control strategies is a key technology in next-generation energy-efficient building systems. However the case studies show that traditional control strategies are still being used in most of the buildings subsystems even with the development of better alternatives presented over the past years. In addition, the majority of studies focus on independent components of the building rather than building-wide optimization, neglecting the potential efficiency improvements to be exploited for the entire system in order to achieve significant energy savings.

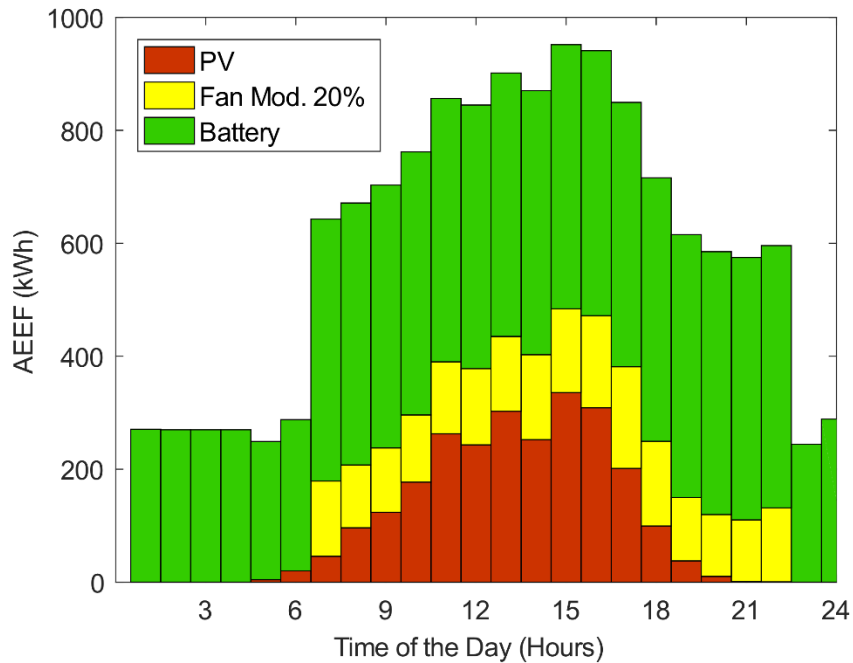


Figure 15.8 Aggregated Available Electrical Energy Flexibility for case study building for summer design day.

Furthermore, the building-wide optimization is a non-linear and multivariate problem having no unique solution where competitive objectives arise in practice, involving interdependent issues distributed among multiple building climate zones. In this way, the coordinated operation of interconnected subsystems performing autonomous control is essential to achieve the overall system goals.

In this context, where the control process of buildings should be optimized, there is a need to seek new methods and technologies that provide fast and optimized management and control. Appropriate methods must be efficient and robust, performing inter-context considerations among each building zone micro-climate and ensuring reliability and security in several operating conditions of the system.

# References

- Afram, A. & Janabi-Sharifi, F., 2014. Theory and applications of HVAC control systems - A review of model predictive control (MPC). *Building and Environment*, 72, pp.343–355.
- Afram, Abdul, and Farrokh Janabi-Sharifi. "Theory and applications of HVAC control systems—A review of model predictive control (MPC)." *Building and Environment* 72 (2014): 343-355.
- Ahmed, K. et al. (2017) 'Occupancy schedules for energy simulation in new prEN16798-1 and ISO/FDIS 17772-1 standards', *Sustainable Cities and Society*. Elsevier, 35(January), pp. 134–144. doi: 10.1016/j.scs.2017.07.010.
- Ali, Adhra, and Hussain Kazmi. "Minimizing Grid Interaction of Solar Generation and DHW Loads in nZEBs Using Model-Free Reinforcement Learning." *International Workshop on Data Analytics for Renewable Energy Integration, ECML-PKDD*. Springer, 2017.
- Arendt, K., Jradi, M., Wetter, M. & Veje, C. T., 2018. ModestPy: An Open-Source Python Tool for Parameter Estimation in Functional Mock-up Units. Cambridge, MA, USA, s.n.
- Arnold, M. & Andersson, G., 2011. Model predictive control of energy storage including uncertain forecasts. *Power Systems Computation Conference (PSCC)*, Stockholm, Sweden.
- ASHRAE (2017). *ASHRAE Handbook: Fundamentals*. SI edition, American Society of Heating, Refrigerating and Air-conditioning Engineers Inc., Atlanta, USA.
- ASHRAE, 2013. ANSI/ASHRAE Standard 55: Thermal Environmental Conditions for Human Occupancy. Ashrae.
- ASHRAE. "ASHRAE Standard 55-2010: thermal environmental conditions for human occupancy." 2010.
- Aswani, A. et al., 2012. Reducing transient and steady state electricity consumption in HVAC using learning-based model-predictive control. *Proceedings of the IEEE*, 100(1), pp.240–253.
- Bacher, P. & Madsen, H., 2011. Identifying suitable models for the heat dynamics of buildings. *Energy and Buildings*, 43(7), pp.1511–1522.
- Barrett, Enda, and Stephen Linder. "Autonomous HVAC control, a reinforcement learning approach." *Joint European Conference on Machine Learning and Knowledge Discovery in Databases*. 2015.
- Beghi, A. et al., 2014. Energy efficient control of HVAC systems with ice cold thermal energy storage. *Journal of Process Control*, 24(6), pp.773–781. Available at: <http://dx.doi.org/10.1016/j.jprocont.2014.01.008>.
- Bengio, X. Glorot and Y. "Understanding the difficulty of training deep feedforward networks." *Thirteenth International Conference on Artificial Intelligence and Statistics*. 2010. 249–256.
- Berkenkamp, F. & Gwerder, M., 2014. Hybrid model predictive control of stratified thermal storages in buildings. *Energy and Buildings*, 84, pp.233–240. Available at: <http://dx.doi.org/10.1016/j.enbuild.2014.07.052>.
- Bianchini, G. et al., 2016. Demand-response in building heating systems: A Model Predictive Control approach. *Applied Energy*, 168, pp.159–170. Available at: <http://dx.doi.org/10.1016/j.apenergy.2016.01.088>.

- Blochwitz, T. & Otter M., Å. J., 2016. Functional Mockup Interface 2.0: The Standard for Tool Independent Exchange of Simulation Models. s.l., s.n., pp. 173-184.
- Brattebø, H. et al. (2014) Typologier for norske boligbygg - Eksempler på tiltak for energieffektivisering. Available at: [http://episcopo.eu/fileadmin/tabula/public/docs/brochure/NO\\_TABULA\\_TypologyBrochure\\_NTNU.pdf](http://episcopo.eu/fileadmin/tabula/public/docs/brochure/NO_TABULA_TypologyBrochure_NTNU.pdf).
- BRECSU (1999). Energy use in offices (Energy Consumption Guide 19), BRECSU.
- Büchner, J. et al., 2017. Neue Preismodelle für Energie - Grundlagen einer Reform der Entgelte, Steuern, Abgaben und Umlagen auf Strom und fossile Energieträger.
- Burnett, J. et al., 2004. Hong Kong building environmental assessment method. HK-BEAM version 4/04 new buildings. Hong Kong: HK-Beam Society;. Available from: <<http://ira.lib.polyu.edu.hk/handle/10397/54498>>.
- Bygningsstyrelsen, 2016. Best practice Ventilation syddansk Universitet i Odense Bygning 44, Odense: SDU.
- C, F. et al., 2018. Review of applied and tested control possibilities for energy flexibility in buildings, s.l.: Annex 67.
- Camacho, E.F. & Bordons, C., 2007. Model Predictive control, London: Springer London. Available at: <http://link.springer.com/10.1007/978-0-85729-398-5>.
- Candanedo, J., Dehkordi, V. & Lopez, P., 2013. A control-oriented simplified building modelling strategy. Proceedings of BS2013: 13th Conference of International Building Performance Simulation Association, Chambéry, France, Aug. 26-28, pp.3682–3689.
- Candanedo, José A., Saberi Derakhtenjani, Ali, D'Avignon, Katherine, Athienitis, Andreas K. (2018). "A Pathway for the Derivation of Control-oriented Models for Radiant Floor Heating Applications." Proceedings of esim 2018 conference, May 2018, Montreal, Quebec.
- Carvalho, A.D. et al., 2015. Ground source heat pumps as high efficient solutions for building space conditioning and for integration in smart grids. Energy Conversion and Management, 103, pp.991–1007. Available at: <http://dx.doi.org/10.1016/j.enconman.2015.07.032>.
- CEN, "EN 15251: Indoor environmental input parameters for design and assessment of energy performance of buildings addressing indoor quality, thermal environment, lighting and acoustic." European Committee for Standardization, Brussels, Belgium, 2007.
- CEN, 2007. EN 15521: Indoor environmental input parameters for design and assessment of energy performance of buildings addressing indoor quality, thermal environment, lighting and acoustic.
- Clausen, A., Demazeau, Y. & Jørgensen, B. N., 2014. An agent-based framework for aggregation of manageable distributed energy resources. Salamanca - Spain, PAAMS.
- Clauß, J. et al. (2018) 'A generic methodology to evaluate hourly average CO<sub>2</sub>eq . intensities of the electricity mix to deploy the energy flexibility potential of Norwegian buildings', in to be published in Proceedings of the 10th International Conference on System Simulation in Buildings. Liege, Belgium.
- Clauß, J., Stinner, S., Sartori, I., et al. (2019) 'Predictive rule-based control to activate the energy flexibility of Norwegian residential buildings: Case of an air-source heat pump and direct electric heating', Applied Energy. Elsevier, 237, pp. 500–518. doi: 10.1016/J.APENERGY.2018.12.074.

Clauß, J., Stinner, S., Solli, C., et al. (2019) 'Evaluation method for the hourly average CO<sub>2</sub>eq . intensity of the electricity mix and its application to the demand response of residential heating', submitted to *energies*, pp. 1–25.

Coffey, B. et al., 2010. A software framework for model predictive control with GenOpt. *Energy and Buildings*, 42(7), pp.1084–1092.

D. Christantoni, D. Flynn, D.P. Finn, Modelling of a Multi-purpose Commercial Building for Demand response Analysis, *Energy Procedia*. 78 (2015) 2166–2171. doi:10.1016/J.EGYPRO.2015.11.308.

D. Christantoni, S. Oxizidis, D. Flynn, D.P. Finn, Implementation of demand response strategies in a multi-purpose commercial building using a whole-building simulation model approach, *Energy Build.* 131 (2016) 76–86. doi:10.1016/J.ENBUILD.2016.09.017.

Dahl Knudsen, M. & Petersen, S., 2016. Demand response potential of model predictive control of space heating based on price and carbon dioxide intensity signals. *Energy and Buildings*, 125, pp.196–204. Available at: <http://linkinghub.elsevier.com/retrieve/pii/S0378778816303188>.

Damien Ernst, Pierre Geurts, Louis Wehenkel. "Tree-Based Batch Mode Reinforcement Learning." *Journal of Machine Learning Research* (2005): 503-556.

Dar, U.I. et al., 2014. Advanced control of heat pumps for improved flexibility of Net-ZEB towards the grid. *Energy and Buildings*, 69, pp.74–84. Available at: <http://dx.doi.org/10.1016/j.enbuild.2013.10.019>.

De Boer, Pieter-Tjerk, et al. "A tutorial on the cross-entropy method." *Annals of operations research* 134.1 (2005): 19-67.

De Coninck, R. & Helsen, L., 2016. Quantification of flexibility in buildings by cost curves - Methodology and application. *Applied Energy*, 162, pp.653–665.

De Coninck, R. et al., 2010. Modelling and simulation of a grid connected photovoltaic heat pump system with thermal energy storage using Modelica. 8th International Conference on System Simulation in Buildings, (June), pp.1–21.

De Coninck, R. et al., 2014. Rule-based demand-side management of domestic hot water production with heat pumps in zero energy neighbourhoods. *Journal of Building Performance Simulation*, 7(4), pp.271–288. Available at: <http://dx.doi.org/10.1080/19401493.2013.801518>.

De Dear, Richard J., and Gail S. Brager. "Thermal comfort in naturally ventilated buildings: revisions to ASHRAE Standard 55." *Energy and buildings* 34.6 (2002): 549-561.

Deru, Michael, Kristin Field, Daniel Studer, Kyle Benne, Brent Griffith, Paul Torcellini, Bing Liu, et al. 2011. "U.S. Department of Energy Commercial Reference Building Models of the National Building Stock." Publications (E). doi:NREL Report No. TP-5500-46861.

DesignBuilder. 2012. "DesignBuilder Software Ltd." <<https://www.designbuilder.co.uk/>>

DIN EN 12831, 2010. DIN Deutsches Institut für Normung e. V - Energetische Bewertung von Gebäuden - Verfahren zur Berechnung der Norm-Heizlast.

DIN V 4108-6, 2003. DIN Deutsches Institut für Normung e. V - Wärmeschutz und Energie-Einsparung in Gebäuden. Teil 6: Berechnung des Jahresheizwärme- und des Jahresheizenergiebedarfs.

- Dong, B. & Lam, K.P., 2014. A real-time model predictive control for building heating and cooling systems based on the occupancy behavior pattern detection and local weather forecasting. *Building Simulation*, 7(1), pp.89–106.
- Doukas, H., Patlitzianas, K. D., Iatropoulos, K. & Psarras, J., 2007. Intelligent building energy management system using rule sets. *Building and Environment*, Volume 42, pp. 3562 - 3569.
- Dounis, A.I. & Caraiscos, C., 2009. Advanced control systems engineering for energy and comfort management in a building environment-A review. *Renewable and Sustainable Energy Reviews*, 13, pp.1246–1261.
- ECOFYS, 2013. National plan for increasing the number of nearly zero energy buildings in Denmark, Denmark: ECOFYS.
- Ellis, Peter G, Paul A Torcellini, and Drury B Crawley. 2007. "Simulation of Energy Management Systems in Energyplus." *Building Simulation 2007*, 1346–53. [http://www.ibpsa.org/proceedings/BS2007/p189\\_final.pdf](http://www.ibpsa.org/proceedings/BS2007/p189_final.pdf).
- EnEV 2009, 2009. Verordnung zur Änderung der Energieeinsparverordnung.
- EQUA (2015) EQUA Simulation AB. Available at: <http://www.equa.se/en/ida-ice>.
- European Environment Agency (EEA), 2004. Annual European community greenhouse gas inventory 1990–2002, s.l.: EEA.
- F.-F. Li, A. Karpathy, and J. Johnson. CS231n: Convolutional neural networks for visual recognition. n.d. 13 4 2017. <<http://cs231n.github.io>>.
- Fatima, S. & Kattan, A., 2011. Evolving optimal agendas for package deal negotiation. New York - USA, ACM.
- Feist, W., 1994. Interne Gewinne werden überschätzt. *Sonnenenergie & Wärmetechnik* 1/94.
- Filippidou, Faidra, Nico Nieboer, and Henk Visscher. "Are we moving fast enough? The energy renovation rate of the Dutch non-profit housing using the national energy labelling database." *Energy Policy* 109 (2017): 488-498.
- Finck, C. et al., 2018. Review of applied and tested control possibilities for energy flexibility in buildings, s.l.: IEA.
- Finck, C., Li, R. & Zeiler, W., 2019. Economic model predictive control for demand flexibility of a residential building. *Energy*, p. 176.
- Fiorentini, M. et al., 2015. Hybrid model predictive control of a residential HVAC system with PVT energy generation and PCM thermal storage. *Energy Procedia*, 83, pp.21–30.
- Fischer, D. et al. (2017) 'Impact of PV and variable prices on optimal system sizing for heat pumps and thermal storage', *Energy and Buildings*. Elsevier B.V., 128, pp. 723–733. Available at: <http://dx.doi.org/10.1016/j.enbuild.2016.07.008>.
- Fortin, Félix-Antoine, et al. "DEAP: Evolutionary algorithms made easy." *Journal of Machine Learning Research* (2012): 2171-2175.
- Fraunhofer IWES, S. U. F. I., 2014. Power-to-Heat zur Integration von ansonsten abgeregeltem Strom aus Erneuerbaren Energien (Agora Energiewende). <http://www.power-to-heat.eu/power-to-heat/>.

Gagnon, Pieter, Robert Margolis, Jennifer Melius, Caleb Phillips, and Ryan Elmore. 2016. "Rooftop Solar Photovoltaic Technical Potential in the United States: A Detailed Assessment." NREL/TP-6A20-65298. doi:<https://www.nrel.gov/docs/fy16osti/65298.pdf>.

Garnier, A. et al., 2015. Predictive control of multizone heating, ventilation and air-conditioning systems in non-residential buildings. *Applied Soft Computing Journal*, 37, pp.847–862. Available at: <http://dx.doi.org/10.1016/j.asoc.2015.09.022>.

Ghisi, E., & Tinker, J.A., 2004. Window sizes required for the energy efficiency of a building against window sizes required for view, *Proceedings of the CIB World Building Congress*. <http://www.irbnet.de/daten/iconda/CIB10258.pdf>

Ghoreishi, S., Sørensen, J. & Jørgensen, B., 2015. Enhancing State-of-the-art Multi-objective Optimization Algorithms by Applying Domain Specific Operators. s.l., IEEE.

Gill, D. "Building Automation and Controls Systems: Integrated Room Control for Personalized Comfort and Increased ROI." 2014.

Goia, F., Finocchiaro, L. and Gustavsen, A. (2015) '7 . Passivhus Norden | Sustainable Cities and Buildings The ZEB Living Laboratory at the Norwegian University of Science and Technology : a zero emission house for engineering and social science experiments', in. Copenhagen.

Gurobi Optimization, "Gurobi." <http://www.gurobi.com>, 2018a.

Gurobi Optimization, "Mixed-Integer Programming (MIP) - A Primer on the Basics," 2018b. [Online]. Available: <http://www.gurobi.com/resources/getting-started/mip-basics>. [Accessed: 05-Dec-2018].

Halvgaard, R. et al., 2012. Economic model predictive control for building climate control in a smart grid. *Innovative Smart Grid ...*, pp.1–6. Available at: [http://ieeexplore.ieee.org/xpls/abs\\_all.jsp?arnumber=6175631](http://ieeexplore.ieee.org/xpls/abs_all.jsp?arnumber=6175631).

Hamdy, Mohamed, Ala Hasan, and Kai Siren. "A multi-stage optimization method for cost-optimal and nearly-zero-energy building solutions in line with the EPBD-recast 2010." *Energy and Buildings* 56 (2013): 189-203.

Hartmann, T., 2010. Innere Wärmelasten in Wohnungen für die energetische Bewertung nach DIN V 18599.

Hong LüLei JiaShulan KongZhaosheng Zhang, 2007. Predictive functional control based on fuzzy T-S model for HVAC systems temperature control. *Journal of Control Theory and Applications*, 5(1), pp.94–98.

Hong, J. et al., 2012. Discrete demand side control performance under dynamic building simulation: A heat pump application. *Renewable Energy*, 39(1), pp.85–95. Available at: <http://dx.doi.org/10.1016/j.renene.2011.07.042>.

Höök, Mikael, and Xu Tang. "Depletion of fossil fuels and anthropogenic climate change—A review." *Energy Policy* 52 (2013): 797-809.

Huang, G., 2011. Model predictive control of VAV zone thermal systems concerning bi-linearity and gain nonlinearity. *Control Engineering Practice*, 19(7), pp.700–710.

Huang, H., Chen, L. & Hu, E., 2014. Model predictive control for energy-efficient buildings: An airport terminal building study. In *IEEE International Conference on Control and Automation, ICCA*. pp. 1025–1030.

- Huchtemann, K., 2015. Supply temperature control concepts in heat pump heating systems
- HVAC China. Design code for HVAC for civil building (GB 50736-2012). 2012. China Construction Industry Press. Available from: <<https://www.chinesestandard.net/PDF/English.aspx/GB50736-2012>>.
- Intergovernmental Panel on Climate Change. "Climate change 2014: mitigation of climate change." Vol. 3. (2015).
- ISO17772-1 (2017) Energy performance of buildings - Indoor environmental quality - Part1: Indoor environmental input parameters for the design and assessment of energy performance of buildings.
- J, C., C, F., P, V.-F. & P., B., 2017. Control strategies for building energy systems to unlock demand side flexibility – A review, s.l.: 15th Int. Conf. Int. Build. Perform. Simul. Assoc..
- J. Le Dréau and P. Heiselberg, "Energy flexibility of residential buildings using short term heat storage in the thermal mass," *Energy*, vol. 111, no. 1, pp. 1–5, 2016.
- J. Lofberg, "YALMIP : a toolbox for modeling and optimization in MATLAB," 2004 IEEE Int. Conf. Robot. Autom. (IEEE Cat. No.04CH37508), pp. 284–289, 2004.
- J. Ortiz, A. Fonseca, J. Salom, N. Garrido, P. Fonseca, and V. Russo, "Cost-effective analysis for selecting energy efficiency measures for refurbishment of residential buildings in Catalonia," *Energy Build.*, vol. 128, pp. 442–457, 2016.
- Jensen, M. & Jørgensen, B. N., 2011. Decouplink : Dynamic Links for Java. s.l., Springer.
- Jensen, M. L. R. & Jørgensen, B. N., 2010. Composing Objects in Open Contexts Using Dynamic Links. Marina Del Rey - USA, IASTED Software Engineering and Applications (SEA 2010).
- Jiménez, M.J., Madsen, H. & Andersen, K.K., 2008. Identification of the main thermal characteristics of building components using MATLAB. *Building and Environment*, 43(2), pp.170–180.
- Jin, X. et al., 2014. Model Predictive Control of Heat Pump Water Heaters for Energy Efficiency Modeling of Heat Pump Water Heaters. , pp.133–145.
- Jordan, U. V., 2003. DHW Calc-Tool: Werkzeug zur Generierung von Trinkwasser-Zapfprofilen auf statistischer Basis.
- Junker, R. G. et al., 2018. Characterizing the energy flexibility of buildings and districts. *Applied Energy*, , 225(), pp. 175-182.
- Kajgaard, M.U. et al., 2013. Model predictive control of domestic heat pump. In 2013 American Control Conference. pp. 2013–2018. Available at: <http://ieeexplore.ieee.org/document/6580131/>.
- Kalyanmoy, D. & Dhish, K. S., 2005. On Finding Pareto-Optimal Solutions Through Dimensionality Reduction for Certain Large-Dimensional Multi-Objective Optimization Problems. s.l., Kangal report.
- Kandler, C., Wimmer, P. & Honold, J., 2015. Predictive control and regulation strategies of air-to-water heat pumps. *Energy Procedia*, 78, pp.2088–2093.
- Kathirgamanathan, Anjukan, Killian Murphy, Mattia De Rosa, Eleni Mangina, and Donal P Finn. 2018. "Aggregation of Energy Flexibility of Commercial Buildings." In *Proceedings of ESIm 2018*, May 9-10, 2018, 173–82. Montreal.

- Kattan, A., Ong, Y.-S. & Galvan-Lopez, 2013. Multi-agent multi-issue negotiations with incomplete information: A genetic algorithm based on discrete surrogate approach. s.l., IEEE.
- Kazmi, H., et al. "Generalizable occupant-driven optimization model for domestic hot water production in NZEB." *Applied Energy* 175 (2016): 1-15.
- Keshtkar, A., 2015. Development of an Adaptive Fuzzy Logic System for Energy Management in Residential Buildings.
- Kiliccote, S., Piette, M. A., Mathieu, J. L., and Parrish, K. (2010). Findings from seven
- Kilpeläinen S, Lu M, Cao S, Hasan A and Chen S. 2018. Composition and Operation of a Semi-Virtual Renewable Energy-based Building Emulator. *Future Cities and Environment*, 4(1): 1, pp. 1–14, DOI: <https://doi.org/10.5334/fce.7>
- Kitapbayev, Y., Moriarty, J. & Mancarella, P., 2015. Stochastic control and real options valuation of thermal storage-enabled demand response from flexible district energy systems. *Applied Energy*, 137, pp.823–831. Available at: <http://dx.doi.org/10.1016/j.apenergy.2014.07.019>.
- Le Dréau, J. & Heiselberg, P., 2016. Energy flexibility of residential buildings using short term heat storage in the thermal mass. *Energy*, 111(1), pp.1–5.
- Lee, K.-H., Joo, M.-C. & Baek, N.-C., 2015. Experimental Evaluation of Simple Thermal Storage Control Strategies in Low-Energy Solar Houses to Reduce Electricity Consumption during Grid On-Peak Periods. *Energies*, 8(9), pp.9344–9364. Available at: <http://www.mdpi.com/1996-1073/8/9/9344/>.
- Leith, D.J. & Leithead, W.E., 2000. Survey of gain-scheduling analysis and design. *International Journal of Control*, 73(11), pp.1001–1025. Available at: <http://www.tandfonline.com/doi/abs/10.1080/002071700411304>.
- Lindelöf, D. et al., 2015. Field tests of an adaptive, model-predictive heating controller for residential buildings. *Energy and Buildings*, 99, pp.292–302. Available at: <http://dx.doi.org/10.1016/j.enbuild.2015.04.029>.
- Löfberg, J., 2012. Oops! i cannot do it again: Testing for recursive feasibility in MPC. *Automatica*, 48(3), pp.550–555. Available at: <http://dx.doi.org/10.1016/j.automatica.2011.12.003>.
- Ma, J. et al., 2012. Demand reduction in building energy systems based on economic model predictive control. *Chemical Engineering Science*, 67(1), pp.92–100. Available at: <http://dx.doi.org/10.1016/j.ces.2011.07.052>.
- Ma, J., Qin, S.J. & Salsbury, T., 2014. Application of economic MPC to the energy and demand minimization of a commercial building. *Journal of Process Control*, 24(8), pp.1282–1291. Available at: <http://dx.doi.org/10.1016/j.jprocont.2014.06.011>.
- Maasoumy, M. M., Rosenberg, C., Vincentelli, A. S. & Callaway, D. S., 2014. Model predictive control approach to online computation of demand-side flexibility of commercial buildings HVAC systems for Supply Following. Portland, s.n.
- Madsen, H. & Holst, J., 1995. Estimation of continuous-time models for the heat dynamics of a building. *Energy and Buildings*, 22(1), pp.67–79.
- Madsen, H., 2007. Time series analysis. s.l.:Chapman and HALL.

- Masy, G. et al., 2015. Smart grid energy flexible buildings through the use of heat pumps and building thermal mass as energy storage in the Belgian context. *Science and Technology for the Built Environment*, 21:6, pp.800–811.
- Mattsson, S. & Elmqvist, H., 1997. Modelica - An international effort to design the next generation modeling language. Gent - Belgium, CACSD, pp. 28-30.
- May-Ostendorp, P.T. et al., 2012. Extraction of supervisory building control rules from model predictive control of windows in a mixed mode building. *Journal of Building Performance Simulation*, 1493(March 2014), pp.1–21.
- Mendoza-Serrano, D.I. & Chmielewski, D.J., 2014. Smart grid coordination in building HVAC systems: EMPC and the impact of forecasting. *Journal of Process Control*, 24(8), pp.1301–1310.
- Miara, M. et al., 2014. Simulation of an Air-to-Water Heat Pump System to Evaluate the Impact of Demand-Side-Management Measures on Efficiency and Load-Shifting Potential. *Energy Technology*, 2(1), pp.90–99. Available at: <http://doi.wiley.com/10.1002/ente.201300087>.
- Moroşan, P.-D. et al., 2010. Building temperature regulation using a distributed model predictive control. *Energy and Buildings*, 42(9), pp.1445–1452. Available at: <http://linkinghub.elsevier.com/retrieve/pii/S0378778810000915>.
- Nagy, A., Kazmi, H., Cheaib, F., Driesen, J., 'Deep reinforcement learning for building optimization', presented at IBPSA Building Simulation and Optimization, BSO 2018, Cambridge, England <https://arxiv.org/ftp/arxiv/papers/1805/1805.03777.pdf>
- Naidu, D.S. & Rieger, C., 2011a. Advanced control strategies for heating, ventilation, air-conditioning, and refrigeration systems—An overview: Part I: Hard control. *HVAC&R Research*, 17(1), pp.2–21. Available at: <http://www.tandfonline.com/doi/abs/10.1080/10789669.2011.540942>.
- Naidu, D.S. & Rieger, C., 2011b. Advanced control strategies for HVAC&R systems—An overview: Part II: Soft and fusion control. *HVAC&R Research*, 17(2), pp.144–158. Available at: <http://www.informaworld.com/openurl?genre=article&doi=10.1080%2F10789669.2011.555650&magic=crossref%7C%7CD404A21C5BB053405B1A640AFFD44AE3>.
- NISSAN LEAF Specs. Available from: [http://www.mynissanleaf.com/wiki/images/0/06/NISSAN\\_LEAF\\_SpecSheet\\_FINAL\\_US\\_2.pdf](http://www.mynissanleaf.com/wiki/images/0/06/NISSAN_LEAF_SpecSheet_FINAL_US_2.pdf)
- Nord Pool Spot (2016) [www.nordpoolspot.com/historical-market-data](http://www.nordpoolspot.com/historical-market-data). Available at: [www.nordpoolspot.com/historical-market-data](http://www.nordpoolspot.com/historical-market-data).
- Oldewurtel, F. et al., 2013. Towards a standardized building assessment for demand response. *Proceedings of the IEEE Conference on Decision and Control*, pp.7083–7088.
- OpenStreetMap (2017) Shiny weather data. Available at: <https://rokka.shinyapps.io/shinyweatherdata/> (Accessed: 20 May 2017).
- Ovaska, S.J., VanLandingham, H.F. & Kamiya, A., 2002. Fusion of soft computing and hard computing in industrial applications: An overview. *IEEE Transactions on Systems, Man and Cybernetics Part C: Applications and Reviews*, 32(2), pp.72–79.
- PAROC, 2017. Danish Building regulations in accordance to BR 10, Denmark: PAROC.
- Pr??vara, S. et al., 2013. Building modeling as a crucial part for building predictive control. *Energy and Buildings*, 56, pp.8–22.

- PRCMC (People's Republic of China Ministry of construction). Urban residents' living water consumption standard (GB/T50331—2002). 2002. Available from <Urban planning communication. <http://netedu.xauat.edu.cn/jpkc/netedu/jpkc2009/szylyybh/content/wlzy/5/zg/GB.pdf>>.
- Reynders, G., Nuytten, T. & Saelens, D., 2013. Potential of structural thermal mass for demand-side management in dwellings. *Building and Environment*, 64, pp.187–199. Available at: <http://dx.doi.org/10.1016/j.buildenv.2013.03.010>.
- Reynders, Glenn. 2015. “Quantifying the Impact of Building Design on the Potential of Structural Storage for Active Demand Response in Residential Buildings.” doi:10.13140/RG.2.1.3630.2805.
- Rosiek, S. & Battles, F.J., 2011. Performance study of solar-assisted air-conditioning system provided with storage tanks using artificial neural networks. *International Journal of Refrigeration*, 34(6), pp.1446–1454. Available at: <http://dx.doi.org/10.1016/j.ijrefrig.2011.05.003>.
- Ruano, A.E. et al., 2006. Prediction of building's temperature using neural networks models. *Energy and Buildings*, 38(6), pp.682–694.
- Ruusuu R, Cao S, Delgado BM, Hasan A. 2019. Direct Quantification of Multiple-Source Energy Flexibility in a Residential Building Using a New Model Predictive High-Level Controller. *Energy Conversion and Management* 180 (2019) 1109–1128. <https://doi.org/10.1016/j.enconman.2018.11.026>
- Ruusuu R, Cao S, Hasan A, Kortelainen J, Karhela T. 2016. Developing an Energy Management System for optimizing the interaction of a residential building with the electrical and thermal grids CLIMA 2016 - the 12th REHVA World Congress May 2016, Aalborg University, Denmark. [vbn.aau.dk/files/233817749/paper\\_129.pdf](http://vbn.aau.dk/files/233817749/paper_129.pdf)
- S Goy, D.P. Finn, Estimating Demand Response Potential in Building Clusters, *Energy Procedia*, Volume 78, 2015, Pages 3391-3396, ISSN 1876-6102, <https://doi.org/10.1016/j.egypro.2015.11.756>.
- Saberi Derakhtenjani, Ali, D'Avignon, Katherine, Athienitis, Andreas K. (2018).” Development of a Predictive Control Methodology for a Hydronic De-icing System for Urban Infrastructure”. *Proceedings of Intelligent Transport Systems (ITS) World Congress 2018*, September 2018. Copenhagen, Denmark.
- Salpakari, J. & Lund, P., 2016. Optimal and rule-based control strategies for energy flexibility in buildings with PV. *Applied Energy*, 161, pp.425–436. Available at: <http://dx.doi.org/10.1016/j.apenergy.2015.10.036>.
- Santos, R.M. et al., 2016. Nonlinear Economic Model Predictive Control Strategy for Active Smart Buildings.
- Sayadi, S., Tsatsaronis, G., Morosuk, T., 2016. Reducing the Energy Consumption of HVAC Systems in Buildings by Using Model Predictive Control. In *CLIMA2016 Conference*, Aalborg, Denmark.
- Schibuola, L., Scarpa, M. & Tambani, C., 2015. Demand response management by means of heat pumps controlled via real time pricing. *Energy and Buildings*, 90, pp.15–28. Available at: <http://dx.doi.org/10.1016/j.enbuild.2014.12.047>.
- Schnieders, J., Pfluger, R. & Feist, W., 2008. Energetische Bewertung von Wohnungslüftungsgeräten mit Feuchterückgewinnung.

Seborg, D. et al., 2011. Process Dynamics and Control, Available at: [http://books.google.pt/books?id=\\_PQ42kOvtfwC](http://books.google.pt/books?id=_PQ42kOvtfwC).

Sichilalu, S.M. & Xia, X., 2015. Optimal power dispatch of a grid tied-battery-photovoltaic system supplying heat pump water heaters. Energy Conversion and Management, 102, pp.81–91. Available at: <http://dx.doi.org/10.1016/j.enconman.2015.03.087>.

Siddique, N., 2014. Intelligent Control, Available at: <http://www.sciencedirect.com/science/article/pii/S095915249285001D%0Ahttp://link.springer.com/10.1007/978-3-319-02135-5>.

SN/TS3031:2016 (2016) 'Bygningers energiytelse, Beregning av energibehov og energiforsyning'.

Sørensen, J. C. & Jørgensen, B. N., 2017. An Extensible Component-Based Multi-Objective Evolutionary Algorithm Framework. s.l., Association for Computing Machinery, pp. 191-197.

Stadtwerke Wolfhagen, 2013. Electricity data.

Sturzenegger, D. et al., 2013. Model Predictive Control of a Swiss office building. In 11th REHVA World Congress. p. 10. Available at: [http://www.opticontrol.ethz.ch/Lit/Stur\\_13\\_Proc-Clima2013.pdf](http://www.opticontrol.ethz.ch/Lit/Stur_13_Proc-Clima2013.pdf).

Sturzenegger, David, Dimitrios Gyalistras, Manfred Morari, and Roy S. Smith. 2016. "Model Predictive Climate Control of a Swiss Office Building: Implementation, Results, and Cost-Benefit Analysis." IEEE Transactions on Control Systems Technology 24 (1): 1–12. doi:10.1109/TCST.2015.2415411.

Szyperski, C., Gruntz, D. & Murer, S., 2002. Component Software: Beyond Object-oriented Programming. s.l.:ACM Press.

T. Péan, J. Salom, and J. Ortiz, "Environmental and Economic Impact of Demand Response Strategies for Energy Flexible Buildings," in Building Simulation and Optimization BSO 2018, 11-12th September 2018, Cambridge (UK), 2018a.

T. Péan, J. Salom, and R. Costa-Castelló, "Configurations of model predictive control to exploit energy flexibility in building thermal loads," in 57th IEEE Conference on Decision and Control, 2018b.

T. Péan, R. Costa-Castelló, and J. Salom, "Price and carbon-based energy flexibility of residential heating and cooling loads using model predictive control," Sustain. Cities Soc., May 2019.

TCSFR. Travel Characteristics Survey -Final report. 2011. The Government of the Hong Kong special administrative region, Transport Department. [http://www.td.gov.hk/en/publications\\_and\\_press\\_releases/publications/free\\_publications/travel\\_characteristics\\_survey\\_2011\\_final\\_report/index.html](http://www.td.gov.hk/en/publications_and_press_releases/publications/free_publications/travel_characteristics_survey_2011_final_report/index.html). 2011.

University of Wisconsin, 2010. A Transient System Simulation Program - TRNSYS Version 17. USA.

Váňa, Z. et al., 2014. Model-based energy efficient control applied to an office building. Journal of Process Control, 24(6), pp.790–797.

VISSMANN Werke GmbH & Co KG, 2010. VITOCAL 300-G.

Wang, L., Wang, Z. & Yang, R., 2012. Intelligent Multiagent Control System for Energy and Comfort Management in Smart and Sustainable Buildings. IEEE Transactions on Smart Grid, Volume 3, pp. 605-617.

- Wang, S. & Ma, Z., 2008. Supervisory and Optimal Control of Building HVAC Systems: A Review. *HVAC&R Research*, 14(1), pp.3–32. Available at: <http://www.tandfonline.com/doi/abs/10.1080/10789669.2008.10390991>.
- Wang, S. & Xu, X., 2006. Parameter estimation of internal thermal mass of building dynamic models using genetic algorithm. *Energy Conversion and Management*, 47(13–14), pp.1927–1941.
- Weiß, U., 2013. Pehnt, M.: *Marktanalyse Heizstrom - Kurzbericht*. Heidelberg.
- World Business Council for Sustainable Development, 2008. *Energy Efficiency in Buildings, s.l.: Facts and Trends*.
- years of field performance data for automated demand response in commercial buildings. In 2010 ACEEE Summer Study on Energy Efficiency in Buildings, Pacific Grove, CA.
- Yu, Z. et al., 2015. Control strategies for integration of thermal energy storage into buildings: State-of-the-art review. *Energy and Buildings*, 106, pp.203–215. Available at: <http://dx.doi.org/10.1016/j.enbuild.2015.05.038>.
- Zavala, V. M. et al., 2010. *Proactive Energy Management for Next-Generation Building Systems*. New York, s.n.
- Zavala, V. M., 2013. Real-Time Optimization Strategies for Building Systems. *Industrial and Engineering Chemistry Research*, Volume 52, pp. 3137-3150.
- Zemtsov, N. et al., 2017. Economic MPC based on LPV model for thermostatically controlled loads. [Online].
- Zhang, K. et al., 2014. Assessing simplified and detailed models for predictive control of space heating in homes. In *Proceedings of SSB 2014: the 9th International Conference on System Simulation in Buildings*, Liege, Dec 10-12. p. P04.1-20.
- Zhou, Y., & Cao, S., 2019a. Flexibility quantification of residential net-zero energy buildings involved with the dynamic operations of hybrid energy storages and various energy conversion strategies. In progress.
- Zhou, Y., & Cao, S., 2019b. Investigation of the flexibility of a residential net-zero energy building (NZEB) integrated with an electric vehicle in Hong Kong. *Energy Procedia*. Volume 158, pp. 2567-2579
- Zhou, Y. et al., 2019. Energy integration and interaction between buildings and vehicles: A state-of-the-art review. *Renewable and Sustainable Energy Reviews*. DOI: <https://doi.org/10.1016/j.rser.2019.109337>.
- Zhou, Y., & Cao, S., 2019c. Energy flexibility investigation of advanced grid-responsive energy control strategies with the static battery and electric vehicles: A case study of a high-rise office building in Hong Kong. *Energy Conversion and Management*. DOI: <https://doi.org/10.1016/j.enconman.2019.111888>.
- Zong, Y. et al., 2012. Model predictive controller for active demand side management with PV self-consumption in an intelligent building. *IEEE PES Innovative Smart Grid Technologies Conference Europe*, pp.1–8.



Energy in Buildings and  
Communities Programme

[www.iea-ebc.org](http://www.iea-ebc.org)